UNIVERSIDAD AUTÓNOMA DE CHIAPAS

FACULTAD DE CIENCIAS EN FÍSICA Y MATEMÁTICAS

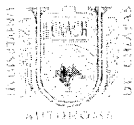# HIGH ENERGY MULTI-WAVELENGTH STUDIES ON PWNE AND UNIDENTIFIED VHE GALACTIC SOURCES

# T E S I S

QUE PARA OBTENER EL GRADO DE:

**MAESTRA EN CIENCAS FÍSICAS**

PRESENTA:

**LAILA VLEESCHOWER CALAS**

ASESORES:

**DR. OMAR TIBOLLA**
**DRA. SARAH KAUFMANN**
**DR. CÉSAR ÁLVAREZ OCHOA**

TUXTLA GUTIÉRREZ, CHIAPAS; MAYO DE 2019.

Tuxtla Gutiérrez, Chiapas
*29 de abril de 2019*
***Oficio No. FCFM/0189/19***

**Dr. Omar Tibolla**
**Director de Tesis**

**Dr. César Álvarez Ochoa**
**Asesor Coadyuvante**
**Presente**

Por este medio me permito informarle que una vez efectuada la revisión de la tesis denominada:

***"High Energy Multi-Wavelegth Studies on PWNE and Unidentified VHE Galactic Sources".***

Ha sido aceptada para sustentar el Examen de Grado de Maestra en Ciencias Físicas de la **C. Lic. Laila Vleeschower Calas**, con matrícula escolar: X131010

Se autoriza su impresión en virtud de cumplir con los requisitos correspondientes.

**Atentamente**
**"Por la conciencia de la necesidad de servir"**
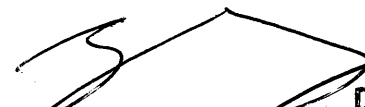
**Dr. Sendic Estrada Jiménez**
**Director**

DIRECCIÓN
FCFM

C.c.p.    Dr. Florencio Corona Vázquez, Secretario Académico de la FCFM.
         Lic. Ana Gabriel Aguilar Avendaño.- Encargada de Servicios Escolares de la FCFM
         Archivo / Minutario
         SEJ /egav

## AGRADECIMIENTOS

Gracias a mis amigos y compañeros que durante esta etapa estuvieron conmigo, por los tiempos tanto de trabajo como de diversión. Gracias Felipe, sin tu apoyo hubiera resultado más difícil.

Gracias Dios por no apartar tu mano de mí.

Agradezco a todos los que hicieron posible la realización y la culminación de esta tesis.

**Laila.**

# ABSTRACT

The cosmic rays were discovered more than 1 century ago and their origin is still unknown, this is in fact the oldest open question in physics (and evidently in astrophysics). In the era of astrophysics of high (very high) energies, we are able to see many astrophysical particle accelerators, but so far, no final answer has been given. With this work we want to help in the explanation on the origin of this radiation by studies of very-high energy gamma rays. In particular, my thesis deals with a fundamental question of very-high energy gamma-ray astronomy. Namely, I analysed three Tera-electron Volt (TeV) unidentified Galactic sources: HESS J1626-490, HESS J1808-204 and HESS J1813-126.

All the identified sources classes (AGNs, PWNe, SNR, etc.) also exhibit emission in the radio and/or X-ray regime. Significant X-ray and radio emission is predicted since the same population of electrons should emit synchrotron radiation at longer wavelengths. Therefore, one of the best ways to identify the sources is looking on X-ray data for lower counterparts.

In this thesis, an analysis of public data acquired by the X-ray satellites Chandra and XMM-Newton was carried out. Furthermore, analysis of *Fermi*-LAT data in HESS J1626-490 was also done. With the final challenging objective of demonstrate (or help

demonstrate) that the unidentified sources are old Pulsar Wind Nebulae (PWN).

# CONTENTS

# LIST OF FIGURES

# LIST OF ACRONYMS

**PWN**    Pulsar Wind Nebulae

**LOFAR**  Low-Frequency Array

**H.E.S.S.**  High Energy Stereoscopic System

**VHE**    Very High Energy

**GRB**    Gamma-ray Bursts

**EBL**    Extra-galactic Background Light

**CRs**    Cosmic Rays

**CMB**    Cosmic Microwave Background

**AGN**    Active Galactic Nuclei

**SNR**    Supernova Remnant

**XRB**    X-ray Binaries

**IACTs**  Imaging atmospheric Cherenkov Telescopes

**IC**     Inverse Compton

**LAT**    Large Area Telescope

**MAGIC**  Major Atmospheric Gamma-ray Imaging Cherenkov Telescope

**HAWC**   High-Altitude Water Cherenkov Observatory

**VERITAS**  Very Energetic Radiation Imaging Telescope Array System

**ARGO-YBJ**  Astrophysical Radiation with Ground-based Observatory at YangBaJing

**MCs**    Molecular Clouds

**FRI**    Fanaroff-Riley-I-type

**TS**     Test Statistic

**INTEGRAL**  INTErnational Gamma-Ray Astrophysics Laboratory

**MOST**   Molonglo Galactic Plane Survey

**SGPS**   Southern Galactic Plane Survey

**GMRT**   Giant Metrewave Radio Telescope

**CGRO**   Compton Gamma-Ray Observatory

**CXO**   Chandra X-ray Observatory

**AXAF**   Advanced X-ray Astrophysics Facility

**EPHIN**   Electron, Proton, Helium INstrument

**HRC**   High Resolution Camera

**ACIS**   Advanced X-ray Imaging Camera

**LETG**   Low Energy Transmission Grating

**HETG**   High Energy Transmission Grating

**CCDs**   Charge Coupled Devices

**FI**   Front Illuminated

**BI**   Back Illuminated

**XMM**   X-ray Multi-Mirror Mission

**ESA**   European Space Agency

**EPIC**   European Photon Imaging Cameras

**RGS**   Reflection Grating Spectrometers

**MOS**   Metal Oxide Semi-conductor

**GLAST**   Gamma-ray Large Area Space Telescope

**SSD**   Silicon-Strip Detector

**GBM**   Gamma-ray Burst Monitor

**GRBs**   Gamma-ray Bursts

**TDRSS**   Tracking and Data Relay Satellite System

**TKR**   Tracker

**CAL**   Calorimeter

**ACD**   Anti-Coincidence Detector

**DAQ**   Data Acquisition System

**CDE**   Crystal Detector Element

**IRFs**   Instrument Response Functions

**FGL**   Fermi Gamma-ray LAT

**SAS**   Science Analysis System

**CCF**   Current Calibration File

**CIF**   Calibration Index File

**GTI**   Good Time Interval

**ATNF**   Australia Telescope National Facility

**SIMBAD**  Set of Identifications, Measurements and Bibliography for Astronomical Data

**YSOC**   Young Stellar Object Candidate

**ABC**   Asymptotic Giant Branch Star Candidate

**LMXB**   Low Mass X-ray Binary

**FSSC**   Fermi Science Support Center

**MET**   Mission Elapsed Time

**IEM**   Interstellar Emission Models

**3FHL**   Third Fermi-LAT Catalog of High-Energy Sources

**TS**   Test Statistic

**ROI**   Region of Interest

**SED**   Spectral Energy Distribution

**PSF**   Point Spread Function

**HGPS**  H.E.S.S. Galactic Plane Survey

**SFR**   Star Forming Region

**SCUBA**  Submillimetre Common User Bolometer Array

# INTRODUCTION

The knowledge of cosmic rays had its beginnings since the beginning of the last century by scientists Theodor Wulf ([1], [2]) and Domenico Pacini [3], but it was the Austrian Viktor Hess who clearly established that they were this type of particles which were being detected [4], which marked the beginning of high energy astrophysics. For a little more than a century scientists have studied its composition, spectrum, propagation and acceleration mechanisms, questioning its origin.

Cosmic rays are related to gamma rays since it requires the acceleration of charges and their interaction with matter or fields of radiation for the production of higher energy photons. The very high-energy gamma-ray astronomy window ($10^{10}$ -$10^{14}$ eV, according to [5]) was opened with the detection of TeV gamma rays from the Crab nebula [6]. In the last decades, great advances have been made in this area of astronomy thanks to the development of the science and technology of both terrestrial and space telescope detectors and we have found just over 200 sources of TeV gamma rays. With this, several categories of this class of objects have already been established, which are: Active Nuclei of Galaxies, Pulsar Wind Nebulae, Supernova Remnants, X-ray Binary Stars, and Starburst Galaxies[1]. However, around one third of the TeV sources still can not be identified, that is, they could not be associated with a counterpart in other wavelengths. A counterpart is what could be the same object seen in high energies but identified in other lower frequencies.

---

[1]for a quick idea visit http://tevcat2.uchicago.edu/

This thesis is structured as follows. An introduction to VHE gamma-ray astronomy is given in Chapter 1. TeV unidentified sources and the objectives of this thesis are introduced in Chapter 2. Chapter 3 describes the telescopes that we used for the analysis. The analysis methods on HESS J1626 and its performance are explained in Chapter 4. The analysis results of the X-ray studies on HESS J1808-204 and on HESS J1813-126 are given in Chapters 5 and 6, respectively. Conclusions are added in Chapter 7.

# CHAPTER 1

## VERY HIGH ENERGY GAMMA RAY ASTRONOMY

With the purpose of studying the Universe, it is necessary to catch its "messengers", not only electromagnetic radiation or photons, but also observing cosmic-ray nuclei, electrons, neutrinos, photons, and most recently, gravitational waves. The development of science and technology has allowed scientists to reveal different aspects of the composition and behaviour at different wavelengths and coordinate observations and interpretations of different messenger signals.

Nowadays the Universe is observed by photons with energies ranging from $10^{-7}$ eV (using e.g. the Low-Frequency Array (LOFAR) [7]) to $10^{14}$ eV (with e.g. the High Energy Stereoscopic System (H.E.S.S.) [8]) thanks to the development of new techniques and technologies for making astronomical observations from both ground and space, but also the advances in laboratory physics and the development of high-speed computers. Photons can be named depending on the energies (E): radio (E < $10^2$ eV), infrared ($10^{-2}$ < E < 2 eV), optical (2 < E < 3 eV), UV (3 < E < 100 eV), X-rays (100 < E < 5 $\times$ $10^5$ eV) and gamma-rays (E > 5 $\times$ $10^5$ eV). The energy range between $10^{10}$ and $10^{14}$ eV is known as "very high energy" (VHE), which also includes the study of neutrino and cosmic rays astronomy.

This work has as objective to study the unidentified VHE galactic sources: HESS J1626-490, HESS J1808-304 and HESS J1813-126, which have been observed at TeV energies by using the H.E.S.S. observatory. We analyse X-ray and gamma-ray data of these three sources with the aim of unveiling the origin of its VHE radiation, in order to understand the places in the Universe where the most energetic processes take place, connecting us to the extreme aspect of our Universe. Efficient particle acceleration can occur mostly when there are extreme astronomical objects or phenomena such as neutron stars, black holes, Gamma-ray Bursts (GRB), or supernova explosions. Furthermore, VHE gamma-rays can provide valuable information about some aspects of fundamental astrophysics and cosmology such as deducing the energy spectra of the Extra-galactic Background Light (EBL), probing for the quantum gravity effect and searching for dark matter, among others.

In this chapter we introduce the VHE astronomy by starting in Sect. 1.1 with cosmic rays, though which human started to realize the presence of strong particle acceleration in the Universe. The mechanisms for gamma-ray production will be described in Sect. 1.2. The possible sites for charged particle acceleration and known VHE sources will be depicted in Sect. 1.3. Concluding remarks of this chapter will be given in Sect. 1.4.

## 1.1 Cosmic Rays

Cosmic Rays (CRs) are high-energy particles that can be produced in different locations in the Universe, and are constantly hitting our planet. Most of them are absorbed by the atmosphere, or else life would not have developed on Earth, but also generates secondary particles. Their study has a special place in physics due to the role it has played in the study of elementary particles and its interactions.

### 1.1.1 Discovery of Cosmic Rays

The cosmic rays, as they are know currently, were studied since beginnings of 20th century after the idea that it was an anomalous ionisation observed in the atmosphere of extraterrestrial origin [9]. During the years 1907-1912 Domenico Pacini [3] detected cosmic rays in Lake Bracciano an the Tireno Sea. At the same period, in 1909, Theodor Wulf discovered them on the Eiffel Tower and introduced the german term "Hoehenstrahlung" ("radiation from the above"), he was also the person who invented the electroscope [1] [2]. By using electroscopes in his balloon flights of 1912-1913, was Viktor Hess [4] who confirmed the ionization was more intense increasing with height, concluding that the radiation enters from above our atmosphere. He showed that the cosmic rays were an astrophysical phenomenon making observations during a partial solar eclipse (which could be noted as the first astroparticle experiment, marking the beginning of the high-energy astrophysics). He was awarded by the Nobel Prize in 1936 for this work. In addition, in 1914 Kolhörster made his confirmation [10]. The existence of cosmic radiation was fully accepted since about 1926 [11]. Nevertheless, the English term "Cosmic Rays" was coined by the American scientist R. Millikan who was initially sceptical about the conclusion of his colleagues.

It was established that the cosmic rays are dominated by positively charged particles and as we now know consist mainly of stripped atomic nuclei and having relativistic speeds. Nowadays, the term is used to indicate all the energetic charged particles, ions and electrons ($\sim$86% protons, $\sim$11% alpha particles and the rest heavy nuclei, also electrons $\sim$2%) [12], that hit the Earth's atmosphere at a rate of $\sim$1000 per square metre per second, distinguished by high energies, a very few of them can have ultrarelativistic energies extending up to $10^{20}$ eV ($\sim$20 Joules). For a little more than a century, scientists have been studying its composition, spectrum, propagation and acceleration

mechanisms, questioning its origin, and it is currently a topic of active research.

The percentages showed previously are for particles above a given *magnetic rigidity* $R = pc/z|e|$, where $p$ is the momentum, $c$ is the speed of light in vacuum, and $z|e|$ is the charge of the particle, for particles with the same probability of penetrating to the atmosphere through the Earth's magnetic field.

## 1.1.2 Energy Spectrum of CRs

The energy spectrum of the CRs has been measured by several experiments. It shows a power law in a broad energy range, from $10^{10}$ to $10^{20}$ eV as displayed in Figure 1.1. This such high energies and the power law spectrum indicates that the CRs are produced by non-thermal processes.
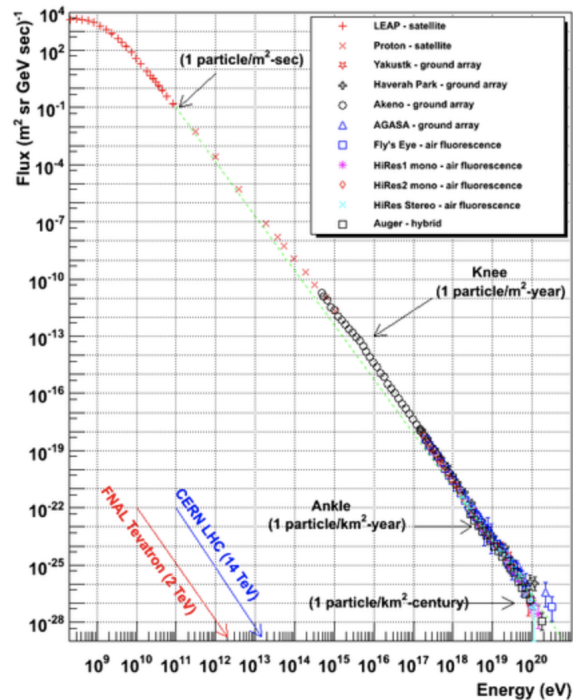


Figure 1.1: Cosmic ray spectrum of various experiments from $\sim 10^8$ to $\sim 10^{20}$ eV. It shows a power law above $10^{10}$ eV, but the index changes at the the called "knee" and "ankle". (Figure from http://www.physics.utah.edu/~whanlon/spectrum.html).

The spectrum does not starts as a power law, below $10^{10}$ eV it is curved in log-log scale, but this is principally due to the effect of the geomagnetic field and the solar wind magnetic field that prevent low energy charged particles from entering the Earth's atmosphere. Above a few GeV energy, the spectrum up to the so-called '*knee*', at $10^{16}$ eV, follows a simple power law as following.

$$N(E)dE = \text{const} \cdot E^{-2.7}dE \quad E < E_{knee} = 10^{16}\text{eV}$$

After the knee, the spectrum becomes steeper with an index of $\sim$-3

$$N(E)dE = \text{const} \cdot E^{-3.0}dE \quad E_{knee} < E < E_{ankle}.$$

The spectrum becomes hard again above the so-called '*ankle*' at $E_{ankle} \approx 4\times 10^{18}$ eV:

$$N(E)dE = \text{const} \cdot E^{-2.69}dE \quad E_{ankle} < E < E_{GZK}.$$

Above $E_{GZK} = 4 \times 10^{19}$ eV, extensive air shower experiments have found that the spectrum appear to fall, presumably because of the 'GZK cut-off' (the Greisen-Zatsepsin-Kuzmin cut-off, see [13]) due to pion production in collisions with Cosmic Microwave Background (CMB) photons (the mean free path of charged particles with E $\gtrsim$ 6 $\times$ $10^{19}$ eV is very short: $\sim$ 30 Mpc for $10^{20}$ eV protons).

## 1.2   Gamma-ray Emission Processes

Cosmic rays are related to gamma-rays due to the acceleration of this charged particles and their interaction with matter or radiation fields is required to the production of energetic photons. In this section, I briefly describe these emission mechanisms that

lead produce the VHE gamma-ray radiation. The information presented in the following subsections are mostly taken from [14] and [15].

## 1.2.1 Decay of a Neutral Pion

When accelerated hadrons (particles made of quarks) collide with other hadrons, there is a production mostly of pions (an up quark and a down anti-quark), of which about a third are neutral pions, $\pi_0$. Each $\pi_0$ has a mass of 135 MeV/c$^2$ and decays almost instantaneously into two photons with a lifetime of $8 \times 10^{-17}$ seconds.

$$p + p \rightarrow \pi_0 + X \rightarrow \gamma + \gamma + X, \tag{1.1}$$

where $X$ denotes associated products such as protons, neutral pions or other mesons (compound particles in a quark-antiquark state).

## 1.2.2 Pair Annihilation

The annihilation of particles and anti-particles can convert energy into two (or more) photons. The most abundant process in astrophysics is the electron-positron annihilation, but this one in particular has a related energy of only 511 keV per photon.

## 1.2.3 Compton Scattering

As an introduction to particle scattering, we will start with the **Thompson scattering**, which is a low-energy interaction between a photon and an electron. This interaction is *elastic*, which means that the photon and the electron collide and modify their momentum direction, but the total kinetic energy remains the same.

If the energy of the scattered photon is greater, then there will be an exchange of energy, and therefore a change in the frequency after the interaction. But as long as

Figure 1.2: Feynman diagram of an electron-positron annihilation resulting in two photons. (Figure by By Manticorp - Own work, CC BY-SA 3.0, https://commons.wikimedia.org/w/index.php?curid=17594913).

the energy of the incident photon is lower than the rest of the stationary electron mass-energy system, namely:

$$h\nu \ll m_e c^2, \tag{1.2}$$

then the interaction will be described by the Thompson scattering.

However, in high energy astrophysics there are many inelastic interactions, so the photon energy changes after the dispersion.

In the case of Compton scattering, a high-energy photon collides with a static electron and transfers part of its energy and momentum to the electron.

The change in the photon wavelength after Compton scattering is given by:

$$\triangle \lambda = \lambda_i - \lambda_f = \frac{h}{m_e c^2}(1 - \cos\alpha), \tag{1.3}$$

where $\alpha$ is the scattering angle of the photon.

The increase in wavelength during the scattering results in a corresponding decrease in photon energy. The energy of the photon is transferred to the electron in the form of

kinetic energy or momentum.

## 1.2.4  Inverse Compton Scattering

In the Inverse Compton scattering, a relativistic electron interacts with a low energy photon. At the end of the interaction the photon gains energy. The Compton effect and the Inverse Compton effect are exactly the same process, but the order of the energy and momentum transferred are reversed.

Relativistic effects become important in the Inverse Compton scattering since it involves high-energy electrons (i.e, high-velocity electrons). The maximum energy gained by the photons through the Compton scattering is equal to its initial energy multiplied by the square of twice the Lorentz factor (where the square Lorentz factor is given by $\gamma^2 = 1/[1 - (v/c)^2]$ and $v$ is the electron speed):

$$E_{max} = (h\nu)_{max} \approx 4\gamma^2 h\nu_0. \tag{1.4}$$

In the general case, the frequency of the scattered photon is given approximately by $\nu \approx \gamma^2 \nu_0$. In many astronomical sources, there are electrons with $\gamma \approx$ 100-1000, and therefore the Inverse Compton scattering is the most relevant scattering radiation process, acting over low energy electrons up to very high energies.

## 1.2.5  Synchrotron Radiation

When an electron is moving and interacting with a magnetic field, its path is bent perpendicularly to the magnetic field due to the Lorentz force and it spirals along the field lines forming a helical path. So that its direction is constantly changing, and thus it is by definition an accelerated charged particle, which yields electromagnetic radiation.

$$e + B \rightarrow e + B + \gamma. \tag{1.5}$$

When a particle is relativistic, the emission is collimated along its direction of movement. This is the so-called *synchrotron radiation* (see [16]).

The Synchrotron radiation is more relevant in the case of electrons, they are lighter than protons and therefore more easily diverted. Due to the magnetic field $B$ the electrons gyro-frequency is:

$$\nu_{gir} = \frac{eB}{2\pi\gamma m_e c} \tag{1.6}$$

The maximum number of photons produced by these electrons occurs at a critical frequency ($\nu_c$) given by:

$$\nu_c = \frac{3}{2}\gamma^3 \nu_{gir} \sin(\theta) \tag{1.7}$$

where $\theta$ is the angle between the momentum of the particle and the magnetic field lines. The radiation can only be observed when the photon beam is aligned with the line of sight as the electrons revolve around the field lines. Because of this, the synchrotron radiation spectrum is the sum of a large number of harmonics of the cyclotron emission basis; the resulting spectrum is sharply chopped, with a maximum emission at $\sim 0.29\,\nu_c$ and a intensity of the form:

$$I(\nu) \propto \left(\frac{\nu}{\nu_c}\right)^{\frac{1}{3}} \tag{1.8}$$

for $\nu \ll \nu_c$, and

$$I(\nu) \propto \left(\frac{\nu}{\nu_c}\right)^{\frac{1}{2}} e^{-(\nu/\nu_c)} \tag{1.9}$$

11

for $\nu \gg \nu_c$.

The spectrum of the synchrotron radiation can be easily represented by an exponential function of the form $ax^b\exp(-x)^d$. Fitting gives as best values for the parameters $a = 1.787$, $b = 0.299$ and $d = 0.992$, which yield the following expression:

$$F(x) \simeq 1.79x^{0.3}\exp(-x).\tag{1.10}$$

See the evaluated function in Figure 1.3.
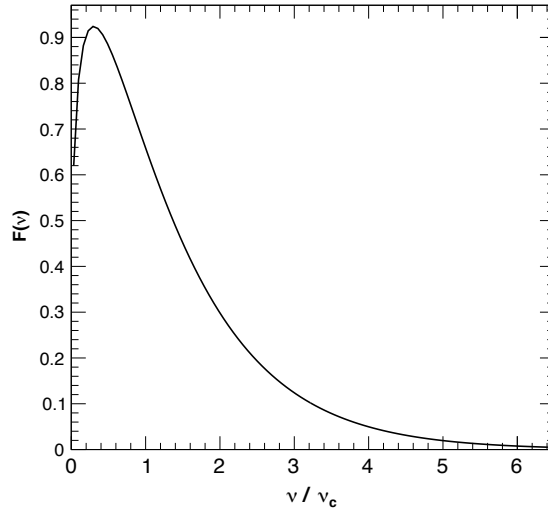


Figure 1.3: Spectrum of synchrotron emission. The flux peak occurs at $0.29\nu_c$, where $\nu_c$ is known as the characteristic frequency. Figure from [14].

Energetic electrons or extremely intense magnetic fields can shift this peak of energy to the gamma-rays domain. An electron with energy $E_e$ under the influence of a field $B$ radiates photons at an energy of:

$$E_\gamma \approx 0.05 \left(\frac{E_e}{TeV}\right)^2 \left(\frac{B}{3\mu G}\right) eV.\tag{1.11}$$

When the magnetic fields are greater than $\sim 10^{13}$G, the quantum and relativistic

effects will result in a magnetic field being so intense that it confines the particles to move along its field lines; in this case the radiation is emitted when the field lines are bent: this process is known as *curvature radiation*.

Depending on the particles distribution, there might be two types of synchrotron radiation: thermal and non-thermal.

**Thermal Synchrotron Radiation**

In this case, the particles distribution follows a Maxwellian of the form:

$$N(E)EdE = N_0E^2 exp\left(-E/E_c\right) \tag{1.12}$$

where $N_0$ is the number of particles and $E_c$ the critical energy.

**Non-thermal Synchrotron Radiation**

When we talk about non-thermal synchrotron emission, the emitting particles generally follow an energy distribution given by a power law:

$$N(E)dE = KE^{-\Gamma} \tag{1.13}$$

where K is a normalization constant and $\Gamma$ is known as the spectral index that ranges in the interval $\sim$ 2-2.5 for this case.

The sources of non-thermal emission are very few because this type of radiation is highly dependent on the energy of the celestial object.

## 1.2.6   Bremsstrahlung

Breaking radiation (from German, *bremsen* "to brake" and *Strahlung* "radiation") or deceleration radiation is electromagnetic radiation produced by the deceleration of a charged

particle, such as an electron (e), when it is deflected by another charged particle, normally an atomic nucleus (with atomic number $Z$):

$$e + Z \rightarrow e + Z + \gamma. \tag{1.14}$$

The lightest particle loses kinetic energy, which is converted into a photon satisfying the energy conservation principle; the cross section depends inversely on the square of the mass of the particle, the bremsstrahlung is extremely efficient for light particles, such as electrons.

By integrating the bremsstrahlung cross section it is possible to obtain an expression for the total intensity $I$ as a function of the photon frequency ($\nu$), the electron velocity ($v_e$) and the impact parameter ($b$):

$$I(\nu) = \frac{(Ze)^2 e^4 n}{12\pi^3 \varepsilon_0^3 c^3 m_e^2 v_e} ln \left( \frac{192 v_e}{Z^{1/3} c} \right) \mathrm{J/cm}^2, \tag{1.15}$$

where $n$ is the density of atoms in the medium in which the particle is immersed and $m_e$ the mass of the electron.

The bremsstrahlung radiation spectrum remains flat until approximately the kinetic energy of the electron ($E_k$), given by:

$$E_k = (\gamma - 1) m_e c^2. \tag{1.16}$$

Then it falls sharply to zero, since all the available kinetic energy of the electron has been transferred to the photon. At high energies, due to relativistic beaming, the average emission angle is given by:

$$\vartheta_\gamma = \frac{mc^2}{E}. \tag{1.17}$$

Therefore, most of the electron energy is released in a narrow cone around its momentum vector.

The description above assumes a single electron interacting with a sea of atomic nuclei; however, in the case of a hot electron-proton plasma, the total emission for all the particles is called thermal *bremsstrahlung*: if T is the plasma temperature and $n_e$ and $n_p$ the density of electrons and protons respectively, the spectral emissivity per unit volume and time is given by:

$$k_\nu = \frac{1}{3\pi^2} \left(\frac{\pi}{6}\right)^2 \frac{(Ze)^2 e^4}{\varepsilon_0^3 c^3 m_e^2} \sqrt{\frac{m_e}{kT}} \, g(\nu, T) \, n_p n_e \, exp\left(-\frac{h\nu}{kT}\right) \mathrm{Wm^{-3} Hz^{-1}}, \qquad (1.18)$$

where $g(\nu, T)$ is the *Gaunt factor* and depends on the collision processes and the approximations used.

## 1.3 Possible Acceleration Sites and known VHE Gamma-ray Sources

The VHE gamma-ray astronomy window was opened with the TeV gama-ray detection of the Crab Nebula using a ground-based atmospheric Cherenkov technique [6]. In recent decades great advances have been made in this area of astronomy thanks to the development of the science and technology of both terrestrial detectors and space telescopes and just over 200 sources of TeV gamma rays have been found. With this, several categories of this class of objects have already been established, which are: Active Galactic Nuclei (AGN), Pulsar Wind Nebulae, Supernova Remnant (SNR), X-ray Binaries (XRB), and Starbursts galaxies (for having a quick look visit TevCat http://tevcat2.uchicago.edu/).

## 1.3.1 Extragalactic sources

**Active Galactic Nuclei**

An active galactic nucleus is a compact region at the center of a Galaxy which is birghter than the standards (the total luminosity of a Galaxy is given by the integral of all the stars in the Galaxy, $10^{11}$) in at least some portion of the electromagnetic spectrum, indicating that the luminosity is not produced by stars. A galaxy with an active core is known as an "active galaxy". In some cases, the central and compact region emits relativistic jets. In some cases high energy emission up to MeV-GeV-TeV energies can be detected in the jets (more radiation than the remaining part of the galaxy), the current theories states that it is powered by Super-massive black hole (with mass around $10^{6}$ to $10^{10}$ $M_{\odot}$) in the center of the host galaxy. This object is surrounded by a disc of accreted material and has two jets perpendicularly to the disc. Inside the jets, particles are accelerated by the Fermi acceleration mechanism (see e.g. [17]) or magnetic reconnection mechanisms (see e.g. [18]).

AGNs are believed to be the most powerful sources of non-thermal energy in the Universe, and currently, these are the most common extragalactic objects emitting VHE gamma-rays (74 are listed in TeVCat).

**Starburst Galaxies**

Starburst galaxies are galaxies in which the rate of the star formation is exceptionally high compared to the observed in most other galaxies (about $10^{3}$ times larger than in a normal galaxy). For this reason, the galaxy will consume all of its gas and dust reservoir within about $10^{8}$ years. Must starburst are observed in a small region around the nucleus. This kind of galaxies experience also a high supernova rate, that makes the CR density also high, resulting in detectable VHE gamma-ray emission (see e.g. [19]). So far, just

two starbusrt galaxies (M82 and NGC 253) have been detected to have VHE gamma-ray emission [20].

**Gamma Ray Bursts**

Gamma-ray bursts are the brightest electromagnetic events that occur in the Universe, meaning that they are due to very violent phenomena; however, this astronomical phenomena can last from miliseconds to several hours [21]. In most of the cases they are followed by residual luminosity of long duration of radiation that can be seen from radio to X-rays.

GRBs are uniformly distributed in the Universe. The emission energy ranges from optical to gamma-rays ($\sim$30 GeV). The strong radiation up to gamma-rays suggests the particle acceleration there. MAGIC recently detected the first GRB at sub-TeV energies [22]. Nevertheless, no GRB has been detected in VHE gamma-rays so far.

## 1.3.2 Galactic Sources

**Supernova Remnants**

Shortly after the discovery of neutrons, in 1934, Baade and Zwicky suggested that when the Iron core of a massive star exceeds the Chandrasekhar limit ($\sim$1.44 $M_\odot$) by the conversion of Silicon into Iron, the star collapse into neutron star producing a *Supernova* [23]. A SNR is the structure which results of the big explosion of the star in a supernova, it is bounded by an expanding shock wave where the supernova ejecta and the interstellar medium collide, and is formed by material expelled from the explosion, and the interstellar material swept along the way.

The energy released ($\sim$10$^{51}$ erg typically) gives as a result the optical and X-ray extended source, which is the gaseous SNR. According to [24], considering the shock

speed, scale of system, magnetic field and explosion rate, SNR can explain basically all features of CRs at least below the knee energy. 11 SNR have been detected to have VHE emission (see TeVCat).

**Pulsars, Pulsar Wind Nebulae**

Pulsars are rotating neutron stars having strong magnetic fields ($\sim 10^{14}$ G) that were discovered in 1967 by Jocellyn Bell and Anthony Hewish [25]. Inside the pulsar magnetosphere, a persistent and strong electric field can exist, and a high density of electrons and positrons exist there and these can be accelerated by the strong electric field.

Highly relativistic winds that consist of electrons and positrons, and possibly a hadronic component are produced in Pulsars [26], these winds carry a significant fraction of the rotational energy loss rate [27]. The pulsar wind nebula (PWN) which emits synchrotron radiation from radio to GeV results of the interaction between the pulsar winds and the ambient medium, TeV can also be produced in these ambient via the inverse Compton (IC) scattering of the background photons off the electrons that emit the synchrotron radiation [28]. PWNe are useful probes of pulsars and their surroundings.

Unidentified TeV sources are most likely to be PWN since many of them have a powerful pulsar located near the edge of the emission region (see e.g. [29], [30]), due to its preferential location in the galactic plane (see Figure 2.2). Forty four TeV sources can be classified as PWN or PWN candidates [31].

More details will be given in the next chapter.

**Binary Systems**

A binary system is a system of two astronomical objects which are close enough that their gravitational attraction causes them to orbit each other around a common center of mass. It can be formed by binary stars, brown dwarfs, neutron stars, or even black holes.

If one of the stars is a compact object like a neutron star or a black hole and the other has a huge mass loss, accretation of the matter to the strong gravitational star may create an accretation disc and relativistic plasma jets, such a system is called a microquasar (microquasar scenario). If both stars have strong stellar winds and they collide, shock waves may exist and particles can be accelerated (wind collision scenario) [32]. There are eleven sources of this nature listed in the TeVCat.

**Open and Globular Clusters**

In a young open cluster, there are numerous young massive stars which have a strong plasma wind. Because of the smaller distance between stars, the winds collide with each other or collective winds collide with surrounding matters. Then, shock will be created which leads to particle acceleration (see e.g. [33]). Similarly, in a globular cluster, plasma winds from many pulsars can accelerate particles. Three massive star clusters and one globular cluster are listed in TeVCat.

## 1.4   Concluding Remarks

In the Universe, there are plenty and a variety of extreme astronomical objects where particles can be accelerated to very high energies. These high energy particles have several channels to produce gamma-rays and one can distinguish them by, for example, the energy spectrum. Therefore, VHE gamma-rays are useful probes for investigating the nature of these extreme objects. VHE gamma-rays are also useful tools for some questions of fundamental physics and cosmology.

TeV sources that cannot been classified due to the lack of a clear lower counterpart will be detailed in the next chapter.

# CHAPTER 2

---

## UNIDENTIFIED TeV SOURCES

---

Very high energy (VHE, E $> 10^{11}$ eV) gamma-rays give the opportunity to study the extreme environments in the local universe in the most direct view that is available nowadays thanks to the invention of Imaging atmospheric Cherenkov Telescopes (IACTs), such as H.E.S.S. Their production can be explained by the presence of relativistic electrons of either non-thermal bremsstrahlung or Inverse Compton (IC) scattering on background photon fields by high-energy electrons, also whereas protons (and atomic nuclei) can generate $\gamma$-rays via the decay of $\pi^0$s produced in hadronic interactions with ambient material. VHE $\gamma$-radiation is therefore expected from the acceleration sites of particles with energies above 1 TeV ($10^{12}$ eV). In particular, $\gamma$-rays can be seen as a probe of sources of nucleonic cosmic rays in our Galaxy and may thus provide part of the explanation on the origin of this radiation.

In this chapter, TeV unidentified sources are introduced, starting in sect. 2.1 where all this kind of sources known to the date are depicted, and I describe the steps that we followed to select, among all of them, the three sources that we would study following our selection criteria, that is also pointed out in this part of the thesis. Besides, a table with the number of X-ray observations carried out on each source is shown, this information

was indispensable at the time of making the selection. In sect. 2.2 I briefly describe all the TeV unidentified sources that are known so far, showing their position, their TeV flux, their spectral index, if it is extended or not and the size of the extension; moreover, I summarize information found in all the available literature of each of the sources trying to find their possible associations. Finally, concluding remarks of this chapter and the selection of the sources as topic of this thesis are given in Sect. 2.3

## 2.1   Introduction

Presently identified VHE gamma-ray sources have been found to be either AGN, PWN, SNR, Starburst Galaxies, or XRB. However, many sources detected at TeV gamma-rays do not have a clear lower counterpart or they do not have a reasonable emission model, making these unidentified. Currently there are 65 TeV unidentified sources that have been detected by all the VHE gamma-ray instruments that have existed so far [31]. In this chapter, I make a brief description of all these sources known to the date. This was a result of doing a review in all the available literature, with the aim to have a better understanding about them and to know the studies that have been done on each of them, and finally to be able to choose three as object of study of the thesis. Following the next selection criteria we chose HESS J1626-490, HESS J1808-204, and HESS J1813-126, these sources will be described in more detail in the chapters 4, 5 and 6.

- We want to study PWN evolution: young PWN ($\lesssim$ 1000 years), medium age and old ($\gtrsim$ 10000 years).

- Unidentified source that have not hardly studied or well known.

- Available X-ray and gamma-ray data.

- With interesting features ("dark sources") by its possible explanation as pulsars,

PWN or magnetars.

In the Figure 2.1 we can find all the sources classified as unidentified VHE gamma-ray sources.

| unidentified VHE γ-ray sources | |
|---|---|
| MAGIC J0223+403 | HESS J1843-033 |
| ARGO J0409-0627 | 0FGL J1844.1-0335 |
| 2HWC J0819+157 | 2HWC J1844-032 |
| 2HWC J1040+308 | HESS J1844-030 |
| 2HWC J1309-054 | HESS J1848-018 |
| HESS J1457-593 | 2HWC J1852+013 |
| HESS J1503-582 | HESS J1852-000 |
| HESS J1614-518 | HESS J1857+026 |
| HESS J1626-490 | MAGIC J1857.6+0297 |
| HESS J1634-472 | HESS J1858+020 |
| HESS J1641-463 | 0FGL J1900.0+0356 |
| HESS J1646-458 (Wd1?) | 2HWC J1902+048 |
| HESS J1729-345 | 1HWC J1904+080c |
| HESS J1741-302 | 2HWC J1907+084 |
| HESS J1745-303* (hot spot C) | ARGO J1910+0720 |
| VER J1746-289 | HESS J1912+101 |
| HESS J1746-285 | 2HWC J1914+117 |
| MAGIC J1746.4-2853 | 2HWC J1921+131 |
| HESS J1747-248 (Terzan 5?) | 2HWC J1928+177 |
| HESS J1804-216 | 2HWC J1938+238 |
| HESS J1808-204 | HESS J1943+213 |
| HESS J1809-193 | 2HWC J1949+244 |
| HESS J1813-126 | 2HWC J1953+294 |
| 2HWC J1825-134 | 2HWC J1955+285 |
| HESS J1826-130 | 2HWC J2006+341 |
| HESS J1828-099 | VER J2016+371 |
| 2HWC J1829+070 | VER J2019+368 |
| HESS J1832-085 | MGRO J2019+37 |
| HESS J1834-087 | TeV J2020+380d |
| 2HWC J1837-065 | VER J2019+407 |
| HESS J1841-055 | MGRO J2031+41 |
| 1HWC J1842-046c | TeV J2032+4130 |

Figure 2.1: Unidentified gamma-ray sources known to the date as described in the text. Table from [31]. The sources which are object of study in this work are marked with red rectangles.

More information about the TeV unidentified sources can be found on TeVCat [1], which is an online catalog for TeV Astronomy developed by Deirdre Horan and Scott Wakely [34].

In Figure 2.2 we can see all the unidentified sources to the date, all of them will be described with more detail in the next subsections. All of them are named starting with the observatory they were discovered, after the J indicates 2000.0 coordinates followed by the source's right ascension and declination. The color of the points depends

---

[1] http://tevcat2.uchicago.edu

22
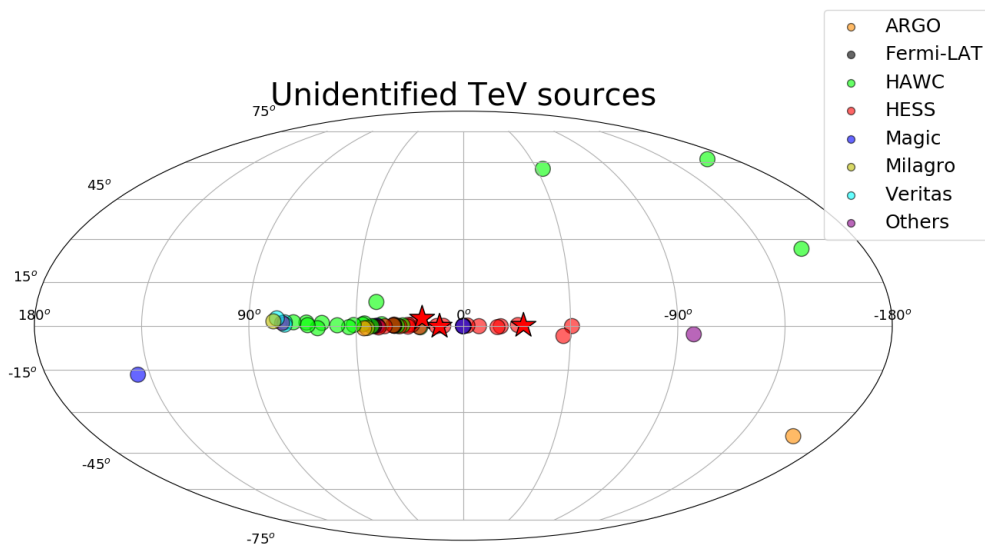
Figure 2.2: Unidentified gamma-ray sources known to the date, described in the text.

on the observatory by which they were discovered. Orange circles shows the sources detected by the Astrophysical Radiation with Ground-based Observatory at YangBa-Jing (ARGO-YBJ); sources found using *Fermi*-LAT (Large Area Telescope) are marked with black color; the blue color shows the sources detected using the Major Atmospheric Gamma-ray Imaging Cherenkov Telescope (MAGIC); sources that were first detected by the High-Altitude Water Cherenkov Observatory (HAWC) are represented in green color; the red color indicates the HESS sources, three of them were highlighted as stars, which were the ones that were analysed in this work; sources detected using Milagro experiment are presented in yellow color; color cyan displays the sources detected by the Very Energetic Radiation Imaging Telescope Array System (VERITAS); with purple color are marked the sources that have other names.

All the identified sources classes also exhibit emission in the radio and/or X-ray regime. Significant X-ray and radio emission is predicted since the same population of electrons should emit synchrotron radiation at longer wavelengths. For typical Galactic

magnetic field strengths, the energy flux of the X-ray component of the photon spectrum in the keV range is predicted to be comparable to the energy flux in the TeV range. If gamma-rays are produced only via $\pi^0$ decay, a strong X-ray or radio signal may not be present; however, proton interactions also produce charged pions and cascades of secundary electrons that should generate a continuum of X-ray and radio synchrotron emission.

With the purpose of knowing which of these sources have been observed with X-ray satellites, I searched in the NASA's HEASARC website using the Browse Mission interface for X-ray observations made with Chandra, XMM-Newton, Swift, NuSTAR and/or Suzaku (visit https://heasarc.gsfc.nasa.gov/cgi-bin/W3Browse/w3browse.pl).

A table with summarized information on these results can be seen in 2.1. This information was key to decide which of the sources we would analyse following the selection criteria.

Table 2.1: Search for X-ray observations. The size of the extension is given in degrees.

| Source | RA | DEC | Extended | Size | $\Gamma$ | XMM | Chandra | Swift | Suzaku | NuStar |
|---|---|---|---|---|---|---|---|---|---|---|
| 0FGL J1844.1-0335 | $18^h\,44^m\,08^s$ | -03° 35' 21" | Yes | - | - | - | 4 | - | - | - |
| MAGIC J0223+403 | $02^h23^m12^s$ | +43°00'42" | No | - | 3.1 | 2 | 1 | 91 | - | - |
| ARGO J0409-0627 | $04^h\,09^m\,24^s$ | -06° 27' 00" | No | - | - | - | - | 1 | - | - |
| 2HWC J0819+157 | $08^h\,19^m\,55^s$ | +15° 47' 24" | Yes | 0.5, 0.5 | 1.5 | - | - | - | - | - |
| Vela Region | $08^h\,33^m\,39^s$ | -45° 00' 10" | No | - | - | - | 29 | 22 | 1 | - |
| 2HWC J1040+308 | $10^h\,40^m\,53^s$ | +30° 52' 12" | Yes | 0.0, 0.0 | 2.08 | - | - | - | - | - |
| 2HWC J1309-054 | $13^h\,09^m\,14^s$ | -05° 29' 24" | No | - | 2.55 | - | - | - | - | - |
| HESS J1427-608 | $14^h\,27^m\,52^s$ | -60° 51' 00" | Yes | 0.04, 0.08 | 2.16 | 1 | - | 10 | 1 | - |
| HESS J1507-622 | $15^h\,06^m\,53^s$ | -62° 21' 00" | Yes | 0.15, 0.15 | 2.24 | 2 | 1 | 3 | 1 | - |
| HESS J1626-490 | $16^h\,26^m\,04^s$ | -49° 05' 13" | Yes | 0.07, 0.10 | 2.18 | 3 | 3 | 20 | - | - |
| HESS J1634-472 | $16^h\,34^m\,58^s$ | -47° 16' 12" | Yes | 0.11, 0.11 | - | 6 | 14 | 214 | 6 | - |
| HESS J1641-463 | $16^h\,41^m\,02^s$ | -46° 18' 13" | No | - | 2.07 | 1 | 10 | 52 | 1 | 3 |
| HESS J1702-420 | $17^h\,02^m\,44^s$ | -42° 00' 57" | Yes | 0.30, 0.15 | 2.07 | - | 2 | 13 | 1 | - |
| HESS J1708-410 | $17^h\,08^m\,24^s$ | -41° 05' 24" | Yes | 0.30, 0.15 | 2.07 | 1 | - | 13 | 1 | - |
| HESS J1729-345 | $17^h\,29^m\,35^s$ | -34° 32' 22" | Yes | 0.14, 0.14 | 2.24 | 1 | - | 27 | - | - |
| HESS J1741-302 | $17^h\,41^m\,15^s$ | -30° 22' 37" | No | - | 2.3 | 1 | 4 | 156 | 3 | - |
| Galactic Centre Ridge | $17^h\,45^m\,40^s$ | -29° 00' 22" | Yes | 2.00, 0.20 | 2.29 | 60 | 184 | 1000 | 19 | 44 |
| Galactic Centre | $17^h\,45^m\,40^s$ | -29° 00' 22" | No | - | 2.1 | 77 | 193 | - | - | - |

| Source | RA | DEC | Extended | Size | $\Gamma$ | XMM | Chandra | Swift | Suzaku | NuStar |
|---|---|---|---|---|---|---|---|---|---|---|
| VER J1746-289 | $17^h\ 46^m\ 20^s$ | -28° 57' 58" | Yes | 0.00 , 0.00 | - | 63 | 190 | 1000 | 19 | 25 |
| HESS J1746-285 | $17^h\ 46^m\ 24^s$ | -28° 52' 33" | No | | 2.19 | 10 | 37 | 1000 | 2 | 11 |
| MAGIC J1746.4-2853 | $17^h\ 46^m\ 25^s$ | -28° 52' 55" | No | - | - | 65 | 195 | 1000 | 6 | 7 |
| HESS J1804-216 | $18^h\ 04^m\ 31^s$ | -21° 42' 00" | Yes | 0.16 , 0.27 | - | 3 | 1 | 21 | 1 | - |
| HESS J1808-204 | $18^h\ 08^m\ 37^s$ | -20° 25' 36" | Yes | 0.10 , 0.10 | 2.3 | 16 | 14 | 50 | 3 | 3 |
| HESS J1809-193 | $18^h\ 10^m\ 31^s$ | -19° 18' 00" | Yes | 0.53 , 0.25 | - | 24 | 31 | 1 | 3 | |
| HESS J1813-126 | $18^h\ 13^m\ 22^s$ | -12° 41' 14" | Yes | 0.21 , 0.21 | - | 1 | 1 | 12 | 1 | 1 |
| 2HWC J1825-134 | $18^h\ 25^m\ 50^s$ | -13° 24' 00" | No | - | 2.58 | 2 | 2 | 15 | - | - |
| HESS J1826-130 | $18^h\ 26^m\ 00^s$ | -13° 02' 02" | Yes | 0.17 , 0.17 | 1.6 | 1 | 3 | 15 | - | - |
| HESS J1828-099 | $18^h\ 28^m\ 59^s$ | -09° 59' 34" | No | - | - | - | 10 | - | - | - |
| 2HWC J1829+070 | $18^h\ 29^m\ 22^s$ | +07° 01' 48" | No | - | 2.69 | - | - | - | - | - |
| HESS J1832-085 | $18^h\ 32^m\ 32^s$ | -08° 30' 35" | No | - | - | 1 | 1 | 20 | - | - |
| HESS J1834-087 | $18^h\ 34^m\ 45^s$ | -08° 45' 36" | Yes | 0.09 , 0.09 | - | 4 | 5 | 75 | 1 | 3 |
| 2HWC J1837-065 | $18^h\ 37^m\ 26^s$ | -06° 34' 48" | No | - | 2.9 | 2 | 2 | 50 | 1 | - |
| HESS J1841-055 | $18^h\ 40^m\ 55^s$ | -05° 33' 00" | Yes | 0.41 , 0.25 | 2.4 | 1 | 4 | 135 | 1 | 1 |
| 1HWC J1842-046c | $18^h\ 42^m\ 00^s$ | -04° 36' 00" | No | - | - | - | - | 172 | - | - |
| HESS J1843-033 | $18^h\ 43^m\ 00^s$ | -03° 18' 00" | Yes | 0.00 , 0.00 | - | 1 | 2 | 19 | - | - |
| 0FGL J1844.1-0335 | $18^h\ 44^m\ 09^s$ | -03° 35' 21" | Yes | 0.00 , 0.00 | - | 1 | 3 | 142 | - | 1 |
| 2HWC J1844-032 | $18^h\ 44^m\ 17^s$ | -03° 15' 00" | No | - | 2.64 | - | 21 | 33 | - | - |

Continued on next page ...

| Source | RA | DEC | Extended | Size | $\Gamma$ | XMM | Chandra | Swift | Suzaku | NuStar |
|---|---|---|---|---|---|---|---|---|---|---|
| HESS J1844-030 | $18^h\ 44^m\ 41^s$ | $-03°\ 05'\ 34"$ | No | - | - | 4 | 19 | 76 | - | - |
| 2HWC J1852+013* | $18^h\ 52^m\ 02^s$ | $+01°\ 22'\ 48"$ | No | - | 2.9 | - | 2 | 8 | - | - |
| HESS J1852-000 | $18^h\ 52^m\ 13^s$ | $-00°\ 00'\ 23"$ | Yes | 0.00, 0.00 | - | - | 4 | 28 | - | - |
| HESS J1857+026 | $18^h\ 57^m\ 11^s$ | $+02°\ 40'\ 00"$ | Yes | 0.11, 0.08 | 2.39 | 1 | 3 | 28 | 1 | - |
| MAGIC J1857.6+0297 | $18^h\ 57^m\ 36^s$ | $+02°\ 58'\ 02"$ | No | - | - | - | 2 | 29 | - | - |
| HESS J1858+020 | $18^h\ 58^m\ 20^s$ | $+02°\ 05'\ 24"$ | Yes | 0.08, 0.02 | 2.17 | - | - | - | - | - |
| 0FGL J1900.0+0356 | $19^h\ 00^m\ 02^s$ | $+03°\ 56'\ 48"$ | No | - | - | - | - | 13 | - | - |
| 2HWC J1902+048* | $19^h\ 02^m\ 02^s$ | $+04°\ 51'\ 36"$ | No | - | 3.22 | 1 | - | 7 | - | - |
| 1HWC J1904+080c | $19^h\ 04^m\ 24^s$ | $08°\ 00'\ 00"$ | No | - | - | - | - | 11 | - | - |
| 2HWC J1907+084* | $19^h\ 07^m\ 10^s$ | $+08°\ 30'\ 00"$ | No | - | 3.25 | - | 1 | 7 | - | - |
| MGRO J1908+06 | $19^h\ 07^m\ 54^s$ | $+06°\ 16'\ 07"$ | Yes | 0.34, 0.34 | 2.1 | 6 | 1 | 14 | - | - |
| ARGO J1910+0720 | $19^h\ 10^m\ 36^s$ | $+07°\ 21'\ 00"$ | No | - | - | - | 3 | 7 | - | - |
| 2HWC J1914+117* | $19^h\ 14^m\ 43^s$ | $+11°\ 43'\ 12"$ | No | - | 2.83 | - | - | 12 | - | - |
| 2HWC J1921+131 | $19^h\ 21^m\ 12^s$ | $+13°\ 07'\ 48"$ | No | - | 2.75 | - | - | 11 | - | - |
| 2HWC J1928+177 | $19^h\ 28^m\ 36^s$ | $+17°\ 46'\ 48"$ | No | - | 2.56 | 4 | 1 | 18 | - | 1 |
| 2HWC J1938+238 | $19^h\ 38^m\ 58^s$ | $+23°\ 48'\ 36"$ | No | - | 2.96 | - | - | 18 | - | - |
| 2HWC J1949+244 | $19^h\ 49^m\ 41^s$ | $+24°\ 27'\ 36"$ | Yes | 1.00, 1.00 | 2.38 | - | - | 5 | - | - |
| 2HWC J1953+294 | $19^h\ 53^m\ 02^s$ | $+29°\ 28'\ 48"$ | No | - | 2.78 | 1 | 2 | 1 | - | - |
| 2HWC J1955+285 | $19^h\ 55^m\ 19^s$ | $+28°\ 35'\ 24"$ | No | - | 2.4 | - | 1 | 1 | - | - |

| Source | RA | DEC | Extended | Size | $\Gamma$ | XMM | Chandra | Swift | Suzaku | NuStar |
|---|---|---|---|---|---|---|---|---|---|---|
| 2HWC J2006+341 | $20^h\,06^m\,12^s$ | $+34°\,10'\,48"$ | No | - | 2.64 | - | - | - | - | - |
| VER J2016+371 | $20^h\,16^m\,02^s$ | $+37°\,11'\,52"$ | No | - | 2.3 | 1 | 2 | 10 | - | 1 |
| VER J2019+368 | $20^h\,19^m\,25^s$ | $+36°\,48'\,14"$ | Yes | 0.34 , 0.13 | 1.75 | 1 | 5 | 8 | 1 | - |
| MilagroDiffuse | $20^h\,20^m\,00^s$ | $+38°\,00'\,00"$ | Yes | 0.00 , 0.00 | - | - | - | - | - | - |
| VER J2019+407 | $20^h\,20^m\,05^s$ | $+40°\,45'\,26"$ | Yes | 0.23 , 0.23 | 2.37 | 5 | 4 | 15 | 1 | - |
| MGRO J2031+41 | $20^h\,28^m\,43^s$ | $+41°\,18'\,36"$ | Yes | 1.80 , 1.80 | 3.22 | - | 1 | - | - | - |

More information about all this sources can be found in the next section of this chapter.

## 2.2  Description of all the unidentified VHE $\gamma$-ray sources

The unidentified VHE $\gamma$-ray sources known to the date are the following:

### 1. MAGIC J0223+403

MAGIC J0223+403

| Parameter | Value |
|---|---|
| R.A. ............. | $02h23m12s$ |
| DEC. ............ | $+43^o00'42''$ |
| Flux (Crab Units) | $0.022$ |
| Energy Threshold | $150\,\mathrm{GeV}$ |
| Spectral Index ... | 3.1 |
| Extended ........ | No |
| Discovery Date .. | $2009.02$ |
| Distance ......... | $-$ |

3C66A and 3C66B are two AGN which are separated 6 arcmin in the sky, with 3C66B is Fanaroff-Riley-I-type (FRI) radio-galaxy, and 3C66A a blazar. MAGIC J0223+403 is located close to the posotion of the blazar 3C66A, considered a candidate TeV blazar. However, an analysis of the MAGIC data shows that the events are rather centered on the position of 3C66B. If the association of the excess with 3C66B will be confirmed, this would be a known TeV emitting radiogalaxy [35].

In [35], they assume that the emission from this source comes from 3C66B, and also, they found that the source is not related to 3C66A with a probability of 95.4%, and propose that it is produced in the misaligned inner structured jet [36]. The "structured jet" is a jet composed by a fast internal spine surrounded by a slower layer. However, since they couldn't detect variations, alternative models invoking emission from more distant regions along the jet cannot be excluded [37].

The best VHE candidates are the radiogalaxies in which the jet axis lies at a relatively small angle with respect to the line of sight, in this model, they assumed an angle of 20 degrees for 3C66B. But after all, the observed spectrum would be a combination from 3C66B and 3C66A as suggested by [35].

This source is likely extragalactic, and as we are interested on Galactic sources, we can say that this is not a good source to analyse for the thesis.

## 2. ARGO J0409-0627

ARGO J0409-0627

| Parameter | Value |
|---|---|
| R.A. ............ | $04h09m24s$ |
| DEC. ........... | $-06^{o}27'00''$ |
| Flux (Crab Units) | $-$ |
| Energy Threshold | $3000$ GeV |
| Spectral Index ... | 3.1 |
| Extended ........ | No |
| Discovery Date .. | 2013.11 |
| Distance ......... | $-$ |

The source was detected to be outside the Galactic plane, at 4.8 standard deviations in a sky survey using the declination band from ?10° to 70°, using data recorded over the past five years using the ARGO-YBJ detector. No counterpart at GeV $\gamma$-ray and X-ray bands, neither at lower energies, has previously been found. Its post-trial significance is the lowest among the sources listed in Table 2 of [38] and is less than 3 standard deviations ($\sigma$).

For the purposes of this thesis, we can say that this source is not interesting, due to it is outside the Galactic plane.

## 3. 2HWC J0819+157

This source was found in the 0.5° radius extended search by HAWC experiment [39], with a Test Statistic (TS) value of 30.7. It is located out of the Galactic plane (b = 26°.52),

30

2HWC J0819+157

| Parameter | Value |
| --- | --- |
| R.A. ............. | $08h19m55.2s$ |
| DEC. ............ | $+15^{o}47'24''$ |
| Flux (Crab Units) | $-$ |
| Energy Threshold | $-$ |
| Spectral Index ... | $1.5 \pm 0.67$ |
| Extended ........ | Yes |
| Discovery Date .. | $2017.02$ |
| Distance ......... | $-$ |

the nearest potentially high-energy source is the AGN 2MASS J08203478+1531114, 0.3 away. However, its distance ($z = 0.14$) seems incompatible with the observed extent and hard spectrum. The fitted index ($-1.50$) is much harder than that of any other source.

Due to the position and characteristics of the source, it is not including among our selection criteria of sources to study in this work.

## 4. Vela Region

Vela Region

| Parameter | Value |
| --- | --- |
| R.A. ............. | $08h33m39s$ |
| DEC. ............ | $-45^{o}00'10''$ |
| Flux (Crab Units) | $-$ |
| Energy Threshold | $-$ GeV |
| Spectral Index ... | $-$ |
| Extended ........ | No |
| Discovery Date .. | $1997.09$ |
| Distance ......... | $-$ |

The Vela region is complex, containing a number of sources of non-thermal radiation, including Vela X, Vela Y and Vela Z (which is part of the sheel of the SNR RX J0852.0-4622) and the young active pulsar PSR B0833-45. Vela X was the first middle-age PWN to be detected, and so the concept of PWN evolution was introduced in this way [40].

In Enemoto et al. 2005 [41], they confirmed, the $\gamma$-ray emission from the Vela PWN at the 4$\sigma$ level, also that the TeV emission from the PWN peaks ~0.5 degrees south of the

pulsar position and has a ~0.6 degree extension, confirming H.E.S.S. report, suggesting this source would require more observations for a detailed morphological study.

Otherwise, observations on the region were carried out with H.E.S.S. observatory and they detected HESS J0835-455 [42], a VHE source situated to the south of the pulsar and the compact X-ray nebula (as seen by Chandra) which appears to be spatially coincident with X-ray (0.4-2.4 keV) emission as seen by ROSAT. But previously, it was suggested that the Vela X feature corresponds to the PWN, by the unequal pressure of the reverse shock from the SNR [43]. This hypothesis is consistent with the H.E.S.S. observations which demonstrate clearly that this feature emits non-thermal radiation [42].

For this source many detailed studies have been done, so it is not a good source for been studied in this thesis.

## 5. 2HWC J1040+308

2HWC J1040+308

| Parameter | Value |
| --- | --- |
| R.A. ............. | $10h40m52.8s$ |
| DEC. ............ | $+30^{o}52'12''$ |
| Flux (Crab Units) | $-$ |
| Energy Threshold | GeV |
| Spectral Index ... | 2.08 $\pm$ 0.25 GeV |
| Extended ........ | Yes |
| Discovery Date .. | $2017.02$ |
| Distance ......... | $-$ |

This source was found in the $0.5°$ radius extended search by HAWC observatory with a TS value of 26.3, having a flux $F_7 = 6.6 \pm 3.5 \times 10^{-15}$ TeV$^{-1}$cm$^{-2}$s$^{-1}$, and no obvious associations were found in catalogs [39]. It is located out of the Galactic plane, which seems in tension with the source extent. No other TeVCat sources were found in a region of $0.5°$ [39]. This source was studied using VERITAS telescopes; however, the exposure was relatively small (1.8~7 hours), and the upper limits were not strongly constraining [44].

For this source no observations have been made in X-rays, and it is out of the Galactic plane, so could no be studied in this thesis project.

## 6. 2HWC J1309-054

| 2HWC J1309-054 | |
|---|---|
| Parameter | Value |
| R.A. ............. | $13h09m14.4s$ |
| DEC. ............ | $-05^{o}29'24''$ |
| Flux (Crab Units) | $-$ |
| Energy Threshold | GeV |
| Spectral Index ... | 2.55 $\pm$ 0.18 GeV |
| Extended ........ | No |
| Discovery Date .. | 2017.02 |
| Distance ......... | $-$ |

Similar to 2HWC J1040+308, the coordinates of this source correspond to a location out of the Galactic plane, with $b = 57.1°$, and having a flux $F_7$ = 12.3 $\pm$ 3.5 $\times$ 10$^{-15}$ TeV$^{-1}$cm$^{-2}$s$^{-1}$. It was foundwith HAWC observatory in the point search with a TS value of 25.3 [39], no obvious associations found in the catalogs. No TeVCat sources were found in a 0.5° search.

Moreover, no X-ray observations have been carried out on this region of the sky, therefore it is not under study for the thesis.

## 7. HESS J1427-608

| HESS J1427-608 | |
|---|---|
| Parameter | Value |
| R.A. ............. | $14h27m52s$ |
| DEC. ............ | $-60^{o}51'00''$ |
| Flux (Crab Units) | $-$ |
| Energy Threshold | GeV |
| Spectral Index ... | 2.16 GeV |
| Extended ........ | Yes |
| Discovery Date .. | 2007.07 |
| Distance ......... | $-$ |

The source is located $\sim 1°$ away from the source G313.2+0.3, which is a X-ray and GeV gamma-ray source located in the *Kookaburra* complex [45]. There are no nearby pulsars or SNR, also the association with the unidentified INTErnational Gamma-Ray Astrophysics Laboratory (INTEGRAL) source IGR J14331-6112 is unlikely due to the fact that there is a large angular distance between both sources.

Moreover, no evidence for significant emission of radio and X-ray significant emission at distances of $0.5°$ or closer to the centroid position of the HESS source was found.

A spatially-independent developed model of PWN was applied to the source, giving as a result reasonable parameters in the PWN framework, concluding that HESS J1427-608 can be identified as evolved PWN [46]. Which is, indeed, the target of this thesis project: to find more objects that can fit in a PWN evolution. Furthermore, this work can be relevant in general for studies in the origin of CRs.

Suzaku and XMM-Newton observations were carried out on the source in [47], where they discovered an intrinsically extended X-ray counterpart ($\sigma = 0'.9 \pm 0'.1$), Suzaku J1427-6051. With XMM-Newton archival data they found several faint point sources in spatial coincidence with HESS J1427-608 in the soft X-ray band. In the same paper, they concluded that the available data were insufficient to confirm if it has a PWN and/or SNR origin.

More than seven years Fermi-LAT data were investigated by [48], in the direction of this TeV source a point GeV source is detected with a significance of $\sim 5.5\sigma$, and the GeV spectrum connects with the TeV spectrum smoothly, which suggests that this is a potentially GeV counterpart of HESS J1427-608.

The absence of shell structure in the X-ray band and the low strength of magnetic field could be telling that the source is a PWN rather than a SNR. But, the SNR scenario is benefited due to its gamma-ray spectrum is flat in a wide energy range. So, the nature of HESS J1427-608 is still unclear and further radio and VHE gamma-ray energies are

crucial to understand its nature [48].

This source was already studied in detail by Voster et al. [46], so we will not concentrate our studies in this source.

## 8. HESS J1507-622

HESS J1507-622

| Parameter | Value |
|-----------|-------|
| R.A. ............. | $15h06m52.8s$ |
| DEC. ............ | $-62^o21'00''$ |
| Flux (Crab Units) | 0.01 |
| Energy Threshold | 500 GeV |
| Spectral Index ... | 2.24 GeV |
| Extended ........ | Yes |
| Discovery Date .. | 2009.12 |
| Distance ......... | – |

There were indications of this source since 2006/2007 during the extension of the H.E.S.S. survey of the Galactic plane [49]. Dedicated observations were performed for 9.7 hours in 2007 and 2008, and HESS J1507-622 was visible with a peak significance at $9.3\sigma$ for the dedicated observations, and showing that the source is slightly extended with intrinsic size (without include the PSF) of $0.15° \pm 0.02°$ [50]. This source was found to be located $\sim$3.5∘ from the Galactic plane and has a flux above 1 TeV of ($1.5 \pm 0.4_{stat}$ $\pm 0.3_{sys}$) $\times 10^{-12}$cm$^{-2}$s$^{-1}$.

No evidence for infrared counterparts were found (see [51], [52]). On the other hand, HESS J1507-622 was found to be on a radio filament at 2.4 GHz (see Figure 3 from [50]). In a complete CO survey [53] the source is located close to the edge of a nearby CO molecular cloud of $\sim$5° $\times$ $\sim$2°. However, due to the difference in extension and the offset of $\sim$1° from the centroid of the HESS source, advise for no association between both sources.

This source was observed also in X-rays, by observations with XMM-Newton and Chandra telescopes [50]. The XMM-Newton observation was severely affected by a

big proton flare reducing significantly the Good Time Interval (GTI) of the observation (originally from 25 ks), and leading to a GTI of 8.0 ks for MOS1 and 9.2 for MOS2 and 0.8 ks for the PN detector. Only one point-like source was found with that observation, which was confirmed by Chandra [50], where 13 sources were detected, one of them was found to be extended.

In [54] a hadronic model involving interactions between high-energy protons with the ambient ISM was assumed with the purpose of investigate the effects of a location at low density environments on the characteristics of such sources. In this case, with increasing distance from the galactic plane, the gamma-ray luminosity monotonically decreases, due to its dependence on the density of the target material. They said that only a young SNR ($\lesssim$ 1000 years) could explain the extension of the source in the case of being linked to the size of the entire remnant. In such scenario, the X-ray emission produced by synchrotron radiation of primary electrons accelerated in the same blast wave as the hadronic CRs would be expected. They also showed that considering a typical value for the energy in cosmic rays for a supernova of $10^{50}$ would suggest that HESS J1507-622 is at a distance of < 2 kpc. Putting that restriction on the distance, it would require a pressure driven age or the remnant of < 1000 years.

In [55] they show the results of the analysis of Chandra data finding a extended Chandra source (magenta source in [55]). Moreover, another discovery of this Chandra observation was the extended source 1RXS J150841.2-621006 (32-40 arcsec, spacial coincident with the radio source MGPS J150850-621025), which is not coincident with the extended source and its outside the $3\sigma$ significance contour of the VHE source emission peak, concluding that is not a plausible counterpart for the source. To sum up, it could be linked to an evoluted PWN still visible at VHE, since the hadronic model appears unlikely unless the distance of a SNR or GRB remnant is fairly small (see also [56]).

A spatially-independent model that can be used to calculate the temporal evolution of the electron/positron spectrum in a spherically expanding PWN was studied in [46]. This model is favoured to explain the nature of HESS J1507-622 as being compressed by the reverse show of the SNR, finding a current age of the PWN of $t_{age}$ = 24 kyr, strengthening the argument that this HESS source can be identified as an old PWN.

This is an interesting source but it has been studied in detail by our research team, leaving it out of the analysis of this thesis.

## 9. HESS J1626-490

HESS J1626-490

| Parameter | Value |
| --- | --- |
| R.A. ............. | $16h26m04s$ |
| DEC. ............ | $-49°05'13''$ |
| Flux (Crab Units) | − |
| Energy Threshold | − GeV |
| Spectral Index ... | $2.18$ |
| Extended ........ | Yes |
| Discovery Date .. | $2007.07$ |
| Distance ......... | − |

Located on the Galactic plane, is a gamma-ray source with an 5 arcmin extent approximately radially-symmetric Gaussian morphology. Toward increasing right asension, there is a slight extension which could mean a second VHE source [57]. There exists some weak radio emission within the gamma-ray emission region, along with the unidentified X-ray source 1RXS J162504-490918, which could be a possible X-ray counterpart since it is located approximately 10' from the centroid position. The shell-type SNR G335.2+00.1 (MSH 16-44) [58] lies outside the significant emission region of this HESS source, as does the LMXB 4U 1624-490 and the HMXB IGR 16283-4838, which are not considered plausible candidates due to their offsets [57].

According to [59], X-ray point sources has been detected, but assuming an IC emission scenario, none of these can be considered as the synchrotron radiation counterpart

to the source. Furthermore, they didn't detect any diffuse X-ray excess emission originating from the region around HESS J1626-490 above the Galactic Background, there is just one bright X-ray point source in the FoV but it is most likely not related to the source due to it is a triple system of active main sequence stars. They used XMM-Newton observations to calculate the a limit for the X-ray flux, but the results disfavors a purely leptonic emission scenario for HESS J1626-490. With these, they could conclude that the most likely origin of the TeV emission is an hadronic interaction betweem cosmic rays and a moderately dense molecular cloud, which was detected with the NANTEN telescope with reasonable physical parameters. They also found that the possible responsible source of accelerated particles for the TeV emission could be SNR G335.2 + 0.1, since the centroid of HESS J1626-490 is found within $0.5°$ of the SNR, in contradiction with [57].

Studies at [60] indicated that it is likely there is a hadronic component to the source due to $NH_3$ (1,1) emission was found towards the TeV peak and also dense gas counterparts to unidentified regions of TeV emission. Furthermore, research carried out indicated a middle-agged or old SNR, at an age similar to other TeV emitting SNRs where the hadronic scenario is supported.

HESS J1626-490 has only one association, with the high-energy $\gamma$-ray source 3FGL J1626.2-4911. A dedicated XMM-Newton observation did not reveal any compelling X-ray counterpart either [59].

Detailed XMM-Newton and Chandra observations can help on answer the question on whether the SNR is or not a plausible counterpart of HESS J1626-490, making this source one of the objectives of this thesis. Results of our X-ray and gamma-ray analysis can be found in Chapter 4.

HESS J1634-472

| Parameter | Value |
|---|---|
| R.A. ............. | $16h34m57.6s$ |
| DEC. ............ | $-47^o16'12''$ |
| Flux (Crab Units) | 0.06 |
| Energy Threshold | 200 GeV |
| Spectral Index ... | $2.38 \pm 0.26$ |
| Extended ........ | Yes |
| Discovery Date .. | 2006.01 |
| Distance ......... | 8.6 kpc |

## 10. HESS J1634-472

The size of the emission region of this unidentified TeV source is 6'.6 $\pm$ 1'.8 [61]. The source was observed with Chandra in the 2-10 keV X-ray band [62]. Two sources has been found to be potential counterpart, one is IGR J16358-4726 located close-by, which belongs to the class of highly absorbed X-ray binary systems [63], and the other is the SNR candidate G337.2+0.1 [64], coincident with AX J1635.9-4719. However the distances of the two objects to HESSJ1634-472 gives as result a correlation unlikely [61].

This source can be a good candidate to make X-ray and Fermi gamma-ray analysis; however this source is not object of study for this work.

## 11. HESS J1641-463

HESS J1641-463

| Parameter | Value |
|---|---|
| R.A. ............. | $16h41m02.1s$ |
| DEC. ............ | $-46^o18'13''$ |
| Flux (Crab Units) | 0.018 |
| Energy Threshold | 640 GeV |
| Spectral Index ... | 2.07 |
| Extended ........ | No |
| Discovery Date .. | 2012.10 |
| Distance ......... | 8.6 kpc |

The discovery of this source was released in [65] using H.E.S.S. telescope, where they showed that exist two potential but weak X-ray counterparts of HESS J1641-463

and they concluded that it is most likely a PWN or a SNR due to spectra, characteristics and the location of the source in the Galactic plane; however, other source types like a binary system cannot be excluded with the data available to the date. The source exhibits one of the hardest spectra observed in VHE $\gamma$-rays.

In [66] Chandra and XMM-Newton observations were used to find possible counterparts. HESS J1641-463 is positionally coincident the SNR G338.5+0.1 and appears a hard spectrum in VHE domain. No obvious X-ray candidate is found as an evident association because of its low brightness and proximity to HESS J1640-465, so the observed feature of HESS J1641-463 is confusing. Due to low statistics, calculating a hardness ratio or spectrum for this source was not possible, and it is unclear whether this may represent a counterpart.

In order to explain the observed VHE gamma-ray spectrum, the most likely scenarios are where protons are accelerated up to hundreds of TeV at the SNR either G338.5+0.1 or G338.3-0.0, and then interact with local gas or nearby massive Molecular Clouds (MCs). Nonetheless, other possible scenarios such as a PWN or a gamma-ray binary cannot be discarded. Moreover, a leptonic emission-based scenario cannot be formally eliminated, although it is severely constrained by the absence of breaks in the gamma-ray spectrum and by the high efficiency required for an accelerator located within the SNR, where strong losses through synchrotron emission are expected [66].

In [67], they analyzed the emission from this source based on the Nonlinear Difusion Shock Acceleration (NLDSA) model considering a scenario proposed by Abramowski et al. (2014 ) [66], where the neighbouring SNR G338.3+0.0 would be a major source of cosmic rays, the escaping protons from the SNR, undergo the Galactic diffusion and collide with the MCs which is positionally coincident with HESS J1641-463, so the TeV emission of the HESS J1641-463 could come from the runaway protons interacting the MC at the region of r > 2R$_f$, the possible X-ray emission of the HESS source is pre-

dicted as being relevant to secondary products of the runaway protons. Future detailed observations will help to a better explanation.

Although the nature of this VHE $\gamma$-ray source is still open, the spectra of this source suggest that the astrophysical objects producing such emission must be capable of accelerating the parental particle population up to energies of at least several hundreds of TeV [68].

Due to its possible explanations and also because we have a lot of X-ray observations, this source is interesting to analyse; moreover, this source is not object of study in this thesis.

## 12. HESS J1702-420

HESS J1702-420

| Parameter | Value |
|---|---|
| R.A. ............. | $17h02m44s$ |
| DEC. ............ | $-42^o00'57''$ |
| Flux (Crab Units) | 0.07 |
| Energy Threshold | 200 GeV |
| Spectral Index ... | 2.07 |
| Extended ........ | Yes |
| Discovery Date .. | 2006.01 |
| Distance ......... | $-$ kpc |

In the H.E.S.S survey of the inner Galaxy [61], they report the detection of the TeV source HESS J1702-420 and discussed possible counterparts. There is a nearby pulsar PSR J1702-4128 (to the north of the VHE emission region) to the source which has enough energy to account for the observed TeV emission by converting toughly 14% of its spin-down luminosity, but an asymmetric PWN would be necessary to be responsible for the emission [61]. However, the association is unlikely since an asymmetric PWN hasn't been detected from this pulsar. Another possible counterpart SNR G344.7-0.1 has a small angular size and is not positionally coincident with the VHE gamma-ray source. Concluding that it was not possible to identify a plausible counterpart of this

source [61].

Another study of the source was carried out in [57], where they talk, about an elongated morphology of the source, there is a emission "tail" extending to positive galactic longitude and latitude statistically significant. They also mention, that the closed-by pulsar PSR J1702-4128 is situated at the edge of the gamma-ray emission and may be a counterpart if it powers the asymmetric PWN. Furthermore, three X-ray binaries that are also nearby the source, but outside the significant emission region.

More recent studies on [69] confirmed that no PWN was found within SNR G344.7-0.1 based on the radio images and the comparison with X-ray and IR observations. Besides, they found that X-ray radiation completely fills in the interior of the SNR, being thermal in nature and originating in heated ejecta and concluded that G344.7-0.1 has evolved within an HI bubble created by the supernova precursor, suggesting that the SNR and its turbulent environment are plausible counterparts of this HESS source.

No evidence to be a PWN, so this is not a good candidate for this thesis work.

## 13. HESS J1708-410

HESS J1708-410

| Parameter | Value |
|-----------|-------|
| R.A. ............. | $17h08m24s$ |
| DEC. ............ | $-41°05'24''$ |
| Flux (Crab Units) | 0.04 |
| Energy Threshold | 200 GeV |
| Spectral Index ... | 2.46 |
| Extended ........ | Yes |
| Discovery Date .. | 2006.01 |
| Distance ......... | $-$ kpc |

This source is located between two sources, a SNR RXJ 1713.7-3946 and HESS J1702-420 [45]. Its detection was reported in [61], and they couldn't find a close-by plausible counterpart. A nearby XMM-Newton observation of the SNR G345.7-0.2 has revealed no X-ray counterpart to the VHE gamma-ray source, but the offset of HESSJ1708-

410 from the centre of the XMM FOV was 15 arc minutes, positioning it close to the edge of the FOV. The source is only marginally extended with respect to the PSF of the instrument. The compact morphology of this HESS source eliminates SNR G345.7-00.2 or closed-by radio hot spots as obvious counterpart candidates. Also, there is an XMM-Newton exposure centered on G345-7-00.2 where no significant emission near the VHE emission is seen. Besides, only a point-like source located over a degree from the HESS source was found on an ASCA exposure.

In [70], they report XMM-Newton observations, archival radio continuum and CO data, and SED modelling of the unidentified HESS source, concluding that the data available did not allow to conclude the nature of the emission of HESS J1708-410. This source is an interesting case due to it has no lower energy candidate counterparts, is rather compact and it has high brightness in gamma-rays which could result in a different type of VHE system than the currently known.

The scenario of ancient PWN has been suggested by [71], and HESS J1708-410 is one of the sources that this scenario is particularly suitable due to the lack of any plausible X-ray counterparts [56].

This source was already studied in detail by [30], [72].

## 14. HESS J1729-345

HESS J1729-345

| Parameter | Value |
|---|---|
| R.A. ............. | $17h29m35s$ |
| DEC. ............ | $-34^o32'22''$ |
| Flux (Crab Units) | – |
| Energy Threshold | – GeV |
| Spectral Index ... | $2.24$ |
| Extended ........ | Yes |
| Discovery Date .. | $2011.05$ |
| Distance ......... | – kpc |

The detection of this source was by HESS collaboration, 2011, where they made

a multi-wavelength analysis to find counterparts [73]. At radio wavelengths, the $\gamma$-ray contours of HESS J1729-345 lie near the HII region G353.381-0.114. Using HI radio recombination line data, the LSR velocity corresponding to this source is either $\sim$54 km/s or $\sim$82 km/s [74]. In the latter case this HII region could be associated with the MC observed around velocities of $\sim$80 km/s. At X-ray energies, no archival dedicated observations were found, and probably due to the high absorption in the line of sight, no emission was detected with ROSAT. However, the multi-wavelength study did not provide a clear understanding of the nature of the source.

In [75] they detected CS(1-0) emission lines towards the HESSJ1731-347/HESSJ1729-345 field corresponding to three Galactic arms: the 3kpc expanding arm, the Norma-Cygnus arm and the Scutum-Crux arm. Also, that they discovered dense molecular gas lies outside the border of HESSJ1729-345, and they found that $\sim$10$^3$ M$_\odot$ is coincident with the gamma-ray emission (at a 4$\sigma$ level).

HESSJ1729-345 is in spatial projection coinciding with known MCs seen through sub-millimetric molecular line emission [73]. The devisable scenario (due to no other local particle accelarators have been found so far) of this emission is in which particles escaping from SNR HESS J1731-347 are penetrating the MCs coincident with HESS J1729-345 and thus lead to enhanced gamma-ray emission, above the emission induced by the sea of cosmic rays that are homogeneously filling the Galaxy [76].

In [76] also demonstrate that, assuming HESS J1731-347 is located at a distance of 3.2 kpc, it is possible that the emission seen in TeV from HESS J1729-345 is produced by cosmic rays escaping from the SNR and illuminating nearby MCs. And considering the HESS source at a distance of $\sim$30 pc away from the center of the SNR, $\gamma$-rays from hadronic interactions from the corresponding MC can very well dominate the TeV emission outside the SNR, when the densest MC region is placed at a larger distance $\sim$100 pc from the SNR.

In [77] were reported no radio emission in spatial coincidence with HESS J1729-345 in the 1390 MHz band, they also found that in the 325 MHz map, the diffuse radio emission towards the west overlaps the region of HESS J1729-345, but the morphology of the emission does not seem to be corresponding to the HESS source, which is $\sim$7 arc min gaussian structure. However, a possible radio counterpart of HESS J1729-345 was found in the 843 MHz Molonglo Galactic Plane Survey (MOST) and the 1.4 GHz Southern Galactic Plane Survey (SGPS) maps. The non-detection in the 1390 MHz Giant Metrewave Radio Telescope (GMRT) map can be due to missing flux. Their GMRT map at 1390 MHz is sensitive to angular scales up to 4 arcmin. Thus significant flux will be missing while imaging a 7 arcmin structure. They obtained a spectral index of 3.0 $\pm$ 0.2, from the 843 MHz MOST map and the 1.4 GHz SGPS map, which is consistent with thermal emission. Which leads to the explanation that the radio emission from this possible counterpart is not synchrotron in nature. The positive spectral index of the possible radio counterpart supports the explanation made by [76], that the VHE emission from the source in a hadronic scenario.

A dense gas clump, traced with emission from the $NH_3$ (1,1) transition seen towards HESS J1729-345, at a velocity of $\sim$16 km/s was reported in [60]. If the molecular clump detected in this study was a counterpart to HESSJ1729-345, the TeV emission could arise from $\pi^0$ decay resulting from p-p collisions between cosmic-rays accelerated in the SNR. The SNR is at a distance of 3.2 kpc (Tian et al. 2008) [78], as is the molecular clump towards HESS J1729-345 traced by $NH_3$ (1,1) in the study. At this distance and with an angular separation between the centre of the SNR and HESS J1729-345 of $\sim$0.5°, the protons would have travelled $\approx$ 30 parsecs. Using the method outlined in the same paper, it would take $\sim$140 yrs for a $10^{14}$ eV proton to diffuse from the SNR (HESS J1731-347) to HESS J1729-345 and $\sim$1400 yrs for a $10^{12}$ eV proton. With a SNR age estimate of 27,000 yrs, protons would have sufficient time to travel and interact with the

molecular gas towards HESS J1729-345 and produce the TeV emission.

Even this source is extremely interesting, our research group already asked X-ray observations in this region; however the observations did not were on time to be analysed in this thesis.

## 15. HESS J1741-302

HESS J1741-303

| Parameter | Value |
|---|---|
| R.A. ............. | $17h41m15.8s$ |
| DEC. ............ | $-30^o22'30.7''$ |
| Flux (Crab Units) | $0.05$ |
| Energy Threshold | 1000 GeV |
| Spectral Index ... | $2.3$ |
| Extended ........ | No |
| Discovery Date .. | $2008.07$ |
| Distance ......... | $-$ kpc |

The source was discovered during a H.E.S.S. survey of the Galactic plane [79], and detected with a significance of $8.1\sigma$ in 143.5 hours of observations [80]. The image of the source at TeV energies appears to exhibit two hot spots, but could not be claimed to be two independent sources due to the poor statistics. Matsumoto et al. (2010) [81] claimed to have detected an X-ray counterpart of one of these sources (J1741A) and a hadronic origin of the TeV $\gamma$-ray emission from this was suggested based on the high TeV to X-ray flux ratio.

There are three pulsars located in the FoV HESS J1741-302. One of them PSR B1737-30 is a powerful source of relativistic particles, and in [81] and in [82] reported no X-ray emission coincident with the location of the pulsar. Due to the large ($\approx 12'$) offset of the pulsar from the peak of the TeV emission of the HESS source, more investigations are required to be able to accept a this source a relic PWN candidate associated to PSR B1737-30.

Another pulsar close to the source is PSR J1741-3016, however it is too old to sustain

a detectable PWN both in X-rays and TeV [80]. The PWN of the third pulsar, PSR J1739-3023 has the pulsar is very offset ($\sim$24' from the HESS source) [83] which makes it a very unlikely counterpart, unless it is a very fast moving pulsar or the ISM density is strongly non-uniform creating the right environment for the host SNR reverse shock to expand asymmetrically.

Hare J. et al. (2016) [83] carried out a multi-wavelength study of this HESS source, where they labeled these hot spots as J1741A and J1741B, respectively. They analysed an observation of Chandra covering the J1741A region were they detected 12 X-ray point sources at a significance level $> 4\sigma$ with no trace of diffuse emission, three of them are found to be AGN, which are unlikely counterparts for the TeV source due to the X-ray flux ratios are 2-3 orders of magnitude smaller than the typical ones responsible for the TeV $\gamma$-rays emission, and an identified star.

On the other hand, seven X-ray point sources were detected in the field of J1741B, one of them was found to be an AGN with low X-ray flux, which makes it an unlikely counterpart to the TeV source, and other two classified sources that appear to be stars. However, the authors of this paper did not yield an obvious candidate for the TeV emission from J1741A/B. Concluding that HESS J1741-302 is not likely an AGN due to the low X-ray to TeV flux ratios, while non-degenerate coronally active stars do not emit TeV $\gamma$-rays, concluding that none of these sources are likely to be associated with the VHE emission of HESS J1741-302.

In the Angüner E. O. et al. (2017) et al. paper [84], they made a multi-wavelength data analysis of three kind of similar sources HESS J1641-463 [66], HESS J1741-302 [79] and HESS J1826-130 [85]. These three sources are tagged as unidentified TeV sources and located near other bright VHE sources, thus their (apparent) emission is contaminated and suffering from source confusion, their best fit positions and extensions are spatially coincident with dense gas regions and none of the sources shows variable

VHE emission, thus indicating possible hadronic VHE emission origin.

For the HESS J1741-302 source, eight MCs were found to be coincident with the best fit position of the source in the FOV [84], this indicating possible hadronic VHE emission origin. However, the studies carried out for this source, not allowed to distinguish whether the scenario for the VHE $\gamma$-ray emission is leptonic or hadronic and they add that for HESS J1741-302, binary scenarios can also be possible.

This source is very close to the Galactic center, making the analysis of the source too complicated since much diffuse emission is expected in X-rays. So, this source was not a good object of study for this thesis.

## 16. Galactic Centre

Galactic Centre

| Parameter | Value |
|---|---|
| R.A. ............. | $17h45m39.6s$ |
| DEC. ............ | $-29^o00'22''$ |
| Flux (Crab Units) | 5 |
| Energy Threshold | $165$ GeV |
| Spectral Index ... | $2.1$ |
| Extended ........ | No |
| Discovery Date .. | $2004.03$ |
| Distance ......... | $-$ kpc |

This region has been very well studied (see e.g. [86], [87]); however, the source and mechanism responsible for the production of HE and VHE gamma radiation in the Galactic center still remain an active topic of discussion. Sgr A* and the PWN G 359.95-0.04 claimed to be able to rule out the nearby SNR Sagittarius A East as a main contributor to the TeV emission.

This is a very complex region with a lot of diffuse emission and a region studied in detail, making this source a not good option to work in this thesis.

## 17. VER J1746-289

VER J1746-289

| Parameter | Value |
| --- | --- |
| R.A. ............. | $17h46m19.71s$ |
| DEC. ............ | $-28^o57'58.4''$ |
| Flux (Crab Units) | 5 |
| Energy Threshold | $-$ GeV |
| Spectral Index ... | $-$ |
| Extended ........ | Yes |
| Discovery Date .. | $2015.07$ |
| Distance ......... | $-$ kpc |

The detection of this extended source was reported on [88] during VERITAS observations of the Galactic Center Ridge from 2010-2014. There is a wealth of non-thermal emission structure that is consistent with the location of VER J1746-289. In the radio band, the Galactic radio arc can be seen adjacent to VER J1746-289. In the gamma-ray regime, an H.E.S.S. excess contours and a Fermi-LAT 3FGL source were found [88]. Both of these give a plausible association to VER J1746-289. The morphology of the VERITAS source is consistent with an association with both the non-thermal X-ray filaments shown and the H.E.S.S. excess in the region. But the peak significance of VER J1746-289 seems to be significantly offset from both these sources.

Whether VER J1746-289 can be associated with the non-thermal X-ray filaments discussed in [89], morphological studies of the TeV emission from the region could help to a better understanding on the nature of particle acceleration in this region, and also the density and distribution of MCs that lies in the inner region of the Galactic Center.

Due to its position in the Galactic center, this source is not good for being studied in this thesis.

HESS J1746-285

| Parameter | Value |
| --- | --- |
| R.A. . . . . . . . . . . . . . | $17h46m23.86s$ |
| DEC. . . . . . . . . . . . . | $-28^o52'33.4''$ |
| Flux (Crab Units) | $-$ |
| Energy Threshold | 350 GeV |
| Spectral Index . . . | 2.19 |
| Extended . . . . . . . . | No |
| Discovery Date . . | 2015.07 |
| Distance . . . . . . . . | $-$ kpc |

## 18. HESS J1746-285

The source was detected for the first time during a study of VHE diffuse emission in the central 200 pc of our galaxy using H.E.S.S. [90]. The source is coincident with an X-ray non thermal filamentary structure G0.13-0.11 associated with a point-source, proposed as a PWN candidate [91].

There is some emission in radio images, but no clear counterpart at these wavelengths. However, HESS J1746-285 and G0.13-0.11, an X-ray non thermal filamentary structure which has been proposed to be a PWN candidate [91], lie between the non-thermal filaments of the Radio Arc and the dense MC G0.13-0.13.

A detailed morphological study of the of the diffuse VHE emission from the GC ridge and a reconstruction of its total spectrum were carried out by the HESS Collaboration using 250 hours of H.E.S.S. data and improved analysis techniques [92], with this research, they could detect HESS J1746-285 in the vicinity of the GC radio arc [93]. The source has no significant extension within uncertainties.

Both MAGIC and VERITAS collaborations have found significant excesses in the vicinity of HESS J1746-285 [94, 95], but their studies do not take into account the contribution of underlying diffuse emission and were based on much lower observation times.

This source is positionally coincident with the confused Fermi-LAT source 3FGL J1746.3-2851c and lies on the edge of the GC radio arc at the centre of the radio arc

bubble, a 9 pc diameter open circular structure visible in mid IR images [96]. This bubble is possibly connected to the Quintuplet cluster (one of the three young massive stellar clusters in the GC region).

The intrinsic spectral index of HESS J1746-285 ($\sim$2.2) and its luminosity ($7\times10^{33}$ erg s$^{-1}$) at the Galactic center distance, twice larger than that of the X-ray nebula, favor a physical association with the PWN. In [92], they showed that the X ray and VHE-ray spectra can be well reproduced by a steady injection of electrons by a pulsar with a spin-down power of a few times $10^{35}$ erg s$^{-1}$ taking into account the radiation energy densities in the vicinity of the Quintuplet cluster. However, the GeV emission is difficult to explain in this scenario, leading them to conclude that the source might be connected to a pulsar itself or the underlying SNR.

This source is interesting due to its possible association with a PWN; however, its position in the Galactic center, makes this source a not good object of study for this thesis.

## 19. MAGIC J1746.4-2853

|  | MAGIC J1746.4-2853 |
| --- | --- |
| Parameter | Value |
| R.A. ............. | $17h46m25s$ |
| DEC. ............ | $-28^o52'55''$ |
| Flux (Crab Units) | $-$ |
| Energy Threshold | $-$ GeV |
| Spectral Index ... | $-$ |
| Extended ........ | No |
| Discovery Date .. | 2016.1 |
| Distance ......... | $-$ kpc |

This source together with the VER J1746-289 and HESS J1746-285 are positionally very close to each other. MAGIC J1746.4-2853 was detected (7.2$\sigma$ local significance lever) during MAGIC observations of Sagittarius A* [97], where they describe it as a significant VHE gamma-ray source close to the Galactic Center Radio Arc. Three sources

are in spatial coincidence with the MAGIC source, the aforementioned VER J1746-289, the EGRET and Fermi sources 3EG J1746-2851 3FGL J1746.3-2851, respectively.

The source has several potential associations. One possible candidate is G0.11-0.11 a giant MC which is located between the Galactic Center Radio Arc and Sgr A*. Gamma-ray emission could be originated during the interaction of the MC with the Galactic Center Radio Arc or from CR interactions inside the dense molecular material in the region. Those CR could be produced in past active episodes of Sgr A* or they could have been accelerated in shocks associated with the several supernova explosions that causes the expansion of the MC [98]. Also, X-ray analysis suggests a possible association with a PWN candidate found in the positional uncertainty of the source [90].

This is not a good source for this thesis due to its position.

## 20. HESS J1804-216

HESS J1804-216

| Parameter | Value |
|---|---|
| R.A. ............. | $18h04m31.2s$ |
| DEC. ............ | $-21^o42'00''$ |
| Flux (Crab Units) | 0.25 |
| Energy Threshold | 200 GeV |
| Spectral Index ... | – |
| Extended ........ | Yes |
| Discovery Date .. | 2005.03 |
| Distance ......... | 6 kpc |

During a scan of the inner part of the Galactic plane with H.E.S.S. from May to July 2004 , the collaboration detected eight unknown VHE sources, with HESS J1804-216 one of them [99]. This source coincides with the southwestern rim of the SNR G8.7-0.1 (W30) of radius 26 arc min. From CO observations [100], the surrounding region is known to be associated with molecular gas where massive star formation is taking place. This SNR could be associated with the nearby (25 arc min), young pulsar PSR J1803-2137 [101]. Furthermore, it is one of three plausible associations with nebulae powered

by sufficiently energetic young pulsars [99].

In summary, this source is more likely to be SNR/MC interaction, disfavouring a PWN association unlikely. So, it is not in the category of object in which we are interested.

## 21. HESS J1808-204

HESS J808-204

| Parameter | Value |
|---|---|
| R.A. . . . . . . . . . . . . . | $18h08m37.3s$ |
| DEC. . . . . . . . . . . . | $-20^o25'36.3''$ |
| Flux (Crab Units) | $-$ |
| Energy Threshold | 1000 GeV |
| Spectral Index . . . | 2.3 |
| Extended . . . . . . . . | Yes |
| Discovery Date . . | 2012.07 |
| Distance . . . . . . . . . | $-$ kpc |

HESS J1808-204 was detected at the TeV band in 2002, it has an extended feature similar in scale and orientation to that of G10.0-0.3, and hence it is argued both sources are associated to each other [102]. Its 0.5-5 TeV energy flux of $1.3 \times 10^{12}$ erg cm$^{-2}$s$^{-1}$ can readily be explained by the intense stellar wind from the luminous blue variable star LBV 1806-20 considering an energetic point of view [102].

The association between Fermi J1808.2-2029 and HESS J1808-204 is suggested by the connection of 300 MeV - 4 TeV spectrum by a power law (cf. Figure 4 of [103]). The gamma-ray spectra of many GeV-detected SNRs have a spectral break at a few GeV [104], in constrast to the power law connection of 300 MeV - 4 TeV spectrum of Fermi J1808.2-2029/HESS J1808-204. Noticeably, the 2.5-500 GeV detection significance at SNR G9.7-0.0 and its OH maser drops to $\lesssim 4.5\sigma$ (cf. Figure 1 of [103]), and the region of HESS J1808-204 is totally inconsistent with that of SNR G9.7-0.0. Therefore, the interacting supernova remnant SNR G9.7-0.0 can only account for the $\gamma$-ray emission from 200 MeV to several GeV, but is unlikely to contribute significantly to the emission at energies above several GeV.

The major mechanism of energy injection for a magnetar is the rapid decay of its strong magnetic field [105]. In the case of SGR 1806-20 (a potentially young age magnetar of 650 yr) its spin-down power is an order of magnitude lower than this threshold, which may account for the PWN-required power for the potential magnertar [103].

Assuming that the loss of magnetic energy of SGR 1806-20 is the major source of emission at energies >4 GeV, this source alone is suffcient to generate a PWN which may account for the flux at energies > 4 GeV. Furthermore, the GeV-TeV spectral connection is also consistent with this PWN scenario. Also, the photon index $2.39 \pm 0.19$ of HESS J1808-204 [102] is consistent with the photon index $2.65 \pm 0.19$ of HESS J1713-381 [106], which is a TeV PWN produced by the magnetar CXOU J171405.7-381031 [107].

However, as the leptonic and/or hadronic nature of HESS J1808-204 is currently unclear. In [103] they speculated the possibility that the emission from several GeV to 4 TeV is leptonic and dominated by a PWN powered by the magnetic-field decay of SGR 1806-20, finding this scenario also consistent with the morphologies observed: The centroid at the $E_{cut,min}$ of 200 MeV is almost equidistant ($\sim 0.19°$) from the SNR G9.7-0.0 center and SGR 1806-20/Cl* 1806-20; in 3-500 GeV, the entire feature is resolved to be two separated clumps (with a $\sim 3\sigma$ significance), whose regions are respectively coincident with HESS J1808-204 and SNR G9.7-0.0

In [108], they made a H.E.S.S. VHE $\gamma$-ray analysis. In this work, they mentioned that the potential counterparts to the VHE gamma-ray source HESSJ1808-204 are the magnetar SGR1806-20, the massive stellar cluster Cl*1806-20, and/or energetic member stars of the cluster, in particular LBV1806-20 and/or the WR stars. However, they could not find a SNR, although there should be to explain SGR 1806-20, or other energetic pulsars in the region of HESS source. But, a prominent multi-wavelength feature is the synchrotron radio nebula G10.0-0.3. Interestingly, HESS J1808-204 is very similar in

intrinsic size to G10.0-0.3 as shown in Figure 5 of the same paper. Based on this, LBV 1806-20 (the possible source of energy for G10.0-0.3) could be considered a plausible counterpart.

The cluster Cl* 1806-20 could easily account for the VHE $\gamma$-ray luminosity of HESS J1808-204 and also of the nearby the 3FGL J1809.2-2016c source due to its likely kinetic stellar wind luminosity of L$_W > 10^{38}$ erg s$^{-1}$. The connection between HESS J1808-204 and the Fermi-LAT GeV source is not so clear given the significant spatial separation between each other and the confused nature of the GeV source.

Given the presence of several molecular clouds along the line of sight towards Cl* 1806-20 [109], a hadronic origin for HESS J1808-204 involving collisions of multi-TeV protons with interstellar gas is well considering. Studies of the molecular cloud morphology are hence needed to ascertain the detailed likelihood of a hadronic origin for the HESSJ1808-204 and the transport properties of particles from the Cl* 1806-20 region. Therefore, the hadronic and/or leptonic origin of the acceleration of the particles responsible for HESS J1804-204 emission, is still unclear. Detailed observations of the molecular gas spatial distribution would be needed for some discrimination of hadronic from leptonic scenarios [109].

The possibility that this source is likely to be identified as a magnetar and the number of X-ray observations, make it a source of our interest and detailed X-ray analysis in this thesis.

## 22. HESS J1809-193

This source together with HESS J1718-385 were found in a search for VHE $\gamma$-ray sources near the pulsars PSR J1718-3825 and PSR J1809-1917 [110]. The nature of HESS J1809-193 is is not yet clear, an ASCA source $G11.0 + 0.0$ [111, 112] was found to be coincident with the peak of the VHE emission, making it a possible X-ray counter-

HESS J1809-193

| Parameter | Value |
| --- | --- |
| R.A. ............. | $18h10m31s$ |
| DEC. ............ | $-19^o18'00''$ |
| Flux (Crab Units) | 0.14 |
| Energy Threshold | 250 GeV |
| Spectral Index ... | 2.2 |
| Extended ........ | Yes |
| Discovery Date .. | 2007.09 |
| Distance ......... | 3.7 kpc |

part of HESS J1809-193. The source distance is estimated to be 2.6 kpc, while PSR J1809-1917 is ∼3.5 kpc away, however, due to large systematic uncertainties of both distance estimates the association between the ASCA source and PSR J1809-1917 is still unclear.

On the other hand, PSR J1809-1917 might also be associated with two SNR candidates (G11.03-0.05 and G11.18+0.11) [112], or with the MAGPIS SNR candidate 10.8750+0.0875 [113], which are all located within the VHE emission region.

The discovery of large scale (∼6') X-ray emission surrounding the compact PWN associated with PSR J1809-1917, and extending toward the VHE centroid [114], strengthens the scenario of a relic PWN crushed by an inhomogeneous SNR interior. The PWN has a cometary morphology and it is attributed to a bow shock created by the pulsar moving supersonically to the southern direction [114]. In summary, several SNR as well as another PWN may contribute to the observed VHE emission.

X-ray studies on HESS J1809-193 were performed using Suzaku in [115], were presence of large scale diffuse emission around the source was found, confirming ASCA results [111]. The extension of the diffuse emission is ∼21' ($3\sigma$ of the gaussian approximation). The diffuse spectrum has the photon index of $\Gamma$ ∼1.7, much harder than those of SNRs with synchrotron X-ray emitting shells ($\Gamma \sim$ 2-3). The hard spectrum could be originated by a PWN [114]. The TeV emission also may have the same origin, because it positionally coincides with the region including the pulsar and the diffuse X-ray emission,

although the center of the TeV emission is offset by $\sim$6' from the pulsar [114].

In [115] they could summarize that that accelerated electrons do not lose their energy when they run from the pulsar to the edge of the emission region because no systematic spatial variation of the photon index was found. To reproduce such phenomena very fast diffusion in an old PWN has to be considered. Assuming that turbulence of the magnetic fields in old PWN systems is smaller than that in young systems, the fast diffusion could be explained.

Multi-wavelength (MW) studies (X-rays, $\gamma$-rays and radio data) were carried out by [116], where they studied the northeast part on HESS J1809-193. In that paper, they said that the spatial morphology and the extent of the TeV emission at the north-east of the HESS source may include XTE J1810-189 position. Nonetheless the X-ray source is an ordinary Type I X-ray burster, and that kind of objects have not been found to produce TeV $\gamma$-rays. The MW classification of the 16 *CXO* sources also did not yield a promising candidate for the putative TeV emission NE of HESS J1809-193. Also, they did an analysis of $\sim$6 years of *Fermi* LAT data and they could not detect the 2FGL 1811.1-1905c source at its catalogued position, but they found tentative evidence of GeV emission at different location (farther from HESS J1809-193 center).

In [117] they pointed that the scenario where the origin of TeV emission from HESS J1809-193 is a PWN, is not completely consistent with the location of the pulsar in the cometary shaped nebula observed in X-rays in the vicinity of PSR J1809-1917, besides that Chandra and Suzaku observations [115] suggest that the pulsar is moving towards the center of the HESS source.

Another work, an analysis of $^{12}$CO in the vicinity of HESS J1809-193 was carried out with the aim of search any other candidate in the FoV that explains the TeV emission. As a result, it was discovered a system of MCs with three main components (called clouds A, B and C) [117] that is well correlated with the TeV source. The total mass and the total

density of the three clouds were calculated and it was found that they satisfied the required amount of target material to explain the high-energy $\gamma$-rays produced by hadrons from HESS J1809-193. The hybrid scenario with contributions from relativistic leptons via IC process in the PSR J1809-1971 operate together with the hadronic process can not be excluded. Additionally, as several bright HII regions lie within the boundary of HESS source, star formation activity can also play a role in the emission.

Many detailed studies have been done on this source, making it not good for the analysis of this thesis.

## 23. HESS J1813-126

HESS J1813-126

| Parameter | Value |
| --- | --- |
| R.A. ............. | $18h13m21.66s$ |
| DEC. ............. | $-12^o41'13.6''$ |
| Flux (Crab Units) | 0.042 |
| Energy Threshold | 200 GeV |
| Spectral Index ... | $-$ |
| Extended ........ | Yes |
| Discovery Date .. | 2015.08 |
| Distance ......... | $-$ kpc |

This source was recently discovered during the HESS Galactic plane survey [118] to be one of few off-plane VHE sources and having an extension of 0.21 $\pm$ 0.032 degrees, and a flux $F(> 1\mathrm{TeV})$ = 1.08 $\pm$ 0.24 $\times$ $10^{-12}$cm$^{-2}$s$^{-1}$.

The intermediate age pulsar PSR J1813-1246 (characteristic age of $\tau_c$=43 kyr) seems coincident with the position of the HESS source, with a spin-down luminosity $\dot{E}$ = 6.2 $\times$ $10^{36}$ erg s$^{-1}$ [39].

X-ray analysis (XMM-Newton and Chandra) were done in this pulsar by [119], which led them to conclude that no extended emission was detected down to a fraction of an arcsec.

This source is of great interest due to its possible explanation as an intermediate/old

pulsar/PWN system, and additionally, long XMM-Newton and Chandra observations have been carried out in the region. All previous, makes this source the third object of study of this thesis work (see Chapter 6)

## 24. HESS J1813-178

HESS J1813-178

| Parameter | Value |
|---|---|
| R.A. . . . . . . . . . . . . . | $18h13m36.0s$ |
| DEC. . . . . . . . . . . . | $-17^o50'24''$ |
| Flux (Crab Units) | 0.06 |
| Energy Threshold | 200 GeV |
| Spectral Index . . . | 2.09 |
| Extended . . . . . . . . | Yes |
| Discovery Date . . | 2005.03 |
| Distance . . . . . . . . . | 4.7 kpc |

HESS J1813-178 was the first source discovered during a survey of the Galactic plane in VHE $\gamma$-rays with H.E.S.S., it has a compact nature with respect to the point-spread function (PSF) of this instrument, it is one of the brightest objects [99], and was also detected by MAGIC [120]

The source has been reported to have positional coincidence with several sources in other wavelengths [**2005astro.ph..5392H**, 121, 122].

The region where HESS J1813-178 was also covered by observations with the VLA (Very Large Array), these showed a faint non-thermal radio source (G12.82-0.02) at the position of HESS J1813-178 [121, 123]. The radio source lies in the projected vicinity of the W 33 region. This region contains ultra-compact HII regions [124] and contains tracers of recent star formation.

With the goal of pinning down the origin of the high-energy X-ray and gamma-ray emission X-ray studies were carried out using XMM-Newton telescope. Due to dense gas in the W 33 region could act as target material for the VHE $\gamma$-ray generation in hadronic interactions, therefore a study of the $^{12}CO(J=1-0)$ distribution performed during

the NANTEN survey of the Galactic plane [125] towards HESS J1813-178 was included in [126].

The most massive molecular cloud in the direction of HESS J1813-178 is in the velocity range 30-40 km/s, see Figure 4 of [126], where can be seen that HESS J1813-178 is located outside of the dense cloud on a scale of $\sim$20 pc and therefore the cloud and the VHE gamma-ray emission are probably unrelated [126].

The radio emission of the source, shows a shell-like structure and the X-ray emission has a compact core with an extended emission towards the north- east, a typical morphology for a PWN (see [127]) [126]. The apparent anti-correlation with the radio shell also suggest a confinement of the X-ray emission within the shell, especially since the tail of the X-ray source extends to the northeast, where a break in the radio shell is present. The non-detection of a pulsar in reasonably deep radio observations may be due to beaming effects. To confirm this scenario, is necessary to find the pulsar within this nebula, either in deep radio or X-ray observations.

The NANTEN data showed a giant MC in the vicinity of HESS J1813-178 in the studies that were performed in [126] that might have played an important role in the evolution of the gamma-ray source. However, G 12.82-0.2 is tentatively established as a composite SNR through its distinct morphology of a central extended non-thermal object within a radio shell. "An upcoming deep Suzaku exposure on HESS J1813-178 will shed more light on the situation in the hard X-ray band and the future GLAST satellite will provide important constraints in the MeV-GeV band" [126].

In [128] they mentioned that HESS J1813-178 is one of the more compact TeV sources to be associated with a SNR. For the majority of the systems, the TeV source is larger than the X-ray PWN. In the case of PSR J1813-1749/HESS J1813-178, the compact TeV source and lack of relative offset can now be explained by its young age, like the Crab and several young pulsars with compact HESS sources that are co-located

with their X-ray PWNe.

Although a possible association of the Fermi source 0FGL J1814.3-1739 with HESS J1813-178/ G12.82-0.02 has been noted by [129], the SNR lies just outside the large, 11' radius 95% confidence Fermi error circle. It leads to conclud that it is not yet possible to identify definitively the GeV emission with the pulsar due to detection of pulsed gamma-rays is required [128].

Too many detailed studies have been done in this source, reason why it is not studied in this thesis.

## 25. 2HWC J1825-134

2HWC J1825-134

| Parameter | Value |
|---|---|
| R.A. ............. | $18h25m50.4s$ |
| DEC. ............ | $-13^o24'00''$ |
| Flux (Crab Units) | $-$ |
| Energy Threshold | 7000 GeV |
| Spectral Index ... | $2.58$ |
| Extended ........ | No |
| Discovery Date .. | $2017.02$ |
| Distance ......... | $-$ kpc |

This HAWC source was first reported as 1HWC J1825-134, it is located between two TeV sources, the PWN HESS J1825-137 and the unidentified HESS J1826-130, at ~0.4 from both. It is connected to the pulsar PSR J1826-1334, 0.°2 away from 2HWC J1825-134, which is the normally considered the offset PWNe [39].

With more HAWC data, future analysis including multiple source fit will help unscramble the different components contributing to 2HWC J1825-134. Also, the TeV binary LS 5039 is 1.4° away from 2HWC J1825-134 and is included in its TS halo in the maps presented in [39].

This source has many options in the identification, making it not a good candidate to develop our analysis.

## 26. HESS J1826-130

HESS J1826-130

| Parameter | Value |
| --- | --- |
| R.A. ............. | $18h26m00.2s$ |
| DEC. ............ | $-13^o2'01.8''$ |
| Flux (Crab Units) | 0.04 |
| Energy Threshold | 1000 GeV |
| Spectral Index ... | 1.6 |
| Extended ........ | No |
| Discovery Date .. | 2015.07 |
| Distance ......... | $-$ kpc |

HESS J1825-137 is one of the brightest and most extensive PWNe detected at TeV energies [130]. The morphology of HESS J1825-137 exhibits a clear asymmetry with respect to PSR J1826-1334, and a MC to the north revealed by [131], with the bulk of the TeV gamma-ray extending up to a degree south of the pulsar. The weak TeV gamma-ray emission component to the north HESS J1826-130 appears to spatially overlap this northern MC, such overlap could result from the interaction of multi-TeV CRs with MCs, and thus raises the possibility of CR acceleration in the vicinity from the progenitor SNR [118].

In the paper [132], where studies using CO and $^{13}$CO survey data (from Nanten telescope) and maps of dense gas tracers with Mopra telescope, it was detected the presence of two SNRs in the region (G018.1 0.1 and G018.6 0.2 [133]). There is also a puslar in the region, PSR J1826-1256 discovered by [134], which is powering the PWN G018.5-0.4 observed at X-rays energies by (Roberts et al. 2007). Therefore, it is possible that TeV emission of HESS J1826-130 could have contributions of each of these sources [132].

HI integrated intensity towards HESSJ1826 130 was also found in [132]. Where they noticed a dip in HI emission towards SNRG018.6-0.2 which did not overlap with the $^{13}$CO(1-0) contour. Furthermore, in the same work, they found that CRs produced by

the P1's progenitor SNR could explain to the TeV gamma-ray emission found in HESS J1826-130. Concluding that the emission of HESS J1826-130 might have a leptonic origin if associated with the PWN G018.5-0.4. If this PWN produces the HESSJ1826-130 emission, the close-by molecular gas may explain the TeV morphology. However, their small angular diameters and their offset position makes the two SNRs unlikely to be associated with HESS J1826-130.

Detailed multi-wavelength studies already exists in this source. excluding this of our analysis.

## 27. HESS J1828-099

HESS J1828-099

| Parameter | Value |
|---|---|
| R.A. .............. | $18h28m58.72s$ |
| DEC. ............. | $-09°59'33.8''$ |
| Flux (Crab Units) | 0.017 |
| Energy Threshold | 200 GeV |
| Spectral Index ... | $-$ |
| Extended ........ | No |
| Discovery Date .. | 2015.07 |
| Distance ......... | $-$ kpc |

This source was recently discovering during the H.E.S.S. Galactic plane survey [118], which appears to be a point-like source and completely dark at lower energies with no apparent associations. There is no evidence for a HE gamma-ray source spatially coincident neither in the 3FGL catalog [135] nor 2FHL catalog (E > 50 GeV) [136].

There were not found X-rays observations on this region, putting this source out of the analysis of this thesis.

## 28. 2HWC J1829+070

This source is found in the point search with a TS value of 25.3. It is located slightly off the Galactic Plane at $b = 8.09°$ , and no associations are found in the catalogs within a

2HWC J1829+070

| Parameter | Value |
| --- | --- |
| R.A. ............. | $18h29m21.6s$ |
| DEC. ............ | $+07^o01'48''$ |
| Flux (Crab Units) | − |
| Energy Threshold | − GeV |
| Spectral Index ... | 2.69 |
| Extended ........ | No |
| Discovery Date .. | 2017.02 |
| Distance ......... | − kpc |

$0.5^\circ$ radius [39].

No X-ray observations were found on this source. Putting away it from our analysis.

## 29. HESS J1832-085

HESS J1832-085

| Parameter | Value |
| --- | --- |
| R.A. ............. | $18h32m31.75s$ |
| DEC. ............ | $-08^o30'35.4''$ |
| Flux (Crab Units) | 0.008 |
| Energy Threshold | 200 GeV |
| Spectral Index ... | − |
| Extended ........ | No |
| Discovery Date .. | 2015.02 |
| Distance ......... | − kpc |

The detection of the source was announced by C. Deil at the 34th ICRC [118].

This is an interesting source because it was newly announced and there is a relatively long XMM-Newton observation of ∼30 ks.

## 30. HESS J1834-087

Too many detailed studies have been done in this source, leaving it out of our studies. (see e.g. )

HESS J1834-087

| Parameter | Value |
|---|---|
| R.A. ............. | $18h34m45.6s$ |
| DEC. ............ | $-08^o45'36''$ |
| Flux (Crab Units) | 0.08 |
| Energy Threshold | 200 GeV |
| Spectral Index ... | − |
| Extended ........ | Yes |
| Discovery Date .. | 2005.03 |
| Distance ......... | 4 kpc |

2HWC J1837-065

| Parameter | Value |
|---|---|
| R.A. ............. | $18h37m26.4s$ |
| DEC. ............ | $-06^o34'48''$ |
| Flux (Crab Units) | − |
| Energy Threshold | 7000 GeV |
| Spectral Index ... | 2.9 |
| Extended ........ | No |
| Discovery Date .. | 2017.02 |
| Distance ......... | − kpc |

## 31. 2HWC J1837-065

2HWC J1837-065 is the principal maximum of an elongated region containing multiple known extended sources [39]. This HAWC source may be associated with the close by HESS J1837-069 (distance of ∼0.4 ). HESS J1837-069 can be considered a candidate PWN [30, 61]. This elongated HAWC region also covers the location of the unidentified source HESS J1841-055, which is a very complex TeV gamma-ray source with many potential counterparts, including the SNRs Kes 73 and G26.6-0.1, three high spindown pulsars: PSR J1841-0524, PSR J1838- 0549, and PSR J1837-0604, and the X-ray binary AX J1841.0-053. ARGO-YBJ also detected emission from this region, ARGO J1839-0627 [137]. This HAWC region will be studied further in a dedicated analysis [39].

This source was already studied in detail in [30].

HESS J1841-055

| Parameter | Value |
| --- | --- |
| R.A. ............. | $18h40m55s$ |
| DEC. ............ | $-05^o33'00''$ |
| Flux (Crab Units) | $-$ |
| Energy Threshold | $540$ GeV |
| Spectral Index ... | $2.4$ |
| Extended ........ | Yes |
| Discovery Date .. | $2007.07$ |
| Distance ......... | $-$ kpc |

## 32. HESS J1841-055

Source that has been studied in much detail. (see e.g. )

## 33. 1HWC J1842-046c

1HWC J1842-046c

| Parameter | Value |
| --- | --- |
| R.A. ............. | $18h42m00s$ |
| DEC. ............ | $-04^o36'00''$ |
| Flux (Crab Units) | $-$ |
| Energy Threshold | $-$ GeV |
| Spectral Index ... | $-$ |
| Extended ........ | No |
| Discovery Date .. | $2015.09$ |
| Distance ......... | $-$ kpc |

A survey of the inner Galaxy region of Galactic longitude between $+15°$ and $+50°$ and latitude between $-4°$ and $+4°$ wascarried out using one-third of the High Altitude Water Cherenkov (HAWC) Observatory operated during its construction phase. To address the ambiguities arising from unresolved sources in the data, a maximum likelihood technique was used to identify point source candidates. Ten sources and candidate sources are identified in this analysis [138].

1HWC J1842-046c has a post-trials significance of $3.4\sigma$ and has no clear gamma-ray association. There is an X-ray source, SNR G 27.4+0.0 (Kes 73), located $\sim 0.4°$ [139] away from this candidate.

## 34. HESS J1843-033

0FGL J1844.1-0335

| Parameter | Value |
|---|---|
| R.A. ............. | $18h44m08.87s$ |
| DEC. ............ | $-03^o35'21.4''$ |
| Flux (Crab Units) | 0.91 |
| Energy Threshold | 3500 GeV |
| Spectral Index ... | $-$ |
| Extended ........ | Yes |
| Discovery Date .. | 2009.04 |
| Distance ......... | $-$ kpc |

Discovered in the same FoV of the young shell-type SNR Kes 75, no obvious coun-terpart for this source was found yet, but a detailed archival search is still ongoing [140].

A likely coincident with the HESS source is ARGO J1841?0332 (even though it is displaced by 0.7°, due to the large systematic pointing error at high zenith angle). It was detected at 3.4 s.d. and was observed at high zenith angles, where large systematic pointing errors are expected. Five other GeV gamma-ray sources surround this region, as shown in Figure 4. of [38]. An observation with improved sensitivity is necessary to clarify this possible TeV emission.

This unidentified source is spatially coincident with 1HWC J1844-031c, which has a post-trials significance of $4.7\sigma$. However, the morphology of the HAWC source appears to extend towards the PWN HESS J1846-029 [138].

Positionally compatible with 2HWC J1844-032 ($\sim 0.3°$). HESS J1843-033 (Hoppe et al. 2008), is a large source with several possible counterparts. A possible X-ray counter-part is AX J1843.8-0352 (G28.60.1), which is an SNR. Also, using Chandra data [141] a source within AX J1843.8-0352 was discovered, CXO J184357-035441, which exhibits a thin thermal spectrum and a jetlike tail. Other possibilities could be AX J1845.0-0258, considered as an anomalous X-ray pulsar (AXP), or SNR G28.8+1.5, whose outer shells may interact with some undiscovered MCs. Further multiwavelength observations are

crucial to identify the origin of the VHE emission [39].

## 35. 0FGL J1844.1-0335

| 0FGL J1844.1-0335 | |
|---|---|
| Parameter | Value |
| R.A. ............. | $18h44m08.87s$ |
| DEC. ............ | $-03^o35'21.4''$ |
| Flux (Crab Units) | 0.91 |
| Energy Threshold | 3500 GeV |
| Spectral Index ... | $-$ |
| Extended ........ | Yes |
| Discovery Date .. | 2009.04 |
| Distance ......... | $-$ kpc |

It has not an associated know source, besides it is an interesting source because it would be extremely bright above 1 TeV if it occurs at a Declination at the edge of Milagro?s sensitivity (if the Milagro observation is real).  Its location is in the region of the Galactic plane surveyed by [61], but was not detected, the reason must be that the source is extended or have a very hard spectrum extending to high energies [142].

## 36. 2HWC J1844-032

| 0FGL J1844.1-0335 | |
|---|---|
| Parameter | Value |
| R.A. ............. | $18h44m08.87s$ |
| DEC. ............ | $-03^o35'21.4''$ |
| Flux (Crab Units) | 0.91 |
| Energy Threshold | 3500 GeV |
| Spectral Index ... | $-$ |
| Extended ........ | Yes |
| Discovery Date .. | 2009.04 |
| Distance ......... | $-$ kpc |

Previously reported by HAWC observatory as 1HWC J1844-031c. This HAWC source has two positionally compatible TeV gamma-ray sources: HESS J1844-030 ($\sim$0.2° distance) and HESS J1843-033 already treated in this work. The PWN Kes 75 is slightly

offset from the HAWC source (0.6° away). The possible associations are: G29.4+0.1, AX J1844.6-0305 (a bright source not yet identified []), and PMN J1844-0306 (complex radio/IR region [143]); therefore SNR or PWN scenarios are considered reasonable.

## 37. HESS J1844-030

Positionally compatible with 2HWC J1844-032 ($\sim$0.2° distance).

In [**HESS_galactic_plane_survey**]: -Several sources lie within the error contours or overlap with this source: SNR (PWN) G29.4+0.1, AX J1844.6-0305 and PMN J1844-0306/GAL 29.39+0.10

The first detailed multiwavelength study of the radio source G29.37+0.1 was reported in [**radio_x-ray_HESS_1844**],which is an as-yet-unclassified object linked to the very-high-energy ?-emitting source HESS J1844-030. The origin of the multiwavelength emission toward G29.37+0.1 has not been clarified so far, leaving open the question about the physical relationship between these sources.

Using observations carried out with the Giant Metrewave Radio Telescope (GMRT), we performed high-quality full- synthesis imaging at 610 MHz of the field containing G29.37+0.1. The obtained data, combined with observations at 1400 MHz from The Multi-Array Galactic Plane Imaging Survey (MAGPIS) were used to investigate in detail the properties of its radio emission. Ad- ditionally, we reprocessed archival data obtained with the XMM-Newton and Chandra observatories in order to get a multiwavelength view of this unusual source.

## 38. 2HWC J1852+013*

It is a new TeV detection by HAWC [39]. There is no known gamma-ray sources close to this location; located 0.6°from its central position is the GeV source 3FGL J1852.8+0158. Do to the source location, there may be a significant contribution of the Galactic diffuse

2HWC J1852+013*

| Parameter | Value |
|---|---|
| R.A. ............. | $18h52m02.4s$ |
| DEC. ............ | $+01^o22'48''$ |
| Flux (Crab Units) | − |
| Energy Threshold | − GeV |
| Spectral Index ... | 2.9 |
| Extended ........ | No |
| Discovery Date .. | 2017.02 |
| Distance ......... | − kpc |

emission to this source.

Multi-wavelength catalog searches reveal several pulsars, several X-ray sources and HII regions in the vicinity of 2HWC J1852+013*. Chandra observations exist of a star cluster and infrared dark cloud IRDC G34.4+0.23 and NaSt1 (WR 122), a Wolf-Rayet binary. The pulsars PSR J1851+0118 and PSR J1850+0124 are located close by [39].

## 39. HESS J1852-000

HESS J1852-000

| Parameter | Value |
|---|---|
| R.A. ............. | $18h52m13s$ |
| DEC. ............ | $-00^o00'23''$ |
| Flux (Crab Units) | − |
| Energy Threshold | − GeV |
| Spectral Index ... | − |
| Extended ........ | Yes |
| Discovery Date .. | 2011.08 |
| Distance ......... | − kpc |

HESS J1852-000 first detection was during deep observations in the region of HESS Galactic Plane Survey ($l = \pm3°$ and $b = \pm80°$), it was found to be an extended VHE gamma-ray source, which lies close to the Galactic Plane. It is close to the SNR Kes 78, so the scenario where all or part of the VHE emission is linked to high-energy CRs produced by Kes 78, however this emission could be due to an undiscovered PWN associated with either the close-by pulsar PSR J1853-0004 or to some other still undetected

pulsar. Furthermore, there is the possibility of source confusion, and that several process are responsible of the TeV emission [144].

## 40. 0FGL J1900.0+0356

0FGL J1900.0+0356

| Parameter | Value |
|---|---|
| R.A. ............. | $19h00m02.21s$ |
| DEC. ............ | $+03^o56'48.3''$ |
| Flux (Crab Units) | $0.43$ |
| Energy Threshold | $3500$ GeV |
| Spectral Index ... | $-$ |
| Extended ........ | No |
| Discovery Date .. | $2009.04$ |
| Distance ......... | $-$ kpc |

This source has no known associations [142].

## 41. 2HWC J1902+048*

2HWC J1902+048*

| Parameter | Value |
|---|---|
| R.A. ............. | $19h02m02.4s$ |
| DEC. ............ | $+04^o51'36''$ |
| Flux (Crab Units) | $-$ |
| Energy Threshold | $-$ GeV |
| Spectral Index ... | $3.22$ |
| Extended ........ | No |
| Discovery Date .. | $2017.02$ |
| Distance ......... | $-$ kpc |

This source appears to be in a confused region, possibly with a large contribution of the Galactic diffuse emission, and will be better disentangled in future analysis with more data. Long Swift observations with a total of 23ks have been performed in the region of 2HWC J1902+048*, due to gamma-ray burst GRB140610. Two Fermi sources within $0.5°$: 1FGL J1902.3+0503c ($0.2°$ away) and 2FGL J1901.1+0427 ($0.5°$ away). Catalog searches reveal several pulsars, several X-ray sources and HII regions in the vicinity of

this HAWC source. The three closest pulsars in the ATNF catalog are: PSR J1901+0459, PSR J1901+0435, and PSR J1901+0510. These pulsars could be powering a PWN which is still undetected because multiwavelength observations has not been carried out for this region [39].

## 42. 1HWC J1904+080c

| 1HWC J1904+080c | |
| --- | --- |
| Parameter | Value |
| R.A. ............. | $19h04m24s$ |
| DEC. ............ | $+08^o00'00''$ |
| Flux (Crab Units) | $-$ |
| Energy Threshold | $-$ GeV |
| Spectral Index ... | $-$ |
| Extended ........ | No |
| Discovery Date .. | 2015.09 |
| Distance ......... | $-$ kpc |

There is currently no previously reported TeV detection near this location. The nearest gamma-ray source is 3FGL J1904.9+0818 at 0.3° away [135]. However, this is a weak detection from the Fermi-LAT 3FGL catalog, at $< 5\sigma$, with no known association.

## 43. 2HWC J1907+084*

| 2HWC J1907+084* | |
| --- | --- |
| Parameter | Value |
| R.A. ............. | $19h07m09.6s$ |
| DEC. ............ | $+08^o30'00''$ |
| Flux (Crab Units) | $-$ |
| Energy Threshold | $-$ GeV |
| Spectral Index ... | 3.25 |
| Extended ........ | No |
| Discovery Date .. | 2017.02 |
| Distance ......... | $-$ kpc |

There may be a large contribution of the Galactic diffuse emission to this source due to the source location and TS value (33.1). Searches in multiwavelength catalog revealed

several pulsars, several X-ray sources, HII regions, and a MC system coincident with or in the vicinity of the VHE emission. The nearest Fermi source is 3FGL J1904.9+0818, located $0.6°$ away from the cen- tral position of 2HWC J1907+084*, and the nearest pulsar from the ATNF catalog is PSR J1908+0839 [39].

## 44. ARGO J1910+0720

ARGO J1910+0720

| Parameter | Value |
|---|---|
| R.A. ............. | $19h10m36s$ |
| DEC. ............ | $+07°21'00''$ |
| Flux (Crab Units) | $-$ |
| Energy Threshold | 3000 GeV |
| Spectral Index ... | $3.25$ |
| Extended ........ | No |
| Discovery Date .. | $2013.11$ |
| Distance ......... | $-$ kpc |

Very close to ARGO J1910+0720, a counterpart in the hard X-ray band, SWIFT J1910.8+0739(4U 1909+07) [145], is located. This ARGO source is detected at only 4.3 s.d., and the nearby source ARGO J1907+0627 could contribute to the observed excess. With the current statistics the possibility of a background fluctuation cannot be excluded. This is an interesting region for follow-up observations with more sensitive instruments [38].

## 45. 2HWC J1914+117*

Given the source location and TS value (33), there may be a large contribution of the Galactic diffuse emission to this source. Several pulsars, several X-ray sources, and HII regions coincident with or in the vicinity of 2HWC J1914+117* were found during multiwavelengths catalog searches. Seven Swift observations have been carried out, but the over-all exposure is too low to identify a possible counterpart. There are no

2HWC J1914+117*

| Parameter | Value |
| --- | --- |
| R.A. ............. | $19h14m43.2s$ |
| DEC. ............ | $+11^o43'12''$ |
| Flux (Crab Units) | – |
| Energy Threshold | – GeV |
| Spectral Index ... | 2.83 |
| Extended ........ | No |
| Discovery Date .. | 2017.02 |
| Distance ......... | – kpc |

possible counterparts in the Fermi-LAT catalogs. There are three pulsars from the ATNF pulsar catalog located in the vicinity of 2HWC J1914+117* are: PSR J1915+1144, PSR J1915+1149, PSR J1913+1145, and PSR B1911+11 [39].

## 46. 2HWC J1921+131

2HWC J1938+238

| Parameter | Value |
| --- | --- |
| R.A. ............. | $19h38m58s$ |
| DEC. ............ | $+23^o48'36''$ |
| Flux (Crab Units) | – |
| Energy Threshold | – GeV |
| Spectral Index ... | 2.96 |
| Extended ........ | No |
| Discovery Date .. | 2017.02 |
| Distance ......... | – kpc |

With a TS value (30.1) there may be a large contribution of the Galactic diffuse emission to this source. Multiwavelength catalog searches re- veal several pulsars, several X-ray sources, and a MC system coincident with or in the vicinity of 2HWC J1921+131. Swift observations exist of the source IGRJ19203+1328. There is no possible counterpart in the Fermi-LAT catalogs within a radius of $1°$ [39].

## 47. 2HWC J1928+177

It is a new TeV source discovered in the point source search with HAWC. It is likely associated with the pulsar PSR J1928+1746 ($0.03°$ away) [39].

## 48. 2HWC J1938+238

2HWC J1938+238

| Parameter | Value |
|---|---|
| R.A. ............. | $19h38m58s$ |
| DEC. ............ | $+23°48'36''$ |
| Flux (Crab Units) | − |
| Energy Threshold | − GeV |
| Spectral Index ... | $2.96$ |
| Extended ........ | No |
| Discovery Date .. | $2017.02$ |
| Distance ......... | − kpc |

2HWC J1938+238 is a new TeV source discovered in the point source search, within the Galactic Plane using HAWC data. There are several optical galaxies, radio galaxies, and an ATNF pulsar within $0.5°$ around the source location. However, none of these sources are known X-ray or gamma-ray sources. The pulsar, PSR J1940+2337, is located $0.4°$ away from 2HWC J1938+238 and is a middle age pulsar (113 kyr) [39].

## 49. 2HWC J1949+244

2HWC J1949+244

| Parameter | Value |
|---|---|
| R.A. ............. | $19h49m40.8s$ |
| DEC. ............ | $+24°27'36''$ |
| Flux (Crab Units) | − |
| Energy Threshold | − GeV |
| Spectral Index ... | $2.38$ |
| Extended ........ | Yes |
| Discovery Date .. | $2017.02$ |
| Distance ......... | − kpc |

The source is discovered in the $1°$ extended search, which, given the low latitude of the source, suggests there can be an important contribution of the Galactic diffuse emission to this source [39]. It is located $0.1°$ away from the unidentified Fermi- LAT source 3FGL J1949.3+2433. The extent of 3FGL J1949.3+2433 is less than $0.1°$ , which is much smaller than the size of the search in which 2HWC J1949+244 was found. The Fermi-LAT measured spectral index of this source is $2.8\pm0.2$, which is slightly softer than the one measured by HAWC. The millisecond pulsar PSR J1950+2414 is also located near 2HWC J1949+244, but this source has not been detected in X-ray or GeV [146].

## 50. 2HWC J1953+294

2HWC J1953+294 is located at $0.2°$ from the PWN DA 495, associated with the SNR G65.7+1.2. It is likely that the 3FGL J1951.6+2926 is associated with the central pulsar of this system [147]. A joint analysis of this region with Fermi-LAT, VERITAS, and HAWC data is ongoing [39].

## 51. 2HWC J1955+285

<div align="center">

2HWC J1953+294

| Parameter | Value |
| --- | --- |
| R.A. ............. | $19h53m02.4s$ |
| DEC. ............ | $+29^o28'48''$ |
| Flux (Crab Units) | − |
| Energy Threshold | − GeV |
| Spectral Index ... | 2.78 |
| Extended ........ | No |
| Discovery Date .. | 2017.02 |
| Distance ......... | − kpc |

</div>

This source may be associated with the shell-type SNR G065.1+00.6, located 0.5° away [39]. The first gamma-ray source in the region of SNR G065.1+00.6 was reported by the COS-B satellite as 2CG 065+00 [148], then confirmed by the EGRET

detection 3EG J1958+2909 [149]. 2HWC J1955+285 is near the Fermi-LAT pulsar PSR J1954+2836. Fermi-LAT also reported a nonobservation of the SNR in [104]. Milagro reported a 4.3$\sigma$ excess at this location [142]. MAGIC reported a non detection and set a flux limit at 2?3% of the Crab Nebula flux at 1 TeV [150].

## 52. 2HWC J2006+341

| 2HWC J2006+341 | |
|---|---|
| Parameter | Value |
| R.A. ............. | $20h06m12s$ |
| DEC. ............ | $+34^o10'48''$ |
| Flux (Crab Units) | $-$ |
| Energy Threshold | $-$ GeV |
| Spectral Index ... | $2.64$ |
| Extended ........ | No |
| Discovery Date .. | $2017.02$ |
| Distance ......... | $-$ kpc |

2HWC J2006+341 is observed with a TS value of 36.9 and is unassociated with any known TeV detections. Milagro has reported a 3.3$\sigma$ excess at this location. The nearest gamma-ray source is 0.7° away, an unidentified Fermi-LAT source 3FGL J2004.4+3338. This source was also reported in the 1FHL catalog but not the 2FHL catalog. Within a 1° radius there are no nearby SNRs from the Manitoba catalog. The nearest pulsar from the ATNF pulsar catalog is PSR J2004+3429, 0.4° away [39].

## Other sources

Sources like HESS J1857+026, MAGIC J1857.6+0297, HESS J1858+020, 2HWC J1902+048*, MGRO J1908+06, VER J2016+371, VER J2019+368, MilagroDiffuse, VER J2019+407, MGRO J2031+41 have been already studied in much detail and are not being described in this thesis due to they are not possible candidates to our analysis.

## 2.3  Concluding Remarks and the Topic of this Thesis

All the information obtained during the review that was described previously in this chapter and once we knew the X-ray observations we have for each source, we could decide the best targets of study:

1. HESS J1626-490

2. HESS J1808-204

3. HESS J1813-126

All three sources were analysed with both Chandra and XMM-Newton. HESS J1626-490 was also analysed using *Fermi*-LAT data. A brief description of the telescopes we used and the analysis that was done on these three sources is described in the next chapters.

# CHAPTER 3

---

## X-RAY AND GAMMA-RAY TELESOCOPES

---

## 3.1 Introduction

Our planet is constantly bombarded with electromagnetic radiation and particles, but the atmosphere protects us from the exposure that can be harmful for life, otherwise life could not exist. The Earth's atmosphere reflects, absorbs and scatters electromagnetic radiation. In portions of the electromagnetic spectrum, significant amounts of energy are not reaching the Earth's surface. In specific most X-ray and gamma-rays are blocked by the atmosphere, making the use of ballons, sounding rockets or satellites necessary to carry the telescopes. So, X-ray and gamma-ray astronomy could not have developed until it was possible to get the detectors above all or most of the atmosphere. Nowadays, we know that gamma-ray studies can been also done from ground-based telescopes, by observing Cherenkov radiation produced when a gamma ray strikes Earth's upper atmosphere.

The first gamma-ray telescope was carried on board the American satellite Explorer 11 in 1961. In the 1960s the Vela defence satellites designed to detect gamma rays from clandestine nuclear testing serendipitously discovered GRBs coming from deep

79

space. However, it was until 1991, NASA launched the Compton Gamma-Ray Observatory (CGRO) a "great observatory" for gamma-ray astronomy, improving the spatial and temporal resolution of gamma-ray observations. Seventeen years later NASA launched the Fermi Gamma-ray Space Telescope. In this thesis we show the Fermi analysis on the HESS J1626-490 unidentified source. This telescope will be described later this Chapter.

On the other hand, the first imaging X-ray telescope was made by a team of scientists in Cambridge, MA. It was flown in a small sounding rocket in 1963 making images of hot spots in the atmosphere of the Sun. Chandra X-ray Observatory (CXO) and XMM-Newton are among the most recent observatories launched in 1999. We used data from both telescopes to study the unidentified VHE sources HESS J1626-490, HESS J1808-204 and HESS J1813-126. More details about X-ray telescopes are given in the next subsections.

In this chapter we will introduce the electronics and technical details about the three telescopes that we used for the data analysis on this thesis. Sect. 3.2 is dedicated to the Chandra Observatory, in sect. 3.3 I present technical details of XMM-Newton satellite and in sec. **??** the *Fermi*-LAT is described.


## 3.2   Chandra Observatory

The Chandra telescope, originally named Advanced X-ray Astrophysics Facility (AXAF) renamed the Chandra X-ray Observatory in honour of the Nobel Laureate Subrahmanyan Chandrasekhar was launched on July 23, 1999 by the Space Shuttle mission STS-93 and deployed by the orbiter Columbia from its payload bay. The observatory was placed in a highly elliptical orbit with a period of 63.5 hours and the first X-rays focussed by the telescope were observed on August 12, 1999. Due to the X-rays are absorbed by the

Earth's atmosphere, it has to orbit it at a high of 139,000 km in the space.

The spacecraft system provides the support structure and environment necessary for the telescope and the science instruments to work as an observatory. In order to provide motion to the observatory, Chandra has two different sets of thrusters: one for propulsion and the other for momentum unloading. The propulsion thrusters were used immediately after launch to help propel Chandra into its final orbit, which is elliptical and very high in altitude. The momentum unloading thrusters are periodically used to apply torques to Chandra and, thereby, lower the accumulated momentum in its reaction wheels, which are used to control Chandra's attitude.

The Chandra Observatory was specially designed to detect X-ray emission from very hot regions of the Universe such as exploded stars, clusters of galaxies, and matter around black holes combining the mirrors of four instruments to capture X-rays from these astronomical sources. The incoming X-rays are focused by the mirrors to a tiny spot (about half as wide as a human hair) on the focal plane, about 30 feet away.

There is a particle detector mounted near the telescope, the Electron, Proton, Helium INstrument (EPHIN) used to monitor the local charged particle environment. Furthermore, there are two X-ray Imaging detectors aboard: the High Resolution Camera (HRC) and Advanced X-ray Imaging Camera (ACIS). There are also two sets of transmission gratings: the Low Energy Transmission Grating (LETG) which is optimized for longer X-ray wavelengths, and the High Energy Transmission Grating (HETG) optimized for the shorter wavelengths [151].

X-ray telescopes must use a different design than optical telescopes. The high-energy photons like to penetrate mirrors instead of reflecting of of them. The mirrors that focus x-rays are made to be almost parallel to the incoming rays. The x-rays will then glance off of the coated (usually with gold or nickel) mirrors. The mirrors used on the Chandra X-ray Observatory are coated with iridium.

The focal plane science instruments, ACIS and HRC, are well matched to capture the sharp images formed by the mirrors and to provide information about the incoming X-rays: their number, position, energy and time of arrival.

For the Chandra data analysis we carried out in during this thesis work, we used observations made with the ACIS instrument, which is described below.

### 3.2.1 ACIS

The Advanced X-ray Imaging Camera is made up of two Charge Coupled Devices (CCDs) arrays, a 4-chip arranged in a 2×2 array (ACIS-I), and 6 arranged in a 1×6 array (ACIS-S) and each CDD covers a field of about 8'×8', either of which may be place at the focus of the telescope. ACIS-I was designed for imaging and spectrometry; ACIS-S can be used both for imaging spectrometry and also for high-resolution spectroscopy in conjunction with the HETG. Moreover, the ACIS instrument has two types of CCDs. ACIS-I is comprised of 4 Front Illuminated (FI) CCDs, and ACIS-S has 4 FI and 2 Back Illuminated (BI), one of which is at the best focus when the array is translated into position in the focal plane (ACIS-I3 and ACIS-S3). The response of the BI devices extends to energies below that accessible to the FI chips, and the energy resolution is mostly independent of position. The FI CCD is more efficient at higher energies, but the energy resolution varies with position due to radiation damage caused by protons reflected though the telescope during radiation-zone passages early in the mission. A schematic drawing of the ACIS focal plane can be seen on Figure 3.1.

The ACIS detector is working in the energy range of 0.3 - 10 keV with a good angular resolution of 1 arcsec. Each CCD is a 1024 × 1026-pixel frame-transfer imager, each of them of 24 micrometers. The FOV of the ACIS intrument is of 17 arcmin × 17 arcmin. A complete description of the ACIS CCDs can be found in [152].

# ACIS FLIGHT FOCAL PLANE
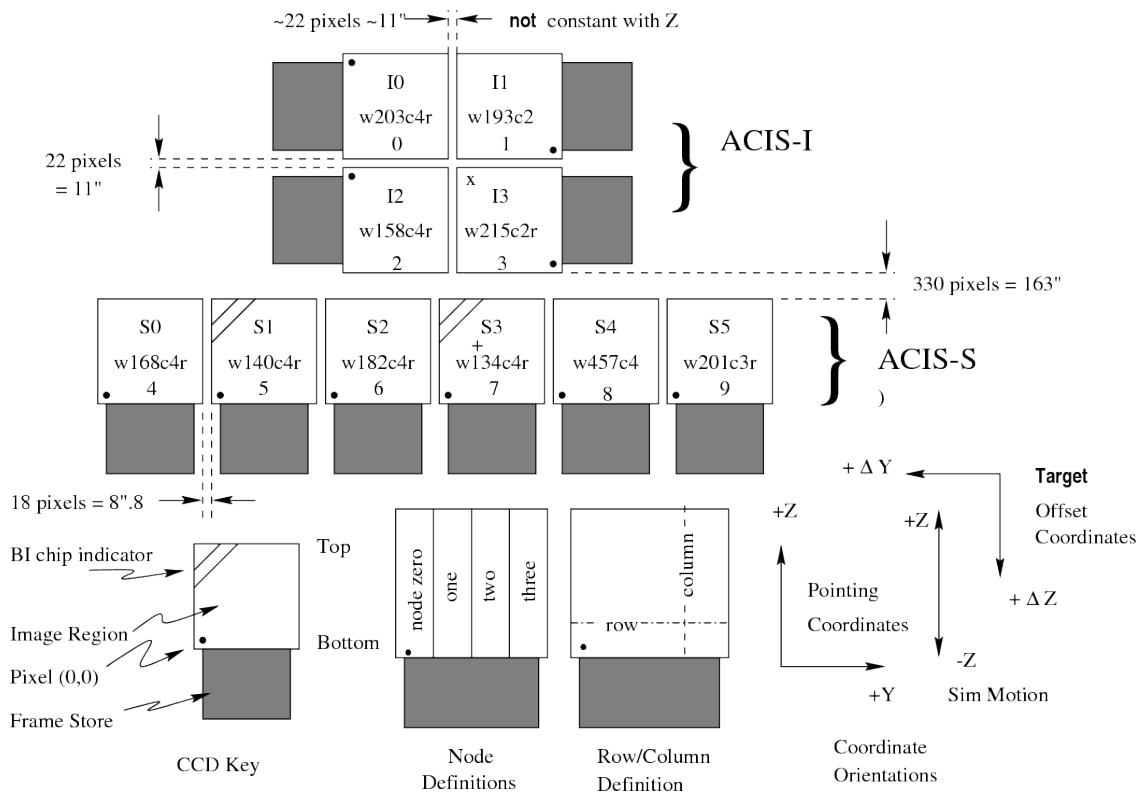


Figure 3.1: A schematic drawing of the ACIS focal plane; insight to the terminology is given in the lower left. Description in the text. Figure from http://cxc.harvard.edu/proposer/POG/html/chap6.html.

Note the aimpoints: on S3 (the '+') and on I3 (the 'x'). Note also the (Y, Z) coordinate system and the target offset convention as well as the SIM motion (+/?Z). This view is along the optical axis, from the sky toward the detectors, (-X). The numerous ways to refer to a particular CCD are indicated: chip letter+number, chip serial number, and ACIS chip number (CCD_ID). As indicated, S3 and S1 are back-illuminated (BI) CCDs, and the rest are front-illuminated (FI) CCDs. The node numbering scheme and the row/column directions are illustrated lower center.

## 3.3 XMM-*Newton* Satellite

XMM-Newton (X-ray Multi-Mirror Mission) is a X-ray space observatory launched by the European Space Agency (ESA) in December, 1999. Named for physicist and astronomer Sir Isaac Newton, the spacecraft is tasked with investigating X-ray sources, performing broad-range spectroscopy and the first simultaneous imaging of objects in both X-ray and optical wavelengths. The instruments on board XMM-Newton are three (EPIC), two Reflection Grating Spectrometers (RGS), and an Optical Monitor. With this observatory we have very sensitive observations due to the large collecting area and ability to make long uninterrupted exposures.

For this analysis we used only the EPIC instrument, which is described in the next subsection.

### 3.3.1 EPIC Cameras from XMM-*Newton*

EPIC consists of two MOS-CCD (Metal Oxide Semi-conductor, MOS1 and MOS2) cameras and a single PN-CCD camera. A charge-coupled device (CCD) is a silicon (Si) device whose operation is based on the spontaneous conversion of light received into electric current that occurs in some materials (Si in this case).

The EPIC cameras observe simultaneously the same field and perform extremely sensitive imaging observations over the telescope's field of view (FOV) of 30 arcmin and in the energy range from 0.15 to 15 keV. Each camera contains a six-position filter wheel, with three types of X-ray transparent filters, a fully open and a fully closed position allowing several modes of data acquisition; these also contains a radioactive source used for internal calibration. The cameras can be independently operated in a variety of modes, depending on the image sensitivity and readout speed needed, as well as the intensity of the target [153].

The MOS cameras (see Figure 3.2 (left)) are installed behind the X-ray telescopes that are equipped with the gratings of the RGS. The gratings divert about half of the telescope incident flux towards the RGS detectors such that about 44% of the original incoming flux reaches the MOS cameras. The X-ray telescope has an unobstructed beam; the EPIC instrument at the focus of this telescope uses PN CCDs and is referred to as the PN camera[1] (see Figure 3.2 (right)). A PN CCD is a special type of charge couple device with high time resolution and quantum efficiency developed for spectroscopy and imaging of X-rays.

All EPIC CCDs operate in photon counting mode with a fixed, mode dependent frame read-out frequency, producing event lists, i.e. tables with one entry line per received event, listing (among others) attributes of the events such as the position at which they were registered, their arrival time and their energies. The two types of EPIC, however, differ in some major aspects. This does not only hold for the geometry of the CCD arrays and the instrument design but also for other properties, like their readout times. The readout of the PN chips is much faster than that of the MOS cameras, because each pixel column has its own readout node. Another important difference is that the MOS chips are FI, while the PN CCDs are BI, which affects the detector quantum efficiencies decisively.

---

[1]http://www.cosmos.esa.int/web/xmm-newton/technical-details-epic
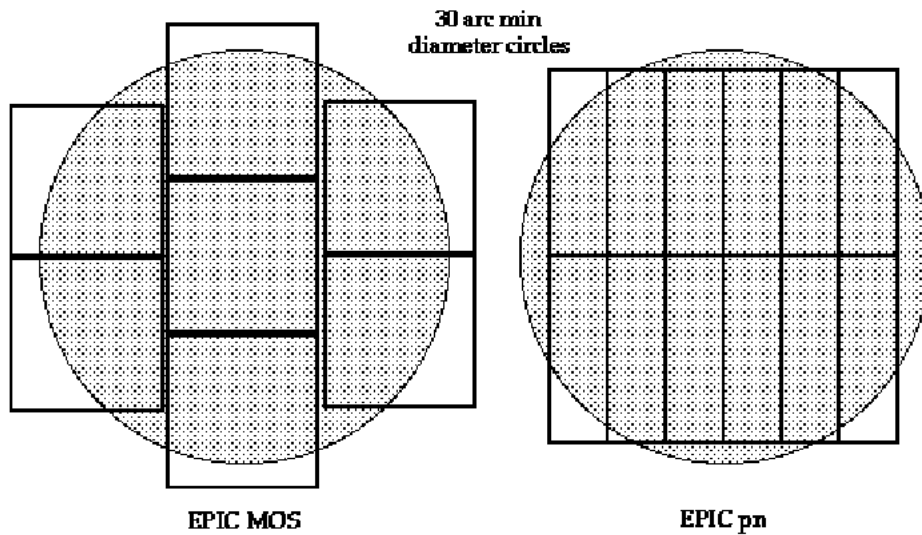
Figure 3.2: A rough sketch of the FOV (30' diameter area, shaded circle) and the of EPIC cameras; MOS (left) and PN (right). [https://heasarc.gsfc.nasa.gov/docs/xmm/uhb/epic.html].

The EPIC cameras allow several modes of data acquisition. The central MOS CCD can be operated separately and the outer ring of 6 CCDs remain in standard imaging mode while. Thus all CCDs are gathering data at all times, independent of the choice of operating mode. The PN camera CCDs can be operated in common modes in all quadrants for Full Frame, Extended Full Frame and Large Window mode, or just with one single CCD for Small Window, Timing and Burst mode, which are listed below:

1. *Full Frame and Extended Full Frame* (PN only): All pixels of all CCDs are read out and thus the full FOV is covered.

2. *Partial Window*: In a Partial Window mode the central CCD of both MOS cameras can be operated in a different mode of science data acquisition, reading out only part of the CCD chip. In the other hand, for PN In Large Window mode only half of the area in all 12 CCDs is read out, whereas in Small Window mode only a part of CCD number 4 is used to collect data. Note that the pn camera in these

windowed modes is operated in such a way that non-read regions of the CCDs are exposed to the sky so that bright sources in these "dark" areas might still affect the observation.

3. *Timming*: For MOS+PN the spatial information is maintained only in one dimension, along the column (RAWX) axis. For pn, the full width of CCD4 is active, whereas for MOS the active area is reduced to about 100 columns around the boresight. Along the row direction (RAWY axis), spatial information is lost due to continuous shifting and collapsing of rows to be read out at high speed. Since the 2 MOS cameras orientations differ by 90 degrees, the "imaging" direction in the 2 MOS are perpendicular to each other. Or else PN only, A special flavour of the Timing mode of the EPIC pn camera is the "Burst" mode, which offers very high time resolution, but has a very low duty cycle of 3%.

For more information about the Science modes of the EPIC cameras visit https://xmm-tools.cosmos.esa.int/external/xmm_user_support/documentation/uhb/epicmode.html.

In Figure 3.2 is shown a rough sketch of both types of EPIC cameras, from which we can see the detector layout and the X-ray telescope FOV. The sensitive area of the detector is about 30 arc min. The two EPIC MOS cameras are rotated $90°$ with respect each other to have a better FOV. The dead spaces between MOS1 and MOS2 are unusable areas due to detector edges (the MOS chips physically overlap each other).

## 3.4 Fermi Satellite

The satellite was launched in 2008 June 11, from Cape Canaveral by a Delta 2920H-10 (also known as a Delta II 'Heavy') into an initial orbit of $\sim$565 km altitude at an 25.6 degree inclination with an eccentricity <0.01. The mission, formerly known as the Gamma-

ray Large Area Space Telescope (GLAST), was named after the physicist Enrico Fermi, who suggested that cosmic rays (particles traveling close to the speed of light) may come from supernova, or violent star explosions. This is an international collaboration from several institutions of the countries Austria, Brazil, France, Germany, Iceland, Italy, Japan, Poland, South Africa, Spain, Sweden and United States of America.

Fermi is performing gamma-ray measurements over the entire sky from low Earth orbit, with a sensitivity factor of 30 or more greater than obtained by earlier gamma-ray missions (EGRET for example), providing improvements in angular resolution, effective area, field-of-view (FOV), energy resolution and range, and time resolution. The field of view is very wide, with useful response out to $\sim 60°$ from the instrument axis, covering about 20% of the sky. The angular resolution depends on the energy of the $\gamma$-ray, its incidence angle, an where it interacts in the Silicon-Strip Detector (SSD). The Point Spread Function (PSF) for on-axis $\gamma$-ray has a 68% containment radius of $\sim 3°$ at 100 MeV ant $0.04°$ for 100 GeV. And the maximun effective is greater than 0.8 m$^2$ at 1 GeV with normal incidence, decreasing at lower and higher energy.

Fermi satellite carries two instruments. The Large Area Telescope (LAT) which detects photons with energy from 20 MeV to > 300 GeV, is the primary instrument and was activated on 2008 June 25. It has a large collecting area, in survey mode it observes the entire sky over two orbits ($\sim$ 3 hours). It is good on study transient phenomena due to its great capability on imaging over a large FOV (sees about 20% of the sky at any given moment), its good time resolution and its low deadtime. Another feature is that LAT provides active background discrimination and rejection against earth albedo gamma rays, the large fluxes of cosmic rays, and trapped radiation that are encountered in orbit.

The orbital period of Fermi is 96.5 minutes, and it is oriented to point the LAT upward at all time, so the earth does not block the view, and has a precession period of 53.4 days. On alternate orbits, Fermi rocks to the left and right, which allows the LAT to cover

more of the sky, thus the whole sky can be surveyed in two orbits. When a strong $\gamma$-ray burst occurs, Fermi points itself at the location of the event for a few hours to collect extra data.

The other instrument is the Fermi Gamma-ray Burst Monitor (GBM), its energy range is 8 keV - 40 MeV. It provides the spectral and temporal context in the classical 10 keV to 25 MeV energy band for Gamma-ray Bursts (GRBs) observed by the LAT, detects and localizes bursts, and alerts the LAT if a burst is in progress. Fermi can autonomously alter its observing plan to observe strong GRBs during and after the low-energy gamma-ray emission, and provides rapid notification to the science community. The primary communication between the spacecraft and the ground is through the Tracking and Data Relay Satellite System (TDRSS), the time and position of the spacecraft are provided by an on-board GPS system.

In this thesis the analysis was carried out using the LAT instrument, which is going to be described in more detail along the next sections.

## 3.4.1   Large Area Telescope: Detector Structure

The principal objective of LAT is to conduct a long term high sensitivity gamma-ray observations of celestial sources. The LAT data are being used for constructing a catalog of celestial gamma-ray sources, resolve the gamma-ray sky of unidentified sources and diffuse emission, spatial mapping and spectra of extended sources such as SNR, MC or PWN, searching for signals from dark matter, measuring the flux and spectrum of cosmic ray electrons, to understand the mechanisms of particle acceleration in AGNs, pulsars, SNRs, among others.

This instrument is composed by four main subsystems that work together to detect gamma-rays and to reject signals generated by cosmic rays, it consists of an array of 16 Tracker modules, 16 Calorimeter modules, a segmented Anti-Coincidence Detector and

a Data Acquisition System Electronics, all contained in 1.8 m square and 0.72 m deep, using only 650 W of electric power. For every gamma-ray photon detected by LAT, 100 000 to one million of cosmic rays has to be filtered. The subsystems are:

- Tracker (TKR): It is the central detector of the LAT, consists of a four-by-four array of tower modules. Each tower module is made of 36 layers of silicon-strip particle tracking detectors interleaved with thin tungsten converter foils, these layers are stacked in 18 mechanical units called trays each equipped with silicon-strip sensors on both sides and readout electronics on the side to minimize dead space between adjacent tower modules [154]. The SSDs in each plane actually consist of two planes of silicon strips, one running in the x and the other in the y direction, these precisely measure the paths of the electron and positron produced from the initial gamma ray in order to reconstruct the direction of the incoming gamma. Multiple scattering of the pair components in the first conversion plane results in an angular deflection that results in a limit to the low angular resolution, especially at low energy. Reconstruction of the interactions from the tracks identify the type of particle as well as its energy and incident direction.

  The pair-conversion signature is also used to help reject the much larger background of cosmic rays. Tungsten tiles are placed at the bottom side of each tray just above the silicon sensors with the aim of place the position sensitive layers as close as possible to the converter and minimize the effect of multiple scattering. A variable thickness of the tungsten layer with thicker tiles at the bottom was placed to achieve a trade-off between resolution and conversion efficiency.

- Calorimeter (CAL): measures the energy of a particle when it is totally absorbed. The LAT Calorimeter is made of cesium iodide (CsI) that produces flashes of light whose intensity is proportional to the energies of the incoming particle. The
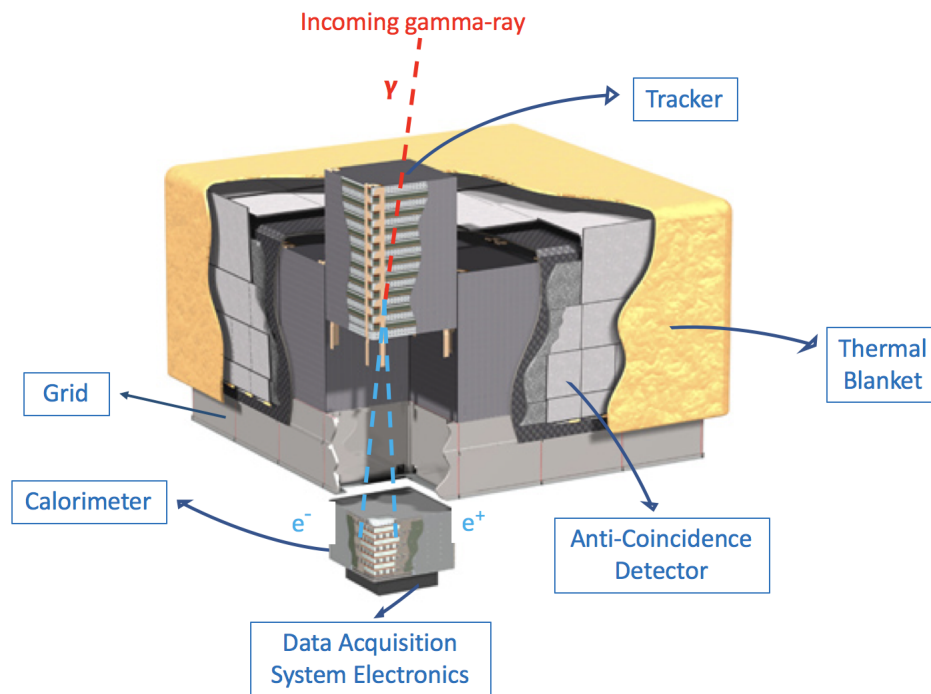
Figure 3.3: Schematic illustration of the Fermi-LAT instrument. Figure adopted from [155]

Calorimeter also helps to reject cosmic rays, since their pattern of energy deposition is different from that of gamma rays. These subsystem modules consists of 96 CsI(Tl) crystals, arranged in a hodoscopic configuration of 8 alternating orthogonal layers of 12 column each, with 1536 crystal total and 8.6 radiation lengths. Each Crystal Detector Element (CDE) is assembled by bonding PIN diodes on each side of a CsI log with the aim that the CDE scintillation light is read out at both ends. The sum of the signals provides the energy deposited in the crystal while the ratio is a measure of the location of the energy deposition along the crystal [154].

• Anti-Coincidence Detector (ACD): is the first line of defence against cosmic rays (mainly protons and electrons) which is 3-5 orders of magnitude more intense that the $\gamma$-rays the LAT should identify. It consists of 1 cm thick scintillator tiles (specially

formulated) that produce flashes of light when hit by charged-particle cosmic rays (but not by gamma rays, which are electrically neutral), with wavelength-shifting fibers spaced 5 mm to bring the signal to the periphery readout electronics . The ACD forms a "hat" that fits over the tracker. The ACS is segmented into 89 tiles and ACD hits far from the reconstructed point of entry are ignored to supress the self-veto induced by back-splash from high-energy particles hitting the calorimeter.

- Data Acquisition System (DAQ): is the brain behind the LAT. It collects information from the Tracker, the Calorimeter, and the ACD and makes the initial distinction between unwanted signals from cosmic rays and real gamma-ray signals in order to reduce the rate of background events that would be relayed to the ground. This system also does an on-board search for gamma-ray bursts. The DAQ processes the event data into a data stream with an average bit rate of 1.2 Mbps for the LAT. The DAQ also performs the command, control, and instrument monitoring; housekeeping, and power switching and consists of specialized electronics and microprocessors. Onboard processing can be modified by uploading new software, if necessary.

### 3.4.2  LAT Detection of $\gamma$-rays and rejection of Cosmic Rays.

When a $\gamma$-ray enters the LAT, it first passes through the ACD without producing a signal. After, the $\gamma$-ray interacts in one of the thin tungsten sheets, coverting the incoming $\gamma$-ray into an electron and positron via pair production (high-energy $\gamma$-rays interact with matter mainly through production of $e^+e^-$ pairs). With this, the Tracker uses the SSDs to measure the paths of the electron and positron to allow the LAT determine the arrival direction of the $\gamma$-ray. Since the $\gamma$-ray energy is larger than the rest mass of the electron and positron, both continue predominantly in the direction of the incident $\gamma$-ray. So the reconstructed direction on the incoming $\gamma$-ray is limited by multiple scatterings of the pair

components the tracker material as well as the spatial resolution of the tracker. Then, these particles enter the Calorimeter, where the measures of the energies of the particles is done, with this we can know the energy of the original $\gamma$-ray. The unwanted cosmic-ray particles produce a signal in the ACD detector telling the DAQ to reject the signal. The detector rejects 99.97% of unwanted signals produced by cosmic rays that enter the LAT. Also, the software in the LAT DAQ also rejects, based on arrival direction, unwanted gamma rays that originate in Earth's atmosphere.

# CHAPTER 4

---

# HESS J1626-490

---

With the objective of helping to demonstrate that unidentified VHE sources are aged PWNe, we carried out detailed X-ray and gamma-ray studies on the TeV unidentified galactic source HESS J1626-490, using observations from the Chandra, XMM-Newton (XMM-N) and Fermi satellite.

In this chapter, first we make a very short description of the HESS source 4.1, after that we show the x-ray data analysis done with this source with both Chandra and XMM-Newton,in specific, the source finding and the spectral analysis of the interesting sources found in the observations (sect. 4.3 and 4.2). The Merging of the X-ray observations is shown in sect. 4.4. In sect. 4.5 the spestral analysis on the selected source of these observations are added. Other section of this chapter (4.6) is dedicated to describe the Fermi data analysis done, for that we obtained the SED of the source. And finally we make the astrophysical discussion of the results that were obtained in sect 4.7.

## 4.1 Introduction

This gamma-ray source was detected by HESS and with no obvious counterpart [57]. It is located at the position R.A. = $16^h26^m04^s$, decl. = 49°05'13", exactly on the Galactic plane, and it was found to have an extension of $0.20 \pm 0.035$ degrees, and its flux (> 1 TeV) is $1.65 \pm 0.33 \times 10^{-12}$ cm$^{-2}$s$^{-1}$, having the 3FGL J1626.2-4911 (Fermi Gamma-ray LAT (FGL)) as an association [8]. The source has an spectrum that follows a power law with a spectral index ($\Gamma$) of $2.47 \pm 0.11$ (see Chapter 2). A gamma-ray and a radio images of this source can be seen in Figure 4.1.
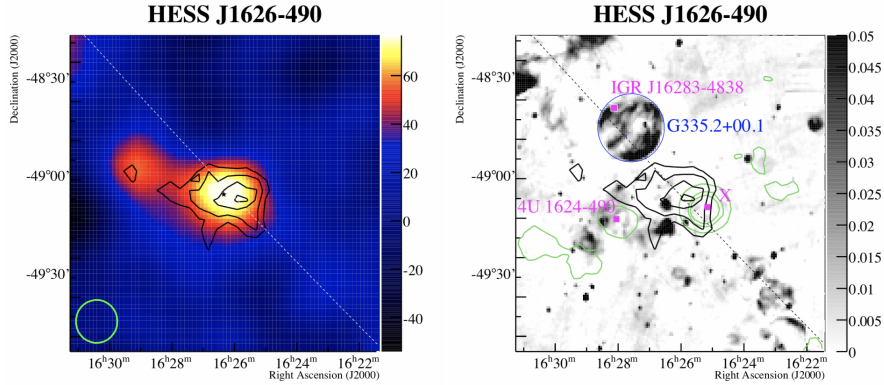


Figure 4.1: *Left:* A VHE gamma-ray excess counts image of HESS J1626-490, the center position was marked with a star. The dashed line represents the Galactic plane. *Right:* A Molonglo radio image in gray scale. An daptively smoothed ROSAT X-ray contours is in green. The significance contours can be seen as the black lines starting at $4\sigma$ in $1\sigma$ steps (in both Left and Right). Also plotted is the SNR G335.2+00.1 (circle marking extent), the HMXB IGR 16283-4838, the LMXB 4U 1624-490, and the unidentified X-ray source 1RXS J162504-490918 (labeled X). Figure from [57].

With the purpose of find counterparts in X-rays, we analyse four X-ray observations that were performed in the region of HESS source, three were performed by XMM-Newton and one with Chandra observatory.

The list of observations that were used for the studies of the HESS source is de-

scribed in Table 4.1, where we can find the ID of the observation, the exact starting date (dd.mm.yy) where the time is also specified, the exposure and the coordinates of the target for each one.

HESS J1626-490

| Mission | Obs ID | Start Date | Exposure | Coordinates |
|---------|--------|------------|----------|-------------|
| XMM-N | 0403280201 | 14.02.07 17:27:08 | 30.6 ks | $16^h26^m19.9^s$, -49°10'20.0" |
| XMM-N | 0403280301 | 14.02.07 16:05:31 | 3.5 ks | $16^h26^m19.9^s$, -49°10'20.0" |
| XMM-N | 0741950101 | 14.08.14 20:16:47 | 37.5 ks | $16^h27^m03.0^s$, -49°12'32.4" |
| Chandra | 13287 | 16.06.12 13:33:57 | 10.0 ks | $16^h27^m03.0^s$, -49°12'32.7" |

Table 4.1: X-ray observations made by XMM-Newton and Chandra telescopes on the position of HESS J1626-490.

## 4.2 XMM-Newton Data Analysis

The data were reprocessed using the XMM-Newton data analysis software Science Analysis System (SAS) version xmmsas 20160201 1833-15.0.0 pipeline, and for their analysis both SAS and FTOOLS software packages were used. The calibration was done using the SAS task `cifbuild`. For using EPIC data, the reprocessing was accomplished by running the default pipeline processing meta tasks `emproc` (for EPIC-MOS) and `epproc` (for EPIC-PN).

The activities carried out so far are:

- Calibration the data.

- Filter event files for flaring particle background.

- Creation of the images using the cleaned event files using ds9.[1]

- Source detection

---
[1] http://ds9.si.edu/site/Home.html

- Identification of X-ray sources using the SIMBAD astronomical database.

- Spectral analysis

### 4.2.1 Observation 0403280201

The observation had an exposure of 30.6 ks and was acquired on February 15, 2007 (ObsID: 0403280201). The three EPIC cameras were operated in Full Frame mode to have the full FOV covered, and a medium filter was also applied for all of them.

The first task to do in the analysis is to calibrate the data. All the XMM-Newton calibration data are organized in a Current Calibration File (CCF) and each constituent of the CCF is uniquely identified by its issue number and date of validity. Access to the CCF is based on the Calibration Index File (CIF), which is generated through the SAS task `cifbuild`. Once we have data already calibrated, at the beginning of the data analysis it is important to filter the event files for flaring particle background.

First, we need to identify intervals of flaring particle background on our instruments: EPIC-MOS and EPIC-PN cameras. To do this, we use the `evselect` task and we obtain the high-energy (>10 keV) light curves (see Figure 4.2), which are dominated by background photons because the influence by X-ray sources is low > 10 keV, therefore the light curves represents flaring events of the background. In the case of the PN detector, the energy range selected for producing the light curves includes events only up to 12 keV and this is because we want to avoid hot pixels being miss-identified as very high energy events.

These plots helped us to delineate a rate (counts/second) to define the "low background" intervals with the purpose of determine where the light curve is low and steady, and finally, to obtain the good time interval of the observation. The rate we used for

EPIC-MOS cameras was 0.35 counts/s as is suggested by the SAS Thread[2]. In the case of the PN detector, the rate we chosen was 1 count/s, to have more or less the same low background interval as with EPIC-MOS.



(a) Light curve above 10 keV from MOS1.

(b) Light curve above 10 keV from MOS2.

(c) Light curve above 12 keV from PN.
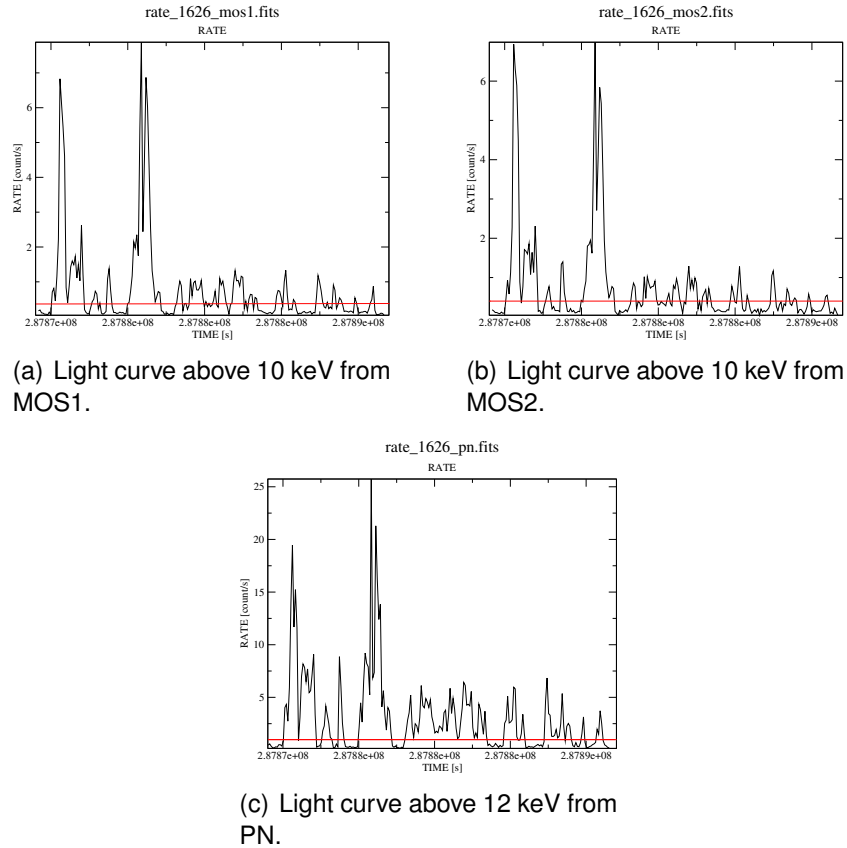
Figure 4.2: Light curves for EPIC-MOS (above 10 keV) and EPIC-PN (above 12 keV) instruments obtained using the ObsID 0403280201 of HESS J1626-490, the red line is to visualize the threshold (count/second) above the low steady background intervals.

After, we can obtain a GTI, as determined by the threshold rate described previously, which is used to create "cleaned" event files (event file with low and steady background). In this case, the obtained GTI for MOS1 was 11.3 ks, for MOS2 was 11.8 ks and for PN, 8.4 ks. In Figure 4.3 the images of the cleaned even files are shown.

Once we have the cleaned images, we added the position of all known pulsars, which

---

[2]http://www.cosmos.esa.int/web/xmm-newton/sas-thread-epic-filterbackground

(a) Cleaned events for MOS1.



(b) Cleaned events for MOS2.



(c) Cleaned events for PN.
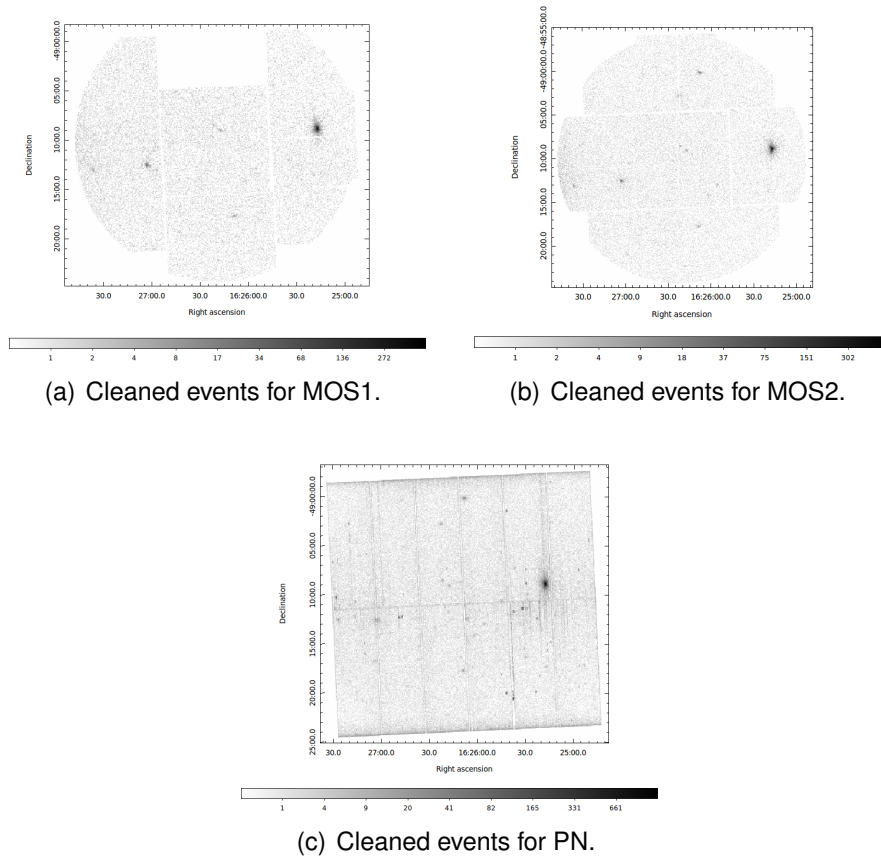
Figure 4.3: Cleaned events images for EPIC MOS and PN EPIC cameras of ObsID 0403280201.

are listed in the Australia Telescope National Facility (ATNF) Pulsar Catalogue [3] [156] within 1 degree of our source HESS J1626-490, just to have a first look, and to know if one of these could be located in the area of the observation, also to know if one of these could be a possible counterpart of the TeV source, the results can be seen on the Figure 4.4.

A source detection was done using the meta-task `edetect_chain`[4], and as a result, nineteen x-ray sources were found in the observation (see Figure 4.5). With the purpose to find reasonable counterparts of the HESS source, a table of the 19 sources (see Ta-

---

[3] http://www.atnf.csiro.au/people/pulsar/psrcat/
[4] https://www.cosmos.esa.int/web/xmm-newton/sas-thread-src-find-stepbystep
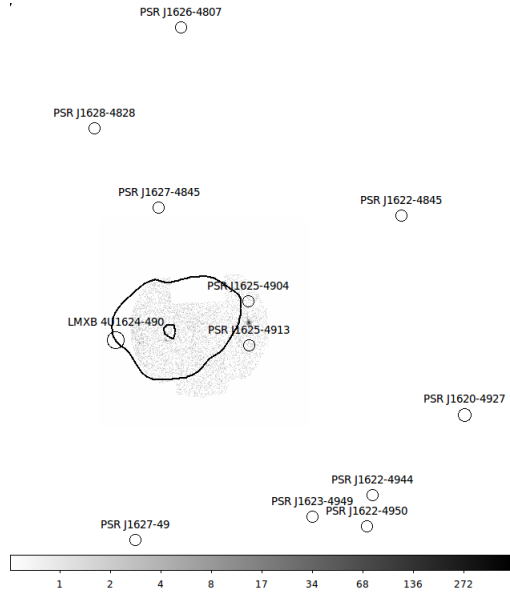
Figure 4.4: The binary star LMXB 4U1624-490, all the pulsars within 1 degree of HESS J1626-490 (black bold contours) and the XMM-Newton observation 0403280201.

bles 4.2.1, 4.2.1) was made with possible counterparts using the astronomical database Set of Identifications, Measurements and Bibliography for Astronomical Data (SIMBAD) [5] which is the biggest astronomical data base currently known. There, we enter the coordinates of the object and we search for sources in a vicinity of 2 arc min. The interesting candidates for TeV emission are the sources that can generate high-energy emission as SNRs, pulsars, X-ray binaries, molecular clouds, FGL objects or even very close stars (counterpart for X-ray emission).

---

[5] http://simbad.u-strasbg.fr/simbad/sim-fcoo
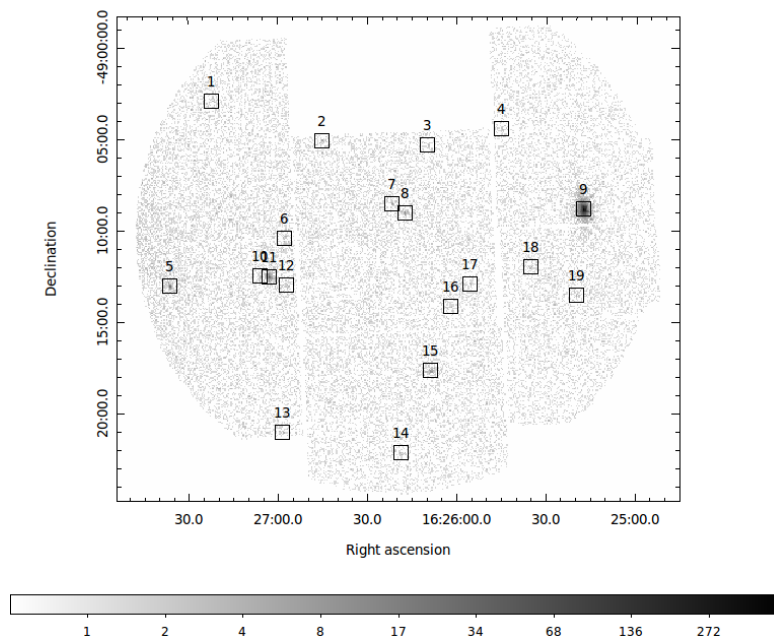
Figure 4.5: Counts map observation obtained for MOS1 using ObsID 0403280201 of HESS J1626-490, the black squares indicate 19 sources detected.

Table 4.2: Possible counterparts of HESS J1626-490 found using MOS1 detector of ObsID 0403280201 (Offset in arcsec), Part 1.

| Src | RA (J2000) | DEC (J2000) | Star | Offset | X-ray source | Offset |
|---|---|---|---|---|---|---|
| 1 | 16:27:21.8 | -49:02:55.7 | SSTGLMC G334.9492-00.0966 | 65.37 | — | — |
| 2 | 16:26:45.12 | -49:05:07.4 | SSTGLMC G334.8495-0.009 | 79.65 | — | — |
| 3 | 16:26:09.6 | -49:05:21.5 | TYC 8320-2072-1 | 54.05 | — | — |
| 4 | 16:25:44.9 | -49:04:28.6 | IRAS 16220-4859 | 102.67 | — | — |
| 5 | 16:27:36.2 | -49:13:03.4 | TYC 8320-1491-1 | 0.86 | — | — |
| 6 | 16:26:57.8 | -49:10:28.2 | — | — | — | — |
| 7 | 16:26:21.6 | -49:08:33.7 | HD 330838 | 16.67 | — | — |
| 8 | 16:26:17.3 | -49:09:03.6 | HD 330838 | 40.49 | — | — |
| 9 | 16:25:17.5 | -49:08:51.7 | HD 147633A | 0.89 | 1RXS J162519.3-49073 | 70.42 |
| 10 | 16:27:05.9 | -49:12:32.8 | TYC 8320-1299-1 | 5.18 | 2XMM J162703.0-491232 | 26.51 |
| 11 | 16:27:02.9 | -49:12:33.5 | TYC 8320-1877-1 | 15.93 | 2XMM J162703.0-491232 | 1.89 |
| 12 | 16:26:56.9 | -49:13:03.0 | TYC 8320-1531-1 | 36.39 | 2XMM J162703.0-491232 | 67.68 |
| 13 | 16:26:58.6 | -49:21:03.6 | EM* VRMF 29 | 86.95 | — | — |
| 14 | 16:26:18.7 | -49:22:13.4 | 2MASS J16261607-4922405 | 37.50 | — | — |

*Continued on next page*

Table 4.2 *Continued from previous page*

| Src | DNe | Offset | HII | Offset | Radio | Offset |
|---|---|---|---|---|---|---|
| 1 | — | — | — | — | AGAL G334.936-00.084 | 38.69 |
| 2 | — | — | — | — | — | — |
| 3 | — | — | — | — | — | — |
| 4 | SDC G334.760+0.108 | 84.45 | — | — | — | — |
| 5 | SDC G334.848-0.198 | 92.50 | — | — | AGAL G334.838-00.201 | 95.88 |
| 6 | — | — | — | — | — | — |
| 7 | G334.778-00.022 | 53.62 | — | — | AGAL G334.784-00.011 | 90.97 |
| 8 | — | — | [JD2012] G334.778-00.022 | 102.76 | — | — |
| 9 | SDC G334.652+0.087 | 58.94 | — | — | — | — |
| 10 | SDC G334.817-0.185 | 118.43 | — | — | AGAL G334.818-00.182 | 107.19 |
| 11 | — | — | — | — | — | — |
| 12 | — | — | — | — | — | — |
| 13 | DOBASHI 6450 | 71.93 | — | — | — | — |
| 14 | SDC G334.585-0.181 | 35.93 | — | — | — | — |

The 2 arcmin region around source number 1 is formed by four sub-millimetric radio sources, being AGAL G334.936-00.084 the closest object found to the source, 38.57 arcsec offset from it. There were found also, two Young Stellar Object Candidate (YSOC): SSTGLMC G334.9492-00.0966 located 65.70 arcsec offset and 2MASS J16272380-4904471 at 113.12 arcsec away; the main sequence star TYC 8320-1835-1, which is 80.32 arcsec from the source, and the Maser MMB G334.935-00.098 at 79.24 arcsec offset. The only object found in the 2 arcmin vicinity of source number 2 in SIMBAD is the YSOC SSTGLMC G334.8495-00.0099, 79.62 arcsec offset. For source number 3, the closest object found was the main sequence star TYC 8320-2072-1, 54.03 arcsec offset, but also the eclipsing binaries UCAC4 205-120748 and UCAC4 205-120673, located 59.55 arcsec and 92.64 arcsec offset, respectively. The bubble source [SPK2012] MWP1G334791+000084 is at 105.25 arcsec from this source. The HESS J1626-490 was found to be at 55.66 arcsec offset from the coordinates given in [57]. Two sources were found in the region of source number 4, the dark nebula SDC G334.760+0.108, located 84.48 arcsec offset and the main sequence star IRAS 16220-4859, 102.60 arcsec away. Source number 5 can be identified to be the spectroscopic binary TYC 8320-1491-1, which was found to be 0.86 arcsec offset. However, in the 2 arcmin region were found five stars which belong to the open cluster NGC 6134 in the constellation Norma, located farther than 39 arcsec offset, as well as two Possible Red Giant Branch star GSC 08320-01103, and TYC 8320-1879-1 located 43.33 arcsec and 93.86 arcsec offset; the YSOC 2MASS J16273180-4912447 at 46.89 arcsec offset; the main sequence star 2MASS J16272878-4913560, at 89.66 arcsec; two dark nebulae SDC G334.848-0.198 and SDC G334.849-0.255, located 92.22 arcsec and 112.10 arcsec offset, respectively; two sub-millimetric radio sources AGAL G334.838-00.201 and AGAL G334.849-00.257, 95.51 arcsec and 118.57 arcsec offset, respectively; the Asymptotic Giant Branch Star Candidate (ABC) 2MASS J16273170-4914319, located 98.91 arcsec;

and the IR source IRAS 16236-4905, at 103.50 arcsec offset. Just an IR object it is found in the neighbourhood of source number 6 MSX6C G334.8128-00.1059, at 49.96 arcsec offset from the source. The closest object to the source number 7 is the main sequence star HD 330838, 16.67 arcsec offset. But there were found also the HII region[JD2012] G334.778-00.022, at 53.61 arcsec; [SPK2012] MWP1G334779-000253 a buble source, 55.43 arcsec offset from the source. Also, two IR sources IRAS 16226-4900, at 76.22 arcsec and IRAS 16225-4903 at 103.73 arcsec offset, and two radio sources AGAL G334.784-00.011 and AGAL G334.796-00.022, 90.97 and 117.36 arcsec offset from the source, respectively. Around source number 8, there were found the star HD 330838, but 40.30 arcsec offset, the IR source IRAS 16225-4903 located 67.79 arcsec offset, the HII region [JD2012] G334.778-00.022 at 102.63 arcsec, the bubble source [SPK2012] MWP1G334779-000253 at 106.46 arcsec, and the carbon star [W71b] 119-02, 109.36 arcsec offset. Source number 9 can be identified to be the visual binary HD 147633 [157], which is located 0.89 arcsec offset in SIMBAD, the proper motion star HD 147633A is located 0.90 arcsec offset and HD 147633B at 3.17 arcsec offset. Other proper motion star was found in the vicinity UCAC2 10696544, 19.70 arcsec offset. Theres is also, the dark nebula SDC G334.652+0.087, 58.94 arcsec offset, the X-ray source 1RXS J162519.3-490743 located 70.45 arcsec offset, the main sequence star TYC 8320-1042-1 at 102.69 arcsec and the YSOC 2MASS J16252857-4908491, 108.73 arcsec offset. In the case of source number 10, it can be identified as the main sequence star TYC 8320-1299-1, which was found to be 5.18 arcsec offset in SIMBAD, the X-ray source 2XMM J162703.0-491232, located 26.51 arcsec offset, as well as two main sequence stars TYC 8320-1877-1 and TYC 8320-1531-1, at 45.10 and 61.15 arcsec offset, respectively; the sub-millimetric radio source AGAL G334.818-00.182 was found 105.82 arcsec offset and the dark nebula SDC G334.817-0.185 at 117.07 arcsec. Source number 11 can be identified as the X-ray source 2XMM J162703.0-491232,

which was found to be located 1.89 arcsec offset, but other three main sequence stars were also found in the vicinity. The closest object found to source number 12 was the main sequence star TYC 8320-1531-1, located 36.19 arcsec offset. The X-ray source 2XMM J162703.0-491232 is located 67.68 arcsec offset and other three TYC stars were also found. The dark nebula DOBASHI 6450 was the closest object found for source 13, at 71.93 arcsec offset. The emission line star EM* VRMF 29 was also in the 2 arcmin region, 86.95 arcsec offset. For source 14, the closest object found in SIMBAD was the dark nebula SDC G334.585-0.181 which is located 35.93 arcsec offset. Furthermore, the YSOCs 2MASS J16261607-4922405 and 2MASS J16261543-4921085 were also found in the locality, 37.39 and 72.25 arcsec offset, respectively, as well as two main sequence stars and the bubbles source [SPK2012] MWP1G334620-001800S located 90.91 arcsec from the source.

Table 4.3: Possible counterparts of HESS J1626-490 found using MOS1 detector of ObsID 0403280201 (Offset in arcsec), Part 2.

| Src | RA (J2000) | DEC (J2000) | Star | Offset | X | Offset |
| --- | --- | --- | --- | --- | --- | --- |
| 15 | 16:26:08.6 | -49:17:43.4 | — | — | — | — |
| 16 | 16:26:01.9 | -49:14:11.8 | SSTGLMC G334.6699-00.0277 | 99.10 | — | — |
| 17 | 16:25:55.4 | -49:12:57.6 | SSTGLMC G334.6699-00.0277 | 31.45 | EXMS B1622-490 | 113.98 |
| 18 | 16:25:35.0 | -49:12:01.4 | — | — | — | — |
| 19 | 16:25:19.7 | -49:13:34.0 | 2MASS J16251207-4912329 | 96.32 | — | — |

| Src | HII | Distance | FGL | Distance | MC | Distance |
| --- | --- | --- | --- | --- | --- | --- |
| 15 | [NNM2015] 3 | 109.33 | 1FGL J1626.0-4917c | 78.95 | [RC2004] G334.6-0.1-112.4 | 86.12 |
| 16 | — | — | — | — | — | — |
| 17 | — | — | — | — | — | — |
| 18 | — | — | — | — | — | — |
| 19 | — | — | — | — | — | — |

*Continued on next page*

Table 4.3 Continued from previous page

| Src | DNe | Offset | Pulsar | Offset | Radio | Offset |
|---|---|---|---|---|---|---|
| 15SDC G334.639-0.078 | 109.26 | | – | – | AGAL G334.661-00.097 | 118.93 |
| 16SDC G334.639-0.078 | 114.85 | | – | – | AGAL G334.639-00.032 | 104.22 |
| 17SDC G334.659-0.001 | 89.52 | | – | – | AGAL G334.639-00.032 | 83.58 |
| 18SDC G334.637+0.028 | 20.16 | | – | – | AGAL G334.662+00.026 | 101.51 |
| 19SDC G334.565+0.023 | 88.77 | | PSR J1625-4913 | 87.76 | – | – |

In the 2 arcmin region around source number 15 there were found: the gamma-ray object 1FGL J1626.0-4917c, located 78.95 arcsec offset; seven molecular clouds that were reported in the catalog [RC2004] (Russeil+Castets, 2004), all of them to be 86.12 arcsec offset from the source; the dark nebula SDC G334.639-0.078, at 109.26 arcsec; the HII region [NNM2015] 3, located 109.33 arcsec offset and the sub-millimetric radio object AGAL G334.661-00.097, 118.93 arcsec offset. Around source number 16 there were found two YSOC: SSTGLMC G334.6699-00.0277 to be 99.10 arcsec and SSTGLMC G334.6365-00.0327, 108.17 arcsec offset; the sub-millimetric radio source AGAL G334.639-00.032 at 104.22 arcsec offset, and the dark nebula SDC G334.639-0.078, 115.84 arcsec offset. The closest object for source 17 is the YSOC SSTGLMC G334.6699-00.0277, located 31.45 arcsec offset, but there were found other two objects of this nature in the two arcmin vicinity, as well as two maser objects Caswell CH3OH 334.635-00.015 at 42.59 arcsec offset, and MMB G334.635-00.015 at 103.98 arcsec offset; the sub-millimetric radio source AGAL G334.639-00.032 at 83.58 arcsec; the dark nebula SDC G334.659-0.001 at 89.52 arcsec; two IR sources IRAS 16220-4906 at 96.77 arcsec, and SSTGLMC G334.6350-00.0146, 103.17 arcsec offset, and the X-ray source EXMS B1622-490, 113.98 arcsec offset. In the 2 arcmin vicinity of source 18, six dark nebulae sources were found, being SDC G334.637+0.028 the closest object to the source at 20.16 arcsec offset. There were found also one sub-millimetric radio source AGAL G334.662+00.026 at 101.51 arcsec and the asymptotic giant branch star candidate 2MASS J16254128-4910213 located 117.39 arcsec offset. The pulsar PSR J1625-4913 was the closest object found to source 19, 87.76 arcsec offset, in the same region there were found also two dark nebulae SDC G334.565+0.023 and SDC G334.611+0.026, located 88.77 arcsec and 99.82 arcsec, respectively and the asymptotic giant branch star candidate 2MASS J16251207-4912329 at 96.32 arcsec offset.

As can be seen on Figure 4.5, the brightest source is the number 9. To have a first

look of which astrophysical source is, we checked on SIMBAD, and the result was 8 possible sources, however, the closest to it was a double star HD 147633, 2.86 arcsec offset.

To identify the sources with mainly non thermal emission that could be interesting candidates for the TeV emission from the HESS source, we create an image of energy range 2.5 - 12 keV and then we performed the source detection tool. The result was that 9 sources remaining and two 'new' were detected (H1 and H2, see Figure 4.6), more details are given in Table 4.4
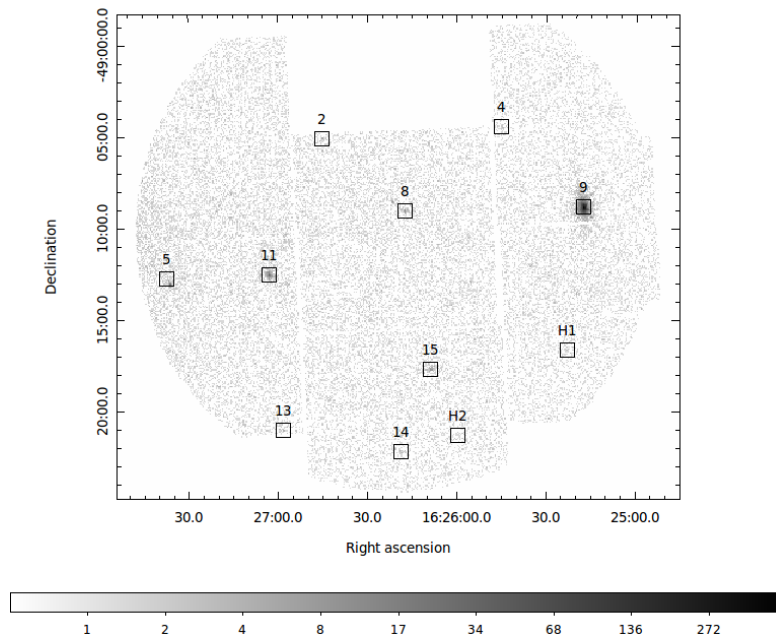


Figure 4.6: Counts map observation of HESS J1626-490 made with MOS1, using a cut in the energy range from 2.5-12 keV, the black squares indicate 11 sources detected by the EPIC source detection tool.

The Table with the coordinates, the possible counterpart, the distance to the source (arcsec), and the flux of the sources dominated by non-thermal emission can bee seen in Table 4.4. Here, the flux was obtained from the FITS file `emllist` which was a result of

Table 4.4: Non-thermal emission sources detected using MOS1 from ObsID 0403280201 of HESS J1626-490. The flux values are in erg cm$^{-2}$s$^{-1}$.

| Src | RA J2000 | DEC J2000 | Possible counterpart | Offset arcsec | Flux E-14 |
|-----|----------|-----------|----------------------|---------------|-----------|
| 2 | 16:26:45.1 | -49:05:07.4 | SSTGLMC G334.8495-0.009 | 79.65 | 2.05 |
| 4 | 16:25:44.9 | -49:04:28.6 | SDC G334.760+0.108 | 84.45 | 1.90 |
| 5 | 16:27:36.2 | -49:13:03.4 | TYC 8320-1491-1 | 0.86 | 3.26 |
| 8 | 16:26:17.3 | -49:09:03.6 | HD 330838 | 40.52 | 4.04 |
| 9 | 16:25:17.5 | -49:08:51.7 | HD 147633 | 0.89 | 38.03 |
| 11 | 16:27:02.9 | -49:12:33.5 | 2XMM J162703.0-491232 | 1.89 | 26.48 |
| 13 | 16:26:58.6 | -49:21:03.6 | DOBASHI 6450 | 71.93 | 4.10 |
| 14 | 16:26:18.7 | -49:22:13.4 | SDC G334.585-0.181 | 35.93 | 3.20 |
| 15 | 16:26:08.6 | -49:17:43.4 | 1FGL J1626.0-4917c | 78.95 | 1.94 |
| H1 | 16:25:22.6 | -49:16:40.1 | AGAL G334.551-00.006 | 13.83 | 3.00 |
| H2 | 16:25:59.5 | -49:21:23.0 | AGAL G334.554-00.144 | 68.23 | 2.41 |

applying the SAS `edetect_chain`. Looking with the positions of the sources in SIMBAD, we can say that: The possible counterpart of source 2 is a YSOC, it is 79.65 arcsec offset from the source, and it is not a plausible counterpart for the TeV source. For source number 4, we have a dark nebula at 84.45 arcsec offset from the source. Source number 5 can be identified to be the spectroscopic binary TYC 8320-1491-1 which is at just 0.86 away from the coordinates we obtained. In the case of source number 8, the main sequence star HD 330838 was found to be located 50.52 arcsec offset. In the 2 arcmin region we also have an IR source (IRAS 16225-4903) at 67.79 arcsec away; the HII region [JD2012] G334.778-00.022 is 102.76 arcsec away; the bubble source [SPK2012] MWP1G334779-000253 is at 106.46 arcsec offset, and the Carbon star [W71b] 119-02 is 109.36 arsec offset. Here I have questions, first, the source that we are seeing with the telescope is very likely the close star, but could it be producing hard X-rays? Could be this star a counterpart of the TeV emission? Maybe it is a result of the interaction with the HII region that is over there? For source number 9, we have the known triple system HD 147633 [158] in this position. The AB binary system contains a double-lined spectroscopic binary which are high proper-motion stars [159]. 19.51 arcsec offset there is

also another high proper-motion star UCAC2 10696544; and a Dark Nebula at 58.94 arcsec known as SDC G334.652+0.087. The source is at also coincident with the ROSAT source 1RXS J162519.3-490743 (described in 2) which was found to be 70.42 arcsec offset. As well as other two stars TYC 8320-1042-1 and 2MASS J16252857-4908491 at more than 100 arcsec offset. The source 11 is very likely to be the X-ray source 2XMM J162703.0-491232, which was found to be at just 1.89 arcsec offset. According to SIMBAD, there are also other 3 stars coincidents with the source, but farther than 30 arcsec. Could the X-ray source be an explanation for the TeV emission? The Dark nebula source DOBASHI 6450 was the closest source found by SIMBAD (71.93 arcsec offset) from source 13. In the 2 arcmin region there is also a emission-line star EM* VRMF 29 but 86.95 arcsec offset. The source 14 has two dark nebulae in the vicinity, SDC G334.585-0.181 and SDC G334.584-0.175 which are 35.93 and 37.72 arcsec offset from the source, respectively. But also two YSOC 2MASS J16261607-4922405 and 2MASS J16261543-4921085 at 37.50 and 72.37 arcsec away, respectively, as well as two main sequence stars and one bubble source ([SPK2012] MWP1G334620-001800S, 90.91 arcsec away). The gamma-ray source 1FGL J1626.0-4917c is located 78.95 arcsec offset from source 15, which was the closest object found. This object could be a counterpart for the TeV emission of the HESS source -Should I search for its extension? There are also, seven molecular clouds in the 2 arcmin region, one dark nebula, one HII region and a sub-millimetric radio source (AGAL G334.661-00.097, 118.93 arcsec offset). Five objects were found in the 2 arcmin vicinity of the source H1, the closest is the sub-millimetric radio source AGAL G334.551-00.006 at 13.83 arcsec offet, two dark nebulae were also found: SDC G334.546-0.002 at 30.64 arcsec offset, and SDC G334.565+0.023 farther, at 109.37 arcsec away from the source. The asymptotic giant branch star candidate 2MASS J16252980-4915362 was found to be 95.37 arcsec offset and there is a main sequence star HD 147634 at 115.42 arcsec. In the case of source

H2, the closest found is the radio source AGAL G334.554-00.144 located 68.23 arcsec away. Moreover, the YSOC SSTGLMC G334.5510-00.1455 is at 80.46 arcsec, and the main sequence star HD 147727 at 102.81 arcsec offset.

In summary, for this observation we could identify source number 5 to be the spectroscopic binary TYC 8320-1491-1; source number 9 the known triple system HD 147633, source 11 to be the X-ray source 2XMM J162703.0-491232. Sources number 9 and 11 were be studied in detail by spectral analysis in section . Source H1 is very likely to be the sub-millimetric radio source AGAL G334.551-00.006 which was found 13.83 arcsec offset. The gamma-ray source 1FGL J1626.0-4917c could explain part of the VHE emission from HESS J1626-490.

## 4.2.2   Observation 0403280301

This short observation was acquired on February 14, 2007 with an ObsID 0403280301. Its duration scheduled to be 3.5 ks, however, the performed duration was longer, 11.3 ks for the MOS cameras and 8 ks for PN (see [6]).

Using the `evselect` task for filter the events file, the rate used for all three EPIC cameras was as suggested by SAS Thread. As can be seen on Figure 4.7. The observation was affected by very high level of radiation, and the telescope was closed to protect the instruments. Therefore the light curve falls and reach a level close to 0.



(a) Light curve above 10 keV from MOS1.

(b) Light curve above 10 keV from MOS2.

(c) Light curve above 12 keV from PN.
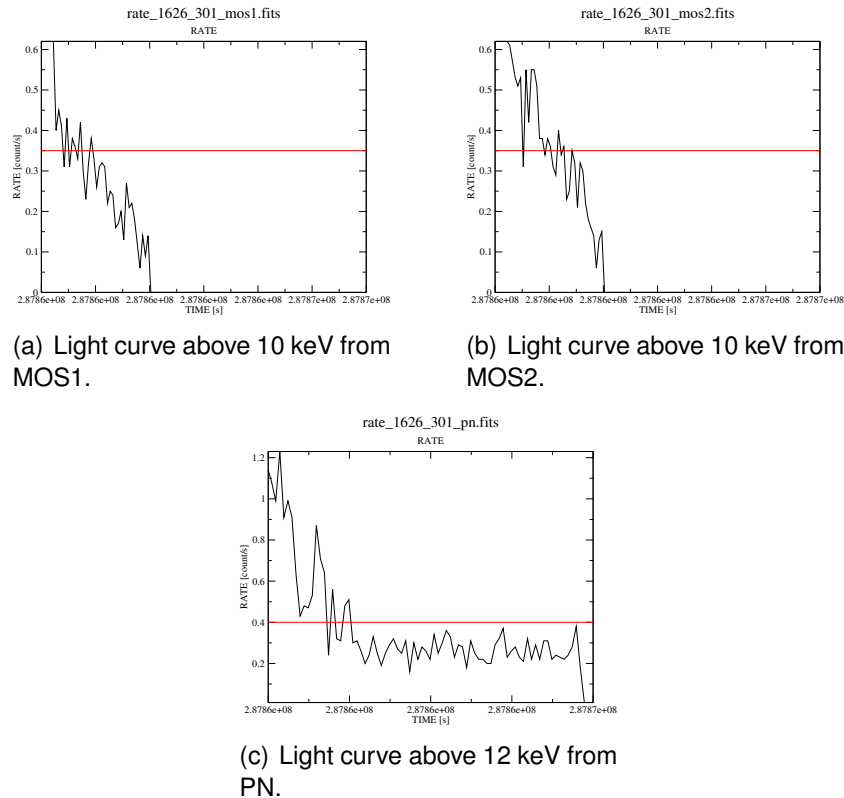
Figure 4.7: Light curves for EPIC-MOS above 10 keV and EPIC-PN above 12 keV instruments obtained using the ObsID 0403280301 of HESS J1626-490, the red line is to visualize the threshold (count/second) above the low steady background intervals.

---

[6]http://xmm2.esac.esa.int/external/xmm_obs_info/obs_view_frame.shtml

Since during this observation a very high level of radiation appeared, the telescope was closed to protect the instruments. Therefore, we cannot perform a data analysis on this data set. Fortunately, we have other two good observations for execute a good analysis of the region.

## 4.2.3   Observation 0741950101

The target of this observation was HESS J1626-490, and was carried out on August 14, 2014 with an exposure of 37.5 ks (ObsID 0741950101). The EPIC-MOS cameras were operated in Large Window mode (an area of 300 x 300 pixels is active), while the PN camera was operated in Small Window mode. A medium filter was used for all three EPIC instruments.

In all the three cases (see Figure 4.8), it was not necessary to establish a rate because the counts per second in each light curve was lower than the value suggested to be particle background.



(a) Light curve above 10 keV from MOS1.

(b) Light curve above 10 keV from MOS2.

(c) Light curve above 12 keV from PN.
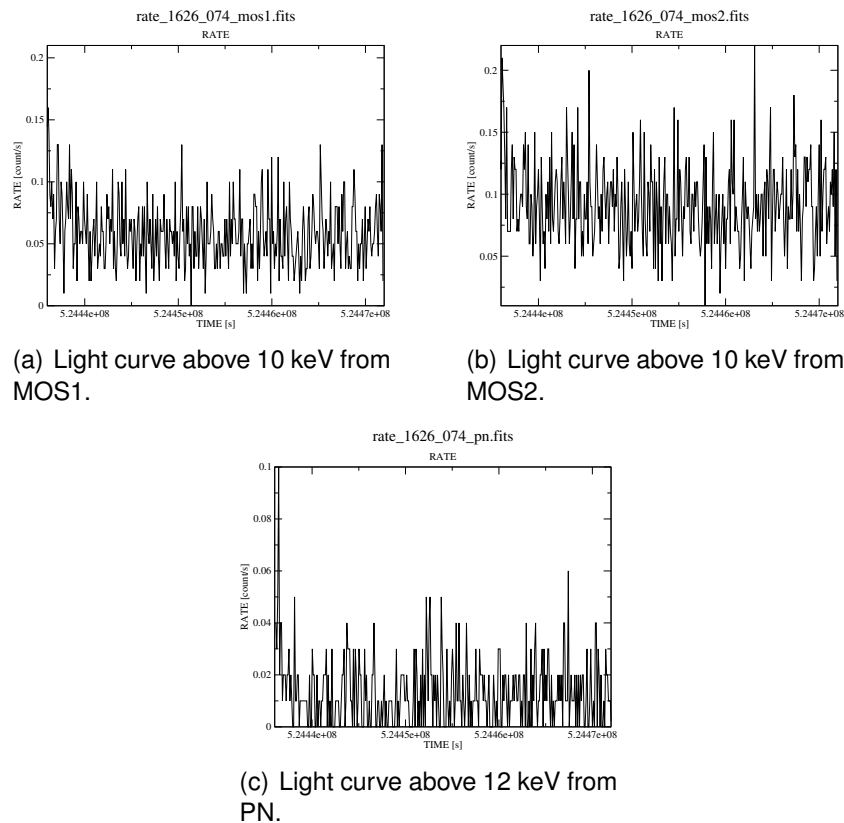
Figure 4.8: Light curves for EPIC-MOS and EPIC-PN instruments of HESS J1626-490 and ObsID 0741950101.

The good time interval was of 36.2 ks for both MOS1 and MOS2 cameras, and 36 ks

for PN . With this interval of time we can obtain the cleaned images, and and using the software ds9 we can visualize them as on Figure 4.9.



(a) Cleaned events for MOS1 in Large Window mode.



(b) Cleaned events for MOS2 in Large Window mode.



(c) Cleaned events for PN in Small Window mode.
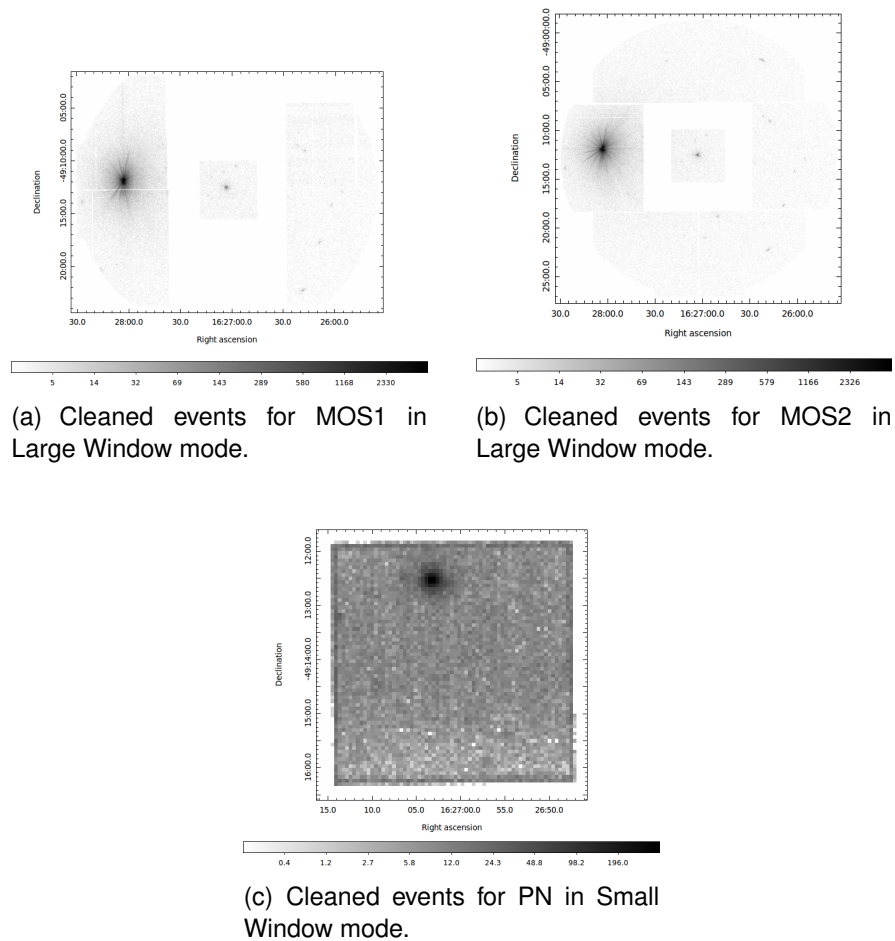
Figure 4.9: Cleaned events images for MOS and PN cameras of the observation ObsID 0741950101.

Once we have the clean images, we can apply the EPIC source detection algorithm. As a result we got twenty eight sources which can be seen on Figure 4.10. The information of the sources can be found on Tables 4.2.3 and 4.2.3.
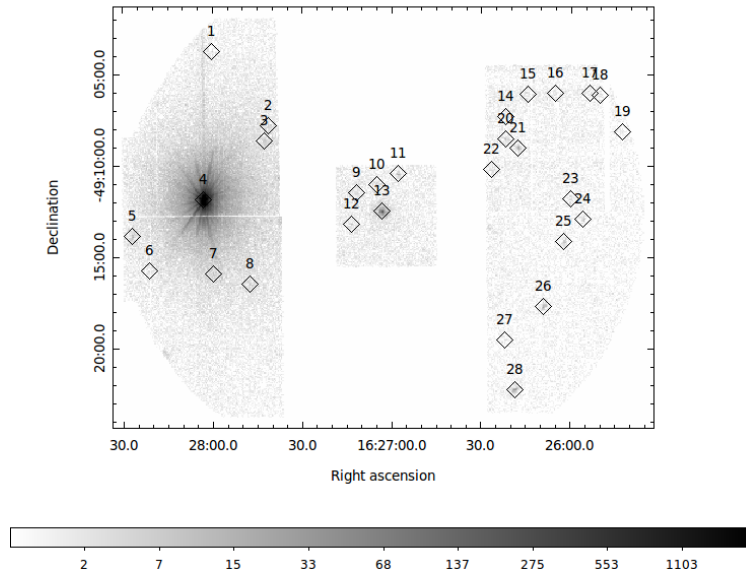
Figure 4.10: Counts map observation of MOS1 on HESS J1626-490 using ObsID 0741950101, the black diamonds indicate 28 sources detected by EPIC source detection.

Table 4.5: Possible counterparts of HESS J1626-490 found using MOS2 detector of ObsID 0741950101 (Offset in arcsec), Part 1.

| Src | RA (J2000) | DEC (J2000) | Star | Offset | X | Offset |
|---|---|---|---|---|---|---|
| 1 | 16:28:00.0 | -49:03:46.4 | TYC 8320-1338-1 | 113.13 | — | — |
| 2 | 16:27:41.3 | -49:07:52.7 | Cl* NGC 6134 PM 101 | 4.97 | — | — |
| 3 | 16:27:42.5 | -49:08:40.6 | Cl* NGC 6134 MMU 27 | 1.62 | — | — |
| 4 | 16:28:03.1 | -49:11:53.5 | 2MASS J16280335-4911535 | 2.40 | 2XMM J162802.8-491154 | 3.05 |
| 5 | 16:28:26.9 | -49:13:54.5 | 2MASS J16283481-4913500 | 77.91 | — | — |
| 6 | 16:28:21.1 | -49:15:47.9 | 2MASS J16282186-4916158 | 28.95 | — | — |
| 7 | 16:27:59.8 | -49:15:57.6 | TYC 8320-1516-1 | 65.79 | — | — |
| 8 | 16:27:47.5 | -49:16:30.4 | 2MASS J16275272-4916111 | 54.45 | — | — |
| 9 | 16:27:11.8 | -49:11:33.0 | TYC 8320-1299-1 | 78.81 | 2XMM J162703.0-491232 | 104.12 |
| 10 | 16:27:04.8 | -49:11:05.3 | TYC 8320-1299-1 | 83.94 | 2XMM J162703.0-491232 | 89.07 |
| 11 | 16:26:57.8 | -49:10:30.0 | — | — | — | — |
| 12 | 16:27:13.4 | -49:13:14.9 | TYC 8320-1299-1 | 86.20 | 2XMM J162703.0-491232 | 110.15 |
| 13 | 16:27:03.1 | -49:12:32.4 | TYC 8320-1877-1 | 18.50 | 2XMM J162703.0-491232 | 0.70 |
| 14 | 16:26:21.6 | -49:07:22.4 | HD 330838 | 87.52 | — | — |

*Continued on next page*

Table 4.5 Continued from previous page

| Src | DNe | Offset | HII | Offset | Radio | Offset |
|---|---|---|---|---|---|---|
| 1 | — | — | — | — | AGAL G335.016-00.166 | 31.75 |
| 2 | — | — | — | — | — | — |
| 3 | — | — | — | — | — | — |
| 4 | - | - | — | — | — | — |
| 5 | SDC G334.938-0.332 | 8.70 | — | — | AGAL G334.939-00.359 | 94.31 |
| 6 | SDC G334.904-0.344 | 5.02 | — | — | [UMM2015] G334.897-00.352 | 35.63 |
| 7 | SDC G334.862-0.304 | 6.04 | — | — | GRS G334.90-00.30 | 80.61 |
| 8 | — | — | — | — | GRS G334.90-00.30 | 112.12 |
| 9 | SDC G334.817-0.185 | 99.46 | — | — | AGAL G334.818-00.182 | 85.38 |
| 10 | — | — | — | — | — | — |
| 11 | — | — | — | — | — | — |
| 12 | SDC G334.817-0.185 | 46.23 | — | — | AGAL G334.818-00.182 | 44.21 |
| 13 | — | — | — | — | — | — |
| 14 | — | — | [JD2012] G334.778-00.022 | 35.35 | AGAL G334.784-00.011 | 22.54 |

There are three bubble sources within the 2 arcmin region around source number 1: [SPK2012] MWP1G335010-001700S, 24.5 arcsec offset (being this one the closest object to the source), [SPK2012] MWP1G335014-001670 at 26.45 arcsec, and [SPK2012] MWP1G335012-001467 at 62.19 arcsec; the sub-millimetric radio source AGAL G335.016-00.166 is 31.75 arcsec offset; and the main sequence star TYC 8320-1338-1 was found to be 113.13 arsec offset. Source number 2 is located in the region of the open cluster NGC 6134 in the constellation of Norma and so, forty one stars of this cluster were found close to the source, The source can be identified to be the star Cl* NGC 6134 PM 101, which was found to be 4.97 arcsec offset. Other twelve stars were in the 2 arcmin region: three variable stars of delta Sct type V* V387 Nor, V* V388 Nor and V* V355 Nor located 34.09 arcsec, 103.84 arcsec, and 109.45 arcsec offset, respectively; one main sequence star HD 330839, six possible red giant branch stars, one asymptotic giant branch star candidate, the UV source MSX6C G334.9455-00.1925 located 105.44 arcsec offset, and the spectroscopic binary TYC 8320-963-1 was found to be 119.09 arcsec offset. The open cluster NGC 6134 was found to be 42.90 arcsec offset and fifty nine stars of this cluster were found in the region of source number 3. This source can be identified to be the possible red giant branch star Cl* NGC 6134 MMU 27, which was located 1.62 arcsec offset. The main sequence star HD 330839 is located 61.40 arcsec offset, other four Variable Star of delta Sct type of the constellation of Norma were found in the region, as well as the UV object MSX6C G334.9455-00.1925, at 111.16 arcsec offset. The closest object found was the main sequence star 2MASS J16280335-4911535, located 2.40 arcsec offset from source number 4, however, this source can be identified to be X-ray object 2XMM J162802.8-491154, found at 3.05 arcsec offset. Two IR objects were also found in the region at 10.83 arcsec and 52.07 arcsec offset. Moreover, the Low Mass X-ray Binary (LMXB) 4U 1624?490 (known as NAME Big Dipper) was found 52.16 arcsec offset. As well as seven stars from the NGC 6134 open

cluster, the main sequence star 2MASS J16275399-4910439 at 113.31 arcsec offset and the possible giant branch star TYC 8320-960-1 at 107.24 arcsec offset. Source marked with number 5 is very likely to be the dark nebula SDC G334.938-0.332 which was found 8.70 arcsec offset, there are also other two objects of this nature, as well as three main sequence stars, the IR source IRAS 16246-4906 at 46.14 arcsec offset, the bubble source [SPK2012] MWP1G334930-003100S is 87.46 arcsec offset, four sub-millimetric radio sources and the maser MMB G334.933-00.307 at 97.39 arcsec offset. There were eleven objects found in the 2 arcmin region around source number 6, the closest was the dark nebula SDC G334.904-0.344, which is a counterpart of the X-ray emission, at 5.02 arcsec offset from the source. There were found also other 4 dark nebulae, three YSOC, three sub-millimetric radio sources, and the main sequence star TYC 8320-1038-1, at 111.51 arcsec offset. Source number 7 is very likely to be the dark nebula SDC G334.862-0.304, which was located 6.04 arcsec offset from the source. In the locality there are also other 4 TYC star, two asymptotic giant branch star candidates GRS G334.90 -00.30 and 2MASS J16280166-4914106 at 70.16 arcsec and 108.60 arcsec offset, respectively, as well as the radio object GRS G334.90 -00.30 at 80.61 arcsec and the IR source IRAS 16243-4910, 108.76 arcsec offset. The 2 arcmin region of source number 8 is composed by the asymptotic giant branch star candidate 2MASS J16275272-4916111 located 54.45 arcsec offset, two TYC stars, the radio source GRS G334.90 -00.30 at 110.40 arcsec and the YSOC SSTGLMC G334.8490-00.2609, 112.12 arcsec offset. For source 9, the closest object is the main sequence star TYC 8320-1299-1, 78.81 arcsec offset. In the region there are also the sub-millimetric radio source AGAL G334.818-00.182 (85.38 arcsec offset), the dark nebula SDC G334.817-0.185 (99.46 arcsec offset) and the X-ray source 2XMM J162703.0-491232 which is located 104.12 arcsec offset. In the 2 arcmin region of source number 10, there were found the stars TYC 8320-1299-1 and TYC 8320-1877-1, located 83.94 arcsec and 99.09 arcsec offset,

and the X-ray source 2XMM J162703.0-491232, 89.07 arcsec offset. Source number 11 is the same source as number 6 in ObsID 0403280201, and the only object found in the vicinity was the IR source MSX6C G334.8128-00.1059 at 51.47 arcsec offset. Six objects were found in the neighbourhood of source 12, the closest object is the sub-millimetric radio source AGAL G334.818-00.182, 44.21 arcsec offset. Two dark nebulae SDC G334.817-0.185 and SDC G334.832-0.197 located 46.23 arcsec and 113.58 arc-sec offset, the IR source SDC G334.817-0.185 at 78.55 arcsec, the main sequence star TYC 8320-1299-1, 86.20 arcsec offset, and the X-ray source 2XMM J162703.0-491232, 110.15 arcsec away. Source 13 is in the same postition as source number 11 of ObsID 0403280201, the X-ray source 2XMM J162703.0-491232, 0.70 arcsec offset. There are also other 3 TYC stars in the vicinity. Source 14 is very likely to be the sub-millimetric radio source AGAL G334.784-00.011, located 22.54 arcsec offset. In the region, there were found the IR source IRAS 16226-4900, 29.95 arcsec offset, the HII region [JD2012] G334.778-00.022, 35.35 arcsec offset, two bubble sources, another sub-millimetric radio source and the main sequence star HD 330838, 87.52 arcsec offset.

Table 4.6: Possible counterparts of HESS J1626-490 found using MOS2 detector of ObsID 0741950101 (Distance in arcsec), Part 2.

| Src | RA (J2000) | DEC (J2000) | Star | Offset | X | Offset |
|-----|-----------|-------------|------|--------|---|--------|
| 15 | 16:26:14.2 | -49:06:07.2 | TYC 8320-2072-1 | 59.07 | – | – |
| 16 | 16:26:05.0 | -49:06:03.2 | TYC 8320-2072-1 | 32.58 | – | – |
| 17 | 16:25:53.5 | -49:06:04.3 | TYC 8320-1731-1 | 35.84 | – | – |
| 18 | 16:25:50.2 | -49:06:09.4 | IRAS 16220-4859 | 34.18 | – | – |
| 19 | 16:25:42.7 | -49:08:09.2 | 2MASS J16255119-4908387 | 34.18 | – | – |
| 20 | 16:26:21.8 | -49:08:33.0 | HD 330838 | 18.12 | – | – |
| 21 | 16:26:17.5 | -49:09:03.2 | HD 330838 | 38.15 | – | – |
| 22 | 16:26:26.4 | -49:10:15.6 | [W71b] 119-02 [h] | 34.97 | – | – |
| 23 | 16:26:00.0 | -49:11:50.3 | SSTGLMC G334.6699-00.0277 | 53.09 | EXMS B1622-490 | 119.36 |
| 24 | 16:25:55.7 | -49:12:56.2 | SSTGLMC G334.6699-00.0277 | 28.70 | EXMS B1622-490 | 114.41 |
| 25 | 16:26:02.2 | -49:14:11.0 | SSTGLMC G334.6699-00.0277 | 99.35 | – | – |
| 26 | 16:26:08.9 | -49:17:44.2 | – | – | – | – |
| 27 | 16:26:21.8 | -49:19:33.6 | SSTGLMC G334.6509-00.1492 | 68.53 | – | – |
| 28 | 16:26:18.5 | -49:22:16.3 | 2MASS J16261607-4922405 | 33.79 | – | – |

*Continued on next page*

124

Table 4.6 Continued from previous page

| Src | HII | Offset | MC | Offset | FGL | Offset |
|---|---|---|---|---|---|---|
| 15 | — | — | — | — | — | — |
| 16 | — | — | — | — | — | — |
| 17 | — | — | — | — | — | — |
| 18 | — | — | — | — | — | — |
| 19 | — | — | — | — | — | — |
| 20 | [JD2012] G334.778-00.022 | 51.89 | — | — | — | — |
| 21 | [JD2012] G334.778-00.022 | 100.94 | — | — | — | — |
| 22 | — | — | — | — | — | — |
| 23 | [NNM2015] 1 | 98.55 | — | — | — | — |
| 24 | — | — | — | — | — | — |
| 25 | — | — | — | — | — | — |
| 26 | [NNM2015] 3 | 110.95 | [RC2004] G334.6-0.1-112.4 | 88.30 | 1FGL J1626.0-4917c81.41 | — |
| 27 | — | — | — | — | — | — |
| 28 | — | — | — | — | — | — |

Table 4.6 Continued from previous page

| Src | DNe | Offset | Radio | Offset | Pulsar | Offset |
|---|---|---|---|---|---|---|
| 15 | — | — | AGAL G334.784-00.011 | 102.36 | — | — |
| 16 | — | — | — | — | — | — |
| 17 | — | — | AGAL G334.718+00.067 | 85.85 | — | — |
| 18 | — | — | AGAL G334.718+00.067 | 54.19 | — | — |
| 19 | SDC G334.717+0.068 | 96.88 | AGAL G334.706+00.034 | 85.17 | — | — |
| 20 | — | — | AGAL G334.784+00.011 | 89.96 | — | — |
| 21 | — | — | — | — | — | — |
| 22 | — | — | GRS G334.90-00.30 | 112.12 | — | — |
| 23 | SDC G334.659-0.001 | 113.19 | — | — | — | — |
| 24 | SDC G334.659-0.001 | 90.42 | AGAL G334.639-00.032 | 85.99 | — | — |
| 25 | SDC G334.639-0.078 | 116.27 | AGAL G334.639-00.032 | 106.57 | — | — |
| 26 | SDC G334.639-0.078 | 111.0 | AGAL G334.661-00.097 | 118.55 | — | — |
| 27 | — | — | — | — | — | — |
| 28 | SDC G334.585-0.181 | 32.29 | — | — | — | — |

For source number 15, the 2 arcmin region is formed with the bubble source [SPK2012] MWP1G334791+000084, 54.78 arcsec offset, the main sequence star TYC 8320-2072-1 is located 59.07 arcsec away, the eclipsing binary UCAC4 205-120748 was found to be 83.65 arcsec offset, the sub-millimetric radio source AGAL G334.784-00.011 is located 192.36 arcsec offset, and it was found that HESS J1626-490 is located at 113.56 arcsec. The closest object found in the region around source 16 is the star TYC 8320-2072-1, located 32.58 arcsec. There was found also the eclipsing binary UCAC4 205-120673 at 33.88 arcsec. HESS J1626-490 is located 51.27 arcsec. In the 2 arcmin region around source number 17, the closest object is TYC 8320-1731-1, a main sequence star located 35.84 arcsec offset. There were found also the molecular cloud PGCC G334.72+00.06 at 58.60 arcsec, the emission line star EM* VRMF 25, 62.27 arcsec off-set, the eclipsing binary UCAC4 205-120673 was found to be 80.92 arcsec offset, the sub-millimetric radio source AGAL G334.718+00.067 at 85.85 arcsec and the dark neb-ula SDC G334.717+0.068 at 89.02 arcsec offset. HESS J1626-490 is located 115.02 arcsec. The closest object to source 18 is the molecular cloud PGCC G334.72+00.06, located 32.59 arcsec offset, but there were also found two main sequence stars, the emission line star EM* VRMF 25, 40.28 arcsec offset, the sub-millimetric radio source AGAL G334.718+00.067 is 54.19 arcsec offset, the dark nebula SDC G334.717+0.068 is at 56.70 arcsec and the eclipsing binary UCAC4 205-120673 is 113.44 arcsec off-set. Two dense cores are close to source 19: MSXDC G334.70+0.02 at 81.28 arcsec (being this the closest object) and [PLW2012] G334.703+00.032-086.5 at 87.24 arc-sec offset, also three radio sources: AGAL G334.712+00.037 at 89.41 arcsec, and AGAL G334.718+00.067 at 95.05 arcsec, the YSOC 2MASS J16255119-4908387 lo-cated 88.26 arcsec offset, the dark nebula SDC G334.717+0.068 at 96.88 arcsec, the Emission-line Star EM* VRMF 25 located 101.98 arcsec offset, and the molecular cloud PGCC G334.72+00.06 at 107.93 arcsec offset. Source number 20 is in the same posi-

tion as source umber 7 of ObsID 0403280201, and is very likely to be the main sequence star HD 330838 located 18.12 arcsec offset. Source number 21 is in the same position of source number 8 of ObsID 0403280201. The closest object of source 22 is the carbon star [W71b] 119-02 located 34.97 arcsec offset. Two main sequence stars were also found in the 2 arcmin region TYC 8320-1346-1 and HD 330838, at 75.35 arcsec and 99.97 arcsec offset, respectively; as well as the IR source IRAS 16225-4903, at 83.01 arcsec offset. In the region around source 23 there were found: two YSOC SSTGLMC G334.6699-00.0277, located 53.09 arcsec offset and 2MASS J16255504-4911009 at 69.28 arcsec offset; two main sequence stars HD 147744 and CD-48 10818B at 64.59 arcsec and 73.01 arcsec offset, respectively; as well as the HII region [NNM2015] 1, 98.55 arcsec offset; the dark nebulae SDC G334.659-0.001 and SDC G334.681+0.010, 113.19 and 117.19 arcsec offset; the maser SDC G334.659-0.001, 115.42 arcsec apart; the dense core AGAL G334.682+00.011 at 118.29 arcsec and the X-ray source EXMS B1622-490, 119.36 arcsec offset. Source 24 is in the same position as source number 17 of ObsID 0403280201. Around source 24, there were found three YSOC, being SSTGLMC G334.6699-00.0277 the closest object, 28.70 arcsec offset. In the 2 arcmin region of source 25, there were found two YSOC: SSTGLMC G334.6699-00.0277 (closest object), and SSTGLMC G334.6365-00.0327 located 99.35 arcsec and 110.57 arcsec offset, respectively. The sub-millimetric radio source AGAL G334.639-00.032 is located 106.57 arcsec offset and the dark nebula SDC G334.639-0.078 at 116.27 arcsec offset. Source as number 16 of ObsID 0403280201 is out of this position. Source number 26 is the same source as source 15 of the ObsID 0403280201, but with a small difference of 2 arcsec in the coordinates. Source number 27 has in the region two YSOC: SSTGLMC G334.6509-00.1492 and 2MASS J16261543-4921085, located 68.53 and 113.76 arcsec offset, respectively; two main sequence stars: TYC 8320-1341-1 and IRAS 16225-4914, at 71.03 and 112.70 arcsec offset, and two bubble sources: [SPK2012] MWP1G334620-

001800S and [SPK2012] MWP1G334660-001400S. Source number 28 is coincident with source number 14 of ObsID 0403280201.

In summary, source number 2 can be identified to be the star Cl* NGC 6134 PM 101, source number 3 to be the possible red giant branch star Cl* NGC 6134 MMU 27, source number 4 to be the X-ray source 2XMM J162802.8-491154. Source number 5 is very likely to be the dark nebula SDC G334.938-0.332, source number 6 the dark nebula SDC G334.904-0.344, source number 7 the dark nebula SDC G334.862-0.304, source number 11 is very likely to be , source 13 was found to be the X-ray source 2XMM J162703.0-491232, and source 14 the sub-millimetric radio source AGAL G334.784-00.011, all of this based on the very small offset of the sources, and source number 20 is very likely to be the main sequence star HD 330838.

For this observation, we also did the cut in the energy band for the EPIC source finding thread, using 2.5-12 keV as the energy range for this tool. The result was that 9 sources remaining and three more were detected, which can be seen on the Figure 4.11

The information about these sources is in the Table 4.7.

Table 4.7: Table of sources dominated by non-thermal emission of HESS J1626-490 ObsID 0741950101. The flux values are in erg cm$^{-2}$s$^{-1}$.

| Src | RA J2000 | DEC J2000 | Possible counterpart | Offset arcsec | Flux E-14 |
|---|---|---|---|---|---|
| 4 | 16:28:03.1 | -49:11:53.5 | 2XMM J162802.8-491154 | 3.05 | 7094.91 |
| 13 | 16:27:03.1 | -49:12:32.4 | 2XMM J162703.0-491232 | 0.70 | 31.34 |
| 21 | 16:26:17.5 | -49:09:03.2 | HD 330838 | 38.15 | 4.63 |
| 24 | 16:25:55.7 | -49:12:56.2 | SSTGLMC G334.6699-00.0277 | 28.70 | 0.89 |
| 25 | 16:26:02.1 | -49:14:11.0 ? | ? | 2.21 | |
| 26 | 16:26:08.9 | -49:17:44.2 | 1FGL J1626.0-4917c | 81.41 | 1.07 |
| 27 | 16:26:21.8 | -49:19:33.6 | SSTGLMC G334.6509-00.1492 | 68.53 | 0.98 |
| 28 | 16:26:18.5 | -49:22:16.3 | SDC G334.585-0.181 | 32.29 | 10.57 |
| H1 | 16:28:01.4 | -49:20:03.1 | 2MASS J16280974-4920054 | 81.19 | 2.45 |
| H2 | 16:27:55.7 | -49:20:34.4 | 2MASS J16280035-4922149 | 110.38 | 1.02 |
| H3 | 16:25:42.0 | -49:15:14.4 | ? | ? | 1.02 |

In the 2 arcmin region around source 4, there were found two 2MASS stars, one
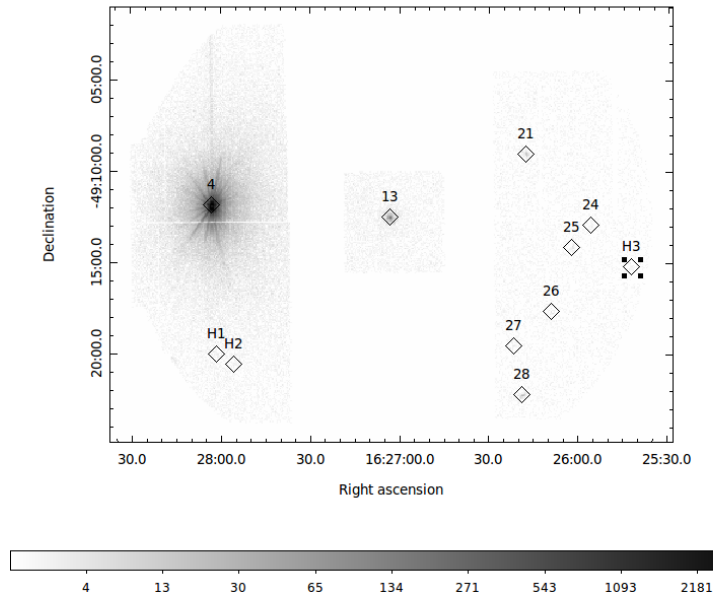
Figure 4.11: Counts map observation of MOS1 for source HESS J1626-490 using ObsID 0741950101 and a cut in the energy range from 2.5 - 12 keV, the black diamonds indicate 11 sources detected by the EPIC source detection.

of them is the closest source to it, 2MASS J16280335-4911535 at 2.40, and 2MASS J16275399-4910439 at 113.31 away. Also, 7 stars in a cluster were found in the region, all of them located at more than 70 arcsec away. However, the counterpart options for this source are: one X-ray source 2XMM J162802.8-491154 located at just 3.05 arcsec away and the LMXB, known as NAME Big Dipper (4U 1624?490) which was found to be 52.16 arcsec away. This binary system is composed of a neutron star and a loss mass companion, and exhibits intense recurrent X-ray dips with a period of $\sim$21 hrs and dip duration of 6-8 hr [160], gamma-ray emission was detected from this source using INTEGRAL [161]. The X-ray dips are believed to be due to the occultation of the X-rays emitted around the compact object by the bulge on the rim of accretion disk, where the fas stream from the companion impacts on it. It has a persistent X-ray emission being the brightest among the dippers ($6 \times 10^{37}$ erg s$^{-1}$ [162]). In the case of the source 13

the clear X-ray counterpart is 2XMM J162703.0-491232 located just 0.70 arcsec offset.

In the other hand, the region of 2 arcmin away from source 21 contains the HD 330838 star, located at 38.15 arcsec away form the source, the IR source IRAS 16225-4903 at 67.96 arcsec away, the HII region known as [JD2012] G334.778-00.022 at 100.94 arcsec away, the bubble source [SPK2012] MWP1G334779-000253 at 104.49 arcsec away and the cluster of stars [W71b] 119-02 located at 108.38 arcsec away. Ten sources were found to be in the 2 arcmin vicinity around source 24, the closest source found was a YSOC SSTGLMC G334.6699-00.0277 located at 28.70 arcsec away, but there are other two objects of this type in the region located at more than 90 arcsec away.

All the 4 sources in the vicinity of source number 25 were found to be further than 95 arcsec away. There are two YSOCs, SSTGLMC G334.6699-00.0277 and SSTGLMC G334.6365-00.0327 at 99.35 and 110.57 arcsec away from the source, respectively. But also, the sub-millimetric radio source AGAL G334.639-00.032 was found to be 106.57 arcsec away and the dark nebula SDC G334.639-0.078 located 116.27 arcsec away.

The closest source to the 26 source was found to be the 1FGL J1626.0-4917c gamma-ray source located 81.41 arcsec away, this source could be a counterpart of HESS J1626-490. Furthermore, seven molecular clouds were also found in the region, all of them located at 88.30 arcsec away. One HII region, one dark nebula and one sub-millimetric radio source were found located further than 100 arcsec away from the source, these are: [NNM2015] 3, SDC G334.639-0.078 and AGAL G334.661-00.097, respectively.

In the region around source 27 were found two YSOC, SSTGLMC G334.6509-00.1492 located at 68.52 arcsec away (the closest source) and 2MASS J16261543-4921085, 113.76 arcsec far. Other two main sequence stars and two bubble sources were found in the vicinity.

In the 2 arcmin vicinity around source 28 there are two dark nebulae, SDC G334.585-0.181 and SDC G334.584-0.175 located 34.39 arcsec away. There are also two young star object candiates 2MASS J16261607-4922405 and 2MASS J16261543-4921085, the first one located 33.79 arcsec away and the second at 73.99 arcsec away.

For the case of source H1, there are one YSOC known as 2MASS J16280974-4920054, at 81.19 arcsec away, one binary star HD 330850 at 81.26 arcsec, the star CD-49 10690 is located 81.31 arcsec away, CCDM J16280-4919B (star in a double system) at 85.66 arcsec away, the IR source 2MASS J16281215-4919571 at 104.90 arcsec away, and the main sequence star HD 330851 at 113.35 arcsec away.

The source H2, has two main sequence star as neighbours, HD 330851 and TYC 8320-1105-1 located 104.67 and 118.79 arcsec away from the source, respectively, very far for being considered as counterparts.

Finally, the source H3 has 7 objects in the 2 arcmin vicinity, two main sequence stars TYC 8320-1536-1 at 90.04 arcsec away and HD 330668 at 93.33 arcsec, SSTGLMC G334.6365-00.0327 which is a YSOC located at 103.27 arcsec away, two IR sources each of them located at 103.54 and 105.02 arcsec away, respectively, one maser source MMB G334.635-00.015 at 103.65 arcsec away, and one sub-millimetric radio source AGAL G334.639-00.032 at 111.05 arcsec offset.

## 4.3 Chandra Data Analysis

Chandra observed HESS J1626-490 on June 16, 2012 with an exposure time of 10.04 ks in total, which result in the ObsID 13287. The observation was made using the ACIS-I, ACIS-S2 (O2), ACIS-S3 (O1) chips of the telescope and an event filter.

The data was analysed making use of the software package CIAO 4.7 (Chandra Interactive Analysis of Observations) provided by the Chadra team and the calibration CALDB v4.7.0 (Calibration Database). The data was reprocessed using the script `chandra_repro`, which runs the commands automatically. This is to identify and eliminate the bad pixels, but also to search and eliminate afterglows and hot pixels.

Using the `dmcopy` we can filter images and select subsets, either spatial, temporal, energy, etc. of an image.

We use the `dmcopy` tool to create the image, and after that, we run the `fluximage` tool to determine and get the exposure map, which creates an image in the 0.5-7 keV energy range and an exposure map of the observation. Once we have all of this, we can use the detection package, for looking to the sources in the observation.

### 4.3.1 Observation 13287

CIAO Science Threads has three tools for the source detection, they are `celldetect`, `vtpdetect` and `wavdetect`. In this analysis, we applied the `celldetect` tool (which is good on detection of well-separated point sources, so it is good to find point sources) and 18 sources were found in this observation. For the detection of extended sources we applied `vtpdetect` tool, which has the advantage to find extended and also faint sources; with this 16 sources were found. For the image, we eliminated the circles of the sources founded by celldetect that were also regions detected with vtpdetect, which are shown in the Figure 4.12. From the 18 sources detected by celldetect, 7 remained and

11 where also detected with vtpdtect.
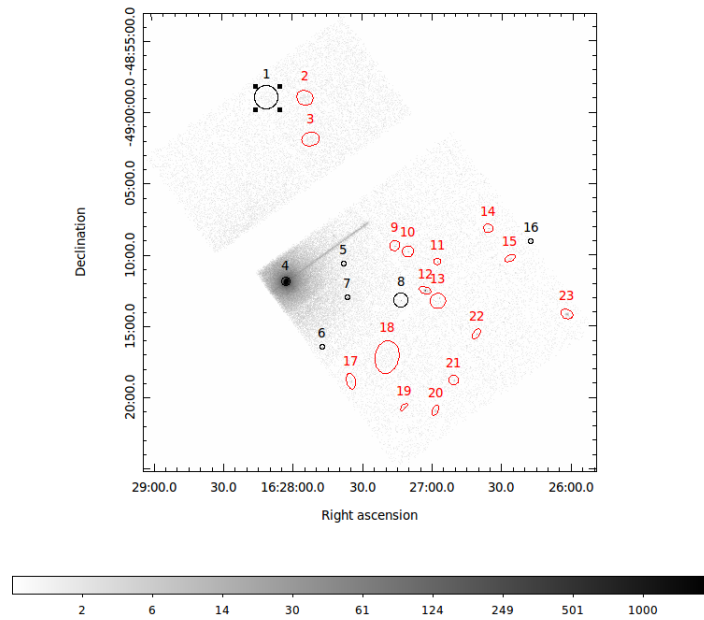


Figure 4.12: Counts map observation of MOS1 with ObsID 13287 for HESS J1626-490, the black circles indicate 7 sources detected by `celldetect`, and the red ellipses are the 16 sources detected with `vtpdetect`.

Information of the position, and the possible counterpart of the sources can be found in the Tables 4.3.1, 4.3.1.

Table 4.8: Possible counterparts of HESS J1626-490 found using ObsID 13287 acquired using Chandra observatory (Offset in arcsec), Part 1.

| Src | RA (J2000) | DEC (J2000) | Star | Offset | X | Offset |
|---|---|---|---|---|---|---|
| 1 | 16:28:10.4 | -48:59:00.8 | 2MASS J16280853-4857441 | 78.99 | – | – |
| 2 | 16:27:54.3 | -48:59:01.8 | TYC 8320-1323-1 | 4.54 | 2XMM J162754.2-485857 | 4.41 |
| 3 | 16:27:51.9 | -49:01:55.5 | 2MASS J16274360-4900579 | 100.25 | – | – |
| 4 | 16:28:02.8 | -49:11:53.6 | 2MASS J16280335-4911535 | 5.71 | 2XMM J162802.8-491154 | 0.79 |
| 5 | 16:27:37.9 | -49:10:41.0 | V* V385 Nor | 1.82 | – | – |
| 6 | 16:27:47.2 | -49:16:32.2 | 2MASS J16275272-4916111 | 58.34 | – | – |
| 7 | 16:27:36.3 | -49:13:03.8 | TYC 8320-1491-1 | 0.38 | – | – |
| 8 | 16:27:13.3 | -49:13:14.0 | TYC 8320-1299-1 | 84.69 | 2XMM J162703.0-491232 | 08.69 |
| 9 | 16:27:15.9 | -49:09:24.8 | IRAS 16234-4901 | 69.77 | – | – |
| 10 | 16:27:10.2 | -49:09:49.1 | IRAS 16234-4901 | 72.74 | – | – |
| 11 | 16:26:57.6 | -49:10:31.1 | – | – | – | – |
| 12 | 16:27:02.9 | -49:12:32.9 | TYC 8320-1877-1 | 15.91 | 2XMM J162703.0-491232 | 1.96 |
| 13 | 16:26:57.4 | -49:13:17.4 | TYC 8320-1531-1 | 33.98 | 2XMM J162703.0-491232 | 71.47 |
| 14 | 16:26:35.7 | -49:08:11.5 | SSTGLMC G334.8182-00.0579 | 90.23 | – | – |

*Continued on next page*

Table 4.8 Continued from previous page

| Src | DNe | Offset | HII | Offset | Radio | Offset |
| --- | --- | --- | --- | --- | --- | --- |
| 1 | — | — | — | — | — | — |
| 2 | — | — | — | — | — | — |
| 3 | SDC G334.953-0.301 | 11.77 | — | — | — | — |
| 4 | — | — | — | — | — | — |
| 5 | — | — | — | — | — | — |
| 6 | — | — | — | — | GRS G334.90 -00.30 | 113.93 |
| 7 | SDC G334.848-0.198 | 92.99 | — | — | AGAL G334.838-00.201 | 96.26 |
| 8 | SDC G334.817-0.185 | 46.95 | — | — | AGAL G334.818-00.182 | 44.48 |
| 9 | — | — | — | — | — | — |
| 10 | — | — | — | — | — | — |
| 11 | — | — | — | — | — | — |
| 12 | — | — | — | — | — | — |
| 13 | — | — | — | — | — | — |
| 14 | — | — | [JD2012] G334.778-00.022 | 115.23 | AGAL G334.796-00.022 | 98.17 |

The only object found in the vicinity of source number 1 is the main sequence star 2MASS J16280853-4857441, located 78.99 arcsec offset. Source number 2 can be identified to be the X-ray source 2XMM J162754.2-485857, which is 4.41 arcsec offset, however there is a main sequence star very close to it, TYC 8320-1323-1 at 4.54 arcsec offset. The closest object found in the 2 arcmin region around source number 3 was the dark nebula SDC G334.997-0.123, located 62.89 arcsec offset. In the region, the bubble [SPK2012] MWP1G335012-001467 was found 74.43 arcsec from the source, as well as the YSOC 2MASS J16274360-4900579 at 100.25 arcsec offset, and the IR object 2MASS J16274158-4901400 located 101.64 arcsec offset. The source number 4 is coincident with the source number 4 of the ObsID 0741950101 made by XMM-Newton satellite. Forty one sources were found in the 2 arcmin region of source number 5, 37 of them being part of the open cluster NGC 6134 in the constellation of Norma. However, this source can be identified as the closest object which is the ellipsoidal variable star V* V385 Nor, also in the constellation of Norma, 1.82 arcsec offset. Three variable stars of delta Sct type were also found in the vicinity, being V* V386 Nor the closest among them, 26.03 arcsec offset, as well as one main sequence star (TYC 8320-1410-1, 72.22 arcsec offset), and the spectroscopic binary TYC 8320-963-1, located 80.45 arcsec offset. The position of source number 6 is coincident with source number 8 of ObsID 0741950101. Source number 7 is in the same position of source number 5 of ObsID 0403280201, identified to be the spectroscopic binary TYC 8320-1491-1. Source number 8 is coincident with source number 12 of ObsID 0741950101. The main sequence star IRAS 16234-4901 was the only object in the region of source number 9, located 69.77 arcsec offset from the source. This star was also the only object found in the vicinity of source number 10. The IR source MSX6C G334.8128-00.1059 is located 51.47 arcsec offset from the detected source number 11. No other objects were found in this region. Source number 12 can be identified to be the X-ray source 2XMM J162703.0-491232, which is 1.96 arc-

sec offset. Three main sequence stars were also found in the 2 arcmin region, sources 11 (ObsID 0403280201) and 13 (ObsID 0741950101) are in the same position. Source 13 is in the same position of source number 12 of ObsID 0403280201. Source number 14 shares the 2 arcmin region with the YSOC SSTGLMC G334.8182-00.0579, located 90.23 arcsec offset; with the sub-millimetric radio source AGAL G334.796-00.022, 98.17 arcsec; with the bubble source [SPK2012] MWP1G334779-000253, 104.14 arcsec; the HII region [JD2012] G334.778-00.022, 115.23 arcsec; and the IR source IRAS 16226-4900 at 118.46 arcsec offset.

Table 4.9: Possible counterparts of HESS J1626-490 found using ObsID 13287 acquired using Chandra observatory (Offset in arcsec), Part 2.

| Src | RA (J2000) | DEC (J2000) | Star | Offset | X | Offset |
|-----|-----------|-------------|------|--------|---|--------|
| 15 | 16:26:26.360 | -49:10:17.43 | [W71b] 119-02 | 33.66 | — | — |
| 16 | 16:26:17.493 | -49:09:04.84 | HD 330838 | 38.99 | — | — |
| 17 [c] | 16:27:34.836 | -49:18:55.24 | 2SSTGLMC G334.7707-00.3109 | 81.98 | — | — |
| 18 [d] | 16:27:19.330 | -49:17:14.07 | 2MASS J16272878-4916592 | 93.71 | — | — |
| 19 | 16:27:11.965 | -49:20:44.02 | No object found | — | — | — |
| 20 | 16:26:58.427 | -49:20:58.18 | EM* VRMF 29 | 81.38 | — | — |
| 21 | 16:26:50.502 | -49:18:50.90 | EM* VRMF 29 | 79.09 | — | — |
| 22 | 16:26:40.701 | -49:15:35.86 | 2MASS J16264954-4916088 | 92.64 | — | — |
| 23 | 16:26:01.920 | -49:14:11.58 | SSTGLMC G334.6699-00.0277 | 98.93 | — | — |

*Continued on next page*

139

Table 4.9 *Continued from previous page*

| Src | DNe | Offset | HII | Offset | Radio | Offset |
|-----|-----|--------|-----|--------|-------|--------|
| 15 | — | — | — | — | — | — |
| 16 | — | — | [JD2012] G334.778-00.022 | 102.33 | — | — |
| 17 | — | — | — | — | — | — |
| 18 | SDC G334.757-0.215 | 93.88 | — | — | AGAL G334.759-00.216 | 91.66 |
| 19 | — | — | — | — | — | — |
| 20 | DOBASHI 6450 | 72.44 | — | — | — | — |
| 21 | — | — | — | — | — | — |
| 22 | — | — | — | — | AGAL G334.728-00.147 | 45.04 |
| 23 | SDC G334.639-0.078 | 116.02 | — | — | AGAL G334.639-00.032 | 104.22 |

Source number 15 is 33.66 arcsec offset from the Carbon star [W71b] 119-02, 75.77 arcsec from the star TYC 8320-1346-1, 82.74 arsec from the IR source IRAS 16225-4903, and 101.34 arcsec from the star HD 330838. Source number 16 is in the same position of soyrce number 8 of ObsID 0403280201 ans source 21 of ObsID 0741950101. In the region of source 17 there are two YSOC SSTGLMC G334.7707-00.3109, at 81.98 arcsec offset and SSTGLMC G334.7858-00.3120 at 86.99 arcsec, there are two main sequence stars: 2MASS J16272581-4918528 at 88.28 arcsec and TYC 8320-2128-1 at 118.91 arcsec, and the IR source IRAS 16239-4912 is at 93.65 arcsec offset. For the case of source 18, the region is composed by the IR source IRAS 16234-4911, located 75.23 arcsec offset, the sub-millimetric radio source AGAL G334.759-00.216, at 91.66 arcsec; the asymptotic giant branch star candidate 2MASS J16272878-4916592, 93.71 arcsec offset, the dark nebula SDC G334.757-0.215, 93.88 arcsec offset and two main sequence stars TYC 8320-1699-1 and 2MASS J16272581-4918528, 113.36 and 117.33 arcsec offset, respectively. No astronomical object was found in the 2 arcmin region of source number 19 in SIMBAD. Source 20 is in the same position of source number 3 of ObsID 0403280201. Two objects were found to be in the 2 arcmin region of source number 21, the emission line star EM* VRMF 29, located 79.09 arcsec offset, and the IR source IRAS 16230-4913 at 115.96 arcsec offset. Around source number 22 there were found three sub-millimetric radio sources AGAL G334.728-00.147 (closest object), located45.04 arcsec offset, AGAL G334.704-00.127 and AGAL G334.694-00.132, at 77.01 and 90.82 arcsec offset respectively. There is another radio source, GRS G334.80 -00.10 at 96.70 arcsec, and a YSOC SSTGLMC G334.6927-00.1296, 99.20 arcsec away from the source; the mm source [CAB2011] G334.70-0.12 is 110.73 arcsec offset; and the star TYC 8320-1431-1 is 115.98 arcsec away. Source number 23 was found to be in the same position of source number 25 of ObsID 0741950101.

As we did for the XMM-Newton images, we carried out a cut in the energy range (2.5 - 8 keV), for let us know about the sources dominated by non-thermal emission. The result can be seen in the Figure 4.13.
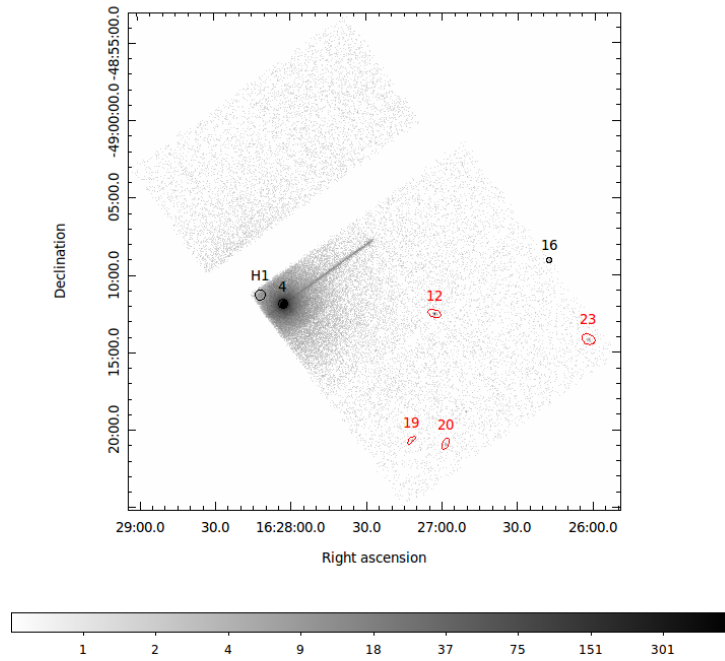


Figure 4.13: Counts map observation using ObsID 13287 made by Chandra of HESS J1626-490 with a cut in the energy range from 2.5 keV to 8 keV, the black circles indicate 7 sources detected by `celldetect` and the red circles the ones detected using `vtpdetect`.

The sources are summarized in Table 4.10.

The source number 4 is coincident with the source number 4 of the ObsID 0741950101 made by XMM-Newton satellite which was found to be the LMXB 4U 1625-490. Source number 12 was found to be the X-ray source 2XMM J162703.0-491232. For the source number 16, the two closest objects are: 1. The YSOC SSTGLMC G334.6699-00.0277 at 28.70 arcsec, and 2. the Maser Caswell CH3OH 34.635-00.015 at 45.21 arcsec. SST-GLMC G334.6699-00.0277 is one of the 18,949 point sources that have intrinsically red

Table 4.10: Table of non-thermal emission sources of HESS J1626-490 ObsID 13287. The flux values are in erg cm$^{-2}$s$^{-1}$

| Src | RA J2000 | DEC J2000 | Possible counterpart | Offset arcsec | SNR |
|-----|----------|-----------|---------------------|--------|------|
| 4 | 16:28:02.782 | -49:11:53.61 | 2XMM J162802.8-491154 | 0.79 | 222.65 |
| 12 | 16:27:02.856 | -49:12:32.87 | 2XMM J162703.0-491232 | 1.96 | 13.42 |
| 16 | 16:25:55.68 | -49:12:56.16 | Not sure | ? | |
| 19 | 16:27:11.965 | -49:20:44.02 | No object found | - | |
| 20 | 16:26:58.427 | -49:20:58.18 | Not sure | - | 3.60 |
| 23 | 16:26:01.920 | -49:14:11.58 | Not sure | - | 4.92 |
| H1 | 16:28:11.527 | -49:11:22.62 | - | - | 3.70 |

mid-infrared color observed by the SPITZER telescope in the Galactic midplane [163]. In the other hand, there is one sub-millimetric radio source in the 2 arcmin vicinity, AGAL G334.639-00.032 located 85.99 arcsec away. Furthermore, there is also one dark nebula in the region at 90.42 arcsec offset, known as SDC G334.659-0.001. Two more YSOC are close, SSTGLMC G334.6365-00.0327 and 2MASS J16255504-4911009 located 95.16 and 115.45 arcsec away, respectively. Also, two IR sources are in the region, and the X-ray source EXMS B1622-490 is 114.41 arcsec away.

In the case of the source 20, which is the same source as number 13 of OsbID 0403280201, the closest source found in SIMBAD was the Dark Cloud Nebula DOBASHI 6450 at 72.44 arcsec that was detected by the 2 Micron All Sky Survey Point Source Catalog (2MASS PSC) [164]. And the other source EM* VRMF 29, which is a emission-line star is at 81.38 arcsec. Could be this a counterpart?

The source 23 is a bit more complicated, there are four sources in the neighbourhood of 2 arcmin and all of them are not close enough, the closest source is the YSOC SSTGLMC G334.6699-00.0277 at 98.93 arcsec, but this source seems more close to the source 16. In the neighbourhood there are also other three sources in the 2 arcmin region, the sub-millimetric radio source AGAL G334.639-00.032 located 104.22 arcsec offset, another YSOC SSTGLMC G334.6365-00.0327, 108.18 arcsec offset and the dark

nebula SDC G334.639-0.078, 116.02 arcsec offset.

The closest object to H1 is an infrared source 2MASS J16280420-4911552, 78.82 arcsec away.  This source is very close to the edge of the chio and close to a bright source, therefor it could be a false detection due to detector chips at the edge of the chip, but the SNR is of 3.70.

# 4.4   Merging XMM-Newton and Chandra observations

In the Figures 4.14, we plot all three X-ray observations of HESS J1626-490 and also the TeV HESS contours with the aim of having a better idea of which X-ray sources could be a good candidate for the counterpart, on both with and without the energy cut showing the sources dominated by non-thermal emission.
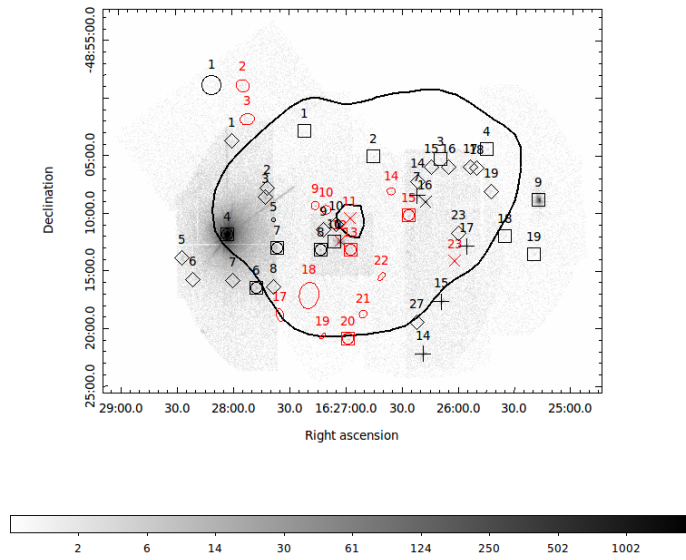
(a) Merged of the three X-ray observations we used to study HESS J1626-490 considering the whole energy range.
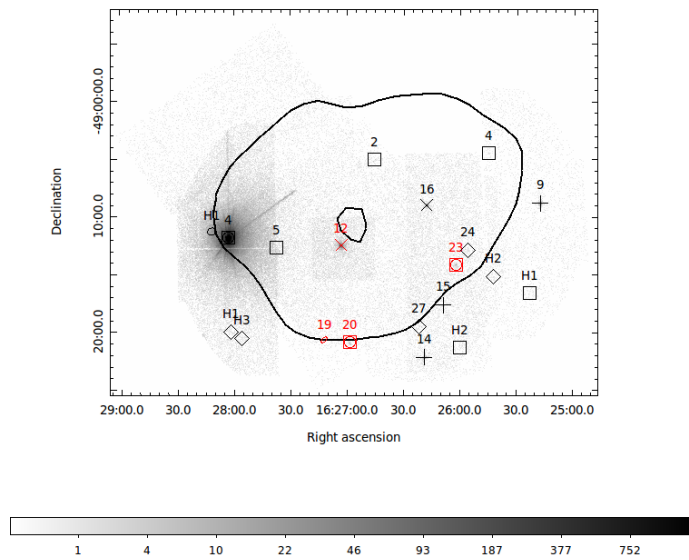


(b) Merged of the three X-ray observations we used to study HESS J1626-490 considering the energy range 2.5 - 12 keV.

Figure 4.14: Merge of the four X-ray observations we analysed and were detailed earlier this chapter for HESS J1626-490. Description in the text.

In Figure 4.14 we can see as black squares the sources detected using XMM-Newton ObsID 0403280201, the black diamonds shows the sources detected with XMM-Newton ObsID 0741950101, the black cross point out the sources detected by both XMM-Newto observations, remaining the number of the first observation. The sources showed with an X indicates the ones detected by both XMM and the Chandra observations, remaining the number of the Chandra observation. The sources indicated as circle inside a box were detected by one of the XMM observations and the Chandra observation, the number of the Chandra observation remained. All the sources marked with color red were detected using `vtpdetect`, the black circles shows the sources detected using `celldetect` of Chandra. The signigicant contours of the HESS source was done by using the H.E.S.S. Galactic Plane Survey (HGPS)significance map with $R_c = 0.2°$, with $R_c$ the correlation radius. This radius defines the circular region over which quantity (e.g. $\gamma$-ray excess) is integrated (for more information see [8]).

## 4.5 Spectral Analysis

The spectrum of a source can give us information about the variation of its flux as function of its energy. In this section, we will carried out the spectral analysis of the sources which are more likely to be counterpart of HESS J1626-490 as found in each observation by both Chandra and XMM-Newton.

For doing the spectrum using the XMM-Newton tools, is necessary to set the regions of the source and the background, and for this, is important to measure the intensity of light as a function of radius (counts/arcsec$^2$), averaging over all the pixels in circular annuli by doing the radial profile, this was done using the `eradial` routine, which extract the radial profile of the source in an image and fits a point spread function to it. This will help us to know at what radius we have a point source, if we have and how big is

its extended emission, and to identify the background. The spectra were extracted using the SAS tasks:

- `evselect`: with the purpose of filter event list data and extracting images.

- `backscale`: this task calculates the area of a source region used to make a spectral file (to re-scale the region).

- `rmfgen`: corrects the instrumental effects specific to the event selection criteria used and writes the result to a specified dataset (the Redistribution Matrix File or RMF) which describes the response of the instrument as a function of energy and PI channel, i.e., changes channels of the telescope to energy.

- `arfgen`: generates the ancillary response file (ARF), takes calibration information provided by the CAL, performs the necessary corrections for instrumental factors depending on the user's requirements, and the state of spectral data, and formats the output. The ARF in conjunction with the RMF can be used to allow fitting of particular spectral models against the observed spectral data.

- `specgroup`: groups the channels in a spectrum. Channels can be defined as BAD (i.e. not to be used) either by using definitions from a calibration file or by specifying the channels or energy range to exclude on the command line.

In the other hand, for the Chandra software, we used a script called `specextract`, which automates the steps for extracting the spectrum for extended and point-like sources observed with the ACIS detector, for this is necessary to extract the regions on the event file, saving separate region files for both source and background. `specextract` runs the following tools:

- `dmextract`: to extract source and (optionally) background spectra. The tool creates the WMAP used as input to `mkacisrmf`.

- `mkarf`: to create ARF(s).

- `arfcorr`: to apply and energy-dependent point-source aperture correction to the source

ARF file.

- `mkrmf` o `mkacisrmf`: to build the RMF(s), depending on which is appropriate for the data and the calibration.

- `dmgroup`: to group the source and/or background spectrum. - `dmhedit`: to update the BACKFILE, RESPFIL and ANCRFILE keys in the source and background spectrum files.

For fitting the spectra we used the XSPEC spectral-fitting package [165], which is designed to be completely detector-independent so that it can be used for any spectrometer.

### 4.5.1   Spectral analysis of source 9, ObsID 0403280201

Once we have the clean image file, we can obtain a radial profile, and to do this, first, we study the region by placing the circle in the center of the source at the brightest pixel (in this case 542 coutns for MOS1 located at coordinates R.A. = $16^h25^m17^s.444$, decl. = $-49°08'52".41$), and we used the `eradial` task to plot the results can be seen in the Figure 4.15.

From the radial profile we can see that, moving away from the beginning, it falls rapidly and then gets a constant, having a very similar behaviour to a Point Spread Function (PSF, see Figure 4.15(a)), from this, we can say that this is a point source, and we can define the regions: from 0-45" we have the source, and after we have background.

The spectrum was obtained using a circular region centred on the point source at R.A. = $16^h25^m17^s.453$, decl. = $-49°08'52".52$ with 45" radius aperture, and a circular region located at R.A. = $16^h25^m26^s.710$, decl. = $-49°03'33".70$ of 140" aperture placed on the left upper of the source region in the same CCD for the source of background. This source spectrum was fitted using a the abs*(mekal+pow) model [7].

Fitting the model result a description of the data with a reduced $\chi^2$ = 1.582 for 62

---

[7]The model "mekal" in XSPEC [166]
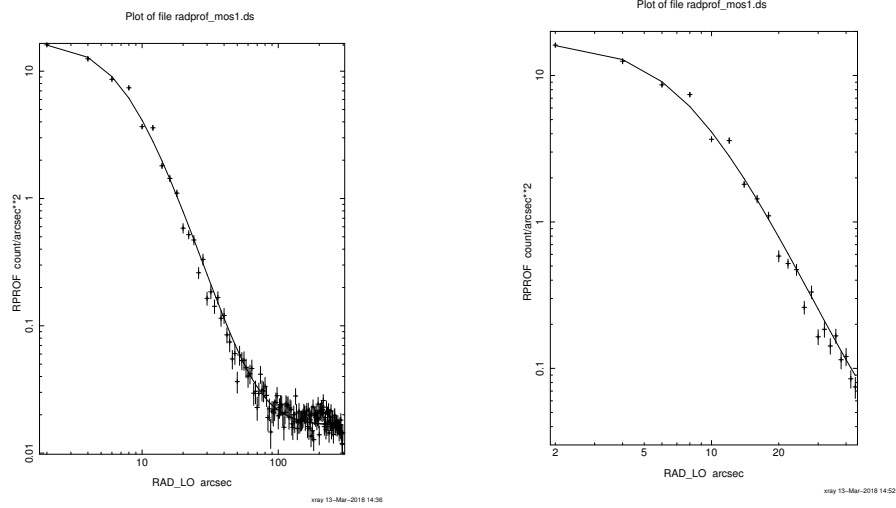
(a) Radial profile of up to 300 arcsec.

(b) Radial profile of up to 45 arcsec.

Figure 4.15: Radial profile of brightest source (number 9) of ObsID 0403280201, using EPIC-MOS1 instrument with a PSF fitted.

degrees of freedom (dof). The spectrum has a photon index $\Gamma$ = 2.63 $\pm$ 0.1, an absorption of $N_H$ = (5.7 $\pm$ 0.1) $\times$ $10^{20}$, a normalization at 1 keV = (15.5 $\pm$ 1) $\times$ $10^{-4}$ keV$^{-1}$ cm$^2$ s$^{-1}$, and a plasma temperature $kT$ = 0.6 $\pm$ 0.01 keV asumming a metal abundance $Abundance$ = 1 (frozen), a redshift $z$ = 0.0 (frozen), a Switch = 1 (interpolate, frozen). The Galactic absorption in the direction of this source is $N_H$=1.72 $\times$ $10^{22}$ cm$^{-2}$ (LAB survey [8], [167]). The resulting flux is $F$ (2-10 keV) = (8.15 $\pm$ 1.1) $\times$ $10^{-13}$ erg cm$^{-2}$ s$^{-1}$ and the absorption corrected flux is $F_{unabs}$ (2-10 keV) = 8.75 $\times$ $10^{-13}$ erg cm$^{-2}$ s$^{-1}$. The result can be seen on Figure 4.16.

## 4.5.2 Spectral analysis of source 11, ObsID 0403280201

This source has 33 counts as the brightest pixel with coordinates R.A. = $16^h27^m03^s$.118, decl. = -49°12'33".35. For the analysis, I did first the radial profile considering as the centre of the source the brightest pixel, and considering a circular region with diameter

---

[8]http://heasarc.gsfc.nasa.gov/cgi-bin/Tools/w3nh/w3nh.pl
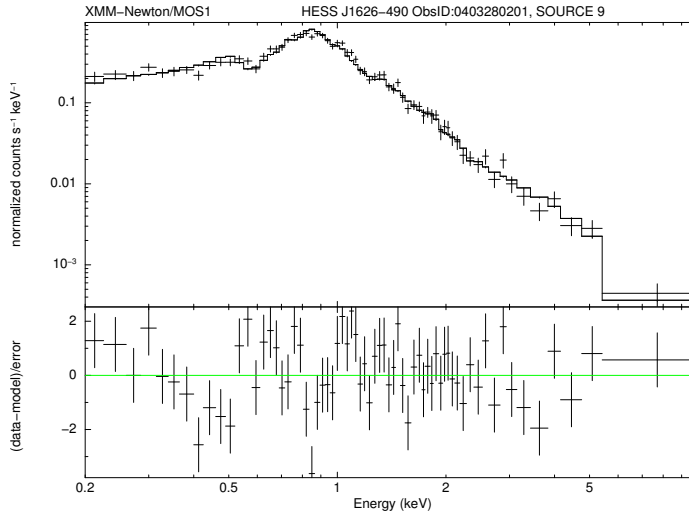
Figure 4.16: Spectrum of the source number 9 (ObsID 0403280201), fitted to the model described in the text. The lower panel shows residuals from the best fit in units of $1\sigma$.

of 17".5. In Figure 4.17 we can see the radial profile obtained.

Where we can identify the regions:

From 0-20 arcsec we have the source. From 20- the background.

Now we can obtain the spectrum of the source using the same circular region as in the radial profile, with 20" radius aperture, and a circular region located at R.A. = $16^h27^m19^s.499$, decl. = -49°13'41".44 from 100" aperture placed on the left lower of the source region on the same CCD. Fitting a power-law model result a description of the data with a reduced $\chi^2$ = 1.8 for 50 dof. The spectrum has a photon index $\Gamma$ = -1.0 $\pm$ 0.2, the absorption was fixed as found in the direction of the source is $N_H$ = 1.68 $\times$ 10$^{22}$ by LAB survey [9], [167], and normalization at 1 keV = (5.2 $\pm$ 1.5) $\times$ 10$^{-6}$ keV$^{-1}$ cm$^2$ s$^{-1}$. The resulting flux is $F$ (2-10 keV) = (2.7 $\pm$ 0.5) $\times$ 10$^{-12}$ erg cm$^{-2}$ s$^{-1}$ and the absorption corrected flux is $F_{unabs}$ (2-10 keV) = 2.8 $\times$ 10$^{-12}$ erg cm$^{-2}$ s$^{-1}$. The result can be seen

---

[9] http://heasarc.gsfc.nasa.gov/cgi-bin/Tools/w3nh/w3nh.pl

Plot of file radprof_src11.ds
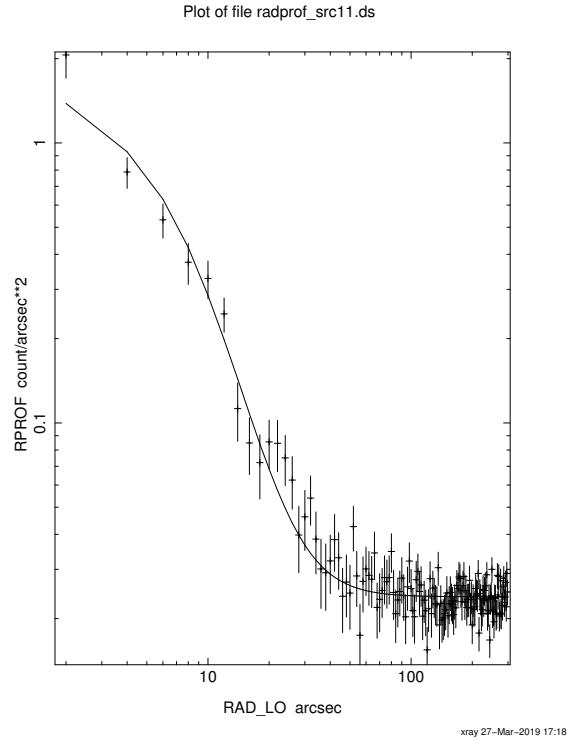


Figure 4.17: Radial profile of source 11 of ObsID 0741950101 using EPIC-MOS1 instrument, with a PSF fitted.

on Figure 4.18.

### 4.5.3 Spectral analysis of source 19, ObsID 0403280201

This source has as brightest pixel 4 counts with physical coordinates R.A. = $16^h25^m19^s.837$, decl. = -49°13'36".80, which was the center of the region for doing the radial profile, and I considered a circle of 12".

From the radial profile we can see the source region is up to 5 arcsec, and after that we have background. Considering this, a spectrum of the point source was extracted using a circular region centred on the point source with coordinates R.A. = $16^h25^m19^s.779$, decl. = -49°13'36".71 of 5" radius aperture, and a circular region located at R.A. =
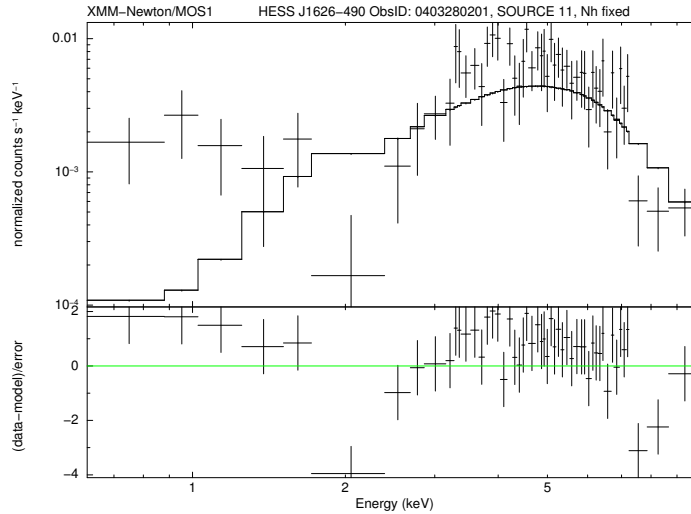
Figure 4.18: Spectrum of source number 11 (ObsID 0403280201) fitted of to the power-law model described in the text. The lower panel shows residuals from the best fit in units of $1\sigma$.

$16^h25^m04^s.075$, decl. = -49°11'42".62 of 50" aperture placed on the right upper of the source region in the same CCD for the source of background. To extract the spectrum, and running the script `specgroup` there is one parameter called `mincounts` which we can define the minimum number of counts regrouped per channel, i.e., the spectrum is rebinned in order to have at least # counts for each background-subtracted spectral channel. For the case of $mincounts$ = 4, I obtained: fitting a power-law model result in a good description of the data with a reduced $\chi^2$ = 0.8 for 1 dof. The spectrum has a photon index $\Gamma$ = 3.1 $\pm$ 1.1, an absorption of $N_H$ = 9.4 $\times 10^{12}$ $\pm$ -1.0, and normalization at 1 keV = (1.1 $\pm$ 0.4) $\times 10^{-5}$ keV$^{-1}$ cm$^2$ s$^{-1}$. The Galactic absorption in the direction of this source is $N_H$=1.72 $\times 10^{22}$ cm$^{-2}$ (LAB survey [10], [167]). The flux neither the absorption corrected flux were not obtained due to the very faint source. The spectrum can be seen on Figure 4.20(a).

---

[10]http://heasarc.gsfc.nasa.gov/cgi-bin/Tools/w3nh/w3nh.pl
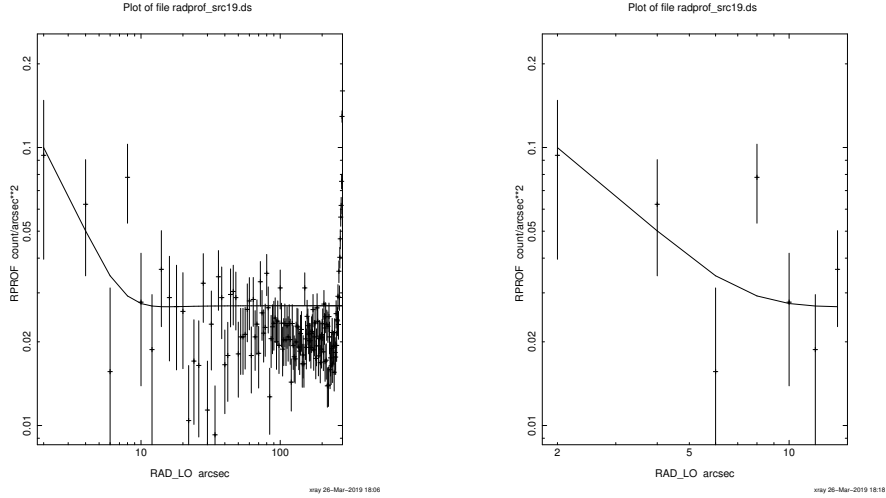
(a) Radial profiel obtained using MOS1 instrument f source 19 of ObsID 0403280201.

(b) Radial profiel obtained using MOS1 instrument f source 19 of ObsID 0403280201, up to 15".

Figure 4.19: Radial profile of source number 19, ObsID 0403280201, using EPIC-MOS1 instrument, with a PSF fitted..

Using a minimum count of `mincounts = 1` in the `specgroup` command, I obtained: a reduced $\chi^2$ = 0.9 for 7 dof, with a photon index $\Gamma$ = 4.8 $\pm$ 2.6, the absorption was fixed with the value provided by LAB survey [11], [167] of $N_H$ = 1.72 $\times$ $10^{22}$, and normalization at 1 keV = (1.2 $\pm$ 1.5) $\times$ $10^{-4}$ keV$^{-1}$ cm$^2$ s$^{-1}$.

The resulting flux is $F$ (2-10 keV) = (2.3 $\pm$ 3.9) $\times$ $10^{-16}$ erg cm$^{-2}$ s$^{-1}$ and the absorption corrected flux is $F_{unabs}$ (2-10 keV) = 3.9 $\times$ $10^{-16}$ erg cm$^{-2}$ s$^{-1}$. The result can be seen on Figure 4.20(b).

### 4.5.4 Spectral analysis of source 4, ObsID 0741950101

This source is the brightest of the observation (see Figue 4.10), it has 4649 counts as the brightest pixel, with coordinates R.A. = $16^h28^m03^s$.023, decl. = -49°11'45".55. We plotted the radial profile with the center in this coordinates and we considered a diameter

---

[11]http://heasarc.gsfc.nasa.gov/cgi-bin/Tools/w3nh/w3nh.pl
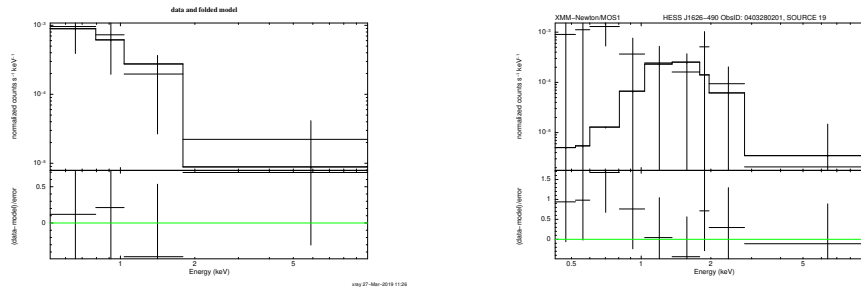
(a) XMM-Newton EPIC MOS1 spectrum of source 19 of ObsID 0403280201, using `mincounts = 4`.

(b) XMM-Newton EPIC MOS1 spectrum of source 19 of ObsID 0403280201 cosidering `mincounts = 1`.

Figure 4.20: Spectra of source number 19 (ObsID 0403280201) fitted to the model described in the text. The lower panel shows residuals from the best fit in units of $1\sigma$.

of 30". In Figure 4.21 we can see the radial profile obtained.

From the plot we can see that there is a clear excess, and we can conclude the source is extended. A spectrum of the point source was extracted using a circular region centred on the point source at coordinates R.A. = $16^h28^m03^s.25$, decl. = -49°11'45".49 with 12" radius aperture, and a circular region located at R.A. = $16^h27^m47^s.984$, decl. = -49°05'24".25 of 75" aperture placed on the right upper of the source region in the same CCD for the source of background. Fitting a power-law model result in a description of the data with a reduced $\chi^2$ = 8.7 for 173 dof. The spectrum has a photon index $\Gamma$ = 1.5 $\pm$ 0.02, an absorption of $N_H$ = (9.0 $\pm$ 0.1) $\times$ $10^{22}$, and normalization at 1 keV = (92 $\pm$ 4.1) $\times$ $10^{-3}$ keV$^{-1}$ cm$^2$ s$^{-1}$.

The Galactic absorption in the direction of this source is $N_H$=1.69 $\times$ $10^{22}$ cm$^{-2}$ (LAB survey [12], [167]). The resulting flux is $F$ (2-10 keV) = (3.3 $\pm$ 0.04) $\times$ $10^{-10}$ erg cm$^{-2}$ s$^{-1}$ and the absorption corrected flux is $F_{unabs}$ (2-10 keV) = 5.3 $\times$ $10^{-10}$ erg cm$^{-2}$ s$^{-1}$. The result can be seen on Figure 4.22.

The source spectrum seems to be affected by the pileup effect which happens for

---

[12]http://heasarc.gsfc.nasa.gov/cgi-bin/Tools/w3nh/w3nh.pl

Plot of file radprof_1626_074mos1_src4.ds
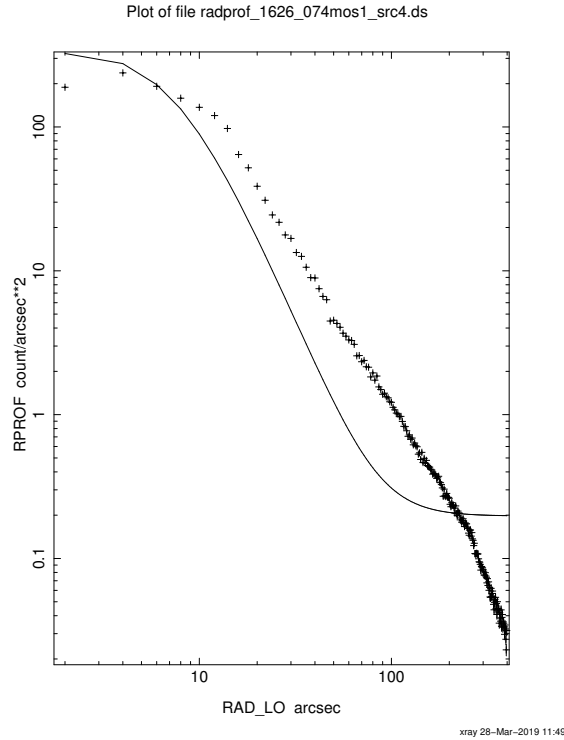


Figure 4.21: Radial profile of source 4, ObsID 0741950101, using EPIC-MOS1 instrument, with a PSF fitted.

very bright sources, which changes the spectrum and can also affect the count rate at the center of the source. Therefore the counts at the center in the radial profile are lower and the PSF does not fit well, and the spectrum cannot be well fitted with the power law.

## 4.5.5  Spectral analysis of source 13, ObsID 0741950101

From the Figure 4.10, we can see there is a source on the center of the MOS detectors, which is the number 13. This source was found to be at coordinates R.A. = $16^h27^m03^s$.050, decl. = -49°12'35".17 and has as brightest pixel 183 counts. To study it in more detail, we made a radial profile, the result can be seen in Figure 4.23(a).

From 4.23(b), we see that the fit is not well adjusting the data, so we changed the
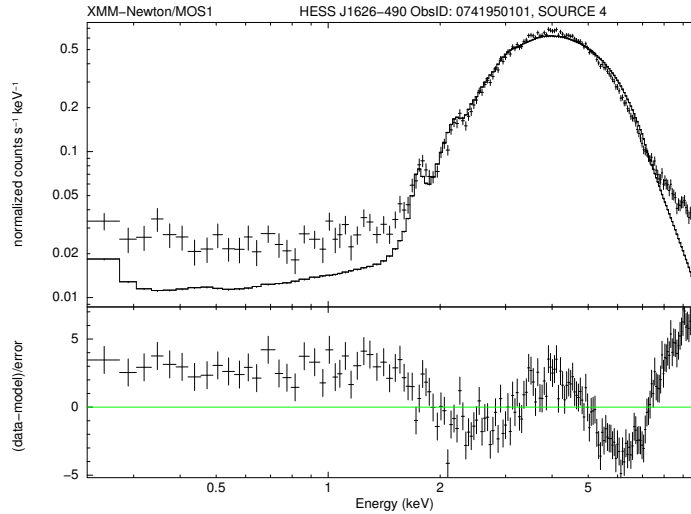
Figure 4.22: Spectrum of source number 4 (ObsID 0741950101) fitted to model described in the text. The lower panel shows residuals from the best fit in units of $1\sigma$.

maximum radius (to 120) used in the program `eradial` to take into account the size of the Large Window Mode. The resulting radial profile was fit with a PSF, see Figure 4.23. Furthermore, as can be seen from the clean image obtained, the source is close to the border of the chip due to the Small Window mode of the observation, so the region of 300 arc sec go over the the size of the observation mode, and therefore the number of counts is decreasing above $\sim$120 arcsec (edge of the Small Window mode). There are some points over the middle of the PSF, which it has to be carefully study in the future with a spectral analysis.

Form Figure 4.23(b) we can see that there is an excess from 20 to 50 arcsec, from 12 to 20 arcsec the region could be dominated by the source due to closeness, and from 0 - 10 we have the source.

A spectrum of the point source was extracted using a circular region centred on the point source with coordinates R.A. = $16^h27^m03^s$.262, decl. = -49°12'34".39 with

(a) Radial profile of up to 300 arcsec.   (b) Radial profile of up to 120 arcsec.
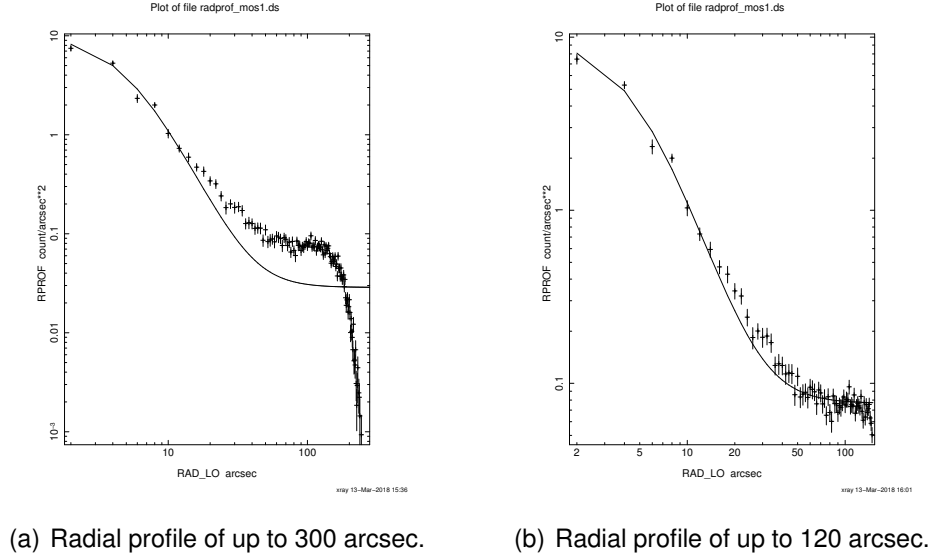
Figure 4.23: Radial profile of source source 13 with a PSF fitted.

12" radius aperture, and a circular region located at R.A. = $16^h27^m47^s$.984, decl. = -49°14'16".01 of 75" aperture placed on the right lower of the source region in the same CCD for the source of background. Fitting a power-law model result in a good description of the data with a reduced $\chi^2$ = 0.9 for 47 dof. The spectrum has a photon index $\Gamma$ = 1.1 $\pm$ 0.2, an absorption of $N_H$ = (14.1 $\pm$ 1.5) $\times$ $10^{22}$, and normalization at 1 keV = (4.4 $\pm$ 1.8) $\times$ $10^{-4}$ keV$^{-1}$ cm$^2$ s$^{-1}$. The Galactic absorption in the direction of this source is $N_H$=1.68 $\times$ $10^{22}$ cm$^{-2}$ (LAB survey [13], [167]). The resulting flux is $F$ (2-10 keV) = (2.7 $\pm$ 0.3) $\times$ $10^{-12}$ erg cm$^{-2}$ s$^{-1}$ and the absorption corrected flux is $F_{unabs}$ (2-10 keV) = 4.7 $\times$ $10^{-12}$ erg cm$^{-2}$ s$^{-1}$. The result can be seen on Figure 4.24.

### 4.5.6   Spectral analysis of source 4, ObsID 13287

From the image 4.12 we can see this source is the brightest, with the maximum of counts to be 5181 and coordinates R.A. = $16^h28^m02^s$.671, decl. = -49°11'50".48. I extracted

---

[13]http://heasarc.gsfc.nasa.gov/cgi-bin/Tools/w3nh/w3nh.pl
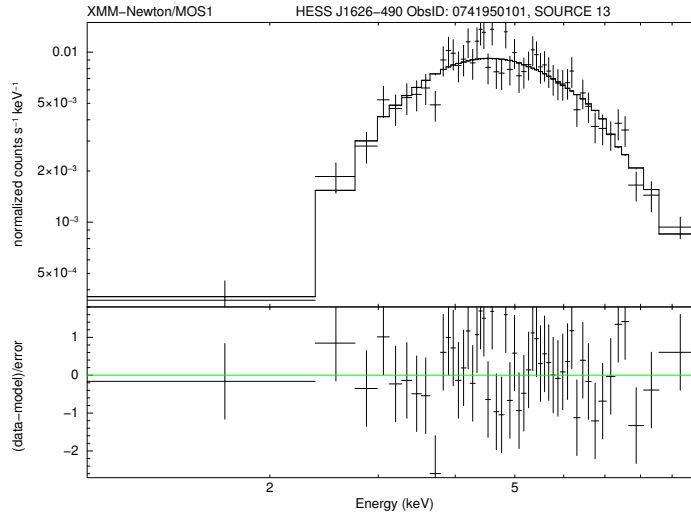
Figure 4.24: Spectrum of source number 13 (ObsID 0741950101) fitted to model described in the text. The lower panel shows residuals from the best fit in units of $1\sigma$.

the spectrum using the `specextract` script. In this case, a spectrum of the point source was extracted using a circular region centred on the point source with coordinates R.A. = $16^h28^m02^s.595$, decl. = -49°11'50".85 with 65" radius aperture, and a circular region located at R.A. = $16^h27^m25^s.220$, decl. = -49°12'10".44 of 80" aperture placed on the right lower of the source region in the same CCD for the source of background. Fitting a power-law model result in a good description of the data (see the Figure 4.25), with a reduced $\chi^2$ = 1.9 for 484 dof. The spectrum has a photon index $\Gamma$ = 0.9 ± 0.02, an absorption of $N_H$ = (7.7 ± 0.1) × $10^{22}$, and normalization at 1 keV = (92.0 ± 3.2) × $10^{-3}$ keV$^{-1}$ cm$^2$ s$^{-1}$. The Galactic absorption in the direction of this source is $N_H$=1.6 × $10^{22}$ cm$^{-2}$ (LAB survey [14], [167]). The resulting flux is $F$ (2-10 keV) = (9.4 ± 0.1) × $10^{-10}$ erg cm$^{-2}$ s$^{-1}$ and the absorption corrected flux is $F_{unabs}$ (2-10 keV) = 1.3 × $10^{-9}$ erg cm$^{-2}$ s$^{-1}$. The result can be seen on Figure 4.25.

---

[14] http://heasarc.gsfc.nasa.gov/cgi-bin/Tools/w3nh/w3nh.pl
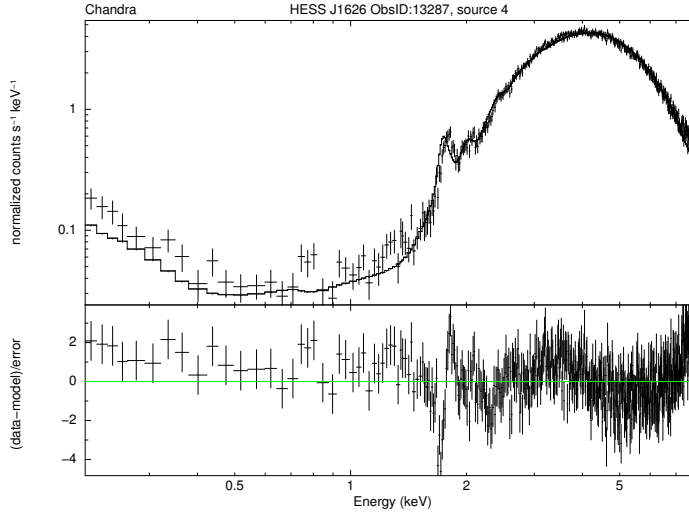
Figure 4.25: Spectrum of source number 4 (ObsID 13287) fitted to model described in the text. The lower panel shows residuals from the best fit in units of $1\sigma$.

### 4.5.7   Spectral analysis of source 12, ObsID 13287

A spectrum of the point source was extracted using a circular region centred on the point source with coordinates R.A. = $16^h27^m03^s.061$, decl.  = -49°12'32".77 with 9" radius aperture, and a circular region located at R.A. = $16^h26^m41^s.965$, decl. = -49°11'48".96 of 60" aperture placed on the right of the source region in the same CCD for the source of background. Fitting a power-law model result in a good description of the data with a reduced $\chi^2$ = 0.7 for 19 dof. The spectrum has a photon index $\Gamma$ = -0.2 $\pm$ 0.2, an absorption of $N_H$ = 1.8 $\times$ $10^{22}$, which was given by the LAB survey ([15], [167]), and normalization at 1 keV = (2.0 $\pm$ 0.8) $\times$ $10^{-5}$ keV$^{-1}$ cm$^2$ s$^{-1}$. The resulting flux is $F$ (2-10 keV) = (2.3 $\pm$ 0.6) $\times$ $10^{-12}$ erg cm$^{-2}$ s$^{-1}$ and the absorption corrected flux is $F_{unabs}$ (2-10 keV) = 2.4 $\times$ $10^{-12}$ erg cm$^{-2}$ s$^{-1}$. The result can be seen on Figure 4.26.

---

[15]http://heasarc.gsfc.nasa.gov/cgi-bin/Tools/w3nh/w3nh.pl
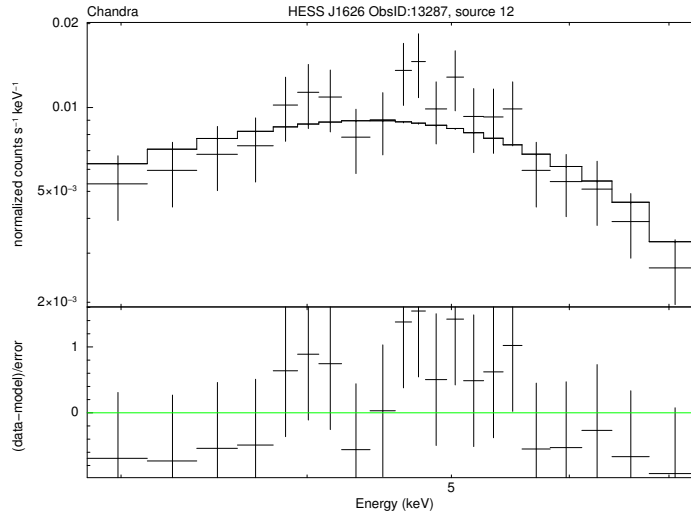
Figure 4.26: Spectrum of source number 12 (ObsID 13287) fitted to model described in the text. The lower panel shows residuals from the best fit in units of $1\sigma$.

## 4.6 Fermi Data Analysis

In [168] studies on $5°$ of the Galactic Plane were performed using 45 months of Fermi-LAT data for energies above 10 GeV with the aim of provide new constraints on PWNe properties and find new clues on the nature of unidentified gamma-ray sources. In this research, 30 sources were detected, however HESS J1626-490 was not, and upper limitis were established (Figure 5 from [168]), in the studies done by the *Fermi*-LAT collaboration. They used data collected from 2008 August 4 to 2012 April 18 and the Pass 7 Clean event class in the energy range of 10 - 316 GeV. This energy range was used in order to avoid systematics associated with the modelling of adjacent sources with soft spectra, and it also helps to reduce systematics associated with imperfect modelling of the Galactic diffuse emission. The maximum energy was picked in order to increase the overlap between the energy range covered by the LAT and thte VHE experiments.

Taking advantage of improvements in the understanding of the LAT and its orbital environment over the course of the mission, the event-level analysis software is periodically updated. New improvements released on 2015 June 24 were implemented on the version of the Fermi LAT data and the Fermi Science Support Center (FSSC) is now serving PASS 8, which is the one we use for the data analysis in this thesis.

In Figure 4.27 were plotted the P8R2_ SOURCE_ V6 (Pass 8 Release 2 Version 6 Instrument Rensponse Functions) integral flux sensitivity (red points) for ten years in 4 bins per energy decade between 31.6 MeV and 1 TeV, the differential flux sensitivity evaluated at different locations which can be found on the LAT Performance website http://www.slac.stanford.edu/exp/glast/groups/canda/lat_Performance.htm (assuming a point source with a power-law spectrum with index 2 and uniform background around it), and in orange, the data points of the SED for the source HESS J1626-490 obtained by H.E.S.S. collaboration [57], all this with the purpose of having a comparison with the upper limits from [168] (blue) and to have an idea of what we could expect of the analysis we will carried out.

From the plots, we can see that the data points of the sensitivity of Fermi are a bit closer to the model proposed in [59], which make this an interesting source for doing the Fermi analysis.

We use 10 years of data for the analysis, collected from 2008 August 4 to 2018 September 13 (Mission Elapsed Time (MET): 239557417 to 558548299) with an energy rage of 10 to 500 GeV and the search radius used was 30 degrees round the position of the HESS source. According to the data server, I got 9 photons file, PH00 got 47097 events, PH01 got 25508, PH02 got 54722, PH03 got 43794, PH04 got 54374, PH05 got 43928, PH06 got 44395, PH07 got 41314, and PH08 got 38645 events.

All the data was plotted on the Figure 4.28.

From the plot 4.28 we can see that there were some times in there when the LAT
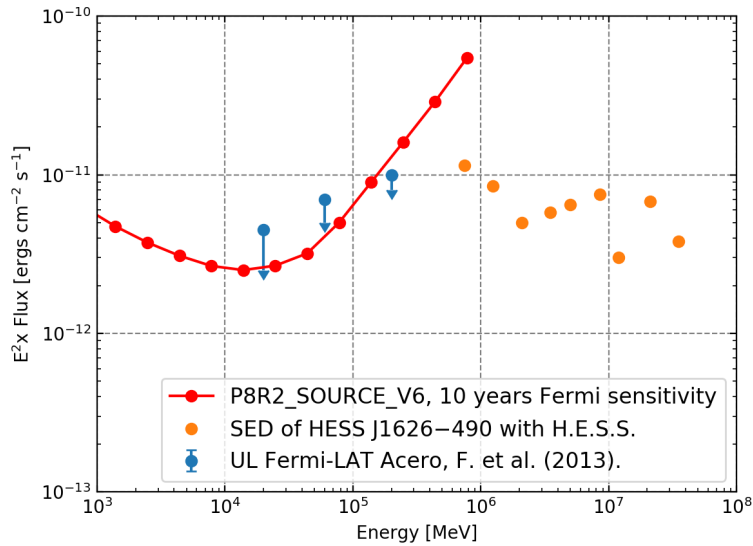
Figure 4.27: Fermi LAT P8R2_ SOURCE_ V6 integral flux sensitivity (red), HESS J1626-490 SED measured by H.E.S.S. [57] (orange) and upper limits obtained by the LAT collaboration [168] (blue).

data quality was less than perfect. We'll need to filter these and figure out which of the events we want to keep. For this and for all the $\gamma$-ray analysis, in our studies we used the python software package *Fermipy* (hosted on GitHub[16]), that facilitates analysis of Fermi LAT data. This software is based on the Fermi ScienceTools, the free software suite provided by NASA for the LAT mission which is primarily written in C++ but includes the python interface named as `pyLikelihood` with the aim of facilitate scripting analysis in python. Fermipy uses `pyLikelihood` to interface with the underlying C++ library. The installation of the packages was done via DockerHub, with a Docker container pre-loaded with many of the necessary tools required for doing Fermi Analysis, including the Fermi Science Tools, the Heasarc Ftools, Python 2.7 an associated libraries along with a host of other programs (see https://github.com/fermi-lat/FermiBottle/wiki/Instructions-for-running-FermiBottle-on-MacOS).

---

[16]https://github.com/Fermipy/fermipy.
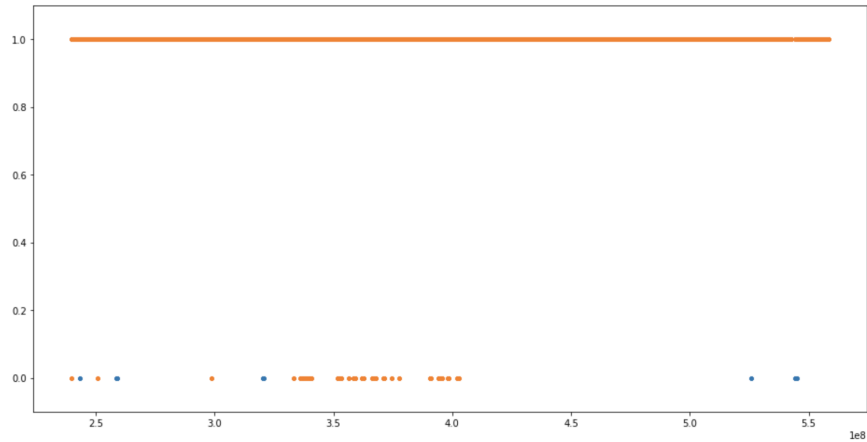
Figure 4.28: All our Fermy data, we can see that not all the data has good quality.

Fermipy was designed around the global analysis object known as GTAnalysis that manages the data and model preparation and provides a set of high-level analysis methods. The package uses a configuration-file that the user needs to prepare according to the needs of its research, and are defined analysis parameters that includes the data selection, Region of Interest (ROI) geometry and model specification. This file has a hierarchical organization that groups parameters into separate dictionaries keyed to a section name (e.g. dta, binning and selection), the format that Fermipy uses for the configuration file is the YAML to read and write in a persistent format.

The configuration file that it used for my analysis of the HESS J1626-490 source can be seen in Figure 4.29, and each section is described below.

In the data section the events and spacecraft files (input data files) are specified with the names of the files for the analysis, for this case, we also add the ltcube fits file, which was precomputed directly using the ST. For the binning section, which control the spatial and spectral binning of the data, we used a roiwidth of 10.0 degrees, even though the suggested ROI for analysis of sources dominated by ~1 GeV events is 15 degrees. The reduction of the size was for decreasing the number of sources due to we are analysing a region close to the galactic plane. The binsz is the spatial bin size in degrees, i.e.

```
data:
  evfile : events.txt
  scfile : SC00.fits
  ltcube : ltcube.fits

binning:
  roiwidth   : 10.0
  binsz      : 0.1
  binsperdec : 8

selection :
  emin : 10000
  emax : 500000
  zmax    : 90
  evclass : 128
  evtype  : 3
  tmin    : 239557417
  tmax    : 558548299
  filter  : null
  glon : 334.7702
  glat : 0.0473
  #target : '3FHL J1626.3-4915'

gtlike:
  edisp : True
  irfs : 'P8R2_SOURCE_V6'
  edisp_disable : ['isodiff','galdiff']

model:
  src_roiwidth : 15.0
  galdiff  : '/data/fermi-summer-school/Likelihood_Advanced/data/gll_iem_v06.fits'
  isodiff  : 'iso_P8R2_SOURCE_V6_v06.txt'
  catalogs : ['gll_psch_v13.xml']
  #catalogs : ['gll_psc_v16.fit']

components:
  - { selection : { evtype : 4  } } # PSF0
  - { selection : { evtype : 8  } } # PSF1
  - { selection : { evtype : 16 } } # PSF2
  - { selection : { evtype : 32 } } # PSF3

fileio:
  outdir : data
```

Figure 4.29: Configuration file used for the analysis. In this, the parameters for the analysis are defined.

the number of degrees per pixel at the center of the image, in this case we selected 0.1 degrees for the size. For the binsperdec, which is the number of energy bins per decade, we selected the standard number of 8.

The selection section gather the parameters of data selection and target definition. In this case, we selected the energy range of 10 - 500 GeV (emin - emax) to avoid systematics related with the modelling of adjacent sources with soft spectra. The maximum zenith angle (zmax) cut helps to exclude photons originating from the Earth's limb, the chosen was 90 degrees. The event class selection for the analysis was the *source* class

designated for the LAT collaboration as evclass=128, and the event type selection was evtype=3, which means we are selecting FRONT and BACK event types. The time of the observation is also defined in this section, for the analysis we used data collected from 2008 August 4 15:43:36, which is the time when the telescope start collecting the data, to 2018 September 13 16:18:14 (MET: 289557417, 558548299). The filter is another option in the section, which is a filter string for gtmktime selection, in our case we did the filter null. For selecting the target, starting with the analysis, we use the 3FHL J1626.3-4915 source, because the 3FHL catalog is the catalog most updated for high-energy sources, it includes data of 7 years of observation and this source is the closest to the HESS J1626-490 source and could be related.

Other section is the *gtlike*, where the control of the setup of the likelihood analysis is established. We used three parameters in this section, edisp, edisp_disable and irfs. With the edips as True, we enable the correction for energy dispertion, and in the other hand, the parameter edisp_disable provide a list of sources for which the edsip correction should be disabled. The Instrument Response Functions (irfs) that we used is the P8R2_SOURCE_V6 IRF which provide the current description of the instrument response for the P8R2 source data release.

For the case of the model section, its purpose is to collect options that rule the inclusion of point-source and diffusce components in the model. For this analysis we setup a ROI width of the source (src_roiwidth) of 15.0 degrees, this parameter states the width of a square region centered on the ROI that selects sources for inclusion in the model. After that, the parameters galdiff and isodiff set the templates for the Galactic Interstellar Emission Models (IEM) and isotropic diffuse respectively. The galdiff sets the path to one or more galactic IEM mapcubes, for isodiff, it sets the path to one or more isotropic templates. In the Catalog section, the catalog which will be used is defined. In this case the Third Fermi-LAT Catalog of High-Energy Sources (3FHL).

The *components* section consist of a list of dictionaries with the same hierarchy as the root analysis configuration. Each line of the list is to define analysis configurations for independent sub-selection of data. The one we used for the analysis defines a joint analysis with four PSF event types as showed previously.

The last section we used was *fileio*, in which are collected the options related to file bookkeeping. The outdir option indicates the root directory of the analysis where all the outpu files will be written, in this case, we use a folder called 'data'.

Once the configuration file was done, its path is passed to the analysis object constructor, so the analysis is executed by creating an instance of GTAnalysis with the config file as its argument. GTAnalysis provides methods to add or remove sources from the model, to fix or free parameters, and to perform a fit to the ROI, also it is used as an envelope over the underlying pyLikelihood classes. After the GTAnalysis initiated, we can run the `setup()` method, which is the one that performs the data preparation and response calculations as selection of the data (gtselect), creation of counts and exposure maps (gtexpcube2), among others needed for the analysis. This could be the slowest step in the analysis depending on the data selection and binning of the analysis chosen. It is recommended tu run the `optimize()` method before any other analysis method, this will loop over all model components in the ROI and fit their normalization and spectral shape parameters, and it also will compute the TS of all sources which can be used in the future to identify sources that could be fixed or deleted from the model. The results can be checked by calling the tool `print_roi()`.

Some sources will result with a $\sqrt{TS} < 3$ and hence without a clear detection. The sources with $\sqrt{TS} > 3$ will be removed from the further analysis to make the model simpler. Furthermore, all the models parameters are initially fixed by default, to free them we use the `free_source()` and `free_sources` methods to free the parameters of the model or also to fix them (using the parameter free = False). In our analysis we

free the normalization of catalog sources within 5 degrees of the ROI center, the sources with $TS > 10$ and all the parameters of isotropic and galactic diffuse components.

To maximize the likelihood with respect to the model parameters that are free, we executed a fit by calling `fit()` after freeing parameters of the model. We can write the results of the fitting with `write_roi`, this will write several output files to know the current status of the model. Once the model is optimized for the ROI, the `residmap()` and `tsmap()` methods can be used to evaluate the fit quality and look for new sources, but before it is necessary to fix the sources.

To check the modelling, and to see if we are doing everything right, we can create a residual map of our region. A residual map calculates the residual between smoothed data and model maps (it is just the left over counts after we've subtracted all of our modelled sources from the ROI.). It is useful for assessing the model goodness-of-fit due to it is sensitive to both positive and negative residuals. The plots 4.30 and 4.31 were obtained in our the analysis.
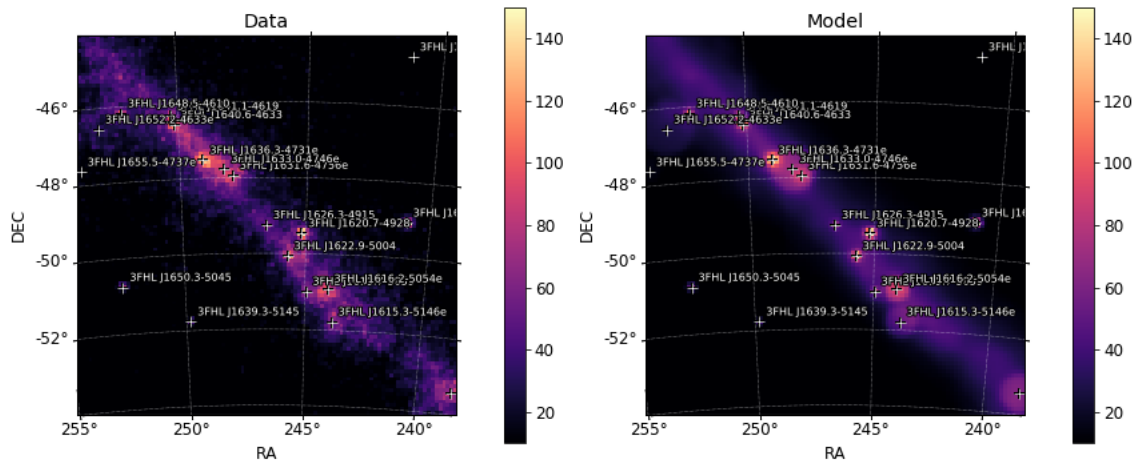


Figure 4.30: Counts map of the region around HESS-J1626-490. The crosses indicate the sources of the 3FHL catalog. Left: Data and Right: Model.
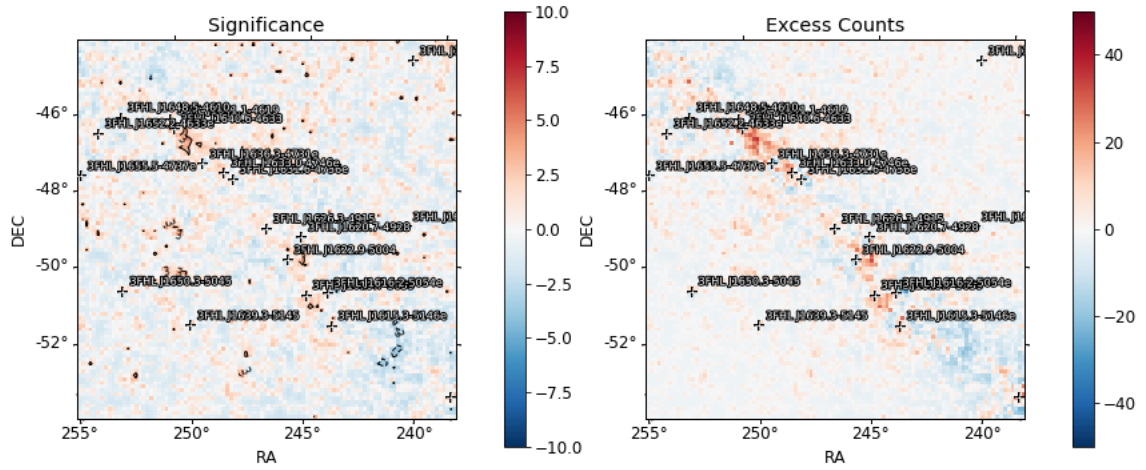
Figure 4.31: Left: Residual Significance Map, and Rigth: Excess Counts Map.

A test statistic map can be also generated, the obtained can be seen in Figure 4.32
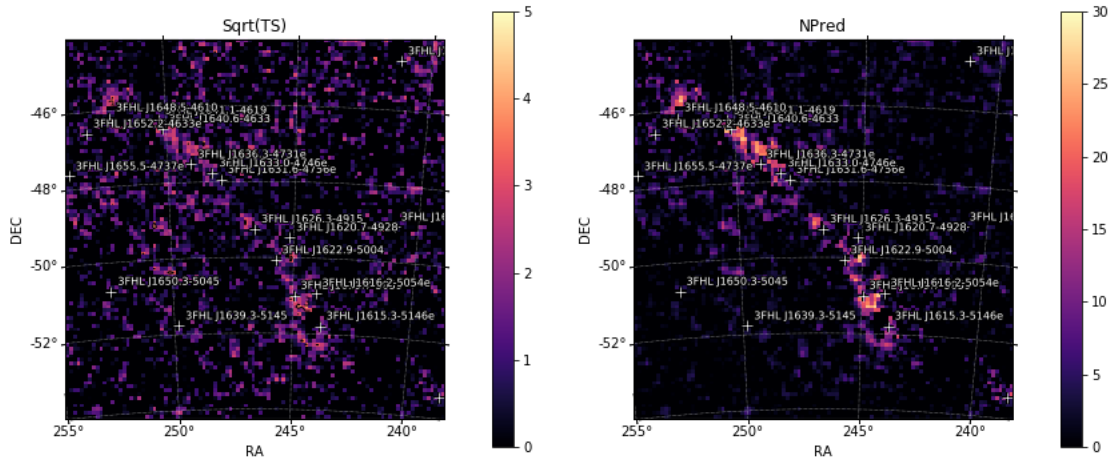


Figure 4.32: Left: Squared root of the TS Map, and Rigth: Number of Predicted Counts (NPred) Map.

**Advanced Analysis Methods**

There are many advanced analysis methods that can be done. To figure out if our source is extended and to know how big is it, we can use the `extension()` method. The source extension analysis is executed for a given source by computing a likelihood ratio test with respect to the point-source (no-extension) hypothesis and a best-fit model for extension. By performing a likelihood profile scan over the source width (68% containment) and fitting for the extension that maximizes the model likelihood is how the best-fit extension is found. Two models for extension are currently supported: a 2D Gaussian (*Radial-Gaussian*) or a 2D (*RadialDisk*). For the 3FHL J1626.3-4915 source we got a best-fit extension of 0.2391 + 0.0736 -0.0738 degrees with a TS = 4.326 which means very low statistics. The symmetric (1 sigma) error was $1\sigma$ = 0.0737 degrees.

In our analysis, the Spectral Energy Distribution (SED) is an important thing, which can help us to understand the nature of the HESS source. The `sed()` method computes a SED by fitting for the flux normalization of a source dividing it in energy bins. The normalization in each bin is fit independently using a power-law spectrum with a fixed index. The SED obtained can be seen on Figure 4.33.
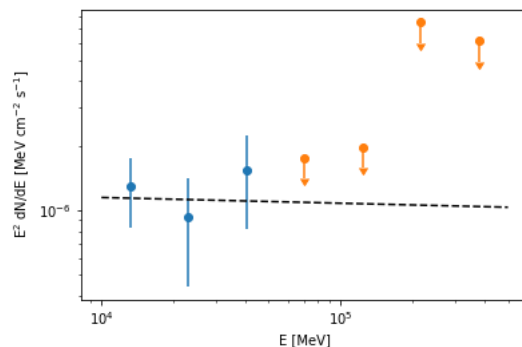


Figure 4.33: Spectral Energy Distribution of the 3FHL J1626.3-4915. The points with arrows are upper limits.

As we can see, the spectra is really flat. Comparing with the Figure 4.27, there are some differences in the spectra.

To have a better understanding of the source localization, we use the `localize()` method, which is used to spatially localize a source. Localization is done scanning the 2D likelihood surface in a local patch around the nominal source position, for more information about the procedure of the method see the Fermipy documentation[17]. The method pass the name of a source as its argument, and it returns a python dictionary with the best-fit position and localization errors and also save this information to the *localization* dictionary of the *Source* object. We used this method to find a better position of our source (see Figure 4.34), which resulted to be ( ra, dec) = ( 246.6061 +/- 0.0318, -49.2642 +/- 0.0337), (glon,glat) = ( 334.6838 +/- 0.0297, -0.1182 +/- 0.0355) offset = 0.0090 r68 = 0.0492 r95 = 0.0795 r99 = 0.0985, which is very close to the original position of the source.
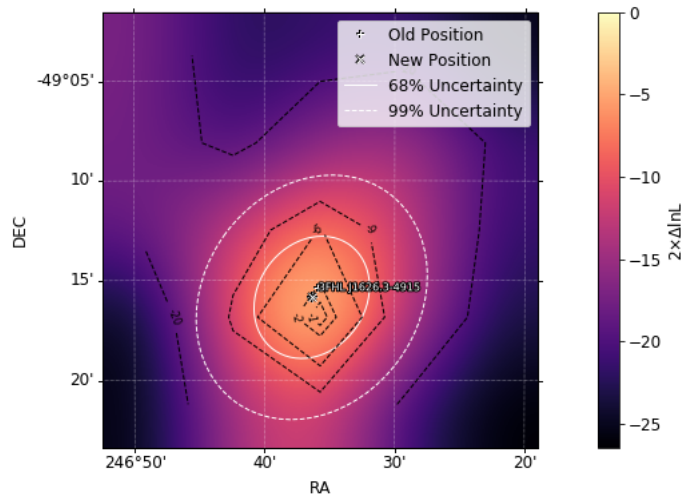


Figure 4.34: Source localization peak, the cross indicates the old position, and the $x$ the new position, the 68% of the uncertanty in the localization is indicated as a circle of a solid line and the 99% as a dotted line.

---

[17]https://fermipy.readthedocs.io/en/0.17.3/advanced/index.html

Once we have the best fit position, I did the extension method again, and I got the following results: Best-fit extension of 0.2367 + 0.0788 - 0.0646 degrees, the TS for the extension was: 4.125 (very low statistics), the 1 $\sigma$ error was 0.071 degrees. The SED was also obtained, as can be seen in the Figure 4.35
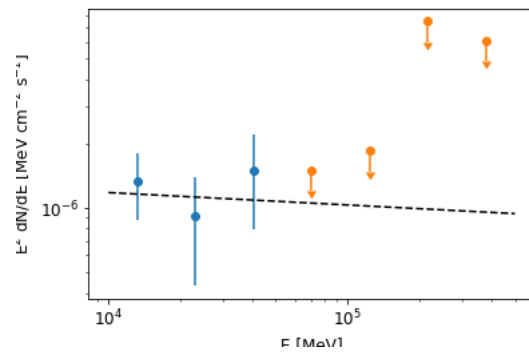


Figure 4.35: Spectral Energy Distribution for the best-fit localization of the 3FHL J1626.3-4915 source.

Comparing the SEDs from both the 3FHL source and the source localization, we can see that these two are very similar. With this and with all the other information, we can say that both can be the same source.

But, with all this analysis that we have described until the moment, can we say that the gamma-ray source is the same source than the HESS J1626-490? Fist, we have to analyse it. To do it, we can change the target in the configuration file, by putting directly the coordinates of HESS J1626-490 as: `glon : 334.7702, glat : 0.0473` [57].

Doing a similar analysis, we obtained the Residual Maps as seen in the Figure 4.36.
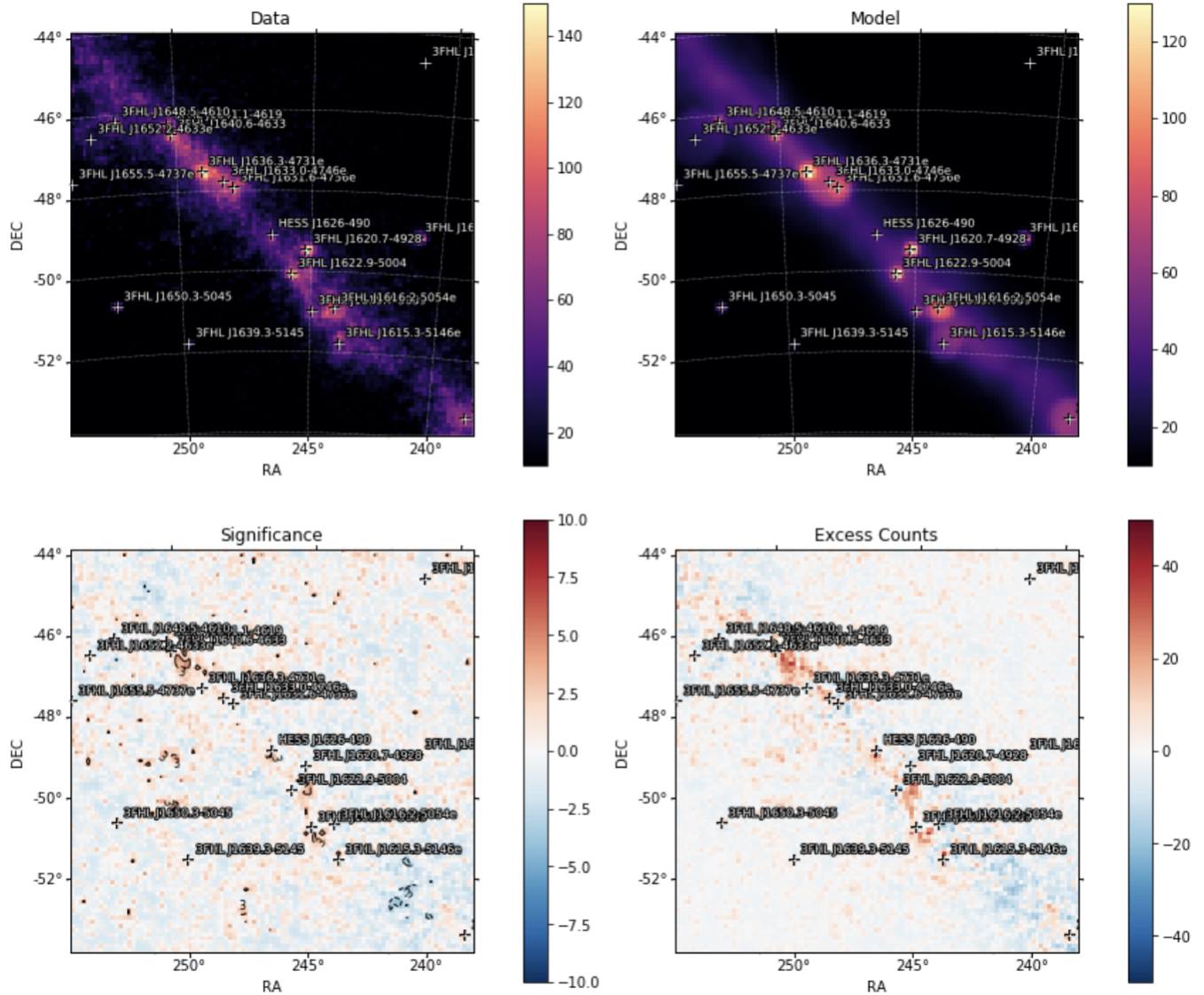
Figure 4.36: Counts map of the region around HESS J1626-490 (left: Data, right: Model). Residual Significance Map (left down) and Excess Counts Map (right down).

The TS map was also generated, see Figure 4.37.
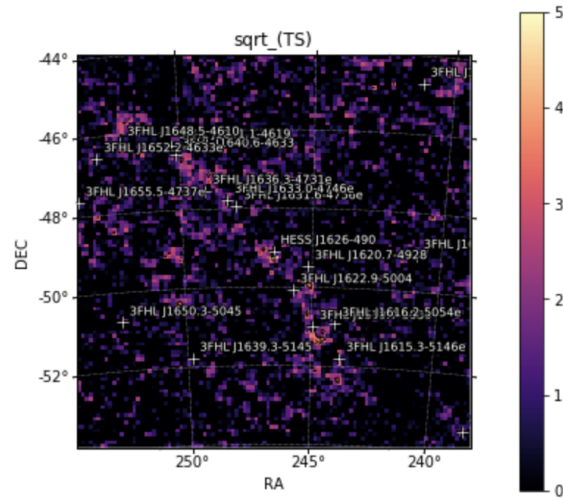
Figure 4.37: $\sqrt{TS}$ map for the HESS J1626-490 source.

The SED obtained for the source at the location of HESS J1626-490 is shown in Figure 4.38:
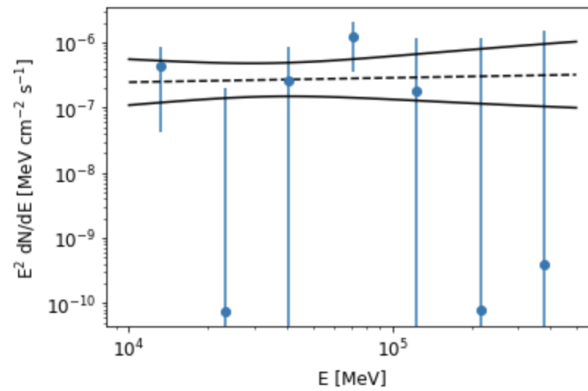


Figure 4.38: SED for the HESS J1626-490 source.

The TS values of the spectral data points are: first point has a TS = 1.48, the second TS = 0.33, the fourth TS = 3.73, the fifth TS = 0.09, for the rest the TS = 0. Therefore, upper limits are shown in the spectrum for HESS J1626-490. See Figure 4.39.
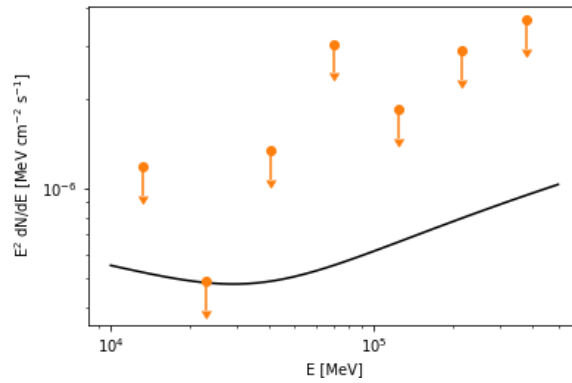
Figure 4.39: SED for the HESS J1626-490 source showing upper limits.

To have a better illustration of the work on Fermi analysis done, the Table 4.40 summarize the results obtained for both sources 3FHL J1626.3-4915 and HESS J1626-490.

| Model | TS | Npred | Glong | GLong_err | GLat | GLat_err | r68 | r95 | r99 | Extension | Extension_err | TS_ext |
|---|---|---|---|---|---|---|---|---|---|---|---|---|
| 3FHL J1626.3-4915 | 30.15 | 46.2 | 334.687 | | -0.11 | | | | | 0.2391 | 0.07 | 4.326 |
| SL 3FHL | 30.11 | 46.3 | 334.6838 | 0.0297 | -0.1182 | 0.0355 | 0.049 | 0.08 | 0.099 | 0.2309 | 0.07 | 4.044 |
| HESS J1626-490 | 1.93 | 10.8 | 334.77 | | 0.047 | | | | | 0.3255 | 0.07 | 22.193 |
| SL HESS | 24.1 | 100 | 334.8 | 0.072 | -0.1148 | 0.0491 | 0.09 | 0.145 | 0.18 | 0.2373 | 0.04 | 29.629 |

Figure 4.40: Table summarizing the results obtained for the analysis of the sources. SL for Source Localization.
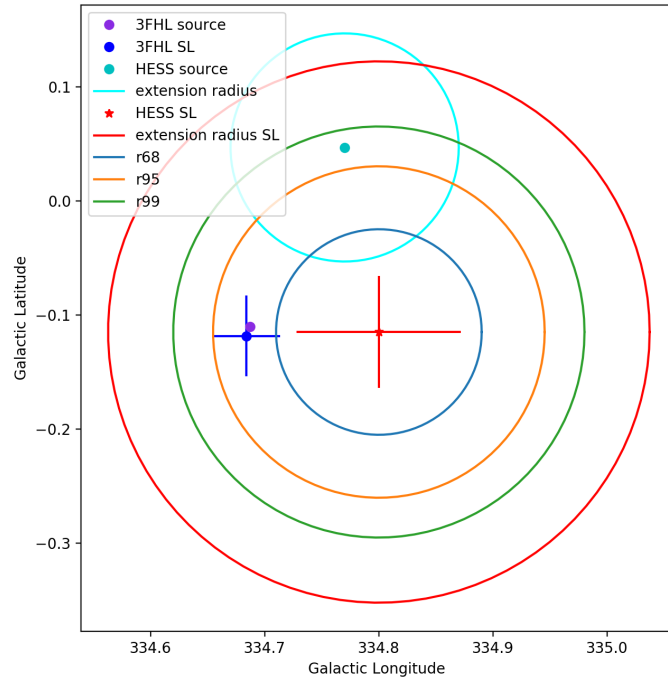
Figure 4.41: Localization of the two sources analized: 3FHL J1616.3-4915 and HESS J1626-490. In this image are also showed the best-fit localization for both sources and the extension radius as well as the error circles of the extension for the 3FHL source.

From the Figure 4.41 we can see that the two sources are within the positional un-certanties. When looking at the HESS position we are seeing a weak signal, that could means that LAT can not see a lot of emission at that position. In the Localization plot, the extension radius of the HESS source showed is 0.1 degree, however, a more exact posi-tion is given from [57], Source Extent: - semi-major axis: 0.07 +/- 0.02 deg - semi-minor axis: 0.10 +/- 0.05 deg - angle: 3 +/- 40 deg measured counter-clock relative to RA axis.

We have a stronger TS at the position outside the errorbar where the HESS position is, that might be an argument that the LAT emission is coming from a different source or maybe LAT is seeing a different part of that source than HESS.

175

## 4.7 Astrophysical Discussion and Conclusions

### X-ray analysis

In this chapter I showed the analysis I did on two XMM-Newton and one Chandra observations made in the region of TeV unidentified source HESS J1626-490. This analysis resulted in the following:

### XMM-Newton

- 19 sources were detected for ObsID 0403280201 considering the full energy range. Among them:

- Source number 5 can be identified to be the spectroscopic binary TYC 8320-1491-1, this source was also found in the detection of the 2.5-12 keV energy range with a flux of $3.26 \times 10^{-14}$ erg cm$^{-2}$ s$^{-1}$, which means it is dominated by non-thermal emission. This binary was also found in the Chandra observation, this time it is shown as source number 7; however it was not detected in the hard range of Chandra, which means ?. For this source we did not obtain its spectrum. This source was not in the FOV of ObsID 0741950101.

- Source number 7 is identified to be the main sequence star HD 330838.

- Source number 9 can be identified to be the triple system HD 147633, composed of two proper motion stars HD 147633A and HD 147633B. The high proper-motion star UCAC2 10696544 was also in the region, 19.70 arcsec offset from source number 9. This source was also detected in the hard energy range, with a flux of $3.8 \times 10^{-13}$ erg cm$^{-2}$ s$^{-1}$. This source was not in the FOV of ObsID 0741950101 neither in the Chandra observation. We extracted the spectrum of the source fit-

ting absorbed Mekal and absorbed power-law, which suggests either a mixture of thermal and non-thermal emission or varying $\Gamma$ or $kT$ within the extracted region.

- Source number 10 is very likely to be the main sequence star TYC 8320-1299-1. This source was not detected in the hard domain, was not in the FOV of ObsID 0741950101 neither of the Chandra observation.

- Source number 11 can be identified to be the X-ray source 2XMM J162703.0-491232 which is still unidentified in the XMM-Newton serendipitous source catalog [169]. It was found in the hard range detection with a flux of $2.65 \times 10^{-13}$ erg cm$^{-2}$ s$^{-1}$. It was also detected in the ObsID 0741950101, marked as source number 13 (center of the observation) and in the hard range with a flux of $3.13 \times 10^{-13}$ erg cm$^{-2}$ s$^{-1}$. This source was also detected in the Chandra observation (source number 12) and in the hard domain of Chandra observation with a SNR of 13.42. In the radial profile (Figure 4.17) we see that with increasing distance from the center, it falls rapidly and then reaches a constant, having a similar behaviour to a PSF, confirming this is a point source.

- For source 15, the gamma-ray source 1FGL J1626.0-4917c was found to be located 78.95 arcsec offset; seven molecular clouds were found at 86.12 arcsec offset. This source was also found in the detection applying the hard range of energy with a flux of $1.94 \times 10^{-14}$ erg cm$^{-2}$ s$^{-1}$. And it was also found as source number 26 in ObsID 0741950101. This was also found in the hard energy range with a flux of $1.07 \times 10^{-14}$ erg cm$^{-2}$ s$^{-1}$.

- Source 18 is very likely to be the dark nebula SDC G334.637+0.028 (20.16 arcsec offset). This source was not detected in the hard energy range and it is outside the FOV of ObsID 0741950101 and ObsId 13287.

- Pulsar PSR J1625-4913 is 87.76 arcsec offset from source 19. This source was not found in the hard energy range and it is outside the FOV of the other observations.

By making the cut in the energy range from 2.5-8 keV, eight sources remained and two more were detected: Sources number 2, 4, 8, 13, 14, H2 can not be identified due to their offsets with their possible counterpart found in SIMBAD. Source H1 is very likely to be the sub-millimetric radio source AGAL G334.551-00.006.

So, in this observation we have the spectroscopic binary, the triple system HD 147633, the X-ray source 2XMM J162703.0-491232, the FGL source, one dark nebula, the pulsar PSR J1625-4913, and the sub-millimetric radio source AGAL G334.551-00.006 to be possible counterparts of the VHE emission from source HESS J1626-490.

The triple system is composed by active main sequence stars and likely to not being related to the HESS source.

Both the FGL source and the pulsar are offset of the HESS VHE emission; besides this pulsar was found to have a characteristic age $\tau_c$ = 1.6 $\times$ 10$^6$ yr and a spin-down luminosity of $\dot{E}$ = 6 $\times$ 10$^{33}$ erg s$^{-1}$. This values indicates the SNR has been already dissipated and a offset PWN would be discarded until the moment. More studies in the unidentified X-ray source 2XMM J162703.0-491232, which is spatially coincident with the HESS source.

In the case of ObsID 0741950101, twenty eight X-ray sources were detected; however, eight of them were detected also in the observation 0403280201. The next sources can be identified for this observation:

- Source number 2 can be identified as the star Cl* NGC 6134 PM 101.

- Source number 3 is very likely to be the possible red giant branch star Cl* NGC 6134 MMU 27.

- Source number 4 can be identified to be the LMXB 4U 1624-490. There was an

X-ray scattering halo caused by this bright binary system. This source was also found in the hard energy cut with a flux of $F = 7.09 \times 10^{-11}$ erg cm$^{-2}$ s$^{-1}$. This is the same source found in the Chandra observation 13287, marked also with number 4, and was found in the hard energy cut with a SNR of 222.65.

- Source number 5 is very likely to be the dark nebula SDC G334.938-0.332.

- Source number 6 can be identified as the dark nebula SDC G334.904-0.344.

- Source number 7 is very likely to be the dark nebula SDC G334.862-0.304.

- Source number 14 is very likely to be the the sub-millimetric radio source AGAL G334.784-00.011. item Source number 28 is likely to be the dark nebula SDC G334.585-0.181 with a flux $F = 10.57 \times 10^{-14}$ erg cm$^{-2}$ s$^{-1}$.

**Chandra**

One Chandra observation was found in the region of HESS J1626-490. With this observation (ObsID 13287), 23 sources were detected; nonetheless, nine of them were detected by the previous observations (0403280201 and 0741950101). For the fourteen remaining we got that:

- Source number 2 is identified to be the X-ray source 2XMM J162754.2-485857. The main sequence star TYC 8320-1323-1 was found to be also very close. This source was not found to be non-thermal emission domain.

- Source number 5 can be identified to be the ellipsoidal variable star V* V385 Nor, in the constellation of Norma and was not found in the hard energy range.

- Source number 15 is likely to be the carbon star [W71b] 119-02, 75.77.

- No astronomical object was found in the 2 arcmin region of source number 19 in SIMBAD. This source was found in the hard energy range.

With all this information, we can say that: we exclude all the stars as possible counterparts of the HESS source, the triple system HD 147633 is also excluded due to it is formed by main sequence stars. So we have the X-ray source 2XMM J162703.0-491232, the FGL source, five dark nebulae and two sub-milimetric radio source spatially coincident of the HESS source. None of these sources alone can explain an extensive and luminous source such as HESS J1626-490, more detailed studies are needed beyond the spatial coincidence.

## Gamma-ray analysis

For the gamma-ray studies working *Fermi*-LAT data, we started the studies by using information of the 3FHL catalog, in specific, using as a target the source 3FHL J1626.3-4915 and applying the FermiPy algorithms, we could obtain its Counts map, TS map, Residual Significance Map, Excess Counts Map, to finally obtain its SED. We did the same, but this time using as a target of the analysis the coordinates of HESS J1626-490. We apply the source localization algorithms on both analysis and we could see they are not the same source; however we cannot say they are not unrelated sources since they are within the positional uncertainties. Moreover, it can also be that the LAT emission is coming from a different source or a different part of the HESS source.

In conclusion, with a TS of 1.93, HESS J1626-490 is not detected in our analysis and upper limits were obtained for this source. Similar results were obtained in [168], in those studies, they used 45 months of data and here we used 10 years and we could not have a real detection of the source, which means that we need to wait for more data time or we need to increase the sensitivity of Fermi to be able to detect sources of this kind.

# CHAPTER 5

## HESS J1808-204

X-ray studies were also carried out on the TeV unidentified galactic source HESS J1808-204 using Chandra and XMM-Newton observations.

In this chapter (sect. 5.1) I make a short description of this HESS J1808-204, in sect. 5.2 I show the X-ray data analysis done on this source using the XMM-Newton (XMM-N) observation and in sect. 5.3 the Chandra analysis on four different observations is shown. The procedure performed in the detection of the X-ray sources is detailed in both cases. The merge of all the observations is presented in sect.5.4. At the end, I indicate the possible counterparts that explains part or all the VHE gamma-ray emission from HESS J1808-204 (sect. 5.5).

The list of observations that have been performed to date in this region are described in Table 5.1, where we can find the ID of the observation, the exact the start date (dd.mm.yy) and the time, the exposure and the coordinates of the objective for each one.

In sect. 5.1 I made a description of HESS J1808-204,

181

## 5.1   Introduction

As was already mentioned previously in Chapter 2, this source was discovered using the H.E.S.S. telescopes [170] as a consequence of joint observations as part of the H.E.S.S. Galactic Plane Survey (HGPS) and a dedicated observation on the magnetar SGR 1806-20 summing a total 94 hours long (from which, 51 were of dedicated and 43 hours of HGPS data, from 2004-2010). In Figure 5.1 we can see a gamma-ray image of the source.
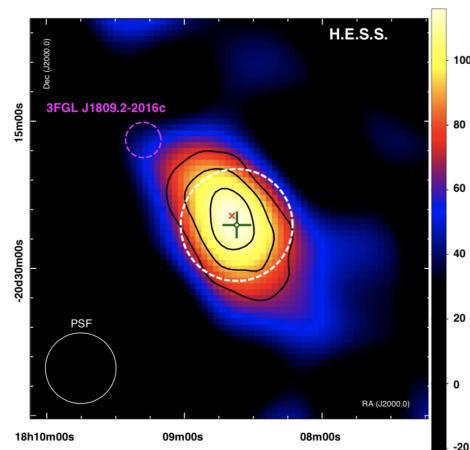


Figure 5.1: A VHE gamma-ray excess counts image of HESS J1808-204, the red cross represents the stellar cluster Cl* 1806-20 in which SGR 1806-20 and LBV 1806-20 are present. The PSF analysis of the source corresponding to 68% containment radius is indicated by the whithe circle (bottom left corner). The white dashed line and the dark green point with error bars ($1\sigma$ statistical) represent the fitted location and radius of the intrinsic Gaussian source model, and the magenta dashed line indicates the 68% location error of the *Fermi*-LAT GeV source. Figure from [170].

SGR 1806-20 is part of the stellar cluster Cl* 1806-20, which harbours (within 0.5 arcmin radius) several energetic stars, among them: four Wolf-Rayet satrs, five O-type stars, and the luminous blue variable LBV 1806-20 [171]. A 2D symmetrical Gaussian model describes well the intrinsic shape of the source with a 68% containment radius

of 15 pc at 8.7 kpc distancd [170]. Its position is R.A. = $18^h08^m37.3^s \pm51^s_{syst}$ and dec. = $-20°25'36.3"\pm71"_{stat}\pm20"_{sys}$, where the systematic errors are due to the telescope pointing and mechanical alignment uncertainties. At that position, the HESS source has a pre-trial excess significance of $+7.1\sigma$, comprising 413 gamma-ray photons within a radius of $0.2°$ [170].

HESS J1808-204 exhibits an energy flux (0.2-10 TeV) of $F_{VHE} \sim 1.7 \times 10^{-12}$ erg cm$^{-2}$ s$^{-2}$ and a luminosity $L_{VHE} \sim 1.6 \times 10^{34}$ (d/8.7kpc)$^2$erg s$^{-1}$.

HESS J1808-204

| Mission | ObsID | Start Date | Exposure | Coordinates |
|---------|-------|------------|----------|-------------|
| XMM-N | 0654230301 | 23.03.11 09:34:32 | 4.4 ks | $18^h08^m39.29^s$, -20°24'29.5" |
| XMM-N | 0654230401 | 23.03.11 11:07:09 | 38.9 ks | $18^h08^m39.29^s$, -20°24'29.5" |
| XMM-N | 0148210101 | 03.04.03 13:35:27 | 55.5 ks | $18^h08^m39.29^s$, -20°24'29.5" |
| XMM-N | 0148210401 | 07.10.03 09:41:25 | 22.4 ks | $18^h08^m39.29^s$, -20°24'29.5" |
| XMM-N | 0164561101 | 06.10.04 16:56:00 | 18.9 ks | $18^h08^m39.29^s$, -20°24'29.5" |
| XMM-N | 0164561301 | 07.03.05 08:20:59 | 24.9 ks | $18^h08^m39.29^s$, -20°24'29.5" |
| XMM-N | 0164561401 | 04.10.05 10:14:24 | 33.0 ks | $18^h08^m39.29^s$, -20°24'29.5" |
| XMM-N | 0205350101 | 06.09.04 09:02:50 | 51.9 ks | $18^h08^m39.29^s$, -20°24'29.5" |
| XMM-N | 0400600301 | 04.04.06 06:42:02 | 29.7 ks | $18^h08^m39.29^s$, -20°24'29.5" |
| XMM-N | 0400600401 | 10.09.06 10:05:30 | 32.4 ks | $18^h08^m39.29^s$, -20°24'29.5" |
| XMM-N | 0502170301 | 26.09.07 15:17:46 | 30.9 ks | $18^h08^m39.29^s$, -20°24'29.5" |
| XMM-N | 0502170401 | 02.04.08 13:09:25 | 32.9 ks | $18^h08^m39.29^s$, -20°24'29.5" |
| XMM-N | 0554600301 | 05.09.08 15:17:46 | 42.3 ks | $18^h08^m39.29^s$, -20°24'29.5" |
| XMM-N | 0554600401 | 03.03.09 15:34:01 | 40.8 ks | $18^h08^m39.29^s$, -20°24'29.5" |
| XMM-N | 0554600501 | 03.03.08 13:21:22 | 6.8 ks | $18^h08^m39.29^s$, -20°24'29.5" |
| XMM-N | 0604090201 | 07.09.09 18:56:14 | 30.9 ks | $18^h08^m39.29^s$, -20°24'29.5" |
| Chandra | 0746 | 15.08.00 17:51:59 | 31.0 ks | $18^h08^m40.32^s$, -20°24'41.1" |
| Chandra | 1827 | 24.07.00 17:51:59 | 4.9 ks | $18^h08^m40.32^s$, -20°24'41.1" |
| Chandra | 6224 | 09.02.05 07:00:06 | 18.8 ks | $18^h08^m39.30^s$, -20°24'39.0" |
| Chandra | 8151 | 26.10.07 07:14:31 | 2.1 ks | $18^h08^m16.80^s$, -20°21'43.2" |

Table 5.1: X-ray observations made by XMM-Newton and Chandra telescopes on the position of HESS J1808-204.

The source is steady and extended towards the blue super-giant star LBV 1806-20,

the cluster Cl* 1806-20, and the magnetar SGR 1806-20. The origin and the nature of the accelerated particles responsible for this VHE emission are not clear so far. This source is of great interest due to the possible high-energy particle acceleration from magnetars, massive stars, and/or stellar clusters.

## 5.2 XMM-Newton Data Analysis

For this source, 16 observations have been carried out to the date using the XMM-Newton observatory using as a the magnetar SGR 1806-20; however, all of them performed in different dates and with different exposure time (see Table 5.1). Consequently, it is optimal to work with the longest GTI observation, in this case 0205350101, having a GTI of 44.4 ks.

The data were reprocessed using the XMM-Newton data analysis software SAS version xmmsas 20160201 1833-15.0.0 pipeline, and for their analysis both SAS and FTOOLS software packages were used. The calibration was done using the SAS task `cifbuild`. For using EPIC data, the reprocessing was accomplished by running the default pipeline processing meta tasks `emproc` (for EPIC-MOS) and `epproc` (for EPIC-PN).

The activities carried out so far are:

- Calibration the data.

- Filter event files for flaring particle background.

- Creation of the images using the cleaned event files using ds9.[1]

- Source detection

- Identification of X-ray sources using the SIMBAD astronomical database.

---

[1] http://ds9.si.edu/site/Home.html

**Observation 0205350101**

The observation was acquired on September 6th, 2004 and it has a duration of 51.9 ks. The MOS cameras were operated in Large Window Mode, and the PN camera on Small Window mode. For the analysis, the first thing to do is the calibration of the data, and after, the event files have to be filtered for times of flaring particle background. In view of this, we obtained the high-energy (>10 keV) light curves with the purpose of identify the intervals of flaring particle background using the `evselect` task. The results can be seen on Figure 5.2.



(a) Light curve above 10 keV from MOS1.

(b) Light curve above 10 keV from MOS2.

(c) Light curve above 12 keV from PN.
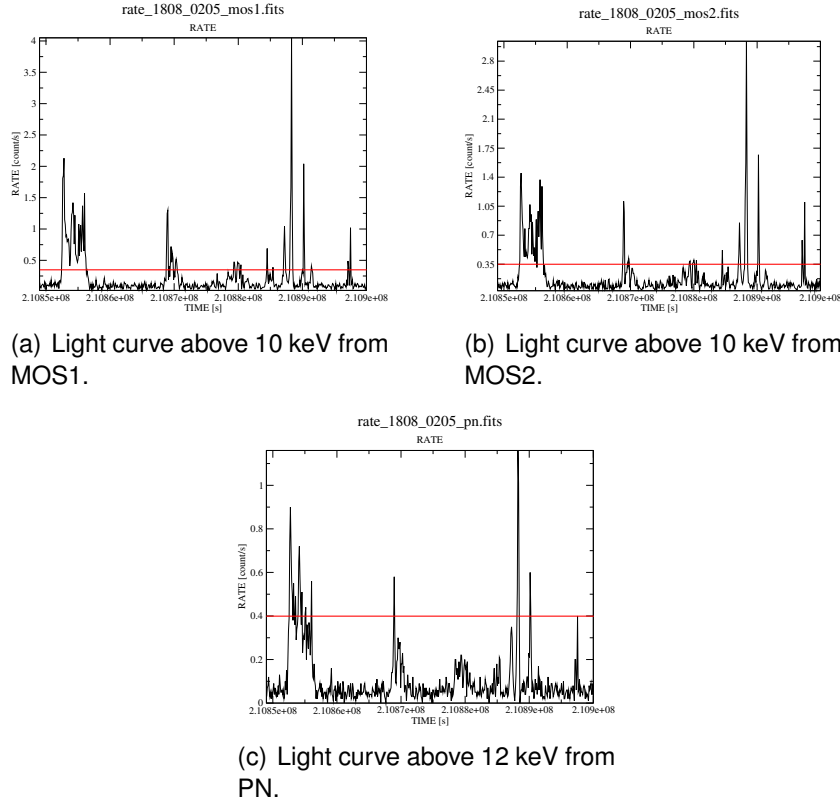
Figure 5.2: Light curves for EPIC-MOS (above 10 keV) and EPIC-PN (above 12 keV) instruments obtained using the ObsID 0205350101 of HESS J1808-204, the red line is to visualize the threshold (count/second) above the low steady background intervals.

The GTI we got for MOS1 was 44.4 ks, for MOS2 was 45.4 ks, and in the case of PN

the result was 48.3 ks. Using this results we created the cleaned event files which can be seen plotted in Figure 5.3.



(a) Cleaned events for MOS1.



(b) Cleaned events for MOS2.



(c) Cleaned events for PN.
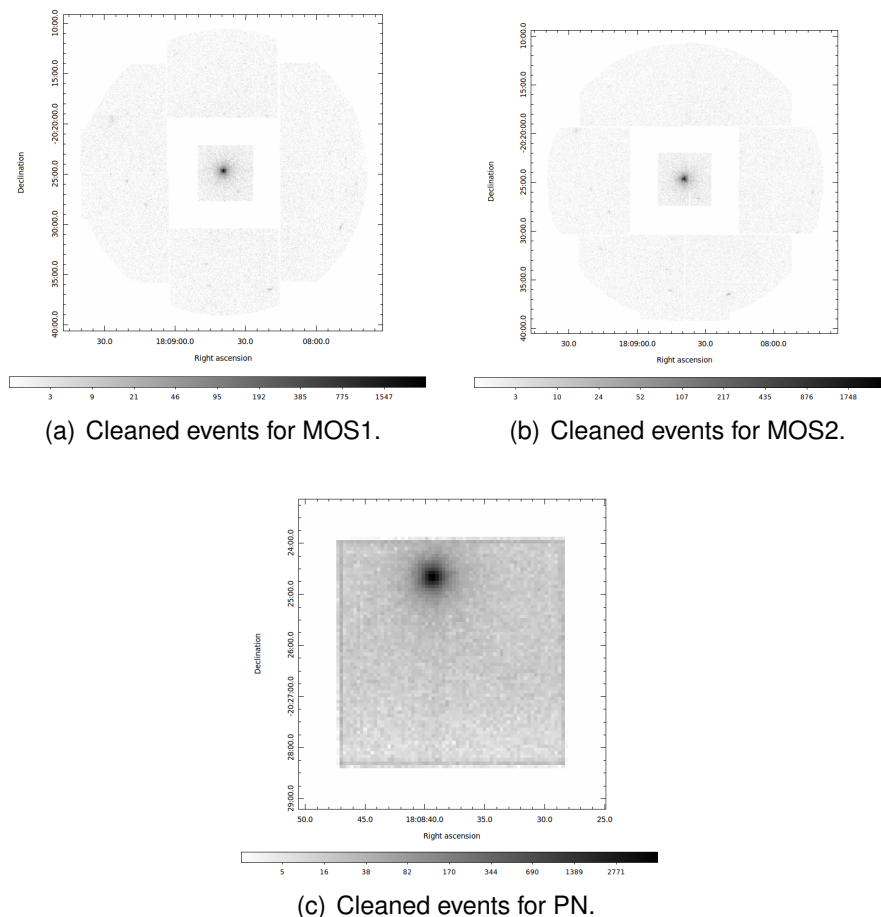
Figure 5.3: Cleaned events images for MOS and PN EPIC cameras of ObsID 0205350101.

The source detection was performed for the MOS1 camera using the EPIC source detection chain, with this, 32 sources were found and are shown in Figure 5.4. As we can see, due to the observation mode some part of the sky is not covered and hence we could be missing some sources that could be important in the search for counterparts of HESS J1808-204. As a consequence, it is better to work with other observation that can covers all the field. On these terms, the ObsID 0554600301, which is another long observation. The analysis on this observation is detailed below.
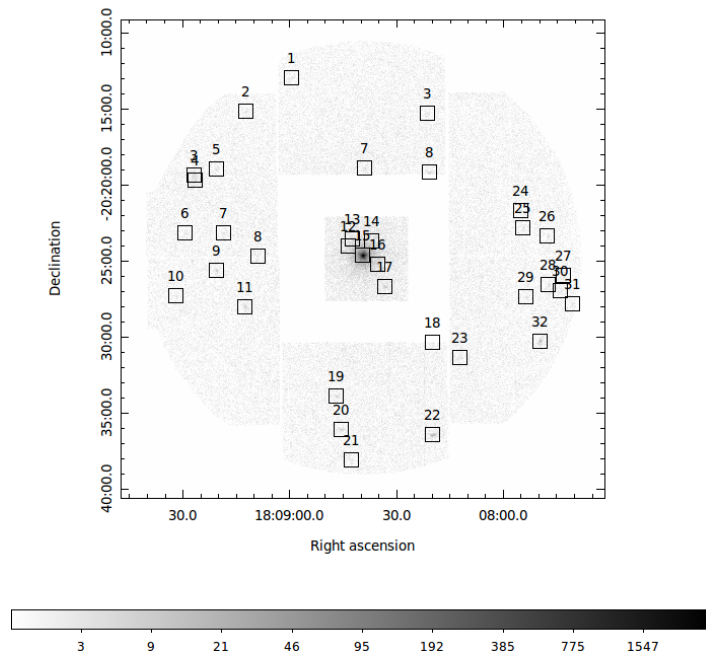
Figure 5.4: Counts map observation obtained for MOS1 using ObsID 0205350101 on HESS J1808-204, the black squares indicate 32 sources detected by an EPIC source detection.

**Observation 0554600301**

Acquired on September 4th, 2008 this observation had a duration of 42.364 ks. On this occasion all three cameras were operated in Full Frame mode (see Figure 5.6), and, in all three cases a medium filter was used.

Once I did the calibration of the data, then I filtered the event files for times of flaring particle background. For that purpose, we extracted the high-energy (>10 keV) light curves using the `evselect` task and a threshold (counts/second) was defined. The rates defined were: 0.35 counts/s for MOS cameras and 0.45 counts/s for the PN detector (See Figure 5.5).

With this threshold established, the GTI obtained were, for both MOS1 and MOS2 of

(a) Light curve above 10 keV from MOS1.



(b) Light curve above 10 keV from MOS2.



(c) Light curve above 12 keV from PN.
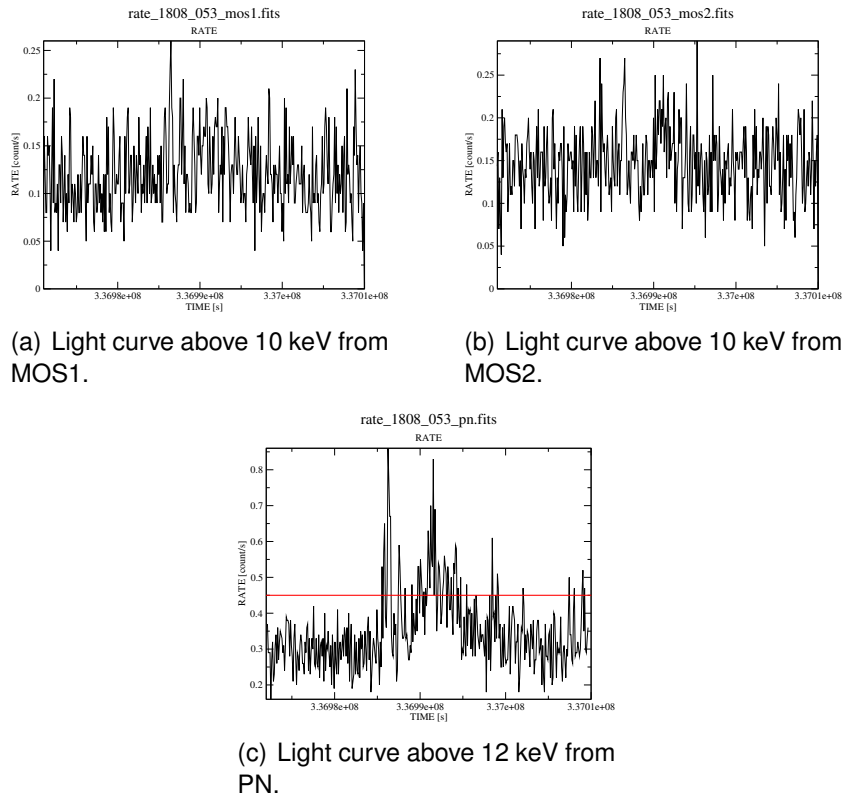
Figure 5.5: Light curves for EPIC-MOS (above 10 keV) and EPIC-PN (above 12 keV) instruments obtained using the ObsID 0554600301 of HESS J1808-204, the red line is to visualize the threshold (count/second) above the low steady background intervals.

39.4 ks, and for PN of 32.1 ks. As a result, the clean images with which we did the data analysis can be seen in the Figure 5.6.

The EPIC source detection chain was applied to the images with the aim of finding the interesting sources that could be part of the counterpart of the HESS source. Forty one source were revealed, these can be seen as black squares in Figure 5.7. More information about all these sources can be found in the Tables 5.2, 5.2, and 5.2.
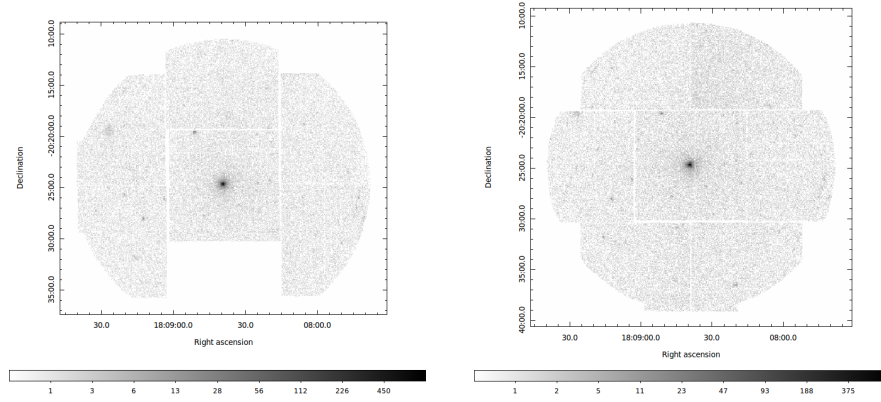
(a) Cleaned events for MOS1.

(b) Cleaned events for MOS2.
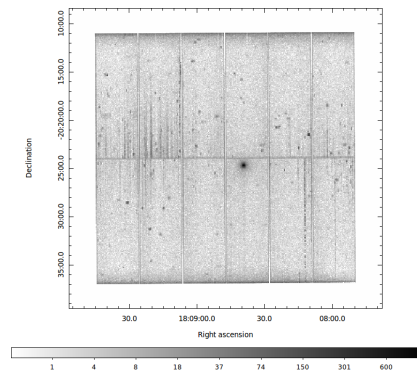


(c) Cleaned events for PN.

Figure 5.6: Cleaned events images for MOS and PN EPIC cameras of ObsID 0554600301.
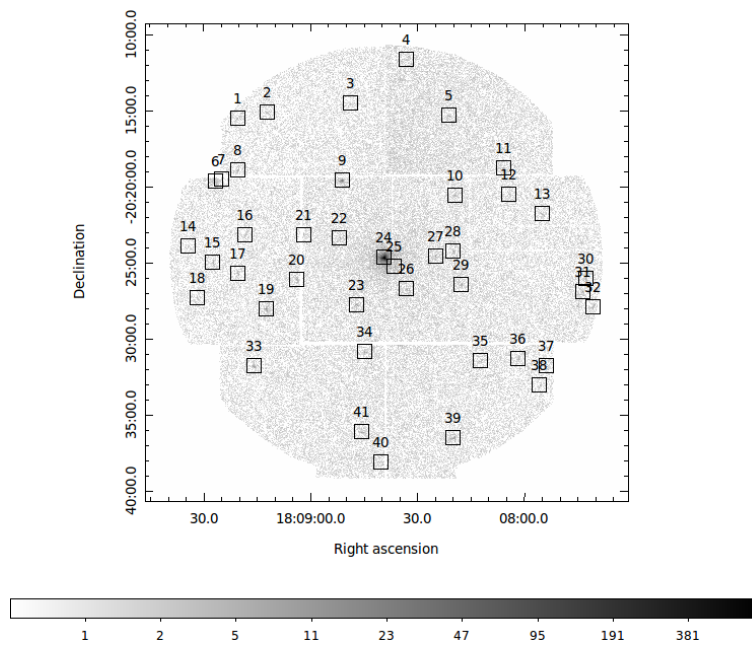
Figure 5.7: Counts map observation obtained for MOS2 using ObsID 0554600301 of HESS J1808-204, the black squares indicate 41 sources detected by an EPIC source detection.

Table 5.2: Possible counterparts of HESS J1808-204 found using MOS2 detector of ObsID 0554600301 (Offset in arcsec), Part 1.

| Src | RA (J2000) | DEC (J2000) | Star | Offset | X | Offset |
|-----|-----------|-------------|------|--------|---|--------|
| 1 | 18:09:20.4 | -20:15:29.5 | HD 312682 | 119.52 | — | — |
| 2 | 18:09:12.0 | -20:15:06.5 | HD 312682 | 3.56 | — | — |
| 3 | 18:08:48.7 | -20:14:31.9 | — | — | — | — |
| 4 | 18:08:33.1 | -20:11:39.1 | No astronomical | — | object found | — |
| 5 | 18:08:21.1 | -20:15:19.8 | 2MASS J18081955-2016047 | 50.06 | — | — |
| 6 | 18:09:26.6 | -20:19:39.4 | 2MASS J18092597-2019383 | 9.34 | 3XMM J180926.9-201930 | 10.01 |
| 7 | 18:09:24.7 | -20:19:28.2 | 2MASS J18092601-2019311 | 18.51 | 3XMM J180926.9-201930 | 30.86 |
| 8 | 18:09:20.4 | -20:18:55.4 | 3XMM J180920.3-201857 | 1.87 | 3XMM J180926.9-201930 | 97.91 |
| 9 | 18:08:51.1 | -20:19:35.4 | — | — | 2XMM J180851.0-201935 | 0.30 |
| 10 | 18:08:19.4 | -20:20:32.6 | SSTGLMC G009.9921-00.1464 | 96.31 | AX J1808.2-2021 | 77.38 |
| 11 | 18:08:05.7 | -20:18:46.4 | TYC 6272-29-1 | 52.83 | — | — |
| 12 | 18:08:04.3 | -20:20:28.3 | HD 312685 | 43.81 | - | - |
| 13 | 18:07:54.9 | -20:21:46.8 | HD 312685 | 109.44 | 2XMM J180754.3-202251 | 65.38 |
| 14 | 18:09:34.3 | -20:23:55.3 | - | - | - | - |

*Continued on next page*

192

Table 5.2 Continued from previous page

| Src | Pulsar | Offset | FGL | Offset | HII | Offset |
|-----|--------|--------|-----|--------|-----|--------|
| 1 | — | — | 3FGL J1809.2-2016c | 93.39 | [CPA2006] N1 | 82.68 |
| 2 | — | — | — | — | — | — |
| 3 | — | — | — | — | — | — |
| 4 | — | — | — | — | — | — |
| 5 | — | — | — | — | — | — |
| 6 | — | — | — | — | [WC89] 010.15-0.34A | 17.8 |
| 7 | — | — | — | — | GAL 010.2-00.3 | 1.87 |
| 8 | — | — | — | — | [WC89] 010.15-0.34B | 30.59 |
| 9 | — | — | UGRS G017.4+2.4 | 27.94 | — | — |
| 10 | — | — | — | — | — | — |
| 11 | — | — | — | — | — | — |
| 12 | — | — | — | — | — | — |
| 13 | — | — | — | — | — | — |
| 14 | — | — | — | — | — | — |

Continued on next page

Table 5.2 Continued from previous page

| Src | MC | Offset | DNe | Offset | Radio | Offset |
|---|---|---|---|---|---|---|
| 1 | SDC G10.201-0.331 | 85.92 | SRBY 15 | 45.49 | [GS70] 010.2-00.3 | 39.77 |
| 2 | DOBASHI 0454 | 106.98 | SRBY 15 | 99.97 | [ERG2015] 2369 | 71.06 |
| 3 | — | — | — | — | — | — |
| 4 | — | — | — | — | — | — |
| 5 | — | — | — | — | BGPS G010.112-00.074 | 119.71 |
| 6 | SDC G10.179-0.360 | 76.21 | — | — | GPSR5 10.161-0.359 | 18.52 |
| 7 | SDC G10.156-0.340 | 51.85 | — | — | GPSR5 10.161-0.359 | 19.47 |
| 8 | SDC G10.156-0.340 | 17.8 | — | — | Kes 62 | 31-87 |
| 9 | — | — | — | — | — | — |
| 10 | SDC G9.991-0.147 | 101.19 | — | — | — | — |
| 11 | — | — | — | — | — | — |
| 12 | — | — | — | — | — | — |
| 13 | — | — | — | — | — | — |
| 14 | SDC G10.111-0.431 | 28.54 | — | — | AGAL G010.104-00.416 | 37.14 |

194

We have the first fourteen sources in Table 5.2. Twenty one objects were found in the 2 arcmin vicinity of source number 1, the closest is the dense core [WWS2012] G010.21-00.31 located at 17.17 arcsec offset, which could be the responsible of the X-ray emission. Also, four dense cores were found in the region [HBM2005] G10.191-0.307 at 70.07 arcsec, AGAL G010.213-00.322 at 62.05 arcsec, [PLW2012] G010.225-00.286+013.2 at 99.29 arcsec, and [TBH2012] 208 at 106.01 arcsec offset. Moreover, ten radio sources were found, being 7 of them sub-millimetric radio sources. The molecular cloud SRBY 15 was found to be at 45.49 arcsec; the HII region [CPA2006] N1, is located 82.68 arcsec away; the dark nebula SDC G10.201-0.331 located at 85.92 arcsec; the gamma-ray source 3FGL J1809.2-2016c was found to be 93.39 arcsec, an the main sequence star HD 312682 was found to be 119.52 arcsec away. Source number 2 can be identified to be the main sequence star HD 312682, located at 3.56 arcsec, another star of this kind was found 62.40 arcsec away (TYC 6272-683-1). Four dense cores were found in the 2 arcmin vicinity, being [TBH2012] 218 the closest at 70.17 arcsec. Eight radio sources were also found in the region, the closest located at 71.06 arcsec, the sub-millimetric radio source [ERG2015] 2369, among them were one mm and six sub-millimetric radio. Moreover, the same molecular cloud and dark nebula as in source number 1 were found. SRBY 15 at 99.97 arcsec and DOBASHI 0454 at 106.98 arcsec away. The only source founded in the 2 arcmin region of source number 3 was the IR source IRAS 18059-2016, located at 110.52 arcsec. No astronomical object was found in the 2 arcmin region around source number 4. The Asymptotic Giant Branch Star candidate 2MASS J18081955-2016047 is the closest object to the source number 5, located at 50.05 arcsec. The OH star OH 10.0 -0.1 was found to be at 84.38 arcsec, the YSOC 2MASS J18081701-2016583 is located at 114.26 arcsec and the sub-millimetric radio source BGPS G010.112-00.074 at 119.71 arcsec offset. Forty seven sources were found in the 2 arcmin of source number 6. The cluster of stars NAME W 31 IR Cluster

was found to be at 10.64 arcsec, so 4 stars were found to be in the vicinity, being the O-type star 2MASS J18092597-2019383 the closest object at 9.34 arcsec. The X-ray source 3XMM J180926.9-201930 was found at 10.01 arcsec; three bubble sources were also found in the vicinity, as well as six HII regions, 16 radio sources, being two mm and nine sub-millimetric radio. Also, two masers, OH 10.2 -0.4 and [TVH89] 253, located at 24.89 and 25.85 arcsec offset, respectively. The Star Forming Region (SFR) [RM2010] SFC 1 was found to be at 75.85 arcsec, as well as three dark nebulae, one Wolf-Rayet star (3XMM J180920.3-201857, located at 97.53 arcsec), the far IR source PLCKERC -070 G010.18-00.35 at 99.49 arcsec, the UV source Lan 75 at 101.98 arcsec away from the source. Source number 7 is located in a region of HII and maser sources, being the HII region GAL 010.2-00.3 at 1.87 arcsec the closest, however five more HII regions were found to be close, [CKW87] 180626.9-202009, [WC89] 010.15-0.34A, GAL 010.15-00.34, JCMTSE J180921.2-201932 and [WC89] 010.15-0.34B, located at 11.19, 18.49, 44.34, 49.66 and 59.40 arcsec away, respectively. The maser sources are close too, [TVH89] 253 at 3.77 arcsec and OH 10.2 -0.4 at 4.33 arcsec. The cluster of stars NAME W 31 IR Cluster is located 32.12 arcsec away, and two stars in a clusters were found, the O-type stars 2MASS J18092601-2019311 at 18.51 arcsec, 2MASS J18092597-2019383 at 20.40 arcsec, 2MASS J18092749-2019482 at 43.80 arcsec, and ALS 19592 at 53.75 arcsec. Two main sequence star; eighteen radio sources, and among them 15 sub-millimetric radio and 2 mm; the x-ray source 3XMM J180926.9-201930 located at 30.86 arcsec; two bubble sources; five dense cores; four dark nebuale; the Wolf-Rayet 3XMM J180920.3-201857 located at 68.37; the far IR source PLCKERC -070 G010.18-00.35 located at 93.85 arcsec; the SFR [RM2010] SFC 1 located at 104.48 arcsec, and the UV source LAN 715 located at 116.90. Source number 8 can be identified to be the WR star 3XMM J180920.3-201857, located 1.87 arcsec offset, the second closest source is the dark nebula SDC G10.156-0.340 located at 17.80 arcsec. Moreover, 6 HII regions were

found in the vinicity, being [WC89] 010.15-0.34B the closest at 30.59 arcsec, as well as 14 radio sources, being Kes 62 is the closest at 31.87 arcsec. Other 6 dense cores, two bubble sources were also found in the region, four dark nebuale; the two masers [TVH89] 253 and OH 10.2 -0.4 at 72.60 and 73.36 arcsec away, the X-ray source 3XMM J180926.9-201930 at 97.91 arcsec; the cluster of stars NAME W 31 IR Cluster located at 99.06 arcsec offset and with this, three stars in a cluster (2 MASS) were also found; and the far IR source PLCKERC -070 G010.18-00.35 at 108.14 arcsec away. Source number 9 can be identified to be the X-ray source 2XMM J180851.0-201935, located 0.30 arcsec offset. The closest object found in the 2 arcmin of source number 10 was the IR source HFE 49 located at 38.41 arcsec, the X-ray source AX J1808.2-2021 is located at 77.38 arcsec offset from the source; as well as two YSOC located at 96.31 and 104.76 arcsec, respectively SSTGLMC G009.9921-00.1464 and SSTGLMC G009.9987-00.1622; and the dark nebula SDC G9.991-0.147 at 101.19 arcsec offset. The closest object of source number 11 was the main sequence star TYC 6272-29-1 at 52.83 arcsec away. Two other sources in the region: The Asymptotic Giant Branch Star candidate SSTGLMC G010.0274-00.0633 at 67.92 arcsec and the OH star OH 10.03 -0.06 at 68.59 arcsec away. Source number 12 was found to be the main sequence star HD 3122685. In the case of source number 13, the X-ray star 2XMM J180754.3-202251 was found to be 65.28 arcsec offset. Fourteen objects were found in the vicinity of source 14, among them 5 dark nebulae were found being SDC G10.111-0.431 the closest source located at 28.54 arcsec away, as well there were found three core sources, one bubble source ([SPK2012] MWP1G010078-004186, at 119.07 arcsec away), and ten radio sources: two mm and eight sub-millimetric radio.

Table 5.3: Possible counterparts of HESS J1808-204 found using MOS2 detector of ObsID 0554600301 (Distance in arcsec), Part 2.

| Src | RA (J2000) | DEC (J2000) | Star | Distance | X | Distance |
|-----|-----------|-------------|------|----------|---|----------|
| 15 | 18:09:27.4 | -20:24:57.6 | — | — | — | — |
| 16 | 18:09:18.2 | -20:23:08.9 | — | — | — | — |
| 17 | 18:09:20.4 | -20:25:40.1 | — | — | — | — |
| 18 | 18:09:31.7 | -20:27:16.9 | TYC 6272-159-1 | 118.14 | - | — |
| 19 | 18:09:12.5 | -20:28:00.8 | HD 312684 | 1.68 | 2XMM J180912.2-202801 | 1.74 |
| 20 | 18:09:03.8 | -20:26:04.6 | SSTGLMC G010.0386-00.3608 | 105.49 | - | — |
| 21 | 18:09:01.9 | -20:23:08.2 | HD 312683 | 43.54 | — | — |
| 22 | 18:08:51.8 | -20:23:21.8 | - | - | — | — |
| 23 | 18:08:47.0 | -20:27:44.65 | - | - | — | — |
| 24 | 18:08:39.4 | -20:24:39.2 | [EGH2001b] A2 | 0.23 | SWIFT J180839.4-202435 | 3.99 |
| 25 | 18:08:36.5 | -20:25:15.2 | 2MASS J18083671-2024542 | 21.21 | SWIFT J180839.4-202435 | 57.36 |
| 26 | 18:08:33.1 | -20:26:43.8 | - | - | — | — |
| 27 | 18:08:24.9 | -20:24:32.0 | USNO-A2.0 0675-24220389 | 0.49 | - | - |
| 28 | 18:08:19.9 | -20:24:15.5 | 2MASS J18081752-2024586 | — | - | — |

*Continued on next page*

Table 5.3 Continued from previous page

| Src | Pulsar | Distance | FGL | Distance | HII | Distance |
|-----|--------|----------|-----|----------|-----|----------|
| 15 | – | – | – | – | [L89b] 10.073-00.412 | 35.76 |
| 16 | – | – | – | – | – | – |
| 17 | – | – | – | – | [L89b] 10.073-00.412 | 93.04 |
| 18 | – | – | – | – | IRAS 18065-2026 | 88.22 |
| 19 | – | – | – | – | – | – |
| 20 | – | – | – | – | – | – |
| 21 | – | – | – | – | – | – |
| 22 | – | – | – | – | – | – |
| 23 | – | – | – | – | – | – |
| 24 | PSR J1808-2024 | 1.00 | – | – | – | |
| 25 | PSR J1808-2024 | 53.23 | – | – | – | |
| 26 | – | – | – | – | – | – |
| 27 | – | – | – | – | – | – |
| 28 | – | – | – | – | – | – |

*Continued on next page*

Table 5.3 Continued from previous page

| Src | MC | Distance | DNe | Distance | Radio | Distance |
|---|---|---|---|---|---|---|
| 15 | — | — | SDC G10.082-0.414 | 21.62 | [ERG2015] 2357 | 22.37 |
| 16 | — | — | — | — | JCMTSE J180913.9-202302 | 61.41 |
| 17 | — | — | SDC G10.069-0.400 | 52.80 | AGAL G010.068-00.407 | 68.28 |
| 18 | — | — | SDC G10.043-0.425 | 74.94 | [SSS2011] BGPS G10.043-0.424 | 80.77 |
| 19 | DOBASHI 0444 | 65.9 | — | — | AGAL G010.019-00.394 | 53.91 |
| 20 | SDC G10.031-0.355 | 76.51 | — | — | AGAL G010.026-00.352 | 56.03 |
| 21 | — | — | — | — | JCMTSE J180902.8-202243 | 28.04 |
| 22 | — | — | — | — | JCMTSE J180844.5-202413 | 115.18 |
| 23 | SDC G9.984-0.267 | 116.07 | — | — | — | — |
| 24 | [CWD97] MC+24 | 0.62 | SDC G9.984-0.267 | 99.83 | JCMTSF J180841.9-202355 | 56.85 |
| 25 | [CWD97] MC+73 | 53.58 | SDC G9.984-0.267 | 109.8 | JCMTSE J180836.4-202400 | 75.25 |
| 26 | — | — | — | — | AGAL G009.959-00.209 | 103.84 |
| 27 | SDC G9.986-0.170 | 95.68 | — | — | [GPD88] 009.972-0.187 | 17.06 |
| 28 | SDC G9.986-0.170 | 77.23 | — | — | [GPD88] 009.972-0.187 | 58.94 |

The next fourteen sources are shown in Table 5.2., and are described with more detail below. Seventeen sources in the 2 arcmin vicinity of source 15: the dark nebula SDC G10.082-0.414 is was the closest found at 21.62 arcsec, but other four sources of the same kind were also found; as well as seven sub-millimetric radio sources (being [ERG2015] 2357 the closest of them at 22.37 arcsec;) two HII regions [L89b] 10.073-00.412 and IRAS 18065-2026 located at 35.76 arcsec and 64.06 arcsec, respectively; the bubble source [SPK2012] MWP1G010078-004186 located at 41.32 arcsec; and two core sources. Five sub-millimetric radio sources in the 2 arcmin region around source 16, all of them were discovered using the JCMTSE Submillimetre Common User Bolometer Array (SCUBA) Survey, being JCMTSE J180913.9-202302 the closest, 60.85 arcsec offset. The closest object to source number 17 was found to be the dark nebula SDC G10.069-0.400 located at 52.80 arcsec, however another dark nebula is also in the 2 arcmin region, SDC G10.067-0.406 at 66.64 arcsec offset. There are also, three sub-millimetric radio sources, one HII region ([L89b] 10.073-00.412 at 93.04 arcsec away) and one core source ([ERG2015] 2356 at 71.67 arcsec away). Nine sources in the 2 arcmin region of source 18, being SDC G10.043-0.425, a dark nebula the closest at 74.94 arcsec away, moreover there is another dark nebula source in the region: SDC G10.086-0.438 at 108.49 arcsec, as well as four radio sources: one mm ([SSS2011] BGPS G10.043-0.424 at 80.77 arcsec) and three sub-millimetric radio; one HII region (IRAS 18065-2026 at 88.22 arcsec); one bubble source /[SPK2012] MWP1G010078-004186 at 112.53 arcsec), and one main sequence star (TYC 6272-159-1 at 118.14 arcsec offset). In the 2 arcmin vicinity of source 19 there are: two main sequence stars, being HD 312684 the closest object at just 1.68 arcsec, the x-ray source 2XMM J180912.2-202801, located also close at 1.74 arcsec offset;as well as seven radio sources: two mm and five sub-millimetric radio; one dark nebula DOBASHI 0444 at 65.90 arcsec, and two core sources, so it can be identified to be the the F-type star HD 312864. In the 2

arcmin region around source number 20 were found: four sub-millimetric radio and one mm sources, being AGAL G010.026-00.352 the closest object at 56.03 arcsec. There are also, one IR source IRAS 18060-2025 at 56.19 arcsec offset; two dense cores; one dark nebula (SDC G10.031-0.355 at 76.51 arcsec); the YSOC SSTGLMC G010.0386-00.3608 was found to be located at 105.49 arcsec offset and one main sequence star TYC 6272-11-1 at 118.17 arcsec away. Three sub-millimetric radio sources and one main sequence stars were the object found in SIMBAD to be in the 2 arcmin region around source number 21, being JCMTSE J180902.8-202243 the closest at 28.04 arcsec away. The 2 arcmin region around source 24 is a bit complicated, eighty sources were found in the vicinity. The main sequence stars [EGH2001b] A2 and [EGH2001b] A3 were found at the same distance, at 0.23 arcsec, but there are other 30 stars of this kind in the region; twelve molecular clouds were also found, all of them 0.62 arcsec offset; four IR sources; the pulsar PSR J1808-2024 is located 1.00 arcsec offset; three Wolf-Rayet stars: WR 111c (the closest) at 3.46 arcsec offset, WR 111d at 3.59 arcsec offset, and WR 111b at 7.64 arcsec; the X-ray source SWIFT J180839.4-202435 was found to be 3.99 arcsec away; the massive stellar cluster Cl* 1806-20 is 5.07 arcsec offset and eleven stars in a cluster were found in the vicinity; also, the interstellar matter AX J1808.6-2024 was found to be 6.01 arcsec away, the object [GKG2005] VLA J180839-202439 is located at the same distance. Other seven sub-millimetric radio sources were found in the 2 arcmin region; as well as two possible supergiant stars [FNG2005] 4 and [EML2004] Star C, at 6.94 and 9.48 arcsec away, respectively; the blue supergiant star [KMN95] Star A is located at 13.52 arcsec offset, and the dark nebula source SDC G9.984-0.267 at 99.83 arcsec away. Seventy seven sources were found in the 2 arcmin vicinity of source number 25, the massive stellar cluster 1806-20 was found to be at 50.68 arcsec offset, so eleven stars in the cluster were found in the region, being the star 2MASS J18083671-2024542 the closest at 21.21 arcsec. Furthermore, thirty one main

sequence stars are also in the region, as well as three Wolf-Rayet stars (WR 111c the closest at 52.66 arcsec offset); four IR sources; the interstellar matter AX J1808.6-2024 is located at 52.87 arcsec; five radio sources (among them four sub-millimetric radio); twelve molecular clouds were also found, all of them at 53.58 arcsec; two possible super giant star [FNG2005] 4 at 56.68 arcsec, and [EML2004] Star C at 62.14 arcsec; the x-ray source SWIFT J180839.4-202435 located at 57.39 arcsec; two objects of unknown nature [KMN95] K and [KMN95] HK both at the same distance (63.69 arcsec); one blue super giant star [KMN95] Star A at 63.76 arcsec offset; one bubble source [CWP2007] CN 141 at 106.05 arcsec and the dark nebula source SDC G9.984-0.267 at 109.80 arcsec. The 2 arcmin region around source 26 composed by the sub-millimetric radio AGAL G009.959-00.209 at 103.84 arcsec offset, the mm source BGPS G009.960-00.206 at 114.27 arcsec, and the bubble source [CWP2007] CN 141 at 114.30 arcsec offset of source number 26. Source number 27 can be identified to be the star USNO-A2.0 0675-24220389 at just 0.49 arcsec offset. In the vicinity there are also four radio sources (two sub-millimetric radio and one mm); two YSOC; one bubble source; one Asymptotic Giant Branch Star candidate (2MASS J18082959-2023030 located at 110.23 arcsec); and two dark nebulae SDC G9.986-0.170 and SDC G9.987-0.164 at 95.68 and 117.37 arcsec offset, respectively. Nine sources found in the 2 arcmin regiond around source marked with number 28, the closest is the bubble source [SPK2012] MWP1G009955-001741 at 36.75 arcsec offset, as well as three YSOC; two radio sources; one main sequence star; and two dark nebulae SDC G9.986-0.170 and SDC G9.987-0.164 at 87.59 and 88.35 arcsec offset, respectively.

Table 5.4: Possible counterparts of HESS J1808-204 found using MOS2 detector of ObsID 0554600301 (Distance in arcsec), Part 3.

| Src | RA (J2000) | DEC (J2000) | Star | Distance | X | Distance |
|---|---|---|---|---|---|---|
| 29 | 18:08:17.8 | -20:26:25.8 | 2MASS J18081769-2026260 | 0.95 | - | — |
| 30 | 18:07:42.7 | -20:26:01.7 | TYC 6259-2696-1 | 39.00 | - | - |
| 31 | 18:07:43.7 | -20:26:53.2 | 2MASS J18074422-2026454 | 10.94 | - | - |
| 32 | 18:07:40.8 | -20:27:52.2 | HD 312693 | 19.86 | - | — |
| 33 | 18:09:15.8 | -20:31:46.6 | IRAS 18061-2032 | 80.35 | — | — |
| 34 | 18:08:44.6 | -20:30:50.8 | 2MASS J18084028-2029433 | 91.09 | - | — |
| 35 | 18:08:12.2 | -20:31:26.4 | No astronomical | — | object found | — |
| 36 | 18:08:01.7 | -20:31:17.0 | ISOGAL-P J180800.7-203117 | 13.8 | — | — |
| 37 | 18:07:53.8 | -20:31:47.3 | TYC 6259-2681-1 | 16.39 | — | — |
| 38 | 18:07:55.7 | -20:33:02.5 | IRAS 18050-2033A | 79.32 | - | — |
| 39 | 18:08:19.9 | -20:36:29.9 | HD 312696 | 105.35 | 2XMM J180819.7-203629 | 1.21 |
| 40 | 18:08:40.3 | -20:38:05.3 | TYC 6272-323-1 | 86.6 | — | — |
| 41 | 18:08:45.6 | -20:36:07.6 | TYC 6272-323-1 | — 60.66 | — | |

*Continued on next page*

Table 5.4 Continued from previous page

| Src | Pulsar | Distance | FGL | Distance | DNe | Distance |
|-----|--------|----------|-----|----------|-----|----------|
| 29 | — | — | — | — | — | — |
| 30 | — | — | — | — | [HPT2001] 09.85-0.02 | 77.64 |
| 31 | — | — | — | — | [HPT2001] 09.85-0.02 | 108.1 |
| 32 | — | — | — | — | — | — |
| 33 | — | — | — | — | — | — |
| 34 | — | — | — | — | DOBASHI 0442 | 84.45 |
| 35 | — | — | — | — | — | — |
| 36 | — | — | — | — | SDC G9.819-0.141 | 96.07 |
| 37 | — | — | — | — | SDC G9.819-0.141 | 79.04 |
| 38 | — | — | — | — | SDC G9.787-0.156 | 21.5 |
| 39 | — | — | — | — | — | — |
| 40 | — | — | 2FGL J1808.5-2037c | 110.16 | — | — |
| 41 | — | — | — | — | — | — |

*Continued on next page*

Table 5.4 *Continued from previous page*

| Src | HII | Distance | MC | Distance | Radio | Distance |
|-----|-----|----------|-----|----------|-------|----------|
| 29 | — | — | — | — | — | — |
| 30 | — | — | [RBP2006] G09.86-0.04 | 87.93 | BGPS G009.852-00.046 | 77.99 |
| 31 | — | — | [RBP2006] G09.86-0.04 | 112.06 | BGPS G009.852-00.046 | 88.49 |
| 32 | — | — | — | — | JCMTSE J180738.2-202855 | 72.66 |
| 33 | — | — | — | — | — | — |
| 34 | — | — | — | — | — | — |
| 35 | — | — | — | — | — | — |
| 36 | — | — | — | — | — | — |
| 37 | — | — | — | — | AGAL G009.781-00.166 | 119.11 |
| 38 | — | — | — | — | AGAL G009.781-00.166 | 41.06 |
| 39 | — | — | — | — | — | — |
| 40 | — | — | — | — | — | — |
| 41 | — | — | — | — | — | — |

The Table 5.2 give us information about the sources number 29 till 41. More details about them are given below. Source number 29 can be identified to be the asymptotic giant branch star candidate 2MASS J18081769-2026260 just 0.95 arcsec offset. In the 2 arcmin region there is also the YSOC 2MASS J18081752-2024586 is located at 87.19 arcsec, and the [SPK2012] MWP1G009955-001741 bubble source at 97.41 arcsec offset. The closest object found to be in the 2 arcmin vicinity of source number 30 is the main sequence star TYC 6259-2696-1 located 39 arcsec offset, but there is also another star of this kind HD 312693, 103.56 arcsec offset. As well as thirteen YSO; two dark nebula; the mm source BGPS G009.852-00.046 located at 77.99 arcsec; the molecular cloud [RBP2006] G09.86-0.04 at 87.93 arcsec and the far IR source IRAS 18046-2025 at 94.82 arcsec offset. Source number 31 can be identified to be the YSOC 2MASS J18074422-2026454 located at 10.94 arcsec offset. Other objects in the 2 arcmin region are: the main sequence stars TYC 6259-2696-1 and HD 312693 at 51.34 and 69.29 arcsec offset; two sub-millimetric radio sources, one mm source; the molecular cloud [RBP2006] G09.86-0.04 located at 112.06; the dense core source BGPS G009.856-00.102 at 116.28 arcsec; and the dark nebula source SDC G9.864-0.102 located 119.88 arcsec offset. Source number 32 can be identified to be the B-type star HD 312693, in this region 10 young stellar objects were found, being 2MASS J18074263-2027360 the closest, 30.52 arcsec offset. There are also, the sub-millimetric radio source JCMTSE J180738.2-202855, located 72.66 arcsec offset, the main sequence star TYC 6259-2696-1, 85.97 arcsec offset and the mm source BGPS G009.852-00.046 at 92.83 arcsec, The only object found in the 2 arcmin region around source number 33 was the main sequence star IRAS 18061-2032, found at 80.35 arcsec offset. Only three sources in the 2 arcmin vicinity were found in SIMBAD for source number 34: the dark nebula DOBASHI 0442 was found 84.45 arcsec offset, the asymptotic giant branch star 2MASS J18084028-2029433 located at 91.09 arcsec away and the YSOC SSTGLMC

G009.9054-00.2844 at 99.60 arcsec offset. No astronomical object was found in the 2 arcmin region around source number 35. Source number 36 can be identified to be the YSOC ISOGAL-P J180800.7-203117, 13.80 arcsec offset; there are other two objects of this nature in the region; as well as the asymptotic giant branch star candidate 2MASS J18075680-2031247 found to be 68.86 arcsec away; the main sequence star HD 312695 at 79.43 arcsec offset; and two dark nebulae SDC G9.819-0.141 and SDC G9.845-0.138 located 96.07 and 118.55 arcsec offset. Source number 37 can be identified to be the main sequence star TYC 6259-2681-1 located 16.39 arcsec offset. Other star of this nature in the vicinity is HD 312695 located at 107.22 arcsec; two asymptotic giant branch stars were also found in the region, as well as two dark nebuale, two YSOC, the outflow EGO G009.78-0.17 at 117.60 arcsec offset ant the sub-millimetric radio source AGAL G009.781-00.166 at 199.11 arcsec. Source number 38 is very likely to be the dark nebula SDC G9.787-0.156 located 21.50 arcsec offset; in the region there were found also the outflow EGO G009.78-0.17 is at 39.50 arcsec; the sub-millimetric radio source AGAL G009.781-00.166 is at 41.06 arcsec; the dense core source BGPS G009.779-00.166 is at 45.25 arcsec; the YSOC IRAS 18050-2033A is at 79.32 arcsec; the main sequence star TYC 6259-2681-1 is at 94.85 arcsec as well as other two giant branch star candidates. Source number 39 is identified to be the X-ray source 2XMM J180819.7-203629 located 1.21 arcsec offset.In the vicinity there were also: one IR source IRAS 18054-2035 located at 102.63 arcsec, the F-type star HD 312696 at 105.35 arcsec offset, and the YSOC SSTGLMC G009.8086-00.2467 located at 118.68 arcsec away from the source. The IR source IRAS 18056-2039 was found to be the closest object to the source number 40, located at 37.08 arcsec offset, but there were found also two main sequence stars and the gamma-ray source 2FGL J1808.5-2037c at 110.16 arcsec offset. Two main sequence star and one IR source were the objects found in the region around source number 41. TYC 6272-323-1 located at 60.66 arcsec offset,

HD 313763 at 86.53 arcsec and IRAS 18059-2036 at 108.99 arcsec offset, respectively.

With the purpose of knowing which of all the sources are dominated by non-thermal emission and which could be counterpart for the TeV emission of the HESS source, we did a cut in the energy range of the image using the 2.5 -12 keV band and then we performed the source detection tool. The sources found can be seen in the Figure 5.8.
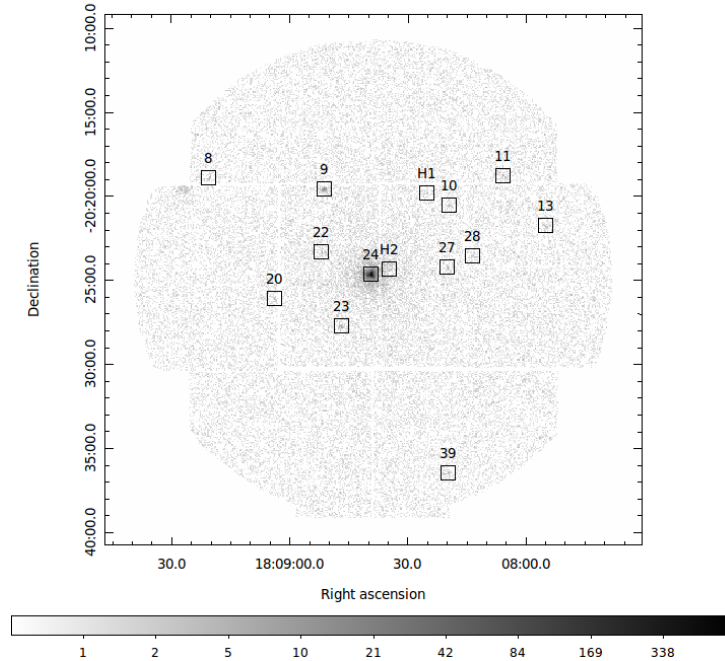


Figure 5.8: Counts map observation using ObsID 0554600301 made by XMM-Newton of HESS J1626-490 with a cut in the energy from 2.5 keV to 12 keV, the black squares indicate 14 sources detected making use of the EPIC source detection tool.

In the Table 5.11 we can find the sources, its position (R.A., dec.), the possible counter part, its offset to the source and their fluxes..

Source number 8 can be identified to be the Wolf-Rayet star 3XMM J180920.3-201857, which is located at just 2.94 arcsec offset. It is known that in the region between two Wolf-Rayet stars the winds collide with speeds of order 1000 km/s, and therefore, massive binary systems are likely sources of high-energy gamma rays, produced either by by inverse-Compton scattering of accelerated electrons, or by acceler-

Table 5.5: Sources dominated by non-thermal emission found using ObsID 0554600301 of HESS J1808-204. The flux values are in erg cm$^{-2}$s$^{-1}$.

| Src | RA J2000 | DEC J2000 | Possible counterpart | Offset arcsec | Flux E-14 |
|---|---|---|---|---|---|
| 8 | 18:09:20.4 | -20:18:54.4 | 3XMM J180920.3-201857 | 2.94 | 2.49 |
| 9 | 18:08:51.1 | -20:19:35.4 | 2XMM J162802.8-491154 | 0.79 | 3.66 |
| 10 | 18:08:19.4 | -20:20:33.4 | - | - | 0.79 |
| 11 | 18:08:05.7 | -20:18:47.2 | - | - | 1.47 |
| 13 | 18:07:54.9 | -20:21:47.2 | 2XMM J180754.3-202251 | 65.02 | 1.60 |
| 20 | 18:09:03.8 | -20:26:05.3 | Not sure | ? | 0.78 |
| 22 | 18:08:51.8 | -20:23:21.5 | JCMTSE J180844.5-202413 | 115.34 | 0.43 |
| 23 | 18:08:46.7 | -20:27:45.0 | SDC G9.984-0.267 | 114.82 | 0.97 |
| 24 | 18:08:39.4 | -20:24:39.2 | PSR J1808-2024 | 1.00 | 98.5 |
| 27 | 18:08:19.9 | -20:24:14.0 | Not sure | - | 0.67 |
| 28 | 18:08:13.4 | -20:23:32.6 | Not sure | - | 0.49 |
| 39 | 18:08:19.7 | -20:36:28.8 | 2XMM J180819.7-203629 | 2.34 | 2.02 |
| H1 | 18:08:25.2 | -20:19:48.4 | Not sure | - | 0.52 |
| H2 | 18:08:34.6 | -20:24:22.7 | Not sure | - | 0.45 |

ation of nuclei followed by collisions with ambient material and gamma-ray production via the decay of pions created in the collision (see [172] and refs. given there, and [173], https://www.mpi-hd.mpg.de/hfm/HESS/pages/home/som/2006/12/). As well as in colliding wind region of early-type binaries gamma-ray flux could be producing in WR+OB systems [174], [175]. Other studies have found gamma-ray emission form Wolf-Rayet stars interacting with AGN jets (see for example[176]), however, there is no evidence isolated WR stars could have gamma-ray emission. Source number 9 is the X-ray source 2XMM J180851.0-201935 which was found to be 0.30 arcsec offset. This object can be identified to be the X-ray counter part, this source could be producing part of the VHE emission of HESS J1808-204; however, it it not extended enough to produce all the emission. There were found five objects around source number 10. The closest is the IR source HFE 49, at 39.03 arcsec offset, the x-ray source AX J1808.2-2021 is at 76.74 arcsec away; two YSOC which are more than 95 arcsec offset, and the dark nebula SDC G9.991-0.147 which is 100.49 arcsec offset. In the case of source number

11, there were found three stars, the closest is a main sequence star TYC 6272-29-1, 52.94 arcsec offset; after we have the asymtotic giant branch star candidate SSTGLMC G010.0274-00.0633 at 68.54 arcsec, and the OH star OH 10.03 -0.06, 69.21 arcsec offset. None of them could explain the VHE emission from HESS source. Source number 13 could be identified as the X-ray source 2XMM J180754.3-202251, which was found to be 65.02 arcsec offset. In the 2 arcmin region around source number 20, eleven sources were found. The closest is the sub-millimetric radio source AGAL G010.026-00.352 at 55.88 arcsec offset, the dense core source [TBH2012] 209 was also found at the same distance; the IR source IRAS 18060-2025 is at 56.91 arcsec; other dense core source was found ([TBH2012] 184 at 59.91 arcsec), three sub-millimetric radio sources more and one mm; the dark nebula SDC G10.031-0.355 located 76.49 arcsec offset, and the YSOC SSTGLMC G010.0386-00.3608 at 105.58 arcsec. The only source found in the 2 arcmin region around source 22 was the sub-millimetric radio source JCMTSE J180844.5-202413 at 115.34 arcsec offset. The only source found in the 2 arcmin vicinity of source 23 was the dark nebula SDC G9.984-0.267 at 114.82 arcsec offset. The region around source 24 is a bit complicated with 80 sources in the 2 arcmin vicinity. Four stars were found 0.23 arcsec offset, [EGH2001b] A1, A2, A3, A4, B1; moreover, 0.62 arcsec offset we can find a set of molecular clouds ([CWD97] MC+73, +87, +4, -16, +94, +38, +44, +30, +24, +13, +13A, +13B) which could strengthen an hadronic scenario. The IR source [EGH2001] J180839.32-202439.5 was found at the same offset and the pulsar PSR J1808-2024 is just 1.00 arcsec offset, this source could be a plausible counterpart of the HESS region if we could find the PWN that could explains the VHE emission. Furthermore, the massive stellar cluster Cl* 1806-20 is located at 5.07 arcsec away and the X-ray source SWIFT J180839.4-202435 located at 3.99 arcsec, etc. The two arcmin region around source number 27 is composed with nine sources found in SIMBAD, the closest is the bubble source [SPK2012] MWP1G009955-001741 at 38.10 arcsec; but

there are also three YSOC, two radio sources, one main sequence star, and two dark nebulae: SDC G9.986-0.170 and SDC G9.987-0.164, 86.17 and 86.97 arcsec offset, respectively. Around source number 28 there were found three YSOC, being SSTGLMC G009.9721-00.1542 the closest object to the source 48.65 arcsec offset, as well as one main sequence star, two bubble sources, and two dark nebulae SDC G9.991-0.147 and SDC G9.987-0.164 at 100.92 and 114.22 arcsec offset, respectively. Source number 39 can be identified to be the X-ray source 2XMM J180819.7-203629 located 2.34 arcsec offset. This object can explain the X-ray but not the VHE emission from the HESS source. There are also one IR source, one main sequence star and one YSOC in the 2 arcmin vicinity, but more than 100 arcsec offset.

There are nine source around the 2 arcmin region of source H1. Being the asymptotic giant branch star candidate 2MASS J18082613-2019115 the closest object, located at 39.08 arcsec; the dark nebula TGU H122 P5 is at 83.05 arcsec offset, there are also four radio sources, one YSOC, one IR and one bubble sources around. Seventy eight sources were found around H2, with the sub-millimetric radio source JCMTSF J180835.9-202400 the closest at 29.48 arcsec offset. The cluster Cl* 1806-20 was found to be 64.52 arcsec away, so ten stars in a cluster were found in the search on SIMBAD, the twelve molecular clouds are at 69.00 arcsec offset and the PSR J 1808-2024 is at 69.20 arcsec offset.

## 5.3 Chandra Observations

Four Chandra observations has been carried out in the region of the HESS J1808-204 source (see Table 5.1), all of them had the SGR 1806-20 as the target. This neutorn star was discovered to be a soft $\gamma$-ray repeater (SGR) [177] and has a X-ray counter part, AX 1805.7-2025 discovered by [178], and the X-ray pulsation having a period of 7.47 s was resolved by [179] The SGRs and anomalous X-ray pulsars are found to be magnetars

[180].

**0746**

This Chandra observation was acquired on August 31st, 2001, (ObsID 0746). The chip S3 of the ACIS-S instrument was used to capture the signal and without using grating. The approved time of the observation was 33.0 ks, however the exposure was of 31.07 ks. Both `celldetect` and `vtpdetect` tools were applied to execute the analysis. Three sources were found with celldetect and two more were detected using vtpdetect, those can be seen as blue ellipses in Figure 5.9(a). Considering the energy cut range from 2.5 to 8 keV to look on sources dominated by non-thermal emission we could find the first two sources with `celldetect` and all the five sources with `vtpdetect`, as well as one new H1 souce, as seen in Figure 5.9(b). More information of all these sources can be found in Table 5.3.
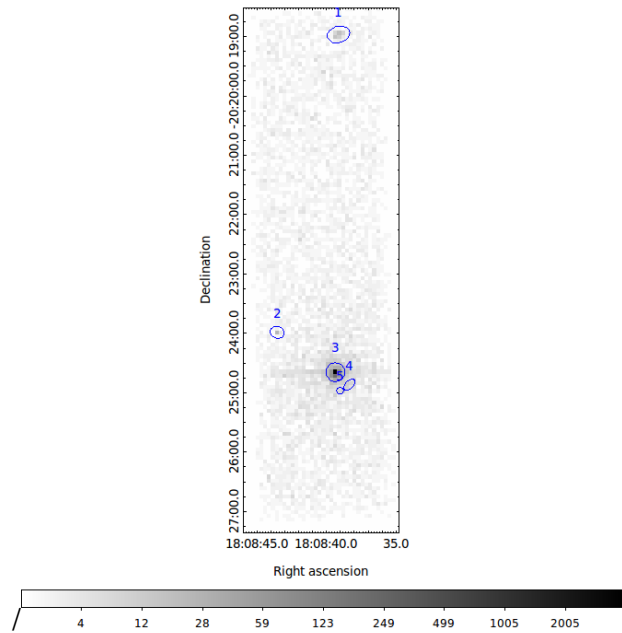
(a) Counts map observation using the energy range 0.5 - 7 keV, the blue squares indicate 5 sources detected making use of vtpdetect tool.
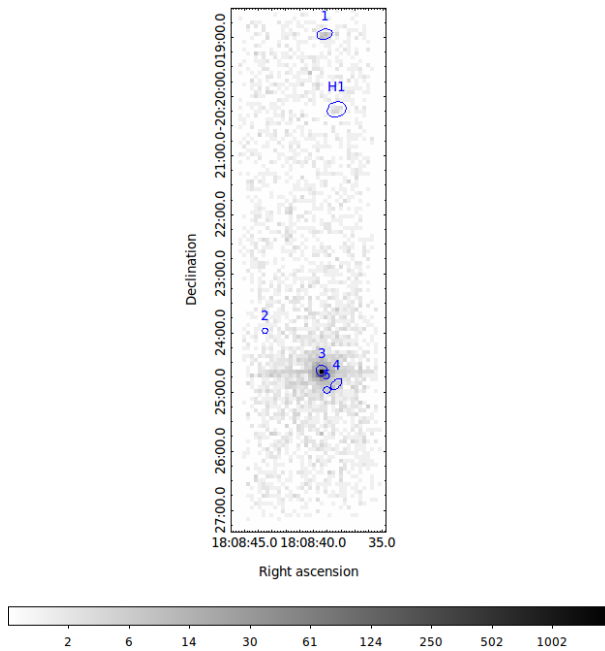


(b) Counts map observation using the hard energy range 2.5 - 8 keV, the blue squares indicate 5 sources detected making use of `celldetecgt` and `vtpdetect` tool.

Figure 5.9: Counts map observations using ObsID 00726 made by Chandra telescope.

Table 5.6: Possible counterparts of HESS J1808-204 found using ObsID 0746 of Chandra Observatory (Distance in arcsec).

| Src | RA (J2000) | DEC (J2000) | Star | Distance | X-ray | Distance |
|-----|-----------|-------------|------|----------|-------|----------|
| 1 | 18:08:39.2 | -20:18:57.4 | TYC 6272-185-1 | 26.53 | – | – |
| 2 | 18:08:43.6 | -20:23:59.4 | 2MASS J18084346-2023591 | 1.40 | SWIFT J180839.4-202435 | 68.56 |
| 3 | 18:08:39.3 | -20:24:39.7 | [EGH2001b] B1 | 0.15 | SWIFT J180839.4-202435 | 4.55 |
| 4 | 18:08:38.3 | -20:24:52.3 | 2MASS J18083812-2024433 | 9.37 | SWIFT J180839.4-202435 | 22.90 |
| 5 | 18:08:38.9 | -20:24:58.4 | [KMN95] Star 7 | 15.21 | SWIFT J180839.4-202435 | 23.84 |
| H1 | 18:08:38.2 | -20:20:13.7 | TYC 6272-633-1 | 3.27 | – | – |

| Src | Pulsar | Distance | FGL | Distance | HII | Distance |
|-----|--------|----------|-----|----------|-----|----------|
| 1 | – | – | – | – | [LPH96] 010.068-0.176 | 79.65 |
| 2 | PSR J1808-2024 | 72.22 | – | – | JCMTSF J180843.2-202343 | 17.22 |
| 3 | PSR J1808-2024 | 0.40 | – | – | [GKG2005] VLA J180839-202439 | 5.94 |
| 4 | PSR J1808-2024 | 18.65 | – | – | [GKG2005] VLA J180839-202439 | 18.91 |
| 5 | PSR J1808-2024 | 18.89 | – | – | [GKG2005] VLA J180839-202439 | 22.41 |
| H1 | – | – | – | – | [LPH96] 010.068-0.176 | 101.31 |

*Continued on next page*

216

Table 5.6 *Continued from previous page*

| Src | MC | Distance | DNe | Distance | Radio | Distance |
|-----|-----|----------|------------------|--------|---------------------|----------|
| 1 | — | — | — | — | BGPS G010.074-00.190 | 25.52 |
| 2 | — | — | SDC G9.984-0.267 | 119.39 | [CWD97] MC+73 | 71.92 |
| 3 | — | — | SDC G9.984-0.267 | 99.71 | [CWD97] MC+73 | 0.25 |
| 4 | — | — | SDC G9.984-0.267 | 100.14 | [CWD97] MC+73 | 19.01 |
| 5 | — | — | SDC G9.984-0.267 | 89.07 | [CWD97] MC+73 | 19.46 |
| H1 | — | — | — | — | | |

Source number 1 can be identified to be the dense core AGAL G010.079-00.196 at 5.16 arcsec offset. However, in the 2 arcmin vicinity of the soirce were found other sources, eight of them are radio, one is a mm source (BGPS G010.074-00.190 at 25.52 arcsec away) and six are sub-millimetric radio sources. There are also two main sequence stars, TYC 6272-185-1 and TYC6272-633-1 at 26.53 and 80.30 arcsec offset. The HII region [LPH96] 010.0.68-00.176 is located at 79.65 arcsec. More than 100 arcsec away there are also a young stellar object candidate and a bubble source. In the case of source number 2, the 2 arcmin is a complex region with eighty objects in the vicinity. The closest source is the 2MASS J18084346-2023591 star at just 1.40 arcsec away. The massive star cluster Cl* 1806-20, is located at 74.44 arcsec, and there are 11 stars of the cluster in the 2 arcmin region, but there are also other thirty two main sequence stars in the vicinity. Also, the blue supergiant star [KMN95] Star A is at 61.93 arcsec, and two possible giant stars, [EML2004] Star C located at 64.73 arcsec and [FNG2005] 4 at 70.44 arcsec. The pulsar PSR J1808-2024 is located 72.22 arcsec offset, seven molecular clouds are located at 71.92 arcsec, three Wolf-Rayet stars are a less than 75 arcsec, WR 111c at 72.56 arcsec, WR 111b at 68.97 arcsec and WR 111d at 67.84 arcsec away. The x-ray source SWIFT J180839.4-202435 is located at 68.56 arcsec. There are also two IR sources located at 72.72 and 104.13 arcsec away ([EGH2001] J18083874-202440.5, and IRAS 18056-2025, respectively). The interstellar matter region AX J1808.6-2024 is located at 73.91 arcsec and the dark nebula SDC G9.984-0.267 is 119.39 arcsec away. Source number 3 is in the same position of source number 24 of the XMM-Newton observation (ObsID 0554600301). However, in this case the closest sources are two stars [EGH2001b] B1 and B3, located at 0.15 and 0.23 arcsec offset, respectively. Twelve molecular clouds are at just 0.25 arcsec and also the IR source [EGH2001] J180839.32-202439.5 is at the same distance. The pulsar PSR J 1808-2024 is 0.40 arcsec away. Farther than this distance, we have 30 stars, 3 more

IR sources, and 11 stars in a cluster and the NAME 1806-20 Star Cluster is located at 5.94 arcsec offset. Furthermore, three WR stars can be found at less than 8 arcsec offset, two possible supergiant stars, and one blue star are also not farther than 15 arcsec away. The x-ray source SWIFT J180839.4-202435 is at just 4.55 arcsec. Furthermore, eight radio sources are also in the 2 arcmin region, there are seven sub-millimetric radio sources among them, as well as two objects of unknown nature ([KMN95] K and HK) located at 13.70 arcsec both of them. By last, the dark nebula SDC SDC G9.984-0.267 is at 99.71 arcsec offset. Due to the proximity of the sources 3, 4 and 5, the same 80 sources are in the 2 arcmin vicinity for all the three cases as well as for source number 2, nevertheless the distances between the sources are a bit different. All five sources were detected when applying the cut in the energy range, and there was one new source detected, H1. Source H1 can be identified to be the main sequence star TYC 6272-633-1, 3.27 arcsec offset. In this region there were found the YSOC SSTGLMC G010.0623-00.1709, 114.16 arcsec offset; and also 6 sub-millimetric radio sources and 1 mm, one core (AGAL G010.079-00.196 at 75.14 arcsec) and the HII region [LPH96] 010.068-0.176, located 100.50 arcsec offset. The SNR obtained for this source was of 3.043067.

**1827**

This observation had the same target as the last observation, it was performed on July 27th, 2001 using the CCDs: I2, I3, S1, S2, S3 and S4 of the instrument ACIS-S. The approved time for this case was of 5.0 ks and we got an exposure time of 4.89 ks. It was done using the exposure mode TE (see Figure 5.10).

For making the analysis, we performed `celldetect` and `vtpdetect` detection tools, and we could find 4 sources with the first tool and one more using the other (source number 5), which can be seen as magenta circles on Figure 5.10(a). A cut in the energy

range was applied to look for sources dominated by non-thermal emission. Four of them were encountered once again, and one more appeared, the results are shown in Figure 5.10(b) and more information can be found in Table 5.3.
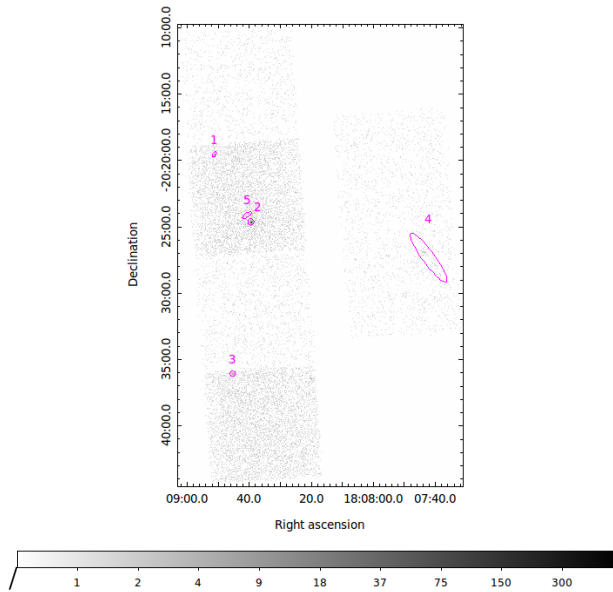
(a) Counts map observation using the energy range 0.5 - 7 keV, the magenta squares indicate 5 sources detected making use of vtpdetect tool.
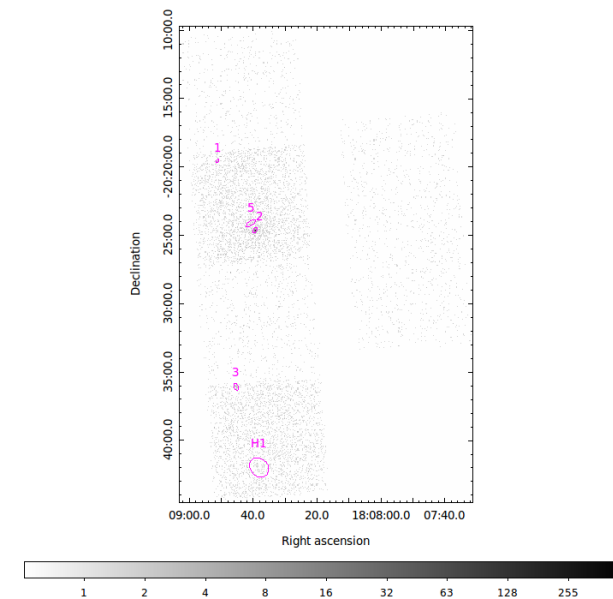


(b) Counts map observation using the hard energy range 2.5 - 8 keV, the magenta squares indicate 5 sources detected making use of `celldetecgt` and `vtpdetect` tool.

Figure 5.10: Counts map observations using ObsID 1827 made by Chandra telescope.

Table 5.7: Possible counterparts of HESS J1808-204 found using ObsID 1827 of Chandra Observatory (Distance in arcsec).

| Src | RA (J2000) | DEC (J2000) | Star | Distance | X-ray | Distance |
|---|---|---|---|---|---|---|
| 1 | 18:08:51.0 | -20:19:34.9 | — | — | 2XMM J180851.0-201935 | 1.09 |
| 2 | 18:08:39.3 | -20:24:39.8 | [EGH2001b] B1 | 0.08 | SWIFT J180839.4-202435 | 4.64 |
| 3 | 18:08:45.2 | -20:36:06.2 | TYC 6272-323-1 | 60.98 | — | — |
| 4 [a] | 18:07:42.2 | -20:27:20.6 | 2MASS J18074263-2027360 | 16.63 | — | — |
| 5 | 18:08:40.6 | -20:24:09.4 | [FNG2005] 13 | 15.77 | SWIFT J180839.4-202435 | 30.80 |
| H1 | 18:08:38.1 | -20:42:01.5 | TYC 6276-1183-1 | 84.61 | — | — |

| Src | Pulsar | Distance | FGL | Distance | MC | Distance |
|---|---|---|---|---|---|---|
| 1 | PSR J1808-2024 | 0.36 | — | — | — | — |
| 2 | — | — | — | — | [CWD97] MC+73 | 0.47 |
| 3 | — | — | — | — | — | — |
| 4 | — | — | — | — | [RBP2006] G09.86-0.04 | 110.03 |
| 5 | PSR J1808-2024 | 35.54 | — | — | [CWD97] MC+73 | 35.04 |
| H1 | — | — | — | — | — | — |

*Continued on next page*

Table 5.7 Continued from previous page

| Src | HII | Distance | DNe | Distance | Radio | Distance |
|-----|-----|----------|-----|----------|-------|----------|
| 1 | — | — | — | — | — | — |
| 2 | — | — | SDC G9.984-0.267 | 99.50 | [GKG2005] VLA J180839-202439 | 6.16 |
| 3 | — | — | — | — | — | — |
| 4 | — | — | [HPT2001] 09.85-0.02 | 100.79 | BGPS G009.852-00.046 | 81.39 |
| 5 | — | — | SDC G9.984-0.267 | 117.49 | JCMTSF J180841.9-202355 | 23.29 |
| H1 | — | — | — | — | — | — |

Source number 1 can be identified to be the X-ray source 2XMM J180851.0-201935, found 1.09 arcsec offset.

The source number 2 is located in the same region of source number 3 of observation 0746, it has the same 80 sources in the vicinity with some difference in the coordinates.

The source number 3 has just three objects in the 2 arcmin vicinity; the first object is a main sequence star TYC 6272-323-1 at 60.98 arcsec offset, the second is also another star HD 313763 at 91.33 arcsec, and the third one is an IR source IRAS 18059-2036, located at 113.54 arcsec.

Source number 4 can be identified to be the YSO 2MASS J18074263-2027360 located at 16.63 arcsec offset. However, this source is located in a region of young stars, in the 2 arcmin vicinity there are thirteen young stellar objects, two main sequence stars, one mm and one sub-millimetric radio sources, as well as the molecular cloud [RBP2006] G09.86-0.04 and the dark nebula [HPT2001] 09.85-0.02, located at 110.03 and 110.79 arcsec offset, respectively. This source was not detected in the hard energy range, so we can say it is dominated by thermal emission.

The source number 5 is also located close to the source number 2, having the same 80 sources in the vicinity, with small differences between the distances.

The new source found with the hard energy cut H1 was found to be at 84.61 arcsec from the main sequence star TYC 6276-1183-1, no other sources were found in SIMBAD in the 2 arcmin vicinity. The SNR obtained for this source was of 3.387602.

**6224**

With the same target name as the other observations, this one had an approved time of 20 ks, but and exposure of 18.82 ks and was acquired on February 9th, 2005. It was done using the instrument ACIS-I, in specific, using the chips I0, I1, I2, I3, S2 and S3 (see Figure 5.11) and as all in the other observations, we carried out the source detection

by using `celldetect` and `vtpdetect` tools.

In the case of this observation, the first 16 sources were detected using both `celldetect` and `vtpdetect` tools, all the others were found just using `vtpdetect`. The sources 13 and 14 were seen by `vtpdetect` as just one marked as 13, 14. See Figure 5.11(a), more information on these sources can be found in Table 5.3.

Making the cut in the energy range to looking for the sources with non-thermal emission dominated, eleven sources were found with this emission. The possible association to all the sources can be seen in Table 5.11.
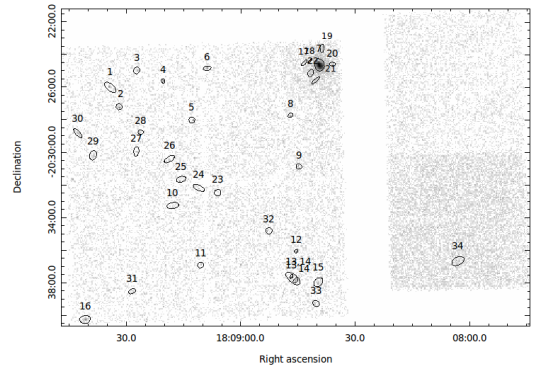
(a) Counts map observation using the energy range 0.5 - 7 keV, the black ellipses indicate 33 sources detected making use of `celldetect` and `vtpdetect` tools.
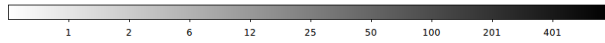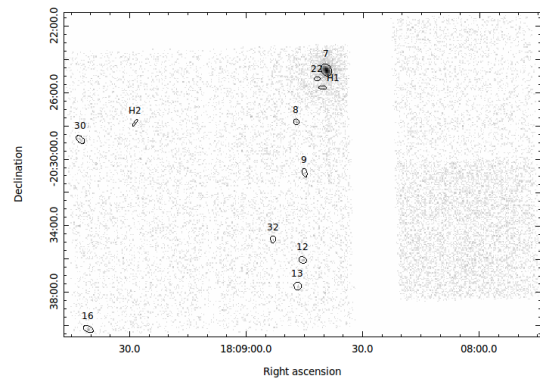


(b) Counts map observation using the hard energy range 2.5 - 8 keV, the black ellipses indicate 11 sources detected making use of `celldetect` and `vtpdetect` tools.

Figure 5.11: Counts map observation of ObsID 6224 using Chandra telescope.

Table 5.8: Possible counterparts of HESS J1808-204 using ObsID 6224 done by Chandra observatory (Distance in arcsec), Part 1.

| Src | RA (J2000) | DEC (J2000) | Star | Distance | X | Distance |
|---|---|---|---|---|---|---|
| 1 | 18:09:34.1 | -20:26:02.4 | – | – | – | – |
| 2 | 18:09:31.8 | -20:27:14.1 | – | – | – | – |
| 3 | 18:09:27.1 | -20:25:00.3 | – | – | – | – |
| 4 | 18:09:20.2 | -20:25:39.0 | – | – | – | – |
| 5 | 18:09:12.7 | -20:28:02.4 | HD 312684 | 4.94 | 2XMM J180912.2-202801 | 4.92 |
| 6 | 18:09:08.7 | -20:24:52.7 | SSTGLMC G010.0386-00.3608 | 70.43 | – | – |
| 7 | 18:08:39.3 | -20:24:39.8 | [EGH2001b] B1 | 0.04 | SWIFT J180839.4-202435 | 4.58 |
| 8 | 18:08:46.9 | -20:27:45.3 | – | – | – | – |
| 9 | 18:08:44.7 | -20:30:54.0 | – | – | 2MASS J18084028-2029433 | 93.68 |
| 10 | 18:09:17.7 | -20:33:17.5 | IRAS 18061-2032 | 119.13 | – | – |
| 11 | 18:09:10.5 | -20:36:56.7 | IRAS 18061-2038 | 60.01 | – | – |
| 12 | 18:08:45.3 | -20:36:05.0 | TYC 6272-323-1 | 62.39 | – | – |
| 13 | 18:08:46.6 | -20:37:38.0 | TYC 6272-323-1 | 42.65 | – | – |
| 14 | 18:08:45.5 | -20:37:53.9 | TYC 6272-323-1 | 48.66 | – | – |

*Continued on next page*

227

Table 5.8 Continued from previous page

| Src | FGL | Distance | Pulsar | Distance | HII | Distance |
|---|---|---|---|---|---|---|
| 1 | – | – | – | – | IRAS 18065-2026 | 73.31 |
| 2 | – | – | – | – | IRAS 18065-2026 | 86.33 |
| 3 | – | – | – | – | [L89b] 10.073-00.412 | 32.76 |
| 4 | – | – | – | – | [L89b] 10.073-00.412 | 95.27 |
| 5 | – | – | – | – | – | – |
| 6 | – | – | – | – | – | – |
| 7 | – | – | PSR J1808-2024 | 0.038 | – | – |
| 8 | – | – | – | – | – | – |
| 9 | – | – | – | – | – | – |
| 10 | – | – | – | – | – | – |
| 11 | – | – | – | – | – | – |
| 12 | – | – | – | – | – | – |
| 13 | – | – | – | – | – | – |
| 14 | – | – | – | – | – | – |

Table 5.8 *Continued from previous page*

| Src | MC | Distance | DN | Distance | Radio | Distance |
|---|---|---|---|---|---|---|
| 1 | — | — | SDC G10.086-0.438 | 26.81 | [BGPS] G010.084-00.436 | 20.65 |
| 2 | — | — | SDC G10.043-0.425 | 76.85 | [SSS2011] BGPS G10.043-0.424 | 82.59 |
| 3 | — | — | SDC G10.082-0.414 | 23.55 | [ERG2015] 2357 | 22.19 |
| 4 | — | — | SDC G10.069-0.400 | 54.72 | AGAL G010.068-00.407 | 70.61 |
| 5 | — | — | DOBASHI 0444 | 68.98 | AGAL G010.019-00.394 | 51.07 |
| 6 | — | — | SDC G10.055-0.355 | 47.65 | BGPS G010.045-00.354 | 37.99 |
| 7 | [CWD97] MC+73 | 0.36 | SDC G9.984-0.267 | 99.61 | [GKG2005] VLA J180839-202439 | 6.05 |
| 8 | — | — | SDC G9.984-0.267 | 115.90 | — | — |
| 9 | — | — | DOBASHI 0442 | 82.78 | — | — |
| 10 | — | — | — | — | — | — |
| 11 | — | — | — | — | — | — |
| 12 | — | — | — | — | — | — |
| 13 | — | — | — | — | — | — |
| 14 | — | — | — | — | — | — |

The 2 arcmin around source number 1 is formed by 4 sub-millimetric radio sources being BGPS G010.084-00.436 the closest. There are also, three dark nebula sources in the vicinity, SDC G10.082-0.414 at 26.81, SDC G10.082-0.414 located at 93.02 arcsec, and SDC G10.094-0.415 at 102.96 arcsec, the HII regions are also close to the source: IRAS 18065-2026 at 73.31 arcsec and [L89b] 10.073-00.412 at 103.70 arcsec offset. The core source [WWS2012] G010.11-00.41 is at 117.51 arcsec away, and the bubble source is [SPK2012] MWP1G010078-004186 is located at 75.99 arcsec. The closest source to the source number 2, found in SIMBAD was to be the dark nebula SDC G10.043-0.425 at 76.85 arcsec, this source is in the same position of source number 18 of the XMM-Newton ObsID 0554600301. In the other hand, the mm source [SSS2011] BGPS G10.043-0.424 is located at 82.59 arcsec and the HII region IRAS 18065-2026 at 86.33 arcsec. There are also 3 sub-millimetric radio sources in the 2 arcmin vicinity, another dark nebula and the bubble source [SPK2012] MWP1G010078-004186 at 110.28 arcsec offset. Source number 3 is in the same position as source number 15 of XMM-Newton ObsID 0554600301. Source number 4 is in the same position of source number 17 of XMM-Newton ObsID 0554600301. Source number 5 is in the same position of source number 19 of XMM-Newton ObsID 0554600301. The closest source to the number 6 is a sub-millimetric radio one, BGPS G010.045-00.354 located at 37.99 arcsec. In the 2 arcmin region, there are also two dark nebulae, being SDC G10.055-0.355 the closest, 47.65 arcsec offset; the IR source IRAS 18060-2025 is at 63.40 arcsec away; the SSTGLMC G010.0386-00.3608 source is catalogued as a YSOC, 70.34 arcsec offset; there are also three sub-millimetric radio sources being AGAL G010.033-00.356 the closest, located 70.25 arcsec away; and two core sources [TBH2012] 184 and [TBH2012] 209, at 81.11 and 109.53 arcsec away, respectively. The source number 7 was found to be the same as source marked with number 3 of ObsID 0746, and source number 24 of ObsID 0554600301. Source number 8 is in the same

position of source 23 of ObsID 0554600301. Source number 9 is in the same position of source number 34 of ObsID 0554600301. 2 arcmin around the source number 10, the only object found was the star IRAS 18061-2032 located very far away, at 119.13 arcsec. The only object found in the 2 arcmin region around source number 11 is the star IRAS 18061-2038, located 60.01 arcsec. The source 12 was found to be in the same of source 41 of ObsID 0554600301. The source number 13 was found to be close to three stars: TYC 6272-323-1 at 42.65 arcsec, HD 313763 at 63.84 arcsec, and IRAS 18057-2039 at 99.52 arcsec away. The star TYC 6272-323-1 is at 48.66 arcsec away from source 14, HD 313763 at 84.46 arcsec, and IRAS 18057-2039 at 85.06 arcsec. The IR source IRAS 18056-2039 was found to be at 105.96 arcsec away. The region marked with 13,14 was found using `vtpdetect` and involves both 13 and 14 sources region.

Table 5.9: Possible counterparts of HESS J1808-204 found using ObsID 6224 of Chandra Observatory, (Distance in arcsec), Part 2.

| Src | RA (J2000) | DEC (J2000) | Star | Distance | X | Distance |
|---|---|---|---|---|---|---|
| 15 | 18:08:39.6 | -20:37:59.5 | TYC 6272-323-1 | 87.90 | – | – |
| 16 | 18:09:40.7 | -20:40:16.7 | VVV J180938.83-204213.7 | 119.82 | – | – |
| 17 | 18:08:43.3 | -20:24:32.2 | 2MASS J18084346-2023591 | 33.13 | SWIFT J180839.4-202435 | 54.54 |
| 18 | 18:08:41.8 | -20:24:24.9 | [KMN95] Star 9 | 19.09 | SWIFT J180839.4-202435 | 34.69 |
| 19 | 18:08:38.6 | -20:23:38.6 | 2MASS J18083856-2024135 | 34.91 | SWIFT J180839.4-202435 | 57.98 |
| 20 | 18:08:35.9 | -20:24:37.6 | 2MASS J18083672-2024277 | 15.47 | SWIFT J180839.4-202435 | 49.89 |
| 21 | 18:08:40.3 | -20:25:37.2 | USNO-A2.0 0675-24234251 | 29.81 | SWIFT J180839.4-202435 | 63.15 |
| 22 | 18:08:41.6 | -20:25:09.9 | USNO-A2.0 0675-24234251 | 3.13 | SWIFT J180839.4-202435 | 46.40 |
| 23 | 18:09:06.9 | -20:32:30.4 | IRAS 18061-2032 | 65.26 | – | – |
| 24 | 18:09:10.9 | -20:32:12.5 | IRAS 18061-2032 | 5.91 | – | – |
| 25 | 18:09:15.5 | -20:31:41.7 | IRAS 18061-2032 | 78.28 | – | – |
| 26 | 18:09:18.6 | -20:30:26.6 | No astronomical | - | was found | – |
| 27 | 18:09:27.3 | -20:29:58.9 | TYC 6272-159-1 | 55.46 | – | – |
| 28 | 18:09:26.1 | -20:28:47.1 | TYC 6272-159-1 | 47.71 | – | – |

Table 5.9 *Continued from previous page*

| Src | HII | Distance | FGL | Distance | MC | Distance |
|-----|-----|----------|-----|----------|-----|----------|
| 15 | — | — | 2FGL J1808.5-2037c | 98.02 | — | — |
| 16 | — | — | — | — | — | — |
| 17 | — | — | — | — | [CWD97] MC+73 | 56.23 |
| 18 | — | — | — | — | [CWD97] MC+73 | 37.37 |
| 19 | — | — | — | — | [CWD97] MC+73 | 61.67 |
| 20 | — | — | — | — | [CWD97] MC+73 | 48.57 |
| 21 | — | — | — | — | [CWD97] MC+73 | 59.35 |
| 22 | — | — | — | — | [CWD97] MC+73 | 43.31 |
| 23 | — | — | — | — | — | — |
| 24 | — | — | — | — | — | — |
| 25 | — | — | — | — | — | — |
| 26 | — | — | — | — | — | — |
| 27 | — | — | — | — | — | — |
| 28 | — | — | — | — | — | — |

*Continued on next page*

Table 5.9 Continued from previous page

| Src | Pulsar | Distance | DNe | Distance | Radio | Distance |
|---|---|---|---|---|---|---|
| 15 | — | — | — | — | — | — |
| 16 | — | — | — | — | AGAL G009.858-00.587 | 100.25 |
| 17 | PSR J1808-2024 | 56.25 | SDC G9.984-0.267 | 86.72 | JCMTSF J180844.0-202431 | 10.11 |
| 18 | PSR J1808-2024 | 37.56 | SDC G9.984-0.267 | 97.59 | JCMTSF J180841.9-202355 | 29.93 |
| 19 | — | — | — | — | JCMTSE J180836.4-202400 | 37.95 |
| 20 | PSR J1808-2024 | 48.65 | — | — | JCMTSF J180835.9-202400 | 37.58 |
| 21 | PSR J1808-2024 | 58.75 | SDC G9.984-0.267 | 51.77 | [GKG2005] VLA J180839-202439 | 63.90 |
| 22 | PSR J1808-2024 | 43.85 | SDC G9.984-0.267 | 56.67 | [GKG2005] VLA J180839-202439 | 49.98 |
| 23 | — | — | — | — | — | — |
| 24 | — | — | — | — | — | — |
| 25 | — | — | — | — | — | — |
| 26 | — | — | — | — | — | — |
| 27 | — | — | — | — | — | — |
| 28 | — | — | SDC G10.043-0.425 | 76.38 | [SSS2011] BGPS G10.043-0.424 | 77.87 |

The source number 15, is close to the IR source IRAS 18056-2039 located at 36.11 arcsec away, the star TYC 6272-323-1 is at 87.90 arcsec and the gamma-ray source 2FGL J1808.5-2037c at 98.02 arcsec offset from this source. It is in the same position as source 40 of ObsID 0554600301. For the case of source 16, the closest object is the far-IR source IRAS 18067-2040, located 53.46 arcsec away. In the region there were found also the sub-millimetric radio source AGAL G009.858-00.587 (100.25 arcsec offset), and the star VVV J180938.83-204213.7 located 119.82 arcsec offset from the source. The source number 17 was found to be in the same region as source number 2 of ObsID 0746, so the same 80 sources were found in the 2 arcmin vicinity but with different distances to this one, the same occurs for source 18 and source 19; however for this last one the dark nebula SDC G9.984-0.267 was not found in the region, the same 79 sources were found in the 2 arcmin vicinity for source 20. The source number 21 is also in the same region, but 78 sources were found in the region. For the source 22 the 80 sources of the same region were found in SIMBAD. In the 2 arcmin region of source 23 was found just one star IRAS 18061-2032, located at 65.26 arcsec offset. However, source number 24 can be identified to be this star, which was found to be 5.91 arcsec offset. Source number 25 is in the same position as source number 33 of ObsID 0554600301. No astronomical object was found in the 2 arcmin region around source 26. The star TYC 6272-159-1 was found to be 55.46 arcsec away from the source 27 and no other source was found in the 2 arcmin region. Around source 28, the star TYC 6272-159-1 was found to be at 44.71 arcsec offset, the dark nebula SDC G10.043-0.425 at 76.38 arcsec and the sub-millimetric radio source [SSS2011] BGPS G10.043-0.424 at 77.87 arcsec away.

Table 5.10: Possible counterparts of HESS J1808-204 found using ObsID 6224 of Chandra Observatory (Distance in arcsec).

| Src | RA (J2000) | DEC (J2000) | Star | Distance | Dark Nebula | Distance |
|-----|-----------|-------------|------|----------|-------------|----------|
| 29 | 18:09:38.6 | -20:30:12.8 | TYC 6272-553-1 | 6.05 | – | – |
| 30 | 18:09:42.6 | -20:28:51.3 | TYC 6272-361-1 | 82.01 | – | – |
| 31 | 18:09:28.4 | -20:38:32.7 | [RMB2008] G009.8980-00.5359 | 67.17 | – | – |
| 32 | 18:08:52.5 | -20:34:50.4 | TYC 6272-383-1 | 50.01 | – | – |
| 33 | 18:08:40.2 | -20:39:17.7 | IRAS 18057-2039 | 85.55 | – | – |
| 34 | 18:08:03.0 | -20:36:41.2 | TYC 6276-1738-1 | 91.64 | SDC G9.737-0.239 | 100.57 |

Source number 29 can be identified to be the main sequence star TYC 6272-553-1, located 6.05 arcsec offset.  Two other objects were found in the region, the main sequence star and TYC 6272-361-1, 79.46 arcsec offset, and the IR source IRAS 18067-2031 located at 105.34 arcsec away.  Three stars were found in the 2 arcmin around source 30, TYC 6272-361-1 at 82.01 arcsec, TYC 6272-553-1 at 93.77 arcsec, and HD 312820 at 98.88. The 2 arcmin around source 31 is composed by the Asymptotic Giant Branch Star candidate [RMB2008] G009.8980-00.5359 at 67.17 arcsec, the Cepheid variable Star VVV J180923.34-203854.7 at 74.20 arcsec away, the main sequence star VVV J180934.64-203805.9 is 91.78 arcsec offset, the IR source IRAS 18066-2038 was found to be located at 102.79 arcsec, the Variable Star of RR Lyr type VVV J180935.96-203835.6 at 106.33 arcsec and the star VVV J180935.43-203725.9 at 119.30 arcsec offset.  The vicinity around source 32 is formed by the IR source IRAS 18059-2036 at 48.99 arcsec, and two stars, TYC 6272-383-1 and TYC 6272-747-1 located at 50.01 and 71.42 arcsec away, respectively.  The closest source to the one marked with number 33 is the IR source IRAS 18056-2039 at 50.61 arcsec away, there are other 2 sources in the 2 arcmin vicinity, the stars IRAS 18057-2039 and TYC 6276-1183-1, located 85.55 and 108.58 arcsec away.  Around source 34 the TYC 6276-1738-1 was found at 91.64 arcsec, the dark nebula SDC G9.737-0.239; at 100.57 arcsec, the Asymptotic Giant Branch Star candidate 2MASS J18080795-2037550; and at 101.70, the YSOC ISOGAL-P J180803.6-203454 at 107.43 arcsec away.

The sources which were found to be dominated by non-thermal emission are shown in Table 5.11.

The source number 7 has several objects in the same field of view, being the pulsar PSR J1808-2024 at 0.45 arcsec offset. This pulsar is of special interest to try to explain the HESS source due to its possible association to a PWNe. The only source found in the 2 arcmin search in SIMBAD was the dark nebula SDC G9.984-0.267 located 118.03

Table 5.11: Sources dominated by non-thermal emission found using ObsID 6224 by
Chandra telescope of HESS J1808-204.

| Src | RA J2000 | DEC J2000 | Possible counterpart | Distance arcsec | SNR |
|---|---|---|---|---|---|
| 7 | 18:08:39.3 | -20:24:39.8 | PSR J1808-2024 | 0.45 | 8.1 |
| 8 | 18:08:47.0 | -20:27:46.9 | SDC G9.984-0.267 | 118.03 | 4.3 |
| 9 | 18:08:44.9 | -20:30:50.4 | DOBASHI 0442 | 81.81 | 3.5 |
| 12 | 18:08:45.4 | -20:36:05.4 | TYC 6272-323-1 | 62.09 | 4.0 |
| 13 | 18:08:46.6 | -20:37:39.7 | TYC 6272-323-1 | 44.36 | 3.2 |
| 16 | 18:09:40.6 | -20:40:14.2 | IRAS 18067-2040 | 51.20 | 4.8 |
| 22 | 18:08:41.7 | -20:25:11.8 | USNO-A2.0 0675-24234251 | 2.74 | |
| 30 | 18:09:42.6 | -20:28:50.7 | TYC 6272-361-1 | 1.00 | 3.5 |
| H1 | 18:08:40.3 | -20:25:43.5 | SDC G9.984-0.267 | 50.22 | |
| H2 | 18:09:28.5 | -20:27:50.3 | SDC G10.043-0.425 | 34.99 | |

arcsec offset of source number 8. In the 2 arcmin region around source number 9 we could fine three sources: the dark nebula, and the asymptotic giant branch star candidate 2MASS J18084028-2029433 located 93.0 arcsec offset and the YSOC SSTGLMC G009.9054-00.2844 at 102.69 arcsec offset, being the dark nebula the closest object. Three sources were also found in the region around source number 12. Two main sequence stars being TYC 6272-323-1 the closest and the IR source IRAS 18059-2036 at 111.37 arcsec offset, none of them could be associated to the VHE emission of HESS source. This source is in the same position as source number 41 of the XMM-Newton observation analysed in the last section. It was not found to be dominated by non-thermal emission. Three main sequence stars in the 2 arcmin vicinity of source 13 were found, being TYC 6272-323-1 the closest, this sources could not be energetic enough to produce VHE emission. The far IR source IRAS 18067-2040 was found to be 51.20 arcsec offseto of source 16, as well as the sub-millimetric radio source AGAL G009.858-00.587 located 102.59 arcsec and the variable star of RR Lyr type VVV J180935.96-203835.6 which is 118.16 arcsec offset. Source number 22 and the source H1 is in the same region as source 7, there were found the same 80 objects in the 2 arcmin vicinity, but

in this case, the main sequence star USNO-A2.0 0675-24234251 is the closet, located 2.74 arcsec offset. This could be associated to the X-ray emission but not for the VHE one. Source number 30 can be identified to be the main sequence star TYC 6272-361-1. The source H1 is in the same region as the source 22, however, only 77 objects were found in the 2 arcmin region, being the main sequence star USNO-A2.0 0675-24234251 the closest at 35.21 arcsec, no mm sources were found this time. For the new source detected using the hard energy range cut, H2, in SIMBAD we found the dark nebula SDC G10.043-0.425 to be at 34.99 arcsec offset; the mm source [SSS2011] BGPS G10.043-0.424 is 41.07 arcsec offset; the sub-millimetric radio source AGAL G010.053-00.417 is at 76.40 arcsec, the star TYC 6272-159-1 at 78.39 arcsec and the HII region IRAS 18065-2026 at 112.37 arcsec offset.

### 8151

This observation got as target name the X-ray source AX J180816-2021 and was performed using the instrument ACIS-S, in specific, the CCDs: I2:O2, I3:O3, S1:O1, S2:O5, S3:Y, and S4:O4, and a observation mode TE-F. The exposure time was of just 2.11 ks and as can be seen from the image we obtained (Figure 5.12), the number of counts is homogeneous so applying the source detection algorithms is not possible to found any source, and this observation is not good for doing an analysis.
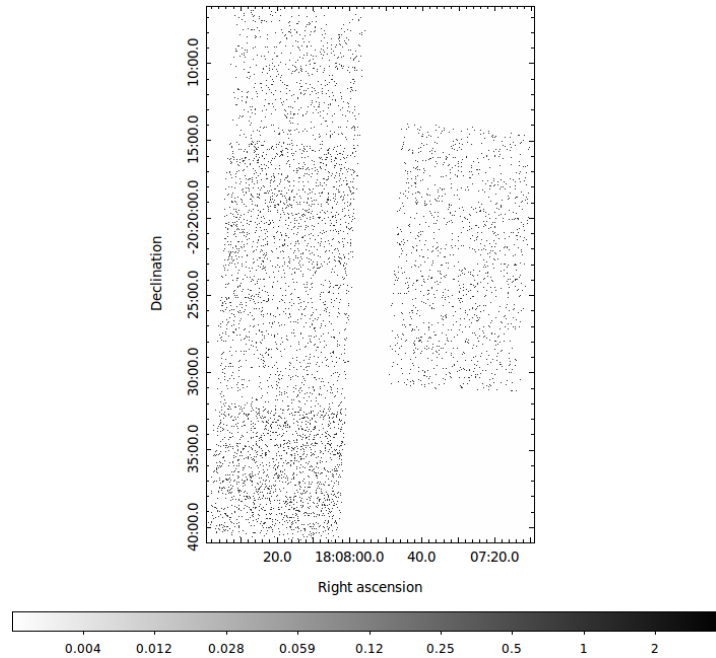
Figure 5.12: Counts map observation using ObsID 8151 made by Chandra.

## 5.4 Merging the XMM-Newton and Chandra Observations

To get all the sources in one image, we did the merge of all the observations in Figure 5.13, where we can see also all the sources detected in both energy ranges.

240
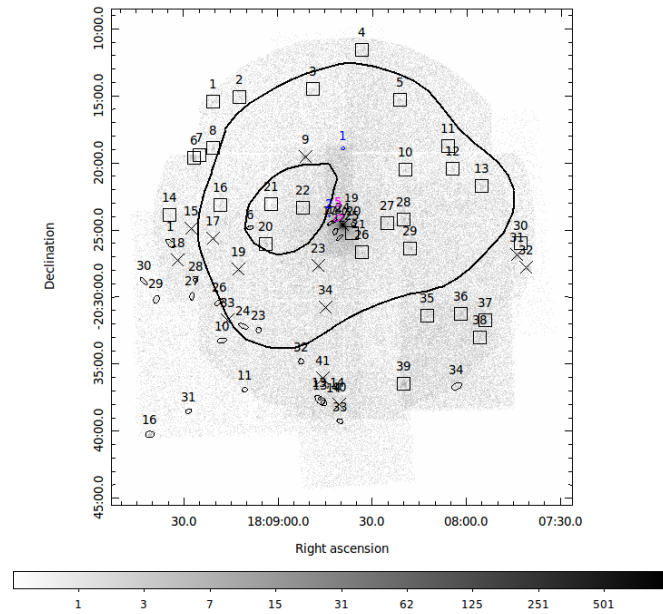
(a) Merge of the two X-ray observations we used to study

HESS J1813-126 considering the full energy range.
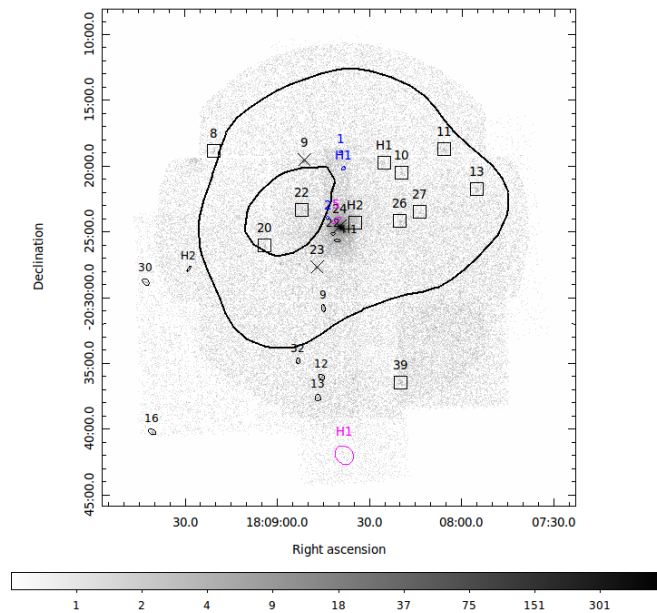


(b) Merge of the four X-ray observations we used to study

HESS J1813-126 considering the energy range 2.5-12 keV.

Figure 5.13: Merge of the four X-ray observations we analysed and were detailed earlier this chapter for HESS J1813-126. Description in the text.

In Figure 5.13 we can see as black squares the sources detected using only XMM-Newton ObsID 0554600301. The sources showed with an X indicates the ones detected by both XMM and the Chandra telescopes, remaining the number of the XMM-Newton observation. The blue ellipses shows the sources detected only in the ObsID 0746; with magenta ellipses are represented the sources were detected using only the ObsID 1827; the black ellipses point out the detections of the ObsID 6224. The signigicant contours of the HESS source was done by using the H.E.S.S. Galactic Plane Survey (HGPS)significance map with $R_c = 0.2°$, with $R_c$ the correlation radius. This radius defines the circular region over which quantity (e.g. $\gamma$-ray excess) is integrated (for more information see [8]).

## 5.5 Astrophysical Discussion and Conclusions

The source HESS J1808-204 was observed using XMM-Newton and Chandra observations. We developed the data analysis by looking into the X-ray detected sources using one observation of XMM and three of Chandra. The results are summarized in this section:

### XMM-Newton

Forty two X-ray sources were detected using ObsID 0554600301 in the region of the HESS source, among them, fourteen were found to be dominated by non-thermal emission, which are the sources more likely to be the counterpart of the VHE emission, and no astronomical sources were found for two of the sources (4 and ).

The sources that were found to be main sequence stars are discarded to be responsible of the VHE TeV emission, due to they are dominated by thermal emission.

Here I summarize the sources that we could find for this observation:

- Source number 1 is very likely to be the dense core source [WWS2012] G010.21-00.31 located at 17.17 arcsec offset, which could be the responsible of the X-ray emission, but not the VHE TeV emission.

- Source number 2 is identified to be the main sequence star HD 312682.

- Source number 6 was found to be 10.64 arcsec offset from the cluster of stars W31 IR Cluster, being the O-type star 2MASS J18092597-2019383 the closest object at 9.34 arcsec. The X-ray source 3XMM J180926.9-201930 was found at 10.01 arcsec. This source was not found in the hard energy range.

- Source number 7 is located in a region of HII and maser sources, being the HII region GAL 010.2-00.3 at 1.87 arcsec the closest, however five more HII regions were found to be close, [CKW87] 180626.9-202009, [WC89] 010.15- 0.34A, GAL 010.15-00.34, JCMTSE J180921.2-201932 and [WC89] 010.15-0.34B, located at 11.19, 18.49, 44.34, 49.66 and 59.40 arcsec away, respectively. The maser sources are close too, [TVH89] 253 at 3.77 arcsec and OH 10.2 -0.4 at 4.33 arcsec. Four O-type stars were found also in the region: 2MASS J18092601-2019311 at 18.51 arcsec, 2MASS J18092597-2019383 at 20.40 arcsec, 2MASS J18092749-2019482 at 43.80 arcsec, and ALS 19592 at 53.75 arcsec. However, this source was not found in the hard energy cut.

- Source number 8 can be identified to be the WR star 3XMM J180920.3-201857, located 1.87 arcsec offset. This source was found in the hard energy range with a flux of $F = 2.49 \times 10^{-14}$ erg cm$^{-2}$ s$^{-1}$.

- Source number 9 can be identified to be the X-ray source 2XMM J180851.0-201935, located 0.30 arcsec offset. This source was also found to be dominated by non-thermal emission with a flux $F = 3.66 \times 10^{-14}$ erg cm$^{-2}$ s$^{-1}$. And it was

also found in the Chandra ObsID 1827, marked with number 1.

- Source number 12 was found to be the main sequence star HD 3122685, which was the only object found in the 2 arcmin radius search in SIMBAD.

- In the case of source number 13, the X-ray star 2XMM J180754.3-202251 was found to be 65.28 arcsec offset. This one was found to be among the sources dominated by non-thermal emission, with a flux $F = 1.6 \times 10^{-14}$ erg cm$^{-2}$ s$^{-1}$.

- Source number 14 is close to the dark nebulae SDC G10.111-0.431, the closest source located at 28.54 arcsec offset. This source was not found to be dominated by non-thermal emission.

- Source number 15 was found to be close to the SDC G10.082-0.414, at 21.62 arcsec and the sub-millimetric radio source [ERG2015] 2357 at 22.37 arcsec, also the HII region [L89b] 10.073-00.412 is located 35.76 arcsec offset. It was not found in the hard energy range. Moreover, this source was also found using Chandra software and was marked with source number 3, and it was not found either in the hard energy range.

- Source 19 can be identified to be the main sequence star HD 312684, located 1.68 arcsec offset, and the X-ray source 2XMM J180912.2-202801, located also close at 1.74 arcsec offset. This source was not found to be dominated by non-thermal emission.

- Source number 21 is likely to be the sub-millimetric radio source JCMTSE J180902.8-202243 which was found at 28.04 arcsec offset. This source was not found to be dominated by non-thermal emission.

- The 2 arcmin region around source number 24 is composed of 32 main sequence stars, twelve molecular clouds, four IR sources, the pulsar PSR J1808-2024, three

WR stars, the X-ray source SWIFT J180839.4-202435, the massive stellar cluster Cl* 1806-20, the interstellar matter AX J1808.6-2024, eight sub-millimetric radio sources, two possible supergiant stars, the super giant star [KMN95] Star A, and the dark nebula SDC G9.984-0.267 at 99.83 arcsec away. This source was found to be dominated by non-thermal emission with a flux $F = 9.8 \times 10^{-13}$ erg cm$^{-2}$ s$^{-1}$, and it is coincident with source number 3 of ObsID 0746, source number 2 of ObsID 1827 and source number 7 of Obs ID 6224. We can see 5 sources around this one with the Chandra observation due to its better angular resolution.

- Source number 27 can be identified to be the X-ray emitting star USNO- A2.0 0675-24220389 at just 0.49 arcsec offset. This source was also found in the hard energy range with a flux $F = 0.67 \times 10^{-14}$ erg cm$^{-2}$ s$^{-1}$.

- Source 28 can be identified to be the bubble source [SPK2012] MWP1G009955-001741 at 36.75 arcsec offset. This source was also found to be dominated by non-thermal emission with a flux $F = 0.49 \times 10^{-14}$ erg cm$^{-2}$ s$^{-1}$. It was not found in the Chandra observations.

- Source number 29 can be identified to be the asymptotic giant branch star candidate 2MASS J18081769-2026260 just 0.95 arcsec offset. This source was not found dominated in the hard energy range neither in the Chandra observations.

- Source number 31 can be identified to be the YSOC 2MASS J18074422-2026454 located at 10.94 arcsec offset. It was not found in the hard energy range. No coincident source was found in the Chandra observations.

- Source number 32 can be identified to be the B-type star HD 312693. It was not found in the Chandra observations.

- Source number 36 can be identified to be the YSOC ISOGAL-P J180800.7-203117,

13.80 arcsec offset. It was not found in the hard energy range and it was not in the FOV of the Chandra observations.

- Source number 37 can be identified to be the main sequence star TYC 6259-2681-1 located 16.39 arcsec offset.

- Source number 38 is close to the dark nebula SDC G9.787- 0.156 located 21.50 arcsec offset; in the region there were found also the outflow EGO G009.78-0.17 is at 39.50 arcsec. It was not found to be dominated by non-thermal emission and it was not in the FOV of Chandra observations.

- Source number 39 is identified to be the X-ray source 2XMM J180819.7-203629 located 1.21 arcsec offset. This source was to be dominated by non-thermal emission with a flux $F = 2.0 \times 10^{-14}$ erg cm$^{-2}$ s$^{-1}$. It was not found in the FOV of Chandra observations.

## Chandra

Forty different X-ray sources were detected using four different observations made by Chandra observatory in the region of HESS J1808-204.  The sources that could be identified by coincidence association are the following:

### 0746

- Source number 2 is identified to be the main sequence star 2MASS J18084346-2023591 at just 1.40 arcsec away.

- Source H1 can be identified to be the main sequence star TYC 6272-633-1, 3.27 arcsec offset.

**1827**

- Source number 1 can be identified to be the X-ray source 2XMM J180851.0-201935, found 1.09 arcsec offset.

- Source number 4 can be identified to be the YSO 2MASS J18074263-2027360 located at 16.63 arcsec offset.

**6224**

- The 2 arcmin around source number 1 is formed by 4 sub-millimetric radio sources being BGPS G010.084-00.436 the closest. There are also, three dark nebula sources in the vicinity, SDC G10.082-0.414 at 26.81 arcsec offset.

- The closest source to the number 6 is a sub-millimetric radio one, BGPS G010.045-00.354 located at 37.99 arcsec.

- Source number 24 can be identified to be the main sequence star IRAS 18061-203, located 5.91 arcsec offset.

- Source number 29 can be identified to be the main sequence star TYC 6272-553-1, located 6.05 arcsec offset.

The sources that were found to be main sequence stars are discarded to be responsible of the VHE TeV emission, due to they are dominated by thermal emission.

So, in this region we have the W31 IR Cluster, in which the O-type star 2MASS J18092597-2019383 was found, this kind of stars are able to produce X-rays but this can not a be counterpart of the VHE TeV emission. Moreover, eight X-ray sources were found in the region, as well as the HII region GAL 010.2-00.3, four dark nebulae, the sub-millimetric radio source JCMTSE J180902.8-202243, twelve molecular clouds, four

IR sources, the pulsar PSR J1808-2024, four WR stars, the massive stellar cluster Cl*

1806-20, the interstellar matter AX J1808.6-2024, ten sub-millimetric radio sources.

# CHAPTER 6

HESS J1813-126

In this chapter, the X-ray analysis on HESS J1813-126 will be described. In sect. 6.1 I give the details that are known to the date about this source. All the information about the analysis I carried out using XMM-Newton observation in the region of this HESS source will be given in sect. 6.2 and in sect. 6.3 the analysis using the Chandra observation. Sect. 6.4 contains the merge of the X-ray observations analysed. Astrophysical discussions and conclusions are shown in 6.5.

## 6.1   Introduction

This source was discovered during the HESS Galactic plane survey [118]. It was found to be at the position of R.A. = $18^h 13^m 21.66^s$, decl. = -12°41'13.60" (one of few off-plane VHE sources) and having an extension of 0.21 $\pm$ 0.032 degrees, and a flux $F(> 1\mathrm{TeV})$ = 1.08 $\pm$ 0.24 $\times$ $10^{-12}$cm$^{-2}$s$^{-1}$. An image of the source can be seen in Figure 6.1.

The only plausible counterpart associated with the emission is the pulsar PSR J18131246 [181], but offset the position with the VHE best-fit centroid. This pulsar has a spin-down luminosity $\dot{E}$ = 6.3 $\times$ $10^{36}$ erg s$^{-1}$ and a characteristic age $\tau_c$ = 43 kyr and is one of
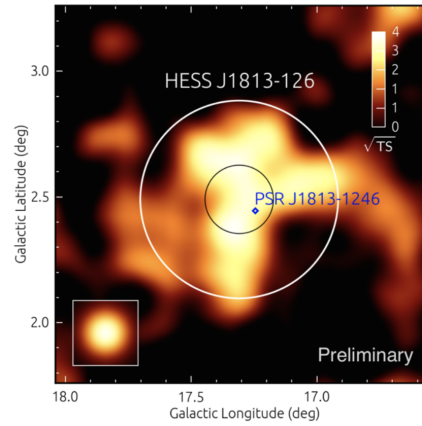
Figure 6.1: A VHE gamma-ray significance ($\approx \sqrt{TS}$) image of HESS J1813-126, show-
ing the PSF of the data set is shown inset. The 68% uncertainty in the best fit
centroid of the VHE emission is represented by the black circle in the center,
and the white circle shows the 70% containment region of the emission. The
position of the pulsar is shown by a blue diamond. The FoV is $1.7° \times 1.7°$.
Figure from [8].

the brightest gamma-ray pulsars (known as 3FGL J1813.4-1246) [135]. No off-pulse

emission have been found so far in other energy bands [8].

The X-ray analysis that were performed on the TeV unidentified galactic source

HESS J1813-126 using observations from the Chandra and XMM-Newton (XMM-N) tele-

scopes. The list of observations that were used for each source are described in Table

6.1, where we can find the ID of the observation, the exact the Start date (dd.mm.yy)

where the time is also specified, the exposure and the coordinates of the objective for

each one.

HESS J1813-126

| Mission | Obs ID | Start Date | Exposure | Coordinates |
|---------|--------|------------|----------|-------------|
| XMM-N | 0693960101 | 10.03.13 17:27:08 | 108.9 ks | $18^h13^m23.41^s$, -12°45'58.8" |
| Chandra | 14399 | 22.07.13 04:42:09 | 50.4 ks | $18^h13^m23.40^s$, -12°45'58.8" |

Table 6.1: X-ray observations made with XMM-Newton and Chandra telescopes on the position of HESS J1813-126.

## 6.2   XMM-Newton Observation

There is one observation performed using the XMM-Newton telescope. This was acquired on March 10th and lasted 108.9 ks (ObsID: 0693960101) with the purpose of studying the radio-quiet gamma-ray pulsar PSR J1813-1246, which was the target name, being this object located in the region of HESS J1813-126. The MOS detectors were operated in Full Frame mode using a medium filter, while the PN camera of the EPIC instrument was operating in Small Window mode and employing the thin optical filter.

The data were reprocessed using the XMM-Newton data analysis software SAS version xmmsas 20160201 1833-15.0.0 pipeline, and for their analysis both SAS and FTOOLS software packages were used. The calibration was done using the SAS task `cifbuild`. For using EPIC data, the reprocessing was accomplished by running the default pipeline processing meta tasks `emproc` and `epproc`.

The activities carried out so far are:

- Calibration of the data.

- Filter event files for flaring particle background

- Creation of the images using the cleaned event files using ds9 [1]

---

[1] http://ds9.si.edu/site/Home.html

- Source detection

- Identification of x-ray sources

In the present case, it was not necessary to filter the event files for flaring particle background, due to the data was found under the terms of the good signal, see Figure 6.2. It is confirmed in the analysis done by [119] were they performed two analysis and those revealed no significant contamination from flares.



(a) Light curve above 10 keV from MOS1.



(b) Light curve above 10 keV from MOS2.



(c) Light curve above 12 keV from PN.
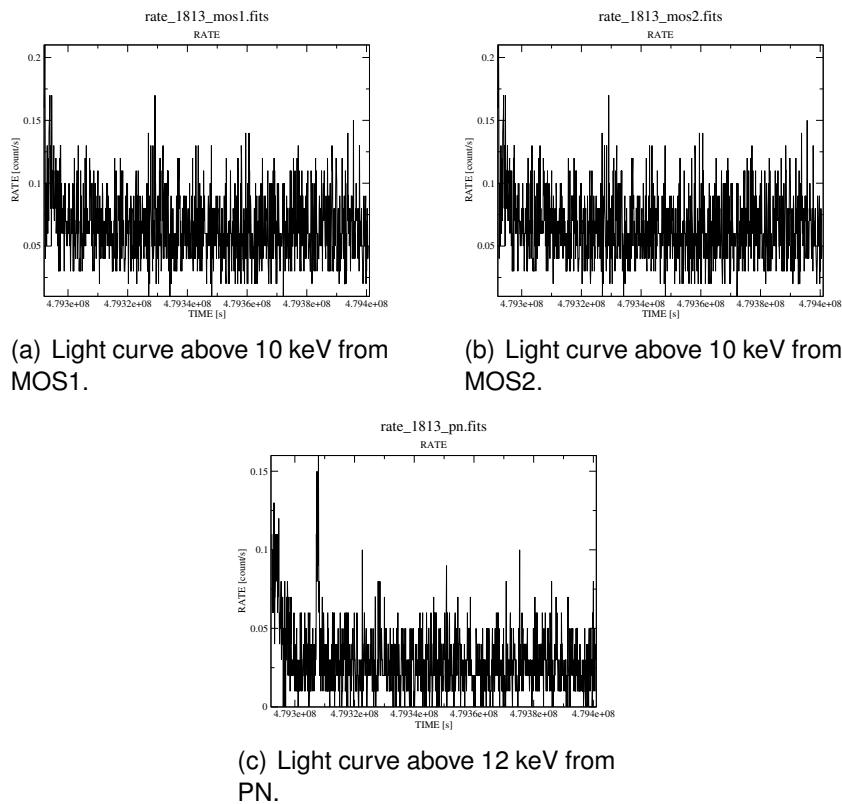
Figure 6.2: Light curves for EPIC-MOS and EPIC-PN instruments of ObsID 0693960101.

The GTI obtained for both MOS1 and MOS2 was 108.6ks, and for PN we got 108.5 ks. In the Figure 6.3 are plotted the cleaned event files that were made by making use of these GTI.

Now, the source detection was carried out on the MOS2 camera, due to the MOS1 detector was damaged and two chips are not plotted. Using the tool EPIC source

(a) Cleaned events for MOS1.

(b) Cleaned events for MOS2.



(c) Cleaned events for PN.
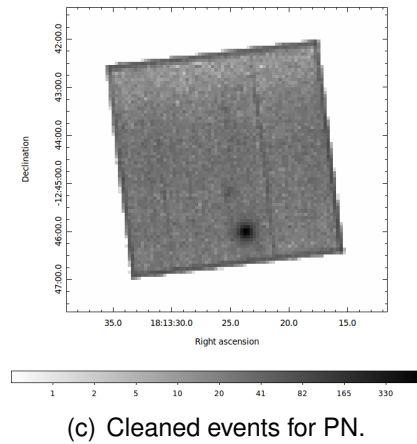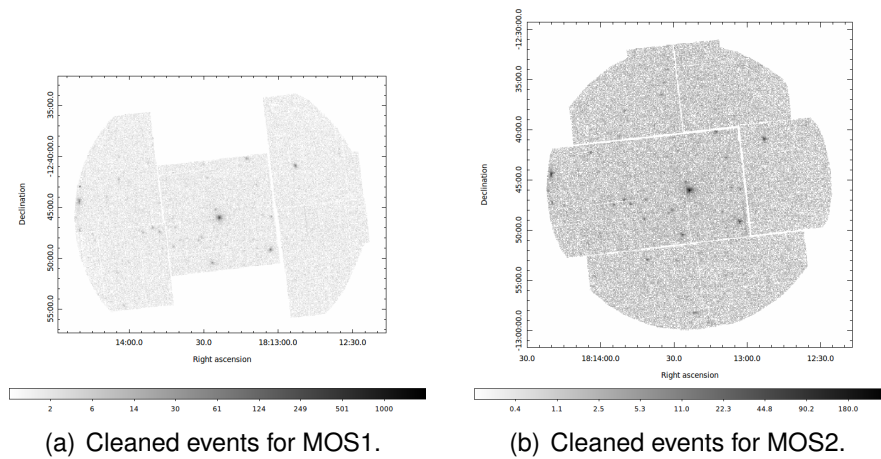
Figure 6.3: Cleaned events images for MOS and PN EPIC cameras of ObsID 0693960101.

detection (edetect_chain), 72 sources were found for this observation (see Figure 6.4).

Information about the sources detected as possible counterparts was done with information from the database SIMBAD can be found in 6.3, 6.2, 6.2, 6.2, 6.2, and 6.2.
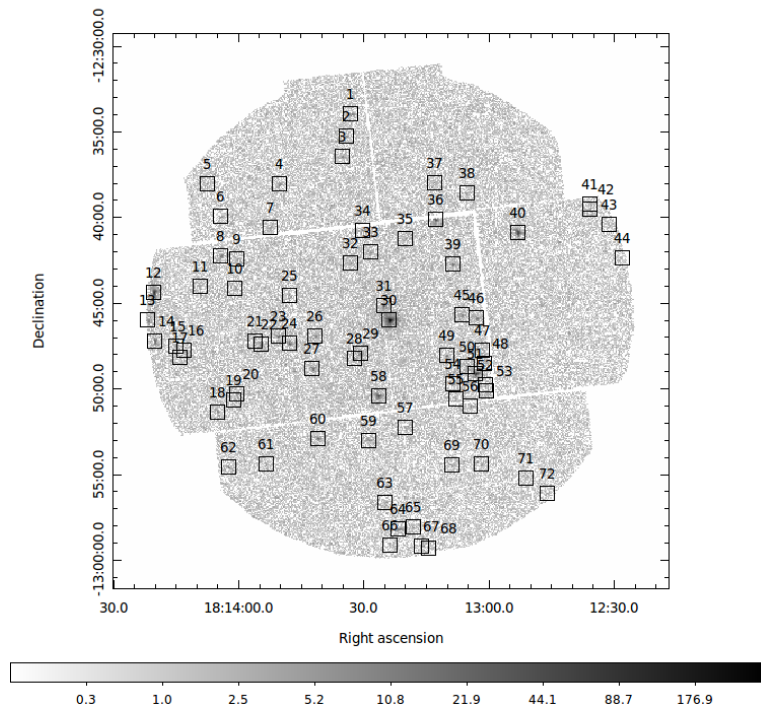
Figure 6.4: Counts map observation of HESS J1813-126 done using MOS2 of ObsID 0693960101, the black squares indicate 72 sources detected by the EPIC source detection tool.

Table 6.2: Possible counterparts of HESS J1813-126 found using MOS2 detector of ObsID 0693960101 (Distance in arcsec), Part 1.

| Src | RA (J2000) | DEC (J2000) | Star | Distance | X | Distance |
|-----|-----------|-------------|------|----------|---|----------|
| 1 | 18:13:33.1 | -12:33:59.8 | No astronomical | — | object found | — |
| 2 | 18:13:34.1 | -12:35:17.9 | No astronomical | — | object found | — |
| 3 | 18:13:35.0 | -12:36:29.2 | No astronomical | — | object found | — |
| 4 | 18:13:50.2 | -12:38:05.3 | No astronomical | — | object found | — |
| 5 | 18:14:07.4 | -12:38:02.4 | — | — | — | — |
| 6 | 18:14:04.1 | -12:39:58.7 | — | — | — | — |
| 7 | 18:13:52.3 | -12:40:36.1 | No astronomical | — | object found | — |
| 8 | 18:14:04.1 | -12:42:14.4 | IRAS 18112-1244 | 53.56 | — | — |
| 9 | 18:14:00.2 | -12:42:27.7 | IRAS 18112-1244 | 59.25 | — | — |
| 10 | 18:14:00.7 | -12:44:08.9 | IRAS 18112-1244 | 72.67 | — | — |
| 11 | 18:14:09.1 | -12:44:02.8 | IRAS 18113-1246 | 81.68 | — | — |
| 12 | 18:14:20.2 | -12:44:22.2 | MSX6C G017.3765+02.2512 | 17.94 | [MHP2014] 3 | 0.80 |
| 13 | 18:14:21.6 | -12:46:01.2 | MSX6C G017.3765+02.2512 | 88.12 | [MHP2014] 9 | 76.14 |
| 14 | 18:14:19.9 | -12:47:13.9 | — | — | [MHP2014] 9 | 0.78 |

Table 6.2 Continued from previous page

| Src | DNe | Distance | FGL | Distance | Radio | Distance |
|-----|-----|----------|-----|----------|-------|----------|
| 1 | — | — | — | — | — | — |
| 2 | — | — | — | — | — | — |
| 3 | — | — | — | — | — | — |
| 4 | — | — | — | — | — | — |
| 5 | DOBASHI 0751 | 44.30 | — | — | — | — |
| 6 | DOBASHI 0751 | 82.04 | — | — | — | — |
| 7 | — | — | — | — | — | — |
| 8 | — | — | UGRS G017.4+2.4 | 61.41 | — | — |
| 9 | — | — | UGRS G017.4+2.4 | 27.94 | — | — |
| 10 | — | — | — | — | — | — |
| 11 | DOBASHI 0749 | 114.97 | — | — | PMN J1814-1245 | 113.80 |
| 12 | DOBASHI 0749 | 54.93 | — | — | — | — |
| 13 | DOBASHI 0749 | 110.78 | — | — | — | — |
| 14 | — | — | — | — | — | — |

There were no found astronomical objects in the 2 arcmin region around sources number 1, 2, 3, 4, and 7. In the vicinity of source number 5 the dark nebula DOBASHI 0751 was found to be 44.30 arcsec offset, the same object was found close to the source number 6, 82.04 arcsec offset. In the 2 arcmin region around source number 8, it was found one main sequence star IRAS 18112-1244, at 53.56 arcsec away, and the gamma-ray source UGRS G017.4+2.4, 61.41 arcsec offset. The same objects were found in the 2 arcmin of source number 9, but in this case, the star is located 59.25 arcsec offset and the gamma-ray source at 27.94 arcsec offset. The vicinity of source number 10 was found just the star IRAS 18112-1244, 72.67 arcsec offset. Around source number 11, the main sequence star IRAS 18113-1246 was found to be 81.68 arcsec offset, as well as the dark nebula DOBASHI 0749, 114.97 arcsec offset; and the radio source PMN J1814-1245, 113.80 arcsec offset. For the case of source number 12, there were found the young stellar object MSX6C G017.3765+02.2512, at 88.12 arcsec offset, the X-ray star [MHP2014] 9 at 76.14 arcsec offset; the X-ray source [MHP2014] 3 that was found to be 0.80 arcsec offset. From this source we can say we identified the X-ray source, however, the VHE emission from the HESS source can not be explained by this source. The dark nebula DOBASHI 0749 was also found in the region, but 54.93 arcsec offset; and there is also an IR source in the neighbourhood, IRAS 18115-1245 at 48.62 arcsec from the source. The young stellar object MSX6C G017.3765+02.2512 was found 88.12 arcsec offset from source number 13. The x-ray source [MHP2014] 9 was also in the 2 arcmin region of this source, 76.14 arcsec offset; as well as the dark nebula DOBASHI 0749, 54.93 arcsec offset, the far IR source IRAS 18115-1245 90.78 arcsec away from the source. The X-ray source [MHP2014] 3 is 100.59 arcsec offset. Source number 14 can be identified to be the X-ray star [MHP2014] 9, located 0.78 arcsec offset.

Table 6.3: Possible counterparts of HESS J1813-126 found using MOS2 detector of ObsID 0693960101 (Distance in arcsec), Part 2.

| Src | RA (J2000) | DEC (J2000) | Star | Distance | X | Distance |
|-----|-----------|-------------|------|----------|---|----------|
| 15 | 18:14:14.9 | -12:47:30.5 | — | — | [MHP2014] 9 | 76.28 |
| 16 | 18:14:13.0 | -12:47:47.8 | — | — | [MHP2014] 9 | 108.03 |
| 17 | 18:14:13.9 | -12:48:10.1 | — | — | [MHP2014] 9 | 104.97 |
| 18 | 18:14:05.0 | -12:51:21.6 | No astronomical | — | object found | — |
| 19 | 18:14:07.4 | -12:38:02.4 | No astronomical | — | object found | — |
| 20 | 18:14:00.2 | -12:50:20.0 | No astronomical | — | object found | — |
| 21 | 18:13:55.9 | -12:47:14.3 | [MHP2014] 11 | 119.98 | — | — |
| 22 | 18:13:54.5 | -12:47:25.1 | [MHP2014] 11 | 98.69 | — | — |
| 23 | 18:13:50.4 | -12:46:57.7 | [MHP2014] 11 | 46.02 | — | — |
| 24 | 18:13:47.8 | -12:47:22.6 | [MHP2014] 11 | 0.50 | — | — |
| 25 | 18:13:47.8 | -12:44:35.2 | — | — | — | — |
| 26 | 18:13:41.5 | -12:46:56.3 | [MHP2014] 11 | 94.55 | — | — |
| 27 | 18:13:42.2 | -12:48:50.8 | [MHP2014] 11 | 119.61 | [MHP2014] 9 | 76.14 |
| 28 | 18:13:32.2 | -12:48:15.5 | No astronomical | — | object found | — |

*Continued on next page*

258

Table 6.3 *Continued from previous page*

| Src | DNe | Distance | Pulsar | Distance | Radio | Distance |
|-----|-----|----------|--------|----------|-------|----------|
| 15 | — | — | — | — | PMN J1814-1245 | 111.54 |
| 16 | — | — | — | — | PMN J1814-1245 | 118.28 |
| 17 | — | — | — | — | — | — |
| 18 | — | — | — | — | — | — |
| 19 | — | — | — | — | — | — |
| 20 | — | — | — | — | — | — |
| 21 | — | — | — | — | — | — |
| 22 | — | — | — | — | — | — |
| 23 | — | — | — | — | — | — |
| 24 | — | — | — | — | — | — |
| 25 | DOBASHI 0748 | 111.61 | — | — | — | — |
| 26 | DOBASHI 0748 | 75.29 | — | — | — | — |
| 27 | — | — | — | — | — | — |
| 28 | — | — | — | — | — | — |

In the case of sources 15 and 16, they have the X-ray star [MHP2014] 9, at 76.28 arcsec from the first source and 108.03 arcsec offset for the second; the radio source PMN J1814-1245 was found to be located 111.54 and 118.28 arcsec offset, respectively. The same X-ray source was found in the 2 arcmin vicinity around the source number 17, located at 104.97 arcsec away, no other object was found in this region. No astronomical objects were found in the 2 arcmin vicinity of the sources with numbers 18, 19, 20, and 28. The X-ray star [MHP2014] 11 was found to be 119.98 arcsec offset from source number 21, 98.69 arcsec offset from source 22 46.02 arcsec offset of source 23 and 0.50 from source 24, so we can say this source is the X-ray star. Moreover, the AGN was found to be 82.36 arcsec offset from the source 21, 65.51 arcsec from source 22, 0.36 arcsec from source 23, and 45.72 arcsec from source 24, we can identify the AGN to be the source 23. For source number 25, the dark nebula DOBASHI 0748 was found to be 111.61 arcsec offset, and no other object was found in the neighbourhood. The same dark nebula was found to be 75.29 arcsec offset from source 26, as well as the x-ray star [MHP2014] 11 which is 94.55 arcsec offset. This star and the X-ray source [MHP2014] 9 were found in the vicinity of source number 27, at 119.61 and 76.14 arcsec offset, respectively. The dark nebula is very likely to be source number 26.

Table 6.4: Possible counterparts of HESS J1813–126 found using MOS2 detector of ObsID 0693960101 (Distance in arcsec), Part 3.

| Src | RA (J2000) | DEC (J2000) | Star | Distance | X | Distance |
|-----|-----------|-------------|------|----------|---|----------|
| 29 | 18:13:30.7 | -12:47:57.8 | No astronomical | – | object found | – |
| 30 | 18:13:23.8 | -12:46:00.1 | [MHP2014] 7 | 54.38 | SWIFT J181323.4-124600 | 5.27 |
| 31 | 18:13:25.2 | -12:45:10.8 | [MHP2014] 7 | 1.11 | SWIFT J181323.4-124600 | 55.80 |
| 32 | 18:13:33.1 | -12:42:40.3 | No astronomical | – | object found | – |
| 33 | 18:13:28.3 | -12:42:02.9 | TYC 5684-695-1 | 78.86 | – | – |
| 34 | 18:13:30.2 | -12:40:46.6 | No astronomical | – | object found | – |
| 35 | 18:13:19.9 | -12:41:14.6 | TYC 5684-695-1 | 63.12 | – | – |
| 36 | 18:13:12.7 | -12:40:09.8 | TYC 5684-797-1 | 119.45 | [MHP2014] 8 | 0.80 |
| 37 | 18:13:13.0 | -12:37:58.4 | TYC 5684-797-1 | 87.15 | – | – |
| 38 | 18:13:05.23 | -12:38:36.2 | No astronomical | – | object found | – |
| 39 | 18:13:08.6 | -12:42:44.6 | No astronomical | – | object found | – |
| 40 | 18:12:53.0 | -12:40:53.4 | – | – | [MHP2014] 5 | 0.36 |
| 41 | 18:12:35.8 | -12:39:15.5 | No astronomical | – | object found | – |
| 42 | 18:12:35.78 | -12:39:33.1 | No astronomical | – | object found | – |

*Continued on next page*

Table 6.4 Continued from previous page

| Src | DNe | Distance | Pulsar | Distance | Radio | Distance |
|-----|-----|----------|--------|----------|-------|----------|
| 29 | — | — | — | — | — | — |
| 30 | — | — | PSR J1813-1246 | 0.52 | — | |
| 31 | — | — | PSR J1813-1246 | 54.05 | — | — |
| 32 | — | — | — | — | — | — |
| 33 | — | — | — | — | — | — |
| 34 | — | — | — | — | — | — |
| 35 | — | — | — | — | — | — |
| 36 | — | — | — | — | — | — |
| 37 | — | — | — | — | — | — |
| 38 | — | — | — | — | — | — |
| 39 | — | — | — | — | — | — |
| 40 | — | — | — | — | — | — |
| 41 | — | — | — | — | — | — |
| 42 | — | — | — | — | — | — |

No astronomical objects were found in SIMBAD in the cases of the sources 29, 32, 34, 38, 39, 41 and 42. In the 2 arcmin region vicinity of source number 30, there were found the X-ray star [MHP2014] 7, located 54.38 arcsec offset, and the X-ray source SWIFT J181323.4-124600 at 5.27 arcsec, furthermore, the pulsar PSR J1813-1246 was found to be located 0.52 arcsec offset from this source. So, we can identify the source number 30 to be the pulsar, which is suitable counterpart of HESS J1813-126. Previous studies in [119] they did not find extended emission down to a fraction of an arcsec, and they said the *Suzaku* detection of a nebula reported in [182] was due to the X-ray star [MHP2014] 7 which is located at ∼50 arcsec from the pulsar. The same two objects were also found in the 2 arcmin region around source 31, however, for this source can be identified to be the X-ray star [MHP2014] 7, located 1.11 arcsec offset. In the neighbourhood of source number 33 there was only found the main sequence star TYC 5684-695-1, located 78.86 arcsec from the source, but it was also found that the source HESS J1813-126 10 is 109.21 arcsec offset. The same star was found 63.12 arcsec from source 35, and HESS J1813-126 10 is 25.48 arcsec offset. The source 36 has as neighbour the main sequence star TYC 5684-797-1, at 119.45 arcsec offset. It can be identified to be the AGN [MHP2014] 8, which was found to be at 0.80 arcsec offset in SIMBAD. The only source found in the 2 arcmin region of source 37 was the main sequence star TYC 5684-797-1, at 87.15 arcsec offset. The source marked with the number 40 can be identified to be the AGN [MHP2014] 5 which was found to be 0.36 arcsec offset.

Table 6.5: Possible counterparts of HESS J1813-126 found using MOS2 detector of ObsID 0693960101 (Distance in arcsec), Part 4.

| Src | RA (J2000) | DEC (J2000) | Star | Distance | AGN | Distance |
|-----|-----------|-------------|------|----------|-----|----------|
| 43 | 18:12:31.2 | -12:40:26.0 | No astronomical | — | object found | — |
| 44 | 18:12:28.1 | -12:42:21.6 | No astronomical | — | object found | — |
| 45 | 18:13:06.5 | -12:45:43.6 | IRAS 18102-1245 | 39.95 | — | — |
| 46 | 18:13:02.9 | -12:45:53.3 | IRAS 18102-1245 | 60.47 | — | — |
| 47 | 18:13:01.4 | -12:47:45.2 | — | — | [MHP2014] 4 | 85.33 |
| 48 | 18:13:01.0 | -12:48:31.7 | — | — | [MHP2014] 4 | 47.36 |
| 49 | 18:13:10.1 | -12:48:06.1 | — | — | [MHP2014] 4 | 118.60 |
| 50 | 18:13:05.0 | -12:48:42.1 | — | — | [MHP2014] 4 | 37.49 |
| 51 | 18:13:03.1 | -12:49:07.3 | — | — | [MHP2014] 4 | 0.36 |
| 52 | 18:13:00.7 | -12:49:48.4 | — | — | [MHP2014] 4 | 54.28 |
| 53 | 18:13:00.5 | -12:50:08.2 | — | — | [MHP2014] 4 | 72.36 |
| 54 | 18:13:08.6 | -12:49:44.4 | TYC 5684-825-1 | 106.77 | [MHP2014] 4 | 88.99 |
| 55 | 18:13:07.9 | -12:50:38.40 | — | — | [MHP2014] 4 | 115.28 |
| 56 | 18:13:04.3 | -12:51:03.24 | — | — | [MHP2014] 4 | 117.60 |

*Continued on next page*

Table 6.5 *Continued from previous page*

| Src | DNe | Distance | Pulsar | Distance | Radio | Distance |
|-----|-----|----------|--------|----------|-------|----------|
| 43 | — | — | — | — | — | |
| 44 | — | — | — | — | — | — |
| 45 | — | — | — | — | — | — |
| 46 | — | — | — | — | — | — |
| 47 | — | — | — | — | NVSS J181303-124908 | 86.72 |
| 48 | — | — | — | — | NVSS J181303-124908 | 47.70 |
| 49 | — | — | — | — | — | |
| 50 | — | — | — | — | NVSS J181303-124908 | 40.09 |
| 51 | — | — | — | — | NVSS J181303-124908 | 2.36 |
| 52 | — | — | — | — | NVSS J181303-124908 | 51.66 |
| 53 | — | — | — | — | NVSS J181303-124908 | 69.79 |
| 54 | — | — | — | — | NVSS J181303-124908 | 89.80 |
| 55 | — | — | — | — | NVSS J181303-124908 | 114.84 |
| 56 | — | — | — | — | NVSS J181303-124908 | 115.96 |

Table 6.6: Possible counterparts of HESS J1813-126 found using MOS2 detector of ObsID 0693960101 (Distance in arcsec), Part 5.

| Src | RA (J2000) | DEC (J2000) | Star | Distance | X | Distance |
|-----|-----------|-------------|------|----------|---|----------|
| 57 | 18:13:19.9 | -12:52:18.1 | TYC 5684-485-1 | 14.92 | — | — |
| 58 | 18:13:26.4 | -12:50:26.2 | [MHP2014] 6 | 2.52 | — | — |
| 59 | 18:13:28.8 | -12:53:01.7 | No astronomical | — | object found | — |
| 60 | 18:13:40.8 | -12:52:54.0 | BD-12 4949 | 3.67 | — | — |
| 61 | 18:13:53.3 | -12:54:23.7 | TYC 5684-584-1 | 110.38 | — | — |
| 62 | 18:14:02.2 | -12:54:36.0 | TYC 5684-167-1 | 2.07 | — | — |
| 63 | 18:13:24.7 | -12:56:38.4 | IRAS 18106-1257 | 52.78 | — | — |
| 64 | 18:13:21.6 | -12:58:12.0 | No astronomical | — | object found | — |
| 65 | 18:13:18.0 | -12:58:05.2 | TYC 5684-147-1 | 79.00 | — | — |
| 66 | 18:13:23.5 | -12:59:08.9 | No astronomical | — | object found | — |
| 67 | 18:13:16.1 | -12:59:11.4 | TYC 5684-147-1 | 33.57 | — | — |
| 68 | 18:13:14.4 | -12:59:20.0 | TYC 5684-147-1 | 22.97 | — | — |
| 69 | 18:13:08.9 | -12:54:28.8 | No astronomical | — | object found | — |
| 70 | 18:13:01.7 | -12:54:25.2 | No astronomical | — | object found | — |

Table 6.7: Possible counterparts of HESS J1813-126 found using MOS2 detector of ObsID 0693960101 (Distance in arcsec), Part 6.

| Src | RA (J2000) | DEC (J2000) | Star | Distance | X | Distance |
|-----|-----------|-------------|------|----------|---|----------|
| 71 | 18:12:51.120 | -12:55:15.60 | No astronomical | — | object found | — |
| 72 | 18:12:45.840 | -12:56:07.80 | No astronomical | — | object found | — |

No astronomical objects were found in the 2 arcmin region around the sources 43 and 44, 59, 64, 66, 69, 70, 71, and 72. The star IRAS 18102-1245 was found to be 39.95 and 60.47 arcsec offset from sources 45 and 46, respectively. The AGN [MHP2014] 4 is located in the vicinity of the sources 47, 48, 49, 50, 51, 52, 53, 54, 55 and 56. However, due to the angular distance to source 51, we can identify it to be the AGN, but the radio source NVSS J181303-124908 is also very close, just 2.36 arcsec offset. This source is also in the 2 arcmin region of sources number 47, 48, 50, 52, 53, 54, 55, 56, but farther away (see Table 6.2). The main sequence star TYC 5684-485-1 was found to be 14.92 arcsec offset from source 57, no other objects were found in the 2 arcmin region around this source. The source number 58 can be identified as the X-ray emitting star [MHP2014] 6, which was found to be 2.52 arcsec offset. Source number 60 was found to be the main sequence star BD-12 4949 which is 3.69 arcsec offset. The only object found in the 2 arcmin region aroud source number 61 was the main sequence star TYC 5684-584-1, located 110.38 arcsec offset from it. The source 62 can be identified as the main sequence star TYC 5684-167-1, which was found to be 2.07 arcsec offset. There was another star found in the vicinity, TYC 5684-584-1, 106.37 arcsec offset. The star IRAS 18106-1257 was the only object found to be in the 2 arcmin region around source 63, 52.78 arcsec offset from it. The main sequence star TYC 5684-147-1 was found to be 79.00 arcsec from source 64, 33.57 arcsec from source 67, and 22.97 arcsec from source 68.

To identify the sources with mainly non-thermal emission that could be interesting candidates for the TeV emission from the HESS J1813-126 source, we chose the 2.5 - 12 keV energy band when doing the EPIC source finding thread. The result was that 36 sources remained, see Figure 6.5.

There were not found any astronomical objects in the 2 arcmin radius search in SIM-BAD for the sources: H1 - H9, 1 - 3, 28, 29, 34, 39, 59. For source number 6, the only

Figure 6.5: Counts map observation of HESS J1813-126 done using MOS2 of ObsID 0693960101, with cut in the energy range from 2.5 - 12 keV, the black squares indicate 36 sources detected by the EPIC source detection tool.

object found in the radius search was the dark cloud (nebula) DOBASHI 0751 located at 82.99 arcsec away from the source. Source number 12 can identified to be the X-ray emitting star [MGP2014] 3, located 1.48 arcsec offset; however, the young stellar object MSX6C G017.3765+02.2512 was found to be 18.40 arcsec away, the molecular cloud PGCC G017.37+02.26 is located at 34.99 arcsec offset, the Far-IR source IRAD 18115-1245 is at 48.80 arcsec and the dark nebula DOBASHI 0749 at 54.64 arcsec offset. In the case of source 14, it can be identified as the X-ray star [MHP2014] 9, which was

found to be 0.78 arcsec offset. The source 22 was found 65.36 arcsec away from the AGN [MHP2014] 10, and 98.68 arcsec away from the star [MHP2014] 11, however the AGN can be identified to be the source 23 located at just 0.72 arcsec offset. The source 26 is located 74.93 arcsec from the dark nebula DOBASHI 0748 and 94.65 arcsec from the X-ray star [MHP2014] 11. The only source found in the 2 arcmin region around source 27, was the star [MHP2014] 11, 119.97 arcsec offset. Source number 30 can be identified to be the pulsar PSR J1813-1246, located 0.52 arcsec offset; moreover, 5.27 arcsec offset was found the X-ray source SWIFT J181323.4-124600, and 54.38 arcsec offset the star [MHP2014] 7. Source number 36 can be identified to be the AGN [MHP2014] 8, it was found to be 0.80 arcsec offset. The source marked with number 40 can be identified as the AGN [MHP2014] 5, which was found 0.36 arcsec away, and no other sources were found in the 2 arcmin region. The only source found in the 2 arcmin radius search around source 45 was the star IRAS 18102-1245 located 39.73 arcsec away. The same source was found in the 2 arcmin vicinity around source 46, however the distance to this one is 60.47 arcsec offset. In the 2 arcmin vicinity of source 48 were found the AGN [MHP2014] 4 and the radio source NVSS J181303-124908, located at 46.03 and 46.31 arcsec offset, respectively. For source 49 the only object in the vicinity found was the same AGN, 118.41 arcsec away. The same objects found for source 48 were found for source 50, but at 40.87 and 43.45 arcsec away, respectively. Nonetheless, this AGN can be identified to be source 51, which was found to be 0.00 arcsec away. The radio source NVSS J181303-124908 is located 2.62 arcsec away from this source. Source 54 is in the same region, the distance to the AGN is 88.99 arcsec offset and to the radio source of 89.90 arcsec, and the star TYC 5684-825-1 is located 106.77 arcsec offset. Source number 58 is identified to be the X-ray star [MHP2014] 6, 2.37 arcsec offset, no other sources were found in the 2 arcmin radius search.

## 6.3 Chandra observation

Chandra observed the PSR J1813-1246 during 50.40 ks on 2013 July, 22 (ObsID: 14399) using the ACIS-S instrument on-board the telescope, in specific, the CCDs that were used are: S1, S2, S3, and S4. This observation was organized together with the XMM-Newton observation 0693960101.

We carried out the source detection using both `celldetect` and `vtpdetect` CIAO tools. The results can be seen in the Figure 6.6. In this Figure the black ellipses indicate the 23 sources detected only by `celldetect`, the red ellipses show the sources that were found using the detection tool `vtpdetect`.


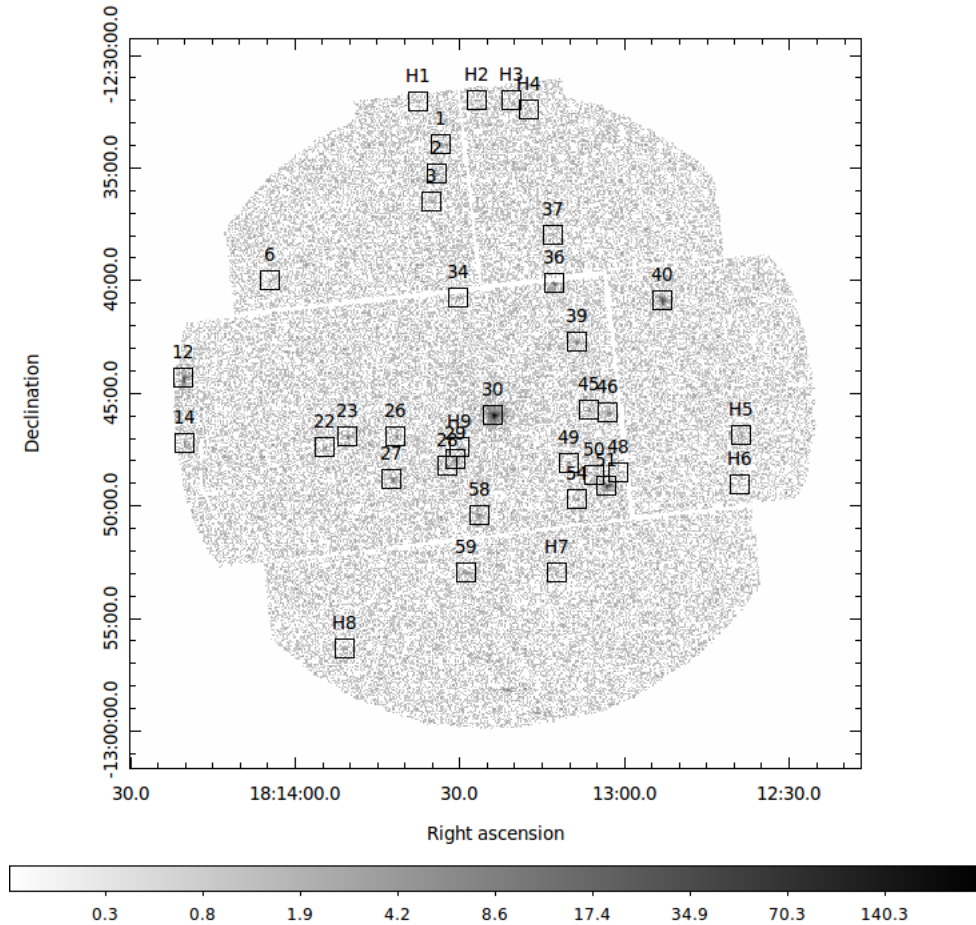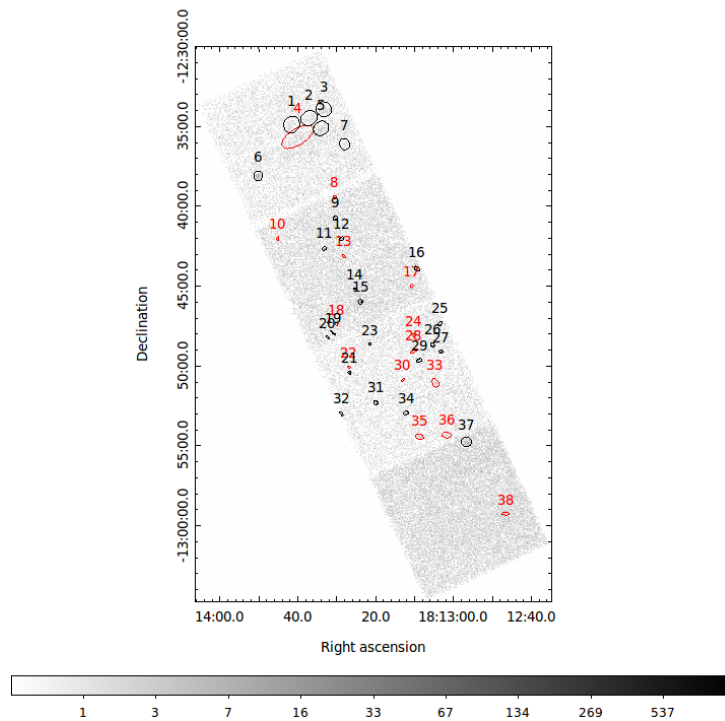
Figure 6.6: Counts map observation of HESS J1813-126 done using MOS2 of ObsID 14399, with cut in the energy range from 2.5-8 keV, showing the sources detected. Description in the text.

Table 6.8: Non-thermal emission sources found using ObsID 0693960101 of HESS J1813-126. The flux values are in erg cm$^{-2}$s$^{-1}$.

| Src | RA J2000 | DEC J2000 | Possible counterpart | Distance arcsec | Flux E-15 |
|---|---|---|---|---|---|
| H1 | 18:13:37.4 | -12:32:03.8 | No astronomical | object found | 5.20 |
| H2 | 18:13:26.9 | -12:31:59.9 | No astronomical | object found | 4.59 |
| H3 | 18:13:20.4 | -12:31:59.5 | No astronomical | object found | 9.84 |
| H4 | 18:13:17.3 | -12:32:24.4 | No astronomical | object found | 7.90 |
| H5 | 18:12:38.6 | -12:46:53.0 | No astronomical | object found | 5.19 |
| H6 | 18:12:38.9 | -12:49:05.2 | No astronomical | object found | 3.06 |
| H7 | 18:13:12.2 | -12:52:59.5 | No astronomical | object found | 2.70 |
| H8 | 18:13:50.9 | -12:56:21.1 | No astronomical | object found | 5.24 |
| H9 | 18:13:30.0 | -12:47:26.2 | No astronomical | object found | 1.73 |
| 1 | 18:13:33.4 | -12:33:59.8 | No astronomical | object found | 5.88 |
| 2 | 18:13:34.1 | -12:35:16.8 | No astronomical | object found | 5.66 |
| 3 | 18:13:35.0 | -12:36:30.5 | No astronomical | object found | 3.18 |
| 6 | 18:14:04.3 | -12:40:01.2 | DOBASHI 0751 | 82.99 | 4.69 |
| 12 | 18:14:20.2 | -12:44:21.5 | [MHP2014] 3 | 1.48 | 76.9 |
| 14 | 18:14:19.9 | -12:47:13.9 | [MHP2014] 9 | 0.78 | 10.4 |
| 22 | 18:13:54.5 | -12:47:24.7 | [MHP2014] 10 | 65.36 | 5.56 |
| 23 | 18:13:50.4 | -12:46:57.4 | [MHP2014] 10 | 0.72 | 9.46 |
| 26 | 18:13:41.5 | -12:46:55.9 | DOBASHI 0748 | 74.93 | 4.03 |
| 27 | 18:13:42.2 | -12:48:50.0 | [MHP2014] 11 | 119.07 | 6.16 |
| 28 | 18:13:32.2 | -12:48:15.5 | No astronomical | object found | 2.95 |
| 29 | 18:13:30.7 | -12:47:57.1 | No astronomical | object found | 4.71 |
| 30 | 18:13:23.8 | -12:46:00.1 | PSR J1813-1246 | 0.52 | 118.0 |
| 34 | 18:13:30.2 | -12:40:46.9 | No astronomical | object found | 2.29 |
| 36 | 18:13:12.7 | -12:40:09.8 | [MHP2014] 8 | 0.80 | 14.0 |
| 37 | 18:13:13.0 | -12:37:59.2 | TYC 5684-797-1 | 86.80 | 2.47 |
| 39 | 18:13:08.6 | -12:42:44.3 | No astronomical | object found | 6.25 |
| 40 | 18:12:53.0 | -12:40:53.4 | [MHP2014] 5 | 0.36 | 42.4 |
| 45 | 18:13:06.5 | -12:45:44.3 | IRAS 18102-1245 | 39.73 | 3.18 |
| 46 | 18:13:02.9 | -12:45:53.3 | IRAS 18102-1245 | 60.47 | 4.85 |
| 48 | 18:13:01.0 | -12:48:33.5 | [MHP2014] 4 | 46.03 | 2.61 |
| 49 | 18:13:10.1 | -12:48:06.5 | [MHP2014] 4 | 118.41 | 3.27 |
| 50 | 18:13:05.3 | -12:48:41.0 | [MHP2014] 4 | 40.87 | 2.23 |
| 51 | 18:13:03.1 | -12:49:07.0 | [MHP2014] 4 | 0.00 | 38.5 |
| 54 | 18:13:08.6 | -12:49:44.4 | [MHP2014] 4 | 88.99 | 2.75 |
| 58 | 18:13:26.4 | -12:50:26.9 | [MHP2014] 6 | 2.37 | 5.63 |
| 59 | 18:13:28.8 | -12:53:01. | No astronomical | object found | 6.73 |

Table 6.9: Possible counterparts HESS J1813-126 found using ObsID 14399 of Chandra Observatory.

| Src | RA (J2000) | DEC (J2000) | Star | Distance | X | Distance |
|---|---|---|---|---|---|---|
| 1 | 18:13:41.4 | -12:34:54.3 | No astronomical | — | object found | — |
| 2 | 18:13:37.0 | -12:34:30.3 | No astronomical | — | object found | — |
| 3 | 18:13:33.2 | -12:33:56.9 | No astronomical | — | object found | — |
| 4 | 18:13:39.9 | -12:35:41.3 | No astronomical | — | object found | — |
| 5 | 18:13:33.9 | -12:35:08.7 | No astronomical | — | object found | — |
| 6 | 18:13:50.0 | -12:38:07.7 | No astronomical | — | object found | — |
| 7 | 18:13:27.8 | -12:36:08.7 | No astronomical | — | object found | — |
| 8 | 18:13:30.4 | -12:39:27.3 | No astronomical | — | object found | — |
| 9 | 18:14:00.2 | -12:42:27.7 | No astronomical | — | object found | — |
| 10 | 18:13:45.0 | -12:42:03.3 | TYC 5684-111-1 | 32.47 | — | — |
| 11 | 18:13:33.1 | -12:42:39.6 | No astronomical | — | object found | — |
| 12 | 18:13:28.6 | -12:42:03.4 | TYC 5684-695-1 | 83.19 | — | — |
| 13 | 18:13:28.1 | -12:43:09.2 | TYC 5684-695-1 | 102.18 | — | — |
| 14 | 18:13:25.3 | -12:45:11.0 | [MHP2014] 7 | 0.52 | SWIFT J181323.4-124600 | 56.21 |

*Continued on next page*

Table 6.9 *Continued from previous page*

| Src | DNe | Distance | Pulsar | Distance | Radio | Distance |
|-----|-----|----------|--------|----------|-------|----------|
| 1 | — | — | — | — | — | — |
| 2 | — | — | — | — | — | — |
| 3 | — | — | — | — | — | — |
| 4 | — | — | — | — | — | — |
| 5 | — | — | — | — | — | — |
| 6 | — | — | — | — | — | — |
| 7 | — | — | — | — | — | — |
| 8 | — | — | — | — | — | — |
| 9 | — | — | — | — | — | — |
| 10 | — | — | — | — | — | — |
| 11 | — | — | — | — | — | — |
| 12 | — | — | — | — | — | — |
| 13 | — | — | PSR J1813-1246 | 54.36 | — | — |
| 14 | — | — | | | — | — |

Table 6.10: Possible counterparts HESS J1813-126 found using ObsID 14399 of Chandra Observatory Part 2.

| Src | RA (J2000) | DEC (J2000) | Star | Distance | X | Distance |
|-----|-----------|-------------|------|----------|---|----------|
| 15 | 18:13:23.8 | -12:46:00.5 | [MHP2014] 7 | 54.65 | SWIFT J181323.4-124600 | 5.49 |
| 16 | 18:13:09.3 | -12:43:56.1 | IRAS 18102-1245 | 89.65 | — | — |
| 17 | 18:13:10.6 | -12:45:01.6 | IRAS 18102-1245 | 74.82 | — | — |
| 18 | 18:13:29.9 | -12:47:24.8 | No astronomical | — | object found | — |
| 19 | 18:13:30.9 | -12:47:57.9 | No astronomical | — | object found | — |
| 20 | 18:13:32.2 | -12:48:14.7 | No astronomical | — | object found | — |
| 21 | 18:13:26.6 | -12:50:26.6 | [MHP2014] 6 | 0.56 | — | — |
| 22 | 18:13:26.7 | -12:50:06.3 | [MHP2014] 6 | 20.87 | — | — |
| 23 | 18:13:21.2 | -12:48:39.5 | TYC 5684-825-1 | 116.51 | — | — |
| 24 | 18:13:47.8 | -12:47:22.6 | — | — | [MHP2014] 4 | 118.93 |
| 25 | 18:13:03.3 | -12:47:22.9 | — | — | [MHP2014] 4 | 104.11 |
| 26 | 18:13:05.3 | -12:48:42.2 | — | — | [MHP2014] 4 | 40.20 |
| 27 | 18:13:03.1 | -12:49:07.3 | — | — | [MHP2014] 4 | 0.42 |
| 28 | 18:13:10.0 | -12:49:05.7 | TYC 5684-825-1 | 102.86 | [MHP2014] 4 | 101.31 |

*Continued on next page*

Table 6.10 *Continued from previous page*

| Src | DNe | Distance | Pulsar | Distance | Radio | Distance |
|-----|-----|----------|--------|----------|-------|----------|
| 15 | — | — | PSR J1813-1246 | 0.16 | — | — |
| 16 | — | — | — | — | — | — |
| 17 | — | — | — | — | — | — |
| 18 | — | — | — | — | — | — |
| 19 | — | — | — | — | — | — |
| 20 | — | — | — | — | — | — |
| 21 | — | — | — | — | — | — |
| 22 | — | — | — | — | — | — |
| 23 | — | — | — | — | — | — |
| 24 | — | — | — | — | — | — |
| 25 | — | — | — | — | NVSS J181303-124908 | 106.11 |
| 26 | — | — | — | — | NVSS J181303-124908 | 42.78 |
| 27 | — | — | — | — | NVSS J181303-124908 | 2.56 |
| 28 | — | — | — | — | NVSS J181303-124908 | 103.11 |

Table 6.11: Possible counterparts HESS J1813-126 found using ObsID 14399 of Chandra Observatory Part 3.

| Src | RA (J2000) | DEC (J2000) | Star | Distance | X | Distance |
|-----|-----------|-------------|------|----------|---|----------|
| 29 | 18:13:08.7 | -12:49:41.20 | TYC 5684-825-1 | 106.83 | [MHP2014] 4 | 88.26 |
| 30 | 18:13:12.9 | -12:50:54.6 | TYC 5684-825-1 | 65.80 | — | — |
| 31 | 18:13:19.8 | -12:52:19.3 | TYC 5684-485-1 | 14.98 | — | — |
| 32 | 18:13:28.6 | -12:53:01.9 | No astronomical | — | object found | — |
| 33 | 18:13:04.6 | -12:51:05.3 | — | — | — | — |
| 34 | 18:13:30.2 | -12:40:46.6 | No astronomical | — | object found | — |
| 35 | 18:13:19.9 | -12:41:14.6 | No astronomical | — | object found | — |
| 36 | 18:13:01.6 | -12:54:21.6 | No astronomical | — | object found | — |
| 37 | 18:12:56.5 | -12:54:47.7 | No astronomical | — | object found | — |
| 38 | 18:12:46.5 | -12:59:16.6 | No astronomical | — | object found | — |

*Continued on next page*

Table 6.11 *Continued from previous page*

| Src | DNe | Distance | Pulsar | Distance | Radio | Distance |
|-----|-----|----------|--------|----------|-------|----------|
| 29 | – | – | – | NVSS J181303-124908 | 89.16 | – |
| 30 | – | – | – | – | – | – |
| 31 | – | – | – | – | – | – |
| 32 | – | – | – | – | – | – |
| 33 | – | – | – | NVSS J181303-124908 | 118.63 | – |
| 34 | – | – | – | – | – | – |
| 35 | – | – | – | – | – | – |
| 36 | – | – | – | – | – | – |
| 37 | – | – | – | – | – | – |
| 38 | – | – | – | – | – | – |

Source number 3 is in the same position of source number 1 of the XMM-Newton observation. Source number 5 is in the same position of source number 2 of XMM-Newton's observation. Source number 6 is in the same position of source number 4 of XMM-Newton's observation. Source number 9 is in the same position of source number 34 of XMM-Newton's observation. Source number 11 is in the same position of source number 32 of XMM-Newton's observation. Source number 12 is in the same position of source number 33 of XMM-Newton's observation. Source number 14 is in the same position of source number 31 of XMM-Newton's observation. Source number 15 is in the same position of source number 30 of XMM-Newton's observation. Source number 19 is in the same position of source number 29 of XMM-Newton's observation. Source number 20 is in the same position of source number 28 of XMM-Newton's observation. Source number 24 is in the same position of source number 49 of XMM-Newton's observation. Source number 26 is in the same position of source number 50 of XMM-Newton's observation. Source number 27 is in the same position of source number 51 of XMM-Newton's observation. Source number 29 is in the same position of source number 54 of XMM-Newton's observation. Source number 31 is in the same position of source number 57 of XMM-Newton's observation. Source number 32 is in the same position of source number 59 of XMM-Newton's observation. Source number 36 is in the same position of source number 56 of XMM-Newton's observation.

No astronomical objects were found in the 2 arcmin region around sources 1 - 9, 11, 18, 19, 20, 32, 34 - 38. The only object found in the region around source number 10 was the main sequence star TYC 5684-111-1, located 32.47 arcsec offset from the source. The main sequence star TYC 5684-695-1 was found to be 83.19 arcsec offset from source 12 and 102.18 arcsec from source 13. The source number 14 is in the same position of source number 31 of XMM-Newton's observation. Source number 15 is in the same position of source number 30 of XMM-Newton's observation. In the region around

source 16, only the main sequence star IRAS 18102-1245 was found, located 89.65 arcsec offset from the source. The same star is 74.82 arcsec offset from source 17. Source 21 is in the same position of source number 58 of XMM-Newton's observation. This source was found 20.87 arcsec offset from the source 22. In the 2 arcmin region around source 23, the only source found was the main sequence star TYC 5684-825-1, located 116.51 arcsec away. Source number 24 is in the same position of source number 49 of XMM-Newton's observation. Source number 26 is in the same position of source number 50 of XMM-Newton's observation. Source number 27 is in the same position of source number 51 of XMM-Newton's observation. The region around source 28 is composed by the main sequence star TYC 5684-825-1, located 102.86 arcsec offset, the AGN [MHP2014] 4, 101.31 arcsec offset and the radio source. Source number 29 is in the same position of source number 54 of XMM-Newton's observation. The main sequence star TYC 5684-825-1, is located 65.80 arcsec offset of source 30. Source number 31 is in the same position of source number 57 of XMM-Newton's observation. The only object found around source 33 was the radio source NVSS J181303-124908, located 118.63 arcsec offset from the source.

We also extracted the sources dominated by non-thermal emission for this observation, which can be seen on Figure 6.7 by doing the cut in the energy range from 2.5 - 8 keV. For the sources that were detected by both `celldetect` and `vtpdetect`, I leaved the region found by `celldetect` (black ellipses), the sources marked with red color were detected only by `vtpdetect`, more information about the source can be found on Table 6.12.

Sources 9, 15, 19, 20, 21, 24, 26, 27, 29, 32 were found in the XMM-Newton observation.

The only object found in SIMBAD in the region of source number 4 was the main sequence star IRAS 18102-1245, but 86.21 arcsec offset. The only object in the region
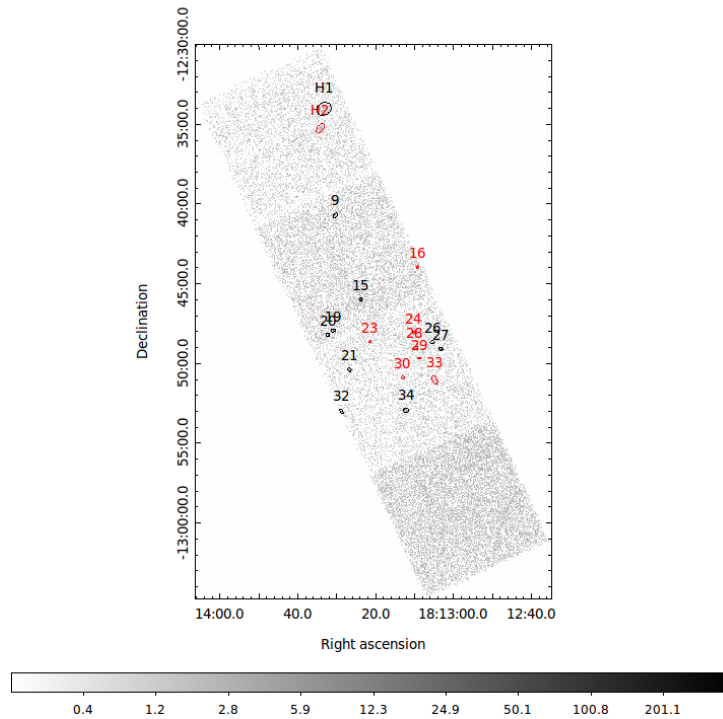
Figure 6.7: Counts map observation of HESS J1813-126 using ObsID 14399 done by Chandra Satellite, with cut in the energy range from 2.5-12 keV, using both `celldetect`, and `vtpdetect` tools. The sources found using just vtpdetect are shown in red color.

of source 23 was the main sequence star TYC 5684-825-1, 116.47 arcsec offset. The only object close to source number 30 was the main sequence star TYC 5684-825-1, 65.42 arcsec. The only object source in the region of source number 33 was the radio source NVSS J181303-124908, 117.34 arcsec offset. No astronomical object was found for sources 34, H1, and H2.

Table 6.12: Non-thermal emission sources found using ObsID 14399 of HESS J1813-126.

| Src | RA J2000 | DEC J2000 | Possible counterpart | Distance arcsec | SNR |
|---|---|---|---|---|---|
| 4 | 18:13:09.1 | -12:43:58.6 | IRAS 18102-1245 | 86.21 | |
| 9 | 18:13:30.2 | -12:40:44.9 | No astronomical | object found | 3.16 |
| 15 | 18:13:23.8 | -12:46:00.3 | PSR J1813-1246 | 0.57 | 8.03 |
| 19 | 18:13:30.9 | -12:47:56.2 | No astronomical | object found | 4.38 |
| 20 | 18:13:32.1 | -12:48:14.4 | No astronomical | object found | 3.34 |
| 21 | 18:13:26.6 | -12:50:26.6 | [MHP2014] 6 | 0.62 | 4.17 |
| 23 | 18:13:21.3 | -12:48:39.9 | TYC 5684-825-1 | 116.47 | |
| 24 | 18:13:10.0 | -12:48:06.2 | [MHP2014] 4 | 118.0 | |
| 26 | 18:13:05.3 | -12:48:42.2 | [MHP2014] 4 | 40.18 | 3.48 |
| 27 | 18:13:03.1 | -12:49:07.3 | [MHP2014] 4 | 0.39 | 13.86 |
| 28 | 18:13:10.0 | -12:49:05.6 | [MHP2014] 4 | 100.20 | |
| 29 | 18:13:08.7 | -12:49:42.4 | [MHP2014] 4 | 88.71 | |
| 30 | 18:13:12.9 | -12:50:54.6 | TYC 5684-825-1 | 65.42 | 3.79 |
| 32 | 18:13:28.7 | -12:53:02.2 | No astronomical | object found | |
| 33 | 18:13:06.5 | -12:45:44.3 | NVSS J181303-124908 | 117.34 | |
| 34 | 18:13:28.8 | -12:53:01.0 | No astronomical | object found | 3.38 |
| H1 | 18:13:33.2 | -12:34:03.9 | No astronomical | object found | 3.17 |
| H2 | 18:13:34.1 | -12:35:17.4 | No astronomical | object found | |

## 6.4   Merging the XMM-Newton and Chandra Observations

To put all the information together, I merged of all the X-ray observations in both, the full energy range and the hard energy range. The Figures can be seen on 6.8.
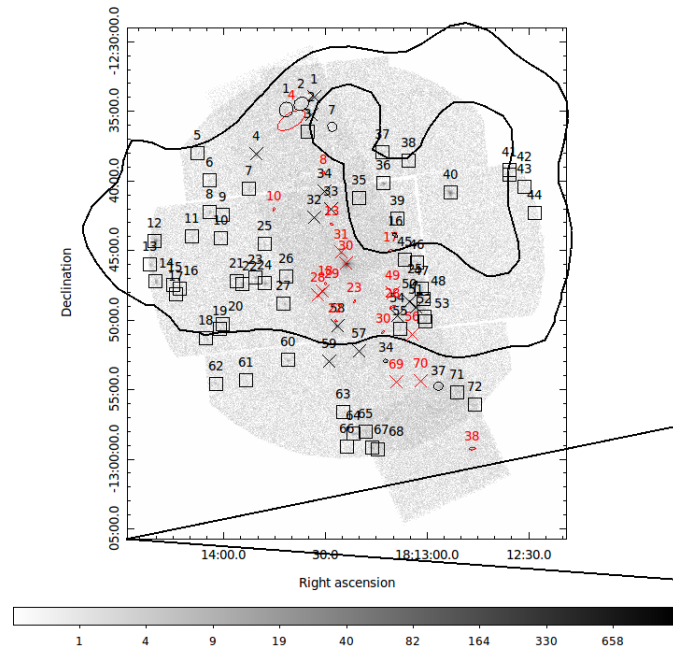
(a) Merged of all the three X-ray observations described previously for the HESS J1626-490 source.
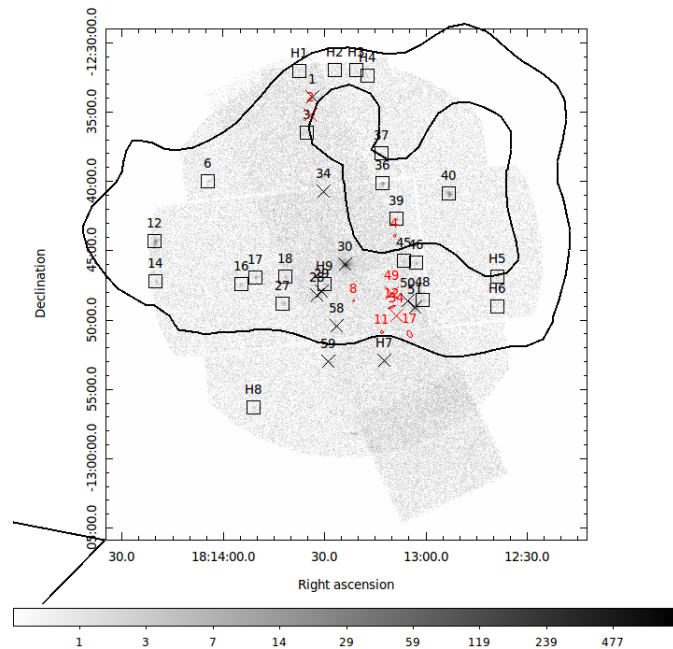


(b) Merge of the two X-ray observations we used to study HESS J1813-126 considering the energy range 2.5-12 keV.

Figure 6.8: Merged of all the two X-ray observations we analysed for HESS J1813-126 Description in the text.

In Figure 6.8 are shown all the sources that were found in the analysing the two X-ray observations on HESS J1813-126. The black squares indicate the sources detected using XMM-Newton data. In the other hand, the sources detected with the `celldetect` tool are shown as black ellipses, the red ellipses points out the sources detected using `vtpdetect`. The sources that were found by both Chandra and XMM-Newton observations were marked with an X, the number of the XMM-Newton source remained, the red color indicates detections using `vtpdetect`.

## 6.5  Astrophysical Discussion and Conclusions

**XMM-Newton observation**

In summary, there were detected 72 sources for the XMM-Newton 0693960101 using the full energy range, and 35 sources were detected in the hard energy range (2.5 - 12 keV), 9 of them were only detected to be dominated by non-thermal emission and no astronomical object was found in the 2 arcmin radius search in the SIMBAD database.

Among all the sources that were found in the full energy range 25 were found to have no astronomical objects in SIMBAD.

- Source number 9 is likely to be the gamma-ray source UGRS G017.4+2.4, 27.94 arcsec offset from the source.

- Source number 12 can be identified to be the X-ray source [MHP2014] 3 that was found to be 0.80 arcsec offset.

- Source number 14 can be identified to be the X-ray star [MHP2014] 9, located 0.78 arcsec offset.

- Source number 23 is identified to be the AGN [MHP2014] 10.

- Source number 24 is identified to be the X-ray emitting star [MHP2014] 11.

  - Source number 30 can be identified to be the pulsar PSR J1813-1246 (0.52 arcsec offset), suitable counterpart of HESS J1813-126. Previous studies showed that extended emission was not found down to a fraction of an arcsec [119], and they said the Suzaku detection of a nebula reported in was due to the X-ray star [MHP2014] 7 which is located at ~50 arcsec from the pulsar.

- Source number 31 can be identified to be the X-ray star [MHP2014] 7, located 1.11 arcsec offset.

- Source number 36 can be identified to be the AGN [MHP2014] 8 (0.80 arcsec offset).

- Source number 40 can be identified to be the AGN [MHP2014] 5 which was found to be 0.36 arcsec offset.

- Source number 51 can be identified to be the AGN [MHP2014] 4. The radio source NVSS J181303-124908 is also very close, just 2.36 arcsec offset.

  - Source number 57 can be identified to be the main sequence star TYC 5684-485-1, which was found to be 14.92 arcsec offset.

- Source number 58 can be identified as the X-ray emitting star [MHP2014] 6, which was found to be 2.52 arcsec offset.

- Source number 60 was found to be the main sequence star BD-12 4949 which is 3.69 arcsec offset.

- Source 62 can be identified as the main sequence star TYC 5684-167-1, which was found to be 2.07 arcsec offset.

So, we have the gamma-ray source UGRS G017.4+2.4, the X-ray source [MHP2014] 3, the X-ray star [MHP2014] 9, the AGN [MHP2014] 10, the X-ray emitting star [MHP2014] 11, the pulsar PSR J1813-1246, the X-ray star [MHP2014] 7, the AGN [MHP2014] 8, the AGN [MHP2014] 5, the AGN [MHP2014] 4, the radio source NVSS J181303-124908, X-ray emitting star [MHP2014] 6 to be possible counterparts of the HESS J1813-126 VHE emission.

X-ray emitting stars could be helping to produce the VHE emission?

From these sources, the the X-ray emitting star [MHP2014] 3, the X-ray star [MHP2014] 9, the AGN [MHP2014] 10, the pulsar PSR J1813-1246, the AGN [MHP2014] 8, the AGN [MHP2014] 5, the AGN [MHP2014] 4, the X-ray emitting star [MHP2014] 6 were found to be non-thermal emission dominated.

So, we have three X-ray emitting stars, four AGNs, and one pulsar in the region to be the possible counterparts of the VHE emission. All these sources could explain part or all the emission from HESS J1813-126; however more detailed analysis are needed, specially in the sources that were found to be AGNs and no previous reports on these sources were found in the literature (see [8]).

**Chandra observation**

In summary, 38 sources were detected; however, 18 of them were also detected with XMM-Newton.

No astronomical objects were found in the 2 arcmin region around sources 1 - 9, 11, 18, 19, 20, 32, 34 - 38.

The sources that were detected by Chandra and not for XMM-Newton were found to be main sequence stars. Which are not plausible counterparts of the VHE emission. For trying to explain the VHE from HESS J1813-126, there were identified the pulsar PSR J1813-1246, two X-ray emitting stars, one AGN and the radio source NVSS J181303-

124908, whose were already detected by XMM-Newton.

# CHAPTER 7

---

## CONCLUSIONS

---

The X-ray analysis of this thesis consisted in analysing 10 different observations made on three different TeV unidentified sources (HESS J1626-490, HESS J1808-204, and HESS J1813-126) and using two different telescopes: XMM-Newton and Chandra. For each observation, I calibrated, filter and cleaned the data, I applied the `edetect_chain` or `celldetect` or `vtpdetect` tool depending on the telescope to look for the X-ray possible counterparts. In addition, I search on the SIMBAD database for astronomical objects in the FOV in other wavelengths that could led me find a clue in the nature on the unidentified source. The most important results obtained are summarized below.

**HESS J1626-490**

Excluding all the stars as possible counterparts of HESS J1626-490, the triple system HD 147633 is also excluded due to it is formed by main sequence stars. We have the X-ray source 2XMM J162703.0-491232, the FGL source, five dark nebulae and two sub-milimetric radio source spatially coincident of the HESS source. None of these sources alone can explain an extensive and luminous source such as HESS J1626-490, more detailed studies are needed beyond the spatial coincidence.

With a TS of 1.93, HESS J1626-490 is not detected in our analysis and upper limits were obtained for this source. Similar results were obtained in [168], in those studies, they used 45 months of data and here we used 10 years and we could not have a real detection of the source, which means that we need to wait for more data time or we need to increase the sensitivity of Fermi to be able to detect sources of this kind.

**HESS J1808-204**

In the region of HESS J1808-204, we have the W31 IR Cluster, in which the O-type star 2MASS J18092597-2019383 was found, this kind of stars are able to produce X-rays but this can not a be counterpart of the VHE TeV emission. Moreover, eight X-ray sources were found in the region, as well as the HII region GAL 010.2-00.3, four dark nebulae, the sub-millimetric radio source JCMTSE J180902.8-202243, twelve molecular clouds, four IR sources, the pulsar PSR J1808-2024, four WR stars, the massive stellar cluster Cl* 1806-20, the interstellar matter AX J1808.6-2024, ten sub-millimetric radio sources.

The pulsar PSR J1808-2024 has a period of 7.5 (s), it has a characteristic age of ∼43 yr. This is a very young pulsar with a spin-down luminosity $\dot{E}$ = 5.0 × $10^{34}$ erg s$^{-1}$ (see http://www.atnf.csiro.au/research/pulsar/psrcat/). Which means this is a good candidate to understand the nature of HESS J1808-204. Moreover, all the sources that are very close to this pulsar, can explain part of the VHE emission. More detailed studies would be needed to clarify the unidentified HESS source.

**HESS J1813-126**

So, we have the gamma-ray source UGRS G017.4+2.4, the X-ray source [MHP2014] 3, the X-ray emitting stars, four AGNs, one radio source and the pulsar PSR J1813-1246 that are possible counterparts of HESS J1813-126. The pulsar has a characteristic age $\tau_c$ = 43 kyr and a spin-down luminosity $\dot{E}$ = 6.54 × $10^{36}$ erg s$^{-1}$, making it the fastest-

spinning known radio-quiet puslar and the second most energetic [119].

In summary: with all the previous information, we given spatial coincidence identification. However, there is a long way to go to fully understand the nature of the VHE emission of these three HESS unidentified sources.

# BIBLIOGRAPHY

1. Wulf, T. Über die in der Atmosphäre vorhandene Strahlung von hoher Durch-dringungsfähigkeit. *Phys. Zeit.* **10,** 152 (1909).

2. Wulf, T. Beobachtungen über die Strahlung hoher Durch-dringungsfähigkeit auf dem Eiffelturm. *Phys. Zeit.* **11,** 811 (1910).

3. Pacini, D. La radiazione penetrante alla superficie ed in seno alle acque. *Nuovo Cimento* **3,** 93 (1912).

4. Hess, V. Über Beobachtungen der durchdringenden Strahlung bei sieben Freibal-lonfahrten. *Phys. Zeit.* **13,** 1084 (1912).

5. Weekes, T. C. Very high energy gamma-ray astronomy. *Physics Reports* **160,** 1–121 (1988).

6. Fazio, G. G., Helmken, H. F., O'Mongain E. andRieke, G. H. & Weekes, T. C. Detection of High-Energy Gamma Rays from the Crab Nebula. *ApJL* **175,** 17 (L1 1972).

7. Morganti, R. *et al.* LOFAR: opening a new window on low frequency radio astron-omy. *arXiv e-prints* (2011).

8. H. E. S. S. Collaboration *et al.* The H.E.S.S. Galactic plane survey. *A&A* **612,** A1 (2018).

9. Wilson, C. T. R. On the Leakage of Electricity through Dust-free Air. *Proc. Camb. Soc.* **11,** 32 (1900).

10. Kolhörster, W. Messungen der durchdringenden Strahlung im Freiballon in gröeren Höhen. *Phys. Zeit.* **14,** 1153 (1914).

11. Janossy, L. Cosmic Rays. *Oxford* **14,** 1153 (1948).

12. Perkins, D. *Particle Astrophysics* Second Edition (Oxford University Press, 2009).

13. Greisen, K. End to the Cosmic-Ray Spectrum? *Phys. Rev. Lett.* **16,** 748–750 (17 1966).

14. Tibolla, O. *Obserbavility of Supernovae Remnants with GLAST* (Ph.D. Thesis, 2007).

15. Saito, T. *Study of the High Energy Gamma-ray Emission from the Crab Pulsar with the MAGIC telescope and Fermi-LAT* (Ph.D. Thesis, 2010).

16. Jackson, J. *Classical Electrodynamics* Third Edition (John Wiley & Sons, INC., 1998).

17. Biermann, P. L. TOPICAL REVIEW: The origin of the highest energy cosmic rays. *Journal of Physics G Nuclear Physics* **23,** 1–27 (1997).

18. Lyutikov, M. Role of reconnection in AGN jets. *New Astronomy Reviews* **47,** 513–515 (2003).

19. Völk, H. J., Aharonian, F. A. & Breitschwerdt, D. *The Nonthermal Energy Content and Gamma Ray Emission of Starburst Galaxies and Clusters of Galaxies* in *TeV Gamma-ray Astrophysics. Theory and Observations* (eds Voelk, H. J. & Aharonian, F. A.) (1996), 279–297.

20. Lacki, B. C., Thompson, T. A., Quataert, E., Loeb, A. & Waxman, E. On the GeV and TeV Detections of the Starburst Galaxies M82 and NGC 253. *The Astrophysical Journal* **734,** 107 (2011).

21. Graham, J. F. & Fruchter, A. S. The Metal Aversion of Long-duration Gamma-Ray Bursts. *The Astrophysical Journal* **774,** 119 (2013).

22. Mirzoyan, R. First time detection of a GRB at sub-TeV energies; MAGIC detects the GRB 190114C. *The Astronomer's Telegram* **12390** (2019).

23. Baade, W. & Zwicky, F. On Super-novae. *Proceedings of the National Academy of Science* **20,** 254–259 (1934).

24. Amato, E. *Particle acceleration in astrophysical sources* in *Frontiers of Fundamental Physics 14 (FFP14)* (2014), 24.

25. Hewish, A., Bell, S. J., Pilkington, J. D. H., Scott, P. F. & Collins, R. A. Observation of a Rapidly Pulsating Radio Source. *Nature* **217,** 709–713 (1968).

26. Cheng, A. F. & Ruderman, M. A. Particle acceleration and radio emission above pulsar polar caps. *The Astrophysical Journal* **235,** 576–586 (1980).

27. Kargaltsev, O. & Pavlov, G. G. *Pulsar Wind Nebulae in the Chandra Era* in *40 Years of Pulsars: Millisecond Pulsars, Magnetars and More* (eds Bassa, C., Wang, Z., Cumming, A. & Kaspi, V. M.) **983** (2008), 171–185.

28. Bîrzan, L., Pavlov, G. G. & Kargaltsev, O. Chandra Observations of the Elusive Pulsar Wind Nebula around PSR B0656+14. *The Astrophysical Journal* **817,** 129 (2016).

29. Mattana, F. *et al.* The Evolution of the $\gamma$- and X-Ray Luminosities of Pulsar Wind Nebulae. *The Astrophysical Journal* **694,** 12–17 (2009).

30. Tibolla, O., Vorster, M., Kaufmann, S., Ferreira, S. & Mannheim, K. Are most of the VHE gamma-ray unidentified sources relic PWNe? *PoS ICRC2013,* 1117 (2013).

31. Kaufmann, S. & Tibolla, O. Ancient Pulsar Wind Nebulae as a natural explanation for unidentified gamma-ray sources. *Nuclear and Particle Physics Proceedings* **297-299.** Cosmic Ray Origin - Beyond the Standard Models, 91–95. ISSN: 2405-6014 (2018).

32. Mirabel, I. F. Very energetic gamma-rays from microquasars and binary pulsars. *Science* **312,** 1759 (2006).

33. Bednarek, W. Gamma-ray production in young open clusters: Berk 87, Cyg OB2 and Westerlund 2. *MNRAS* **382,** 367–376 (2007).

34. Wakely, S. P. & Horan, D. TeVCat: An online catalog for Very High Energy Gamma-Ray Astronomy. *International Cosmic Ray Conference* **3,** 1341–1344 (2008).

35. Tavecchio, F. & Ghisellini, G. 3C66B as a TeV radiogalaxy. *MNRAS,* **394,** 131 (2009).

36. Ghisellini, G., Tavecchio, F. & Chiaberge, M. Structured jets in TeV BL Lac objects and radiogalaxies. Implications for the observed properties. *A&A,* **432,** 401–410 (2005).

37. Stawarz, Ł., Sikora, M. & Ostrowski, M. High-Energy Gamma Rays from FR I Jets. *ApJ,* **597,** 186–201 (2003).

38. Bartoli, B. *et al.* TeV Gamma-Ray Survey of the Northern Sky Using the ARGO-YBJ Detector. *ApJ,* **779,** 27 (2013).

39. Abeysekara, A. U. *et al.* The 2HWC HAWC Observatory Gamma-Ray Catalog. *ApJ,* **843,** 40 (2017).

40. Weiler, K. W. & Panagia, N. VELA X and the evolution of Plerions. *A&A,* **90,** 269–282 (1980).

41. Enomoto, R. *et al.* A Search for Sub-TeV Gamma Rays from the Vela Pulsar Region with CANGAROO-III. *ApJ,* **638,** 397 (2006).

42. Aharonian, F. *et al.* First detection of a vhe gamma-ray spectral maximum from a cosmic source: h.e.s.s. discovery of the vela x nebula. *Astron. Astrophys.* **448,** L43–L47 (2006).

43. Blondin, J. M., Chevalier, R. A. & Frierson, D. M. Pulsar Wind Nebulae in Evolved Supernova Remnants. *ApJ,* **563,** 806–815 (2001).

44. Park, N., VERITAS Collaboration, Fermi-Lat Collaboration & Hawc Collaboration. VERITAS and Fermi-LAT observations of TeV gamma-ray sources from the second HAWC catalog. *International Cosmic Ray Conference* **301,** 696 (2017).

45. Aharonian, F. *et al.* A detailed spectral and morphological study of the gamma-ray supernova remnant with HESS. *A&A* **449,** 223–242 (2006).

46. Vorster, M., Tibolla, O., Ferreira, S. & Kaufmann, S. Time-dependent modelling of pulsar wind nebulae. *ApJ,* **773,** 139 (2013).

47. Fujinaga, T. *et al.* An X-Ray Counterpart of HESS J1427-608 Discovered with Suzaku. *PASJ,* **65,** 61 (2013).

48. Guo, X.-L. *et al.* HESS J1427-608: An Unusual Hard, Unbroken Gamma-Ray Spectrum in a Very Wide Energy Range. *ApJ,* **835,** 42 (2017).

49. Chaves, R. C. G. f. t. H. C. *Extending the H.E.S.S. Galactic Plane Survey* in (2009). arXiv: 0907.0768.

50. Tibolla, O. *et al. EHESS J1507-622: an unique unidentified source off the Galactic Plane* in (2009). arXiv: 0912.4229.

51. Simon, R., Jackson, J. M., M., R. J. & Chambers, E. A Catalog ofMidcourse Space ExperimentInfrared Dark Cloud Candidates. *The Astrophysical Journal* **639,** 227–236 (Mar. 2006).

52. Green, A. J., Cram, L. E., Large, M. I. & Ye, T. The Molonglo Galactic Plane Survey. I. Overview and Images. *The Astrophysical Journal Supplement Series* **122,** 207–219 (1999).

53. Dame, T. M., Hartmann, D. & Thaddeus, P. The Milky Way in Molecular Clouds: A New Complete CO Survey. *The Astrophysical Journal* **547,** 792–813 (2001).

54. Domainko, W. F. Constraints on a hadronic model for unidentified off-plane galactic gamma-ray sources. *Advances in Space Research* **47,** 640–644 (2011).

55. H.E.S.S. Collaboration *et al.* Discovery and follow-up studies of the extended, off-plane, VHE gamma-ray source HESS J1507-622. *A&A* **525,** A45 (2011).

56. Tibolla, O. New developments in the ancient Pulsar Wind Nebulae scenario. *International Cosmic Ray Conference* **6,** 202 (2011).

57. Aharonian, F. *et al.* HESS very-high-energy gamma-ray sources without identified counterparts. *A&A,* **477,** 353–363 (2008).

58. Whiteoak, J. B. Z. & Green, A. J. The MOST supernova remnant catalogue (MSC). *A&AS,* **118,** 329–380 (1996).

59. Eger, P. *et al.* A multi-wavelength study of the unidentified TeV gamma-ray source HESS J1626-490. *ICRC,* **7,** 45–48 (2011).

60. de Wilt, P. *et al.* Dense molecular gas at 12 mm towards Galactic TeV gamma-ray sources. *MNRAS,* **468,** 2093–2113 (2017).

61. Aharonian, F. *et al.* The H.E.S.S. Survey of the Inner Galaxy in Very High Energy Gamma Rays. *ApJ,* **636,** 777–797 (2006).

62. Patel, S. K. *et al.* The Peculiar X-Ray Transient IGR J16358-4726. *ApJL,* **602,** L45 (2004).

63. Revnivtsev, M. *et al.* Igr J16358-4726. *IAU Circ.* **8097** (2003).

64. Combi, J., Benaglia, P., Romero, G. & Sugizaki, M. G337.2+0.1: A new X-ray supernova remnant?. *A&A,* **431,** L9–L12 (2005).

65. Oya, I. *et al.* Discovery of the VHE gamma-ray source HESS J1641-463. *ArXiv e-prints.* arXiv: 1303.0979 (2013).

66. Abramowski, A. *et al.* Discovery of the Hard Spectrum VHE $\gamma$-Ray Source HESS J1641-463. *ApJ,* **794,** L1 (2014).

67. Tang, Y., Yang, C., Zhang, L. & Wang, J. A Self-consistent Explanation of TeV Emissions from HESS J1640-465 and HESS J1641-463. *ApJ,* **812,** 32 (2015).

68. Angüner, E. O. *et al.* Very high energy emission from the hard spectrum sources HESS J1641-463, HESS J1741-302 and HESS J1826-130. *PoS* **ICRC,** 686 (2017).

69. Giacani, E., Smith, M. J. S., Dubner, G. & Loiseau, N. A new study of the supernova remnant G344.7-0.1 located in the vicinity of the unidentified TeV source HESS J1702-420. *A&A* **531,** A138 (2011).

70. Van Etten, A., Funk, S. & Hinton, J. A Multi-Wavelength Investigation of the Unidentified Gamma-Ray Source HESS J1708-410. *ApJ,* **707,** 1717–1722 (2009).

71. de Jager, O. C. *et al.* Unidentified Gamma-Ray Sources as Ancient Pulsar Wind Nebulae. *ArXiv e-prints.* arXiv: 0906.2644 (2009).

72. Kaufmann, S. & Tibolla, O. Ancient Pulsar Wind Nebulae as a natural explanation for unidentified gamma-ray sources. *Nuclear and Particle Physics Proceedings* **297-299,** 91–95 (2018).

73. H.E.S.S. Collaboration *et al.* A new SNR with TeV shell-type morphology: HESS J1731-347. *A&A,* **531,** A81 (2011).

74. Caswell, J. L. & Haynes, R. F. Southern H II regions - an extensive study of radio recombination line emission. *A&A,* **171,** 261–276 (1987).

75. Maxted, N. *et al.* A dense gas survey of the gamma-ray sources HESS J1731-347 and HESS J1729-345. *PoS* **CRISM,** 009 (2014).

76. Cui, Y., Pühlhofer, G. & Santangelo, A. A young supernova remnant illuminating nearby molecular clouds with cosmic rays. *A&A,* **591,** A68 (2016).

77. Nayana, A. J. *et al.* 325 and 610 MHz radio counterparts of SNR G353.6-0.7 also known as HESS J1731-347. *MNRAS,* **467,** 155–163 (2017).

78. Tian, W. W., Leahy, D. A., Haverkorn, M. & Jiang, B. Discovery of the Radio and X-Ray Counterpart of TeV gamma-Ray Source HESS J1731-347. *ApJ,* **679,** L85 (2008).

79. Tibolla, O., Komin, N., Kosack, K., NaumannâGodo, M. & Collaboration, H. A new source discovered close to the Galactic Center: HESS J1741-302. *AIP Conf. Proc.,* **1085,** 249–252 (2008).

80. Tibolla, O. *et al.* New unidentified H.E.S.S. Galactic sources. *PoS* **ICRC.** arXiv: 0907.0574 (2009).

81. Matsumoto, H., Uchiyama, H., Tsuru, T. G., Koyama, K. & Tibolla, O. *Discovery of the X-ray emission from the unidentified TeV object HESS J1741-302* in *PoS 3rd Suzaku Conference* (ed Makishima, K.) (2010), 154–155.

82. Uchiyama, H. *et al.* No X-Ray Excess from the HESS J1741-302 Region, except for a New Intermediate Polar Candidate. *PASJ,* **63,** S865–S872 (2011).

83. Hare, J., Rangelov, B., Sonbas, E., Kargaltsev, O. & Volkov, I. Multi-wavelength Study of HESS J1741-302. *ApJ,* **816,** 52 (2016).

84. Angüner, O. E. *et al.* Very high energy emission from the hard spectrum sources HESS J1641-463, HESS J1741-302 and HESS J1826-130. *International Cosmic Ray Conference* **35,** 686 (2017).

85. Rowell, G. Unidentified TeV sources and the interstellar medium. *AIP Conf. Proc.* **1792,** 020011 (2017).

86. Arca-Sedda, M., Kocsis, B. & Brandt, T. D. Gamma-ray and X-ray emission from the Galactic centre: hints on the nuclear star cluster formation history. *MNRAS* **479,** 900–916 (2018).

87. Chernyshov, D. O., Cheng, K. .-.-S., Dogiel, V. A. & Ko, C. M. Origin of X-Ray and Gamma-Ray Emission from the Galactic Central Region. *The Astrophysical Journal* **835,** 194 (2017).

88. Smith, A. W. & for the VERITAS Collaboration. VERITAS Observations of The Galactic Center Ridge. *C14-10-20.1,* arXiv: 1508.06311 (2015).

89. Ponti, G., Terrier, R., Goldwurm, A., Belanger, G. & Trap, G. Discovery of a Super-luminal Fe K Echo at the Galactic Center: The Glorious Past of Sgr A* Preserved by Molecular Clouds. *ApJ,* **714,** 732–747 (2010).

90. Lemiere, A., Terrier, R., Jouvin, L., Marandon, V. & Khelifi, B. *Study of the VHE diffuse emission in the central 200 pc of our Galaxy with H.E.S.S.* in. **34** (2015), 838.

91. Wang, Q. D., Lu, F. & Lang, C. C. X-Ray Thread G0.13-0.11: A Pulsar Wind Nebula? *ApJ,* **581,** 1148–1153 (2002).

92. H. E. S. S. Collaboration *et al.* Characterising the VHE diffuse emission in the central 200 parsecs of our Galaxy with H.E.S.S. *A&A,* **612,** A9 (2018).

93. Yusef-Zadeh, F., Morris, M. & Chance, D. Large, highly organized radio structures near the galactic centre. *Nature,* **310,** 557–561 (1984).

94. Archer, A. *et al.* TeV Gamma-ray Observations of The Galactic Center Ridge By VERITAS. *ApJ,* **821,** 129 (2016).

95. Ahnen, M. L. *et al.* Search for VHE gamma-ray emission from Geminga pulsar and nebula with the MAGIC telescopes. *A&A,* **591,** A138 (2016).

96. Rodrı/guez-Fernández, N. J., Martı/n-Pintado, J. & de Vicente, P. Large scale ionization of the Radio Arc region by the Quintuplet and the Arches clusters. *A&A,* **377,** 631–643 (2001).

97. Ahnen, M. L. *et al.* Observations of Sagittarius A* during the pericenter passage of the G2 object with MAGIC. *A&A,* **601,** A33 (2017).

98. Oka, T., Hasegawa, T., Sato, F., Tsuboi, M. & Miyazaki, A. A Molecular Cloud and an Expanding Cavity Adjacent to the Nonthermal Filaments of the Galactic Center Radio Arc. *PASJ,* **53,** 779–786 (2001).

99. Aharonian, F. *et al.* A New Population of Very High Energy Gamma-Ray Sources in the Milky Way. *Science* **307,** 1938–1942 (2005).

100. Blitz, L., Fich, M. & Stark, A. A. Catalog of CO radial velocities toward galactic H II regions. *ApJ,* **49,** 183–206 (1982).

101. Kassim, N. E. & Weiler, K. W. A possible new association of a pulsar with a supernova remnant. *Nature,* **343,** 146–148 (1990).

102. Rowell, G., de Naurois, M., Ataï, A. D., Gallant, Y. & H.E.S.S. Collaboration. *Extended VHE γ-ray emission towards SGR1806-20 and stellar cluster C1 1806-20* in (eds Aharonian, F. A., Hofmann, W. & Rieger, F. M.) **1505** (2012), 273–276.

103. Yeung, P. K. H. *et al.* Studying the SGR 1806-20/Cl* 1806-20 Region Using the Fermi Large Area Telescope. *ApJ,* **827,** 41 (2016).

104. Acero, F. *et al.* The First Fermi LAT Supernova Remnant Catalog. *ApJ,* **224,** 8 (2016).

105. Duncan, R. C. & Thompson, C. Formation of very strongly magnetized neutron stars - Implications for gamma-ray bursts. *ApJ,* **392,** L9–L13 (1992).

106. Aharonian, F. *et al.* Chandra and HESS observations of the supernova remnant CTB 37B. *A&A,* **486,** 829–836 (2008).

107. Halpern, J. P. & Gotthelf, E. V. An Energetic Magnetar in HESS J1713-381/CTB 37B. *ApJ,* **725,** 1384–1391 (2010).

108. Abdalla, H. *et al.* Extended VHE gamma-ray emission towards SGR1806-20, LBV1806-20, and stellar cluster Cl*1806-20. *A&A,* **612,** A11 (2018).

109. Corbel, S. & Eikenberry, S. S. The connection between W31, SGR 1806-20, and LBV 1806-20: Distance, extinction, and structure. *A&A,* **419,** 191–201 (2004).

110. Aharonian, F. *et al.* Discovery of two candidate pulsar wind nebulae in very-high-energy gamma rays. *A&A,* **472,** 489–495 (2007).

111. Bamba, A., Ueno, M., Koyama, K. & Yamauchi, S. Diffuse Hard X-Ray Sources Discovered with the ASCA Galactic Plane Survey. *ApJ,* **589,** 253–260 (2003).

112. Brogan, C. L. *et al.* A Low-Frequency Survey of the Galactic Plane Near l=11°: Discovery of Three New Supernova Remnants. *ApJ,* **127,** 355–367 (2004).

113. Helfand, D. J., Becker, R. H., White, R. L., Fallon, A. & Tuttle, S. MAGPIS: A Multi-Array Galactic Plane Imaging Survey. *ApJ,* **131,** 2525–2537 (2006).

114. Kargaltsev, O. & Pavlov, G. G. X-Ray Emission from PSR J1809-1917 and Its Pulsar Wind Nebula, Possibly Associated with the TeV Gamma-Ray Source HESS J1809-193. *ApJ,* **670,** 655–667 (2007).

115. Anada, T., Bamba, A., Ebisawa, K. & Dotani, T. X-Ray Studies of HESS J1809-193 with Suzaku. *PASJ,* **62,** 179–186 (2010).

116. Rangelov, B. *et al.* Multiwavelength Study of the Northeastern Outskirts of the Extended TeV Source HESS J1809-193. *ApJ,* **796,** 34 (2014).

117. Castelletti, G., Giacani, E. & Petriella, A. Unveiling the origin of HESS J1809-193. *A&A,* **587,** A71 (2016).

118. Donath, A. *et al. The H.E.S.S. Galactic plane survey poster* in *34th International Cosmic Ray Conference (ICRC2015)* **34** (2015), 782.

119. Marelli, M. *et al.* On the Puzzling High-Energy Pulsations of the Energetic Radio-Quiet $\gamma$-Ray Pulsar J1813-1246. *The Astrophysical Journal* **795,** 168 (Nov. 2014).

120. Albert, J. *et al.* MAGIC Observations of Very High Energy $\gamma$-Rays from HESS J1813-178. *ApJ,* **637,** L41–L44 (2006).

121. Brogan, C. L. *et al.* Discovery of a Radio Supernova Remnant and Nonthermal X-Rays Coincident with the TeV Source HESS J1813-178. *ApJ,* **629,** L105–L108 (2005).

122. Ubertini, P. *et al.* INTEGRAL IGR J18135-1751 = HESS J1813-178: A New Cosmic High-Energy Accelerator from keV to TeV Energies. *ApJ,* **629,** L109–L112 (Aug. 2005).

123. White, R. L., Becker, R. H. & Helfand, D. J. New Catalogs of Compact Radio Sources in the Galactic Plane. **130,** 586–596 (Aug. 2005).

124. Churchwell, E. Ultracompact H II regions - The impact of newly formed massive stars on their environment. **2,** 79–123 (1990).

125. Mizuno, A. & Fukui, Y. *Physical properties of molecular clouds as revealed by NANTEN CO survey: from the galactic center to the galactic warp* in *Milky Way Surveys: The Structure and Evolution of our Galaxy* (eds Clemens, D., Shah, R. & Brainerd, T.) **317** (Dec. 2004), 59.

126. Funk, S. *et al.* XMM-Newton observations of HESS J1813-178 reveal a composite Supernova remnant. **470,** 249–257 (July 2007).

127. Gaensler, B. M. & Slane, P. O. The Evolution and Structure of Pulsar Wind Nebulae. **44,** 17–47 (Sept. 2006).

128. Gotthelf, E. V. & Halpern, J. P. Discovery of a Highly Energetic X-Ray Pulsar Powering HESS J1813-178 in the Young Supernova Remnant G12.82-0.02. **700,** L158–L161 (Aug. 2009).

129. Abdo, A. A. *et al.* Fermi/Large Area Telescope Bright Gamma-Ray Source List. **183,** 46–66 (July 2009).

130. Aharonian, F. *et al.* Energy dependent $\gamma$-ray morphology in the pulsar wind nebula HESS J1825-137. *A&A,* **460,** 365–374 (2006).

131. Lemiere, A., Terrier, R. & Djannati-Ataï, A. Multi-resolution analysis of the H.E.S.S. Galactic Survey Sources and Search for Counterparts in CO and HI data. *PoS ICRC2005* **4,** 105–108 (2005).

132. Voisin, F. *et al.* ISM gas studies towards the TeV PWN HESS J1825-137 and northern region. *MNRAS,* **458,** 2813–2835 (2016).

133. Brogan, C. L., Gelfand, J. D., Gaensler, B. M., Kassim, N. E. & Lazio, T. J. W. Discovery of 35 New Supernova Remnants in the Inner Galaxy. *ApJ,* **639,** L25–L29 (2006).

134. Ray, P. S. *et al.* Precise $\gamma$-ray Timing and Radio Observations of 17 Fermi $\gamma$-ray Pulsars. *ApJ,* **194,** 17 (2011).

135. Acero, F. *et al.* Fermi Large Area Telescope Third Source Catalog. *The Astrophysical Journal Supplement Series* **218,** 23 (2015).

136. Ackermann, M. *et al.* 2FHL: The Second Catalog of Hard Fermi-LAT Sources. *The Astrophysical Journal Supplement Series* **222,** 5 (2016).

137. Bartoli, B. *et al.* Observation of TeV Gamma Rays from the Unidentified Source HESS J1841-055 with the ARGO-YBJ Experiment. *ApJ,* **767,** 99 (2013).

138. Abeysekara, A. U. *et al.* Search for TeV Gamma-Ray Emission from Point-like Sources in the Inner Galactic Plane with a Partial Configuration of the HAWC Observatory. *ApJ,* **817,** 3 (2016).

139. Ferrand, G. & Safi-Harb, S. A census of high-energy observations of Galactic supernova remnants. *Advances in Space Research* **49,** 1313–1319 (2012).

140. Hoppe, S. The H.E.S.S. survey of the inner Galactic plane. *PoS ICRC2007,* **2,** 579–582 (2008).

141. Ueno, M., Bamba, A., Koyama, K. & Ebisawa, K. Chandra Observations of a Non-thermal Supernova Remnant Candidate AX J1843.8-0352 and Its Surroundings. *ApJ,* **588,** 338–343 (2003).

142. Abdo, A. A. *et al.* Milagro Observations of Multi-TeV Emission from Galactic Sources in the Fermi Bright Source List. *ApJ,* **700,** L127–L131 (2009).

143. Vasisht, G., Gotthelf, E. V., Torii, K. & Gaensler, B. M. Detection of a Compact X-Ray Source in the Supernova Remnant G29.6+0.1: A Variable Anomalous X-Ray Pulsar? *ApJ,* **542,** L49–L52 (2000).

144. Kosack, K., Chaves, R. C. G. & Acero, F. HESS J1852-000: A Very High Energy Gamma-ray source near Supernova Remnant Kes˜78. *PoS ICRC2011* **7,** 76–78 (2011).

145. Tueller, J. *et al.* The 22 Month Swift-BAT All-Sky Hard X-ray Survey. *ApJS,* **186,** 378–405 (2010).

146. Knispel, B. *et al.* Einstein@Home Discovery of a PALFA Millisecond Pulsar in an Eccentric Binary Orbit. *ApJ,* **806,** 140 (2015).

147. Karpova, A., Zyuzin, D., Danilenko, A. & Shibanov, Y. Constraining the parameters of the pulsar wind nebula DA 495 and its pulsar with Chandra and XMM-Newton. *MNRAS,* **453,** 2241–2249 (2015).

148. Swanenburg, B. N. *et al.* Second COS B catalog of high-energy gamma-ray sources. *ApJ,* **243,** L69–L73 (1981).

149. Hartman, R. C. *et al.* The Third EGRET Catalog of High-Energy Gamma-Ray Sources. *ApJS,* **123,** 79–202 (1999).

150. Aleksić, J. *et al.* MAGIC Upper Limits for Two Milagro-detected Bright Fermi Sources in the Region of SNR G65.1+0.6. *ApJ,* **725,** 1629–1632 (2010).

151. Weisskopf, M. C., Tananbaum, H. D., Van Speybroeck, L. & O'Dell, S. Chandra X-ray Observatory (CXO): overview. *Proc. SPIE* **32,** 2005–2011 (2003).

152. Burke, B. E. *et al.* Soft-X-ray CCD imagers for AXAF. *IEEE Transactions on Electron Devices* **44,** 1633–1642 (1997).

153. Turner, M. J. L. *et al.* The European Photon Imaging Camera on XMM-Newton: The MOS cameras : The MOS cameras. *A&A* **365,** L27–L35 (2001).

154. Latronico, L. & Spandre, G. The GLAST large area telescope: Design, construction, test and calibration. *Nucl. Instrum. Methods Phys. Res. A* **581,** 160–163 (2007).

155. Atwood, W. B. *et al.* The Large Area Telescope on the Fermi Gamma-Ray Space Telescope Mission. *The Astrophysical Journal* **697,** 1071–1102 (2009).

156. Manchester, R. N., Hobbs, G. B., Teoh, A. & Hobbs, M. The Australia Telescope National Facility Pulsar Catalogue. *The Astronomical Journal* **129,** 1993–2006 (2005).

157. van Albada-van Dien, E. Photographic observations of visual double stars. *Astronomy and Astrophysics Supplement Series* **52,** 193–202 (1983).

158. Hirshfeld, A. & Sinnott, R. W. *Sky Catalogue 2000.0* Vol. 2 (Cambridge University Press and Sky Publishing Corporation, 1985).

159. Watson, L. *A Photometric and Spectroscopic Study of Selected Southern Chromospherical Active Stars* Ph.D. Thesis (University of Canterbury, 1999).

160. Liao, N.-H., Chou, Y., Hsieh, H.-E. & Chuang, P.-S. The Updated Orbital Ephemeris of Dipping Low Mass X-ray Binary 4u 1624-49. *Publication of Korean Astronomical Society* **30,** 593–594 (2015).

161. Balman, Ş. A Study of the Low-Mass X-Ray Binary Dip Sources XB 1916 - 053, XB 1323 - 619, X 1624 - 490 and 4U 1746 - 371 Observed with INTEGRAL. *The Astrophysical Journal* **138,** 50–62 (2009).

162. Wachter, S. *et al.* Chandra HRC Localization of the Low-Mass X-Ray Binaries X1624-490 and X1702-429: The Infrared Counterparts. *The Astrophysical Journal* **621,** 393–397 (2005).

163. Robitaille, T. P. *et al.* Intrinsically Red Sources Observed by Spitzer in the Galactic Midplane. *The Astronomical Journal* **136,** 2413 (2008).

164. Dobashi, K. Atlas and Catalog of Dark Clouds Based on the 2 Micron All Sky Survey. *Publications of the Astronomical Society of Japan* **63,** S1–S362 (2011).

165. Arnaud, K. A. *XSPEC: The First Ten Years* in *Astronomical Data Analysis Software and Systems V* (eds Jacoby, G. H. & Barnes, J.) **101** (1996), 17.

166. Mewe, R., Lemen, J. R. & van den Oord, G. H. J. Calculated X-radiation from optically thin plasmas. VI - Improved calculations for continuum emission and approximation formulae for nonrelativistic average Gaunt actors. *Astronomy and Astrophysics Supplement Series* **65,** 511–536 (1986).

167. Kalberla, P. M. W. *et al.* The Leiden/Argentine/Bonn (LAB) Survey of Galactic HI. Final data release of the combined LDS and IAR surveys with improved stray-radiation corrections. *A&A* **440,** 775–782 (2005).

168. Acero, F. *et al.* Constraints on the Galactic Population of TeV Pulsar Wind Nebulae Using FERMI Large Area Telescope Observations. *Astrophys. J.* **773,** 77 (2013).

169. Lin, D., Webb, N. A. & Barret, D. Classification of X-Ray Sources in the XMM-Newton Serendipitous Source Catalog. *The Astrophysical Journal* **756,** 27 (2012).

170. H. E. S. S. Collaboration *et al.* Extended VHE $\gamma$-ray emission towards SGR1806-20, LBV 1806-20, and stellar cluster Cl* 1806-20. *A&A* **612,** A11 (2018).

171. Kulkarni, S. R. *et al.* Optical and infrared observations of SGR 1806-20. *The Astrophysical Journal Letters* **440,** L61–L64 (1995).

172. Reimer, A., Pohl, M. & Reimer, O. Nonthermal High-Energy Emission from Colliding Winds of Massive Stars. *The Astrophysical Journal* **644,** 1118–1144 (2006).

173. Bednarek, W. GeV gamma-rays and TeV neutrinos from very massive compact binary systems: the case of WR 20a. *MNRAS* **363,** L46–L50 (2005).

174. Benaglia, P. & Romero, G. E. Gamma-ray emission from Wolf-Rayet binaries. *A&A* **399,** 1121–1134 (2003).

175. Oskinova, L. M., Hamann, W.-R., Feldmeier, A., Ignace, R. & Chu, Y.-H. DISCOVERY OF X-RAY EMISSION FROM THE WOLF-RAYET STAR WR 142 OF OXYGEN SUBTYPE. *The Astrophysical Journal* **693,** L44–L48 (2009).

176. Araudo, A. T., Bosch-Ramon, V. & Romero, G. E. Gamma-ray emission from Wolf-Rayet stars interacting with AGN jets. *AIP Conference Proceedings* **1505,** 614–617 (2012).

177. Laros, J. G. *et al.* A New Type of Repetitive Behavior in a High-Energy Transient. *The Astrophysical Journal* **320,** L111 (1987).

178. Murakami, T. ASCA observations of two SGRs SGR1806-20 and SGR0526-66. *Astrophysics and Space Science* **231,** 57–63 (1995).

179. Kouveliotou, C. *et al.* An X-ray pulsar with a superstrong magnetic field in the soft $\gamma$-ray repeater SGR1806 - 20. *Nature* **393,** 235–237 (1998).

180. Thompson, C. & Duncan, R. C. The soft gamma repeaters as very strongly magnetized neutron stars - I. Radiative mechanism for outbursts. *MNRAS* **275,** 255–300 (1995).

181. Abdo, A. A. *et al.* Detection of 16 Gamma-Ray Pulsars Through Blind Frequency Searches Using the Fermi LAT. *Science* **325,** 840 (2009).

182. Abdo, A. A. *et al.* The Second Fermi Large Area Telescope Catalog of Gamma-Ray Pulsars. *The Astrophysical Journal Supplement Series* **208,** 17 (Oct. 2013).